# Immagine

domenica 27 settembre 2020 10:22

University of Catania

**Dept. of Civil Engineering and Architecture**

**Master Degree in Mechanical Engineering**

# Lecture notes

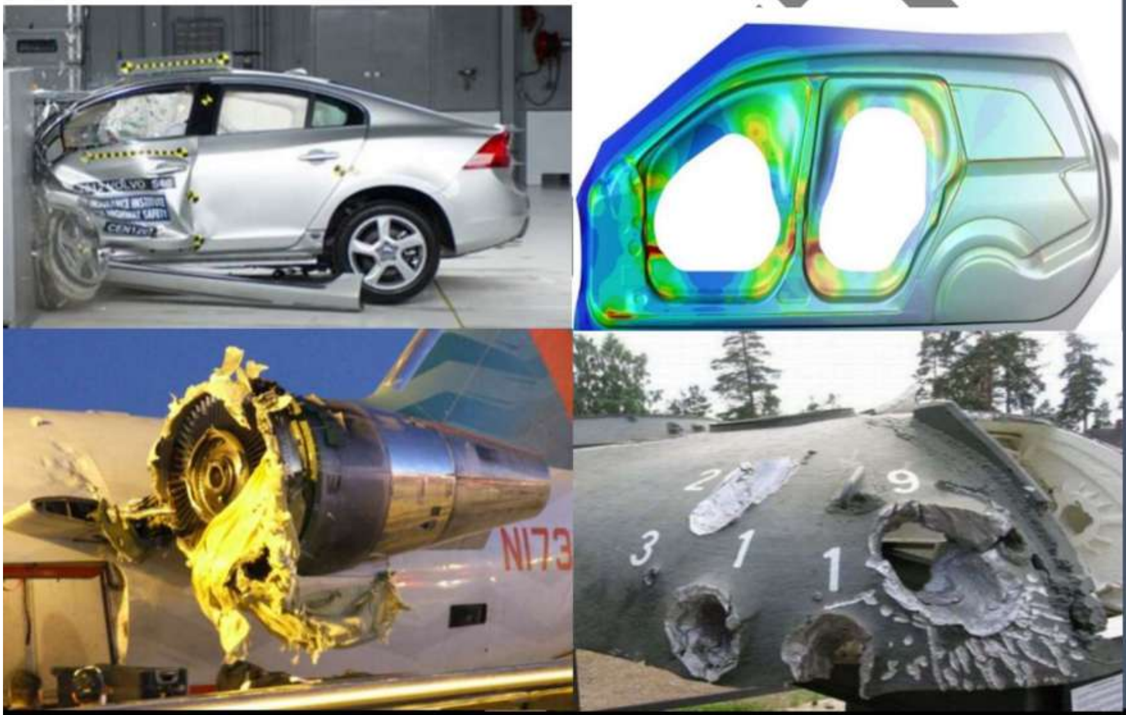

## *Elastoplasticity, Ductile Damage and Dynamics*

**G. Mirone**

**R 2020-09**

# PREFACE

This document is a draft guide of the course of "Advanced Mechanical Design" for Mechanical Engineers available at the University of Catania since the Academic Year 2020-21. It also contains chapters / sections not included within the syllabus of the above course.

The content is based on the research activity and on the lessons held for older courses, although some pargraphs and images are taken from the scientific literature and from the internet.

Some parts of the document are not even yet translated from Italian.

Possible errors and inaccuracies still present in the document can be reported by email at the address giuseppe.mirone@unict.it .

The main sections of the document are aimed at:

Elastoplasticity (Theory + Laboratory experiments + Finite Elements)
Ductile damage (Theory + Laboratory experiments + Finite Elements)
Strain rate effect (Theory + Laboratory experiments + Finite Elements)

.

*Credits for the Cover pictures:*

http://www.sicurauto.it/sistemi-di-sicurezza/news/qual-e-lauto-piu-sicura-degli-ultimi-ventanni.html
http://stampack.com/
http://forums.radioreference.com/colorado-incidents-breaking-news/60891-ntsb-investigates-jet-engine-failure-over-colorado.html
http://image.so.com/i?q=%E7%A9%BF%E7%94%B2%E5%BC%B9%E5%92%8C%E7%A0%B4%E7%94%B2%E5%BC%B9&src=tab_image

# INDEX

# 1 QUICK REVIEW OF TENSORIAL MECHANICS

## 1.1 STRESS TENSOR

Let's consider an elastic body subjected to arbitrary macroscopic loads (forces, moments) and constraints; for determining the effects of all global macroscopic loads on each material point (local microscopic scale), the stress tensor must be defined.

Given an arbitrary Cartesian reference system (RS) with axes $(x, y, z)$, an infinitesimal material cube with faces normal to the RS can be centered on each material point of the body.

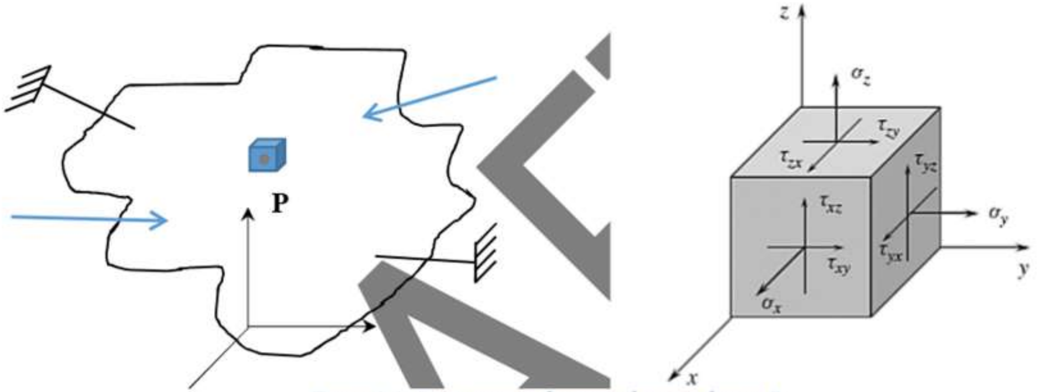

*Figure 1-1: Stress state at the general material point P*

Each face of the cube in Figure 1-1Figure 1-4is subjected to a normal stress perpendicular to the face and two tangential or shear stresses acting parallel to the face. All stresses have the dimension of a force per unit area (N/mm$^2$ = MPa).

For the translational equilibrium the stresses acting on opposite faces have identical magnitude and opposite verses. The rotational equilibrium ensures that:

$$\begin{aligned} \tau_{xy} &= \tau_{yx} \\ \tau_{xz} &= \tau_{zx} \\ \tau_{yz} &= \tau_{zy} \end{aligned} \qquad (1) \qquad ( 1\text{-}1 )$$

So the stress tensor is symmetrical and only 6 different stress values are sufficient for completely identifying the stress state at each material point:

$$\tilde{\sigma}_R(P) = \begin{bmatrix} \sigma_x & \tau_{xy} & \tau_{xz} \\ \tau_{yx} & \sigma_y & \tau_{yz} \\ \tau_{zx} & \tau_{zy} & \sigma_z \end{bmatrix} \qquad (2) \qquad (1\text{-}2)$$

Generally, the stress tensor changes from a material point to another within the same elastic body; however special cases may occur where the stress tensor is identical all over the volume of the body.

## 1.2 CHANGE OF REFERENCE SYSTEM, PRINCIPAL DIRECTIONS AND STRESSES, STRESS INVARIANTS

Assume that a certain stress tensor *σ(P)* expresses the stress state at the point *P* of the elastic body, referred to a RS $R_0$.

Assume that another reference system *R'* is defined in $R_0$ by the coordinates of its three versors; these versors, put in three side-by-side columns define the matrix for changing the reference system from $R_0$ to *R'*.

The change of reference system can also be applied to the stress tensor:

$$\tilde{\sigma}_R = R' \cdot \tilde{\sigma}_{R_0} \cdot R \qquad (3) \qquad (1\text{-}3)$$

NUMERICAL EXAMPLES OF REFERENCE CHANGE (EQUIPM.-DES. YEAR 2019-20 NOTES) !!!!!

Among all the infinite possible RS there is a special one, $R^*$, called “principal reference system”, where the tangential stresses (non-diagonal terms) vanish and the normal stresses, now called principal stresses, are ordered in a descending order:.

$$\tilde{\sigma}_{R*}(P) = \begin{bmatrix} \sigma_1 & 0 & 0 \\ 0 & \sigma_2 & 0 \\ 0 & 0 & \sigma_3 \end{bmatrix} \qquad (4) \qquad (1\text{-}4)$$

The mathematical tool for identifying the principal reference system and the corresponding principal stresses is the "eigenvectors-eigenvalues" operator available in many commercial software for calculus.

If one of the principal stresses is known, then a simple graphical/analytical procedure called "Mohr Circles" can be used for determining the two remaining unkown principal directions and the corresponding principal stresses.

Consider a stress tensor $\tilde{\sigma}_R(P)$ at a material point *P* within the elastic body, expressed in the reference system *R* = (*X, Y, Z*). Let suppose that $\tau_{zx} = \tau_{zy} = 0$ : this means that the *Z* axis of the current reference system is also principal; let suppose that *Z* is coincident to the axis *3* of the unknown principal system *R**, whose axes are labeled (*1,2,3*). Then $\sigma_z = \sigma_3$.
The system *R**can be fully identified by just the angle $\vartheta$ in Figure 1-2, then also the two principal stresses $\sigma_1, \sigma_2$ can be determined through the Mohr circle, so completely defining the stress tensor in the principal reference system $\tilde{\sigma}_{R*}(P)$.

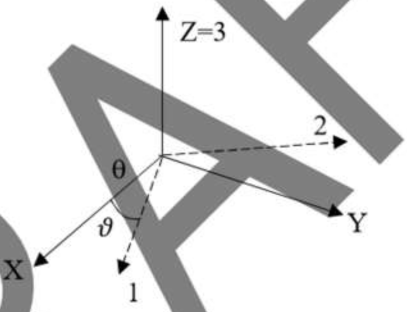

*Figure 1-2 reference systems with common z axis*

$$\tilde{\sigma}_R(P) = \begin{bmatrix} \sigma_x & \tau_{xy} & 0 \\ \tau_{xy} & \sigma_y & 0 \\ 0 & 0 & \sigma_3 \end{bmatrix} \qquad (1\text{-}5)$$

$$\tilde{\sigma}_{R*}(P) = \begin{bmatrix} \sigma_1 & 0 & 0 \\ 0 & \sigma_2 & 0 \\ 0 & 0 & {}_3 \end{bmatrix} \qquad (1\text{-}6)$$

On a $\sigma$ - $\tau$ plane are reported two points of coordinates coordinate (σx, τxy) and (σy, -τxy); such points identify the diameter of a circle which defines all the possible combinations of stress tensors and reference systems having an axis coincident to axis *3*.
Among all such combinations,, the principal stresses correspond to the intersections of the circle with the horizontal axis $\sigma$ and the orientation of the principal axes 1, 2 is identified by the angle $\vartheta$.

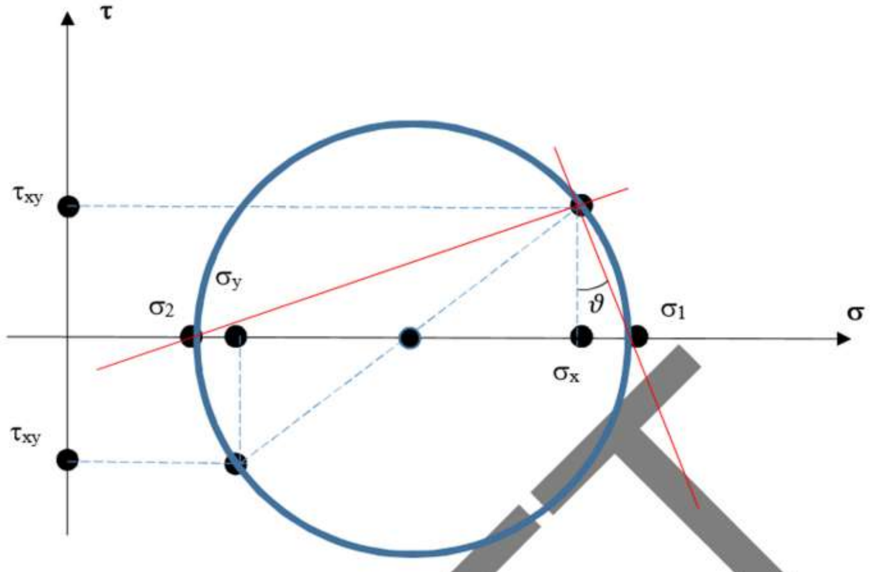

*Figure 1-3 Mohr circle*

By simple geometric considerations, the center of the circle has coordinates ( $\frac{\sigma_x+\sigma_y}{2}$, 0) and the radius of the circle by Pitagora is $r=\sqrt{\left(\frac{\sigma_x-\sigma_y}{2}\right)^2+\tau_{xy}{}^2}$; Then the principal stresses and the angle $\vartheta$ can be simply calculated as follows:

$$\sigma_1=\frac{\sigma_x+\sigma_y}{2}+\sqrt{\left(\frac{\sigma_x-\sigma_y}{2}\right)^2+\tau_{xy}{}^2} \qquad (7)$$ ( 1-7 )

$$\sigma_2=\frac{\sigma_x+\sigma_y}{2}-\sqrt{\left(\frac{\sigma_x-\sigma_y}{2}\right)^2+\tau_{xy}{}^2} \qquad (8)$$ ( 1-8 )

$$\vartheta=Arctan\left(\frac{\sigma_1-\sigma_x}{\tau_{xy}}\right) \qquad (9)$$ ( 1-9 )

As it happens for the vectors, also the tensors can be expressed in whatever different reference systems: the change of RS clearly changes the values of the tensor components but leaves unaltered the nature of the tensor and of the physical entity (stress state) it represents.

For a vector in a fixed plane, the change of RS affects the vector components but cannot affect the modulus nor the orientation of such vector. Similarly, the stress tensor has three invariants independent of the RS:

$$I_1=\sigma_1+\sigma_2+\sigma_3=\ \sigma_x+\sigma_y+\sigma_z \qquad (10)$$

$$\mathrm{I}_2=\sigma_1\sigma_2+\sigma_2\sigma_3+\sigma_1\sigma_3=\left(\sigma_x\sigma_y+\sigma_y\sigma_z+\sigma_z\sigma_x\right)-\tau_{xy}^2-\tau_{yz}^2-\tau_{zx}^2 \qquad (11)$$

$$I_3=\sigma_1\cdot\sigma_2\cdot\sigma_3=\sigma_x\cdot\sigma_y\cdot\sigma_z+2\tau_{xy}\tau_{yz}\tau_{xz}-\left(\sigma_x\tau_{yz}^2+\sigma_y\tau_{xz}^2+\sigma_z\tau_{xy}^2\right) \qquad (12)$$

Equations (10) to (12) report the three invariants expressed in both a general arbitrary reference system (all shear stresses different from zero) and the principal reference system (all shear stresses vanished).

The six numbers inside the stress tensor can greatly change depending on the RS adopted but, given that the physics of the elastic body cannot be affected by a change of RS (shape and material of the body, applied loads and constraints are independent of the given RS), the different sextet of values within $\tilde{\sigma}_R$ and $\tilde{\sigma}_{R_0}$ must reflect such unchanged physics according to eqs. 10-12.

## 1.3 HYDROSTATIC AND DEVIATORIC STRESS COMPONENTS

The mean value of the normal stresses from a general stress tensor is invariant with respect to the RS (it is equal to $I_1/3$), is called hydrostatic stress and allows to decompose a general stress tensor according to the following eq. (13)

$$\tilde{\sigma} = \begin{bmatrix} \sigma_x & \tau_{xy} & \tau_{xz} \\ \tau_{yx} & \sigma_y & \tau_{yz} \\ \tau_{zx} & \tau_{zy} & \sigma_z \end{bmatrix} = \begin{bmatrix} s_x & \tau_{xy} & \tau_{xz} \\ \tau_{yx} & s_y & \tau_{yz} \\ \tau_{zx} & \tau_{zy} & s_z \end{bmatrix} + \begin{bmatrix} \sigma_H & 0 & 0 \\ 0 & \sigma_H & 0 \\ 0 & 0 & \sigma_H \end{bmatrix} = \tilde{\sigma}_{Dev} + \tilde{\sigma}_H \tag{13}$$

with

$$\sigma_H = \frac{\sigma_x+\sigma_y+\sigma_z}{3}\sigma_x \,; \qquad s_i = \sigma_i - \sigma_H \tag{14}$$

The tensor $\tilde{\sigma}_H$ with only diagonal terms is called Hydrostatic and has a first invariant identical to that of the complete tensor $\tilde{\sigma}$, while the tensor $\tilde{\sigma}_{Dev}$ is called Deviatoric and its first invariant is always null.

The hydrostatic stress on elastic bodies generates volume changes without shape variations, while the deviatoric stress generates shape variations at constant volume.

The same decomposition of eq. (13) can be done in the principal reference system:

$$\tilde{\sigma} = \begin{bmatrix} \sigma_1 & 0 & 0 \\ 0 & \sigma_2 & 0 \\ 0 & 0 & \sigma_3 \end{bmatrix} = \begin{bmatrix} s_1 & 0 & 0 \\ 0 & s_2 & 0 \\ 0 & 0 & s_3 \end{bmatrix} + \begin{bmatrix} \sigma_H & 0 & 0 \\ 0 & \sigma_H & 0 \\ 0 & 0 & \sigma_H \end{bmatrix} \tag{15}$$

Again, the first invariant of $\tilde{\sigma}$ goes entirley in $\tilde{\sigma}_H$ while $\tilde{\sigma}_{Dev}$ has a null $I_1$.

The decomposition of a stress tensor in its hydrostatic and deviatoric constituents is importsnt because only $\tilde{\sigma}_{Dev}$ triggers the onset of permanent deformations and the plastic flow, while $\tilde{\sigma}_H$ influences the ductile damage while leaving unaffected the plastic flow.

## 1.4 STRAIN TENSOR AND ELASTICITY LAW

Similarly to what done for the stress tensor, the strain tensor in the general RS can be expressed as follows:

$$\left[\, \tilde{\varepsilon}_{x,y,z} \,\right] = \begin{bmatrix} \varepsilon_x & \varepsilon_{xy} & \varepsilon_{xz} \\ \varepsilon_{yx} & \varepsilon_y & \varepsilon_{yz} \\ \varepsilon_{zx} & \varepsilon_{zy} & \varepsilon_z \end{bmatrix} \tag{16}$$

Under the hypothesis of small displacements and infinitesimal strains, the displacement functions ux and uy are suitable for defining the strains according to Figure 1-4:

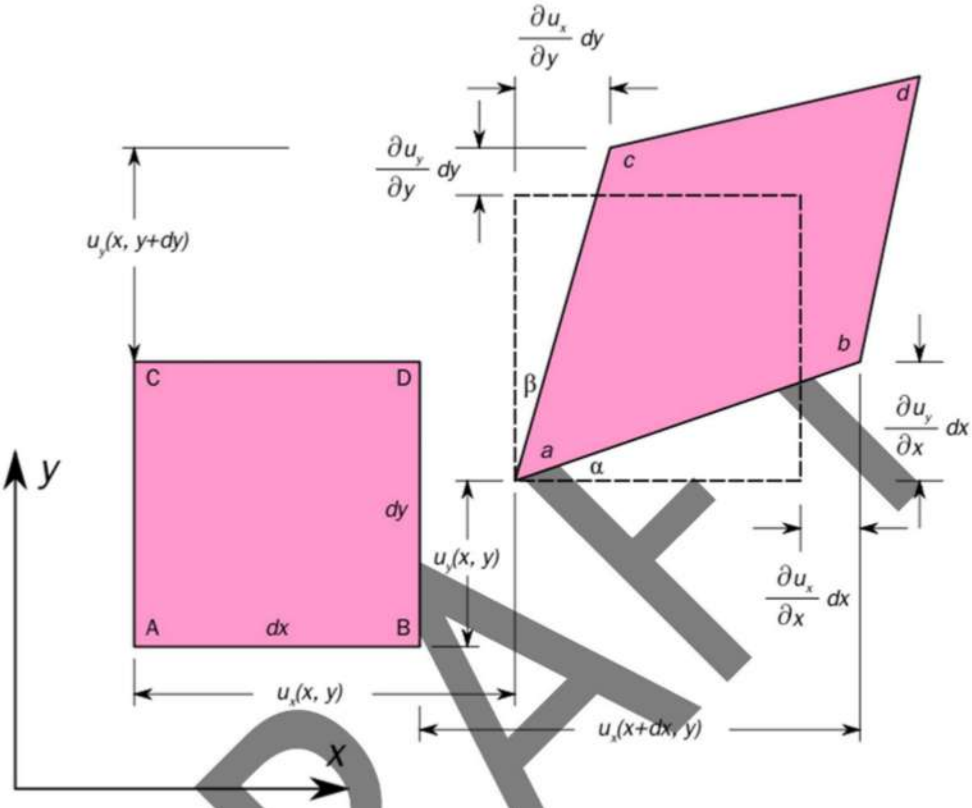

*Figure 1-4: elementary cube for strains definition* CITARE PROVENIENZA FIGURA

Extending the definition to three-dimensional space and displacements *ux, uy, uz*, the components of the strain tensor are defined according to the following derivatives:

$$\epsilon_x = \frac{\partial u_x}{\partial x};\quad \epsilon_y = \frac{\partial u_y}{\partial y};\quad \epsilon_x = \frac{\partial u_z}{\partial z} \tag{17}$$

$$\epsilon_{xy} = \frac{1}{2}\left(\frac{\partial u_x}{\partial y} + \frac{\partial u_y}{\partial x}\right);\quad \epsilon_{xz} = \frac{1}{2}\left(\frac{\partial u_x}{\partial z} + \frac{\partial u_z}{\partial x}\right);\quad \epsilon_{yz} = \frac{1}{2}\left(\frac{\partial u_y}{\partial z} + \frac{\partial u_z}{\partial y}\right) \tag{18}$$

For small displacements and infinitesimal strains, the current deformed configuration of the body can be approximated by the initial undeformed configuration and eqs. (17) and (18) apply.

For large displacements and finite deformations, the current configuration of the body differs from the undeformed configuration, then the current strain is based on the integration of incremental small strains

For small displacements and infginitesimal strains, the strain tensor can be related to the stress tensor through the elastic stress-strain law:

$$\begin{Bmatrix} \epsilon_x \\ \epsilon_y \\ \epsilon_z \\ \epsilon_{xy} \\ \epsilon_{xz} \\ \epsilon_{yz} \end{Bmatrix} = \begin{bmatrix} {}^1/_E & -{}^\upsilon/_E & -{}^\upsilon/_E & 0 & 0 & 0 \\ -{}^\upsilon/_E & {}^1/_E & -{}^\upsilon/_E & 0 & 0 & 0 \\ -{}^\upsilon/_E & -{}^\upsilon/_E & {}^1/_E & 0 & 0 & 0 \\ 0 & 0 & 0 & G & 0 & 0 \\ 0 & 0 & 0 & 0 & G & 0 \\ 0 & 0 & 0 & 0 & 0 & G \end{bmatrix} \begin{Bmatrix} \sigma_x \\ \sigma_y \\ \sigma_z \\ \tau_{xy} \\ \tau_{xz} \\ \tau_{yz} \end{Bmatrix} \text{ or, in contracted form, } \{\bar{\varepsilon}\} = \left[\vec{C}\right]\{\bar{\sigma}\} \qquad (19)$$

With E normal elasticity modulus ( or Young modulus), ν Poisson's coefficients and G tangential elasticity modulus:

$$G = \frac{E}{2\cdot(1+\upsilon)} \qquad (20)$$

Eq. 19 can be easily inverted, therefore within the elastic range a biunivocal relationship exists between the stress and the strain tensors, based on just the two elasticity material constants $E$, $\upsilon$.

# 2 ELASTOPLASTIC BEHAVIOR

## 2.1 GENERAL COSTITUTIVE RELATIONSHIP, BASICS OF NONLINEAR INTEGRATION

When a materiali is stressed beyond the elastic limit (beyond the first yield), its response consists of a total strain tensor which is the sum of an elastic strain tensor (which reverses to zero as the stress is removed) plus a plastic strain tensor (which is irreversible and does not vanishes as the stress is removed):

$$\varepsilon_{ij}^{\ TOT} = \varepsilon_{ij}^{\ EL} + \varepsilon_{ij} \tag{1}$$

While the elastic strain is directly related to the stress through the elasticity equation, the plastic strain cannot be determined by the knowledge of the current stress alone:

$$\begin{gathered} \varepsilon^{EL}{}_i = \frac{1}{E}\left[\sigma_i - \nu\left(\sigma_j + \sigma_k\right)\right] \quad \Longleftrightarrow \quad \sigma_i = \lambda\left(\varepsilon^{EL}{}_i + \varepsilon^{EL}{}_j + \varepsilon^{EL}{}_k\right) + 2\mu\varepsilon^{EL}{}_i \\ \varepsilon_i = \ldots\ldots\ldots\ldots \quad \Longleftrightarrow \quad \sigma_i = \ldots\ldots\ldots\ldots\ldots\ldots \end{gathered} \tag{2}$$

In the plastic range the stress-strain relationship is only incremental, so the calculation of σ and ϵ must be usually performed by numerical integration (finite elements method), determining the entire stresses and strains from the beginning of the loading history up to the current state, at all material points of the component/structure at hand.

This occurs because the differential relationship expressing the elastoplastic behavior, highly dissipative and history-dependent, usually cannot be integrated in a closed form solutions.

When a materiali is gradually loaded, it initially reacts with reversible elastic strains until the elastic range up to the first yield; then, further stresses generate elastoplastic strains.

As the first yield is reached and palstic strains start flowing, the stress can either remain constant (this is the case of ideal plastic materials, e.g. play dough, toothpaste, etc.) or continuously increase beyond the first yield (real elastoplastic materials with hardening response).

The yield phenomena is triggered by a special scalar function, named **yield function** $f(\tilde{\sigma})$ (e.g. the von Mises function), reaching a critical threshold value. The variables of the yield function are the components of the stress tensor (3 or 6 depending on the reference system), and infinite combinations of the input variables can deliver the same outubut value of the yield function.

Given that the reference system where the stress tensor is expressed cannot obviously affect the yield phenomena, thinking to the principal reference system and to the 3 principal stresses as the variables of the yield function $f(\sigma_1, \sigma_2, \sigma_3)$ is preferable, as it allows to visualize such function in a 3-dimensional space.

Given that the first-yield stress is a material constant, $\sigma_{y0}$, all possible combinations of principal stresses delivering the yield stress correspond to the equation

$$f(\tilde{\sigma}) = f(\sigma_1, \sigma_2, \sigma_3) = \sigma_{Eq}(\sigma_1, \sigma_2, \sigma_3) - \sigma_{y0} = 0 \tag{3}$$

with the equivalent stress $\sigma_{Eq}(\sigma_1, \sigma_2, \sigma_3)$ being a properly defined scalar function of the principal stresses.

The yield equation (3) can be plotted in the space of the principal stresses delivering a surface which, for reasons connected to irreversibility and thermodynamics principles, not further investigated here, must be convex at whatever point.

The elastoplastic behavior can be visualized as follows by referring to such surface: as a material point of corrdinates (x, y, z) within the geoemtric reference system of the given structure is gradually loaded, the point $(\sigma_1, \sigma_2, \sigma_3)$ representing its current stress state in the principal stress space starts moving from the origin (unloaded state), according to a certain stress path. While the stress state is elastic the mathematical condition $f(\tilde{\sigma}) < 0$ is satisfied. Then the elastic limit is reached and the stress state point adheres to the inner side of the first yield surface (red surface in Figure 2-1), at point *A,* and the first yield takes place so that $f(\tilde{\sigma}) = 0$;

Then, three different possibilities occur depending on how the loading proceeds and $(\sigma_1, \sigma_2, \sigma_3)$ evolve:

1) Elastic Unloading: the load is gradually released according to whatever path, either equal or different from that of the loading phase, then the stress state point moves back from the inner side of the first-yield surface and $f(\tilde{\sigma}) < 0$ is restored; eventually the stress state returns to the origin at complete unloading. In this case no plastic flow occurred so no residual strains are expeced at the end of the unloading. is satisfied.
2) Constant flow stress loading: principal stresses $(\sigma_1, \sigma_2, \sigma_3)$ change by maintaining constant the yield function, so that so that $f(\tilde{\sigma}) = 0$ is preserved at the first-yield and the equivalent stress remains constant; thus the stress-state point moves remaining attached to the inner side of the first-yield surface and, again, no plastic flow occurs and no plastic strains are generated despite the evolving stresses.
3) Plastic loading: the stresses increase so that $\sigma_{Eq}$ becomes greater than the first yield stress and $\sigma_{Eq}(\sigma_1, \sigma_2, \sigma_3) > \sigma_{y0}$: apparently the condition $f(\tilde{\sigma}) > 0$ applies, but due to the

thermodynamic irreversibility - dissipativity of the plasticity phenomena, such condition can never apply. In fact, in this case the material undergoes plastic strains and a permanent irreversible change of the current yield stress $\sigma_y$ which progressively becomes greater and greater than the first yield stress, so that $\sigma_y > \sigma_{y0}$. In this case $f(\tilde{\sigma}) = 0$ is still preserved, but now $\sigma_y$ continuously increases as the plastic strainikng proceeds, according to the so-called **hardening functions** better discussed ahead. According to the graphic visualization of such phenomena in Figure 2-1, the point A moves outside the first-yield surface but, at the same time, the material evolves in a way that the current position of the stress state (point B), always lies at the inner side of the current evolving yield surface (blue surface).

The plastic straining irreversibly affects the material by changing its current yield surface, so that the current stress state of a general plastic loading path always lies on the inner side of such current yield surface. While in **Errore. L'origine riferimento non è stata trovata.** the yield surface is simply increased in size (which is called isotropic hardening), more general changes of the yield surface may also include rigid motions within the stress space (kinematic hardening) and shape changes not considered here.

The isotropic hardening can be represented by a scalar function $R(\tilde{\varepsilon})$ expressing the current enlargement of the yield surface (or the difference $\sigma_y - \sigma_{y0}$) as in **Errore. L'origine riferimento non è stata trovata.**, while the kinematic hardening is represented by a vectorial function $\tilde{X}(\tilde{\varepsilon})$, expressing the rigid motion of the yield surface within the space of principal stresses, not visualized in Figure 2-1.

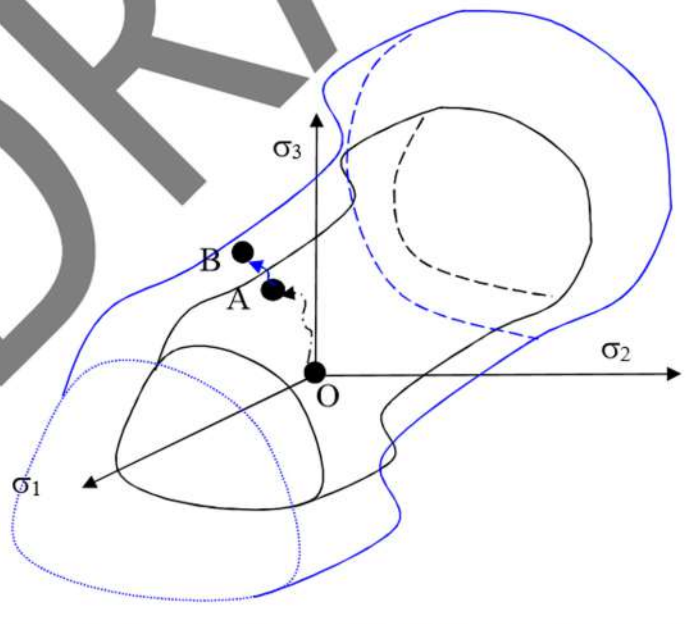

*Figure 2-1 Yield surface and moving stress state point within the principal stress space*

While the kinematic hardening $\tilde{X}(\tilde{\varepsilon})$depends on the entire tensor of plastic strain $\tilde{\varepsilon}$, the hydrostatic hardening on ly depends on a scalar function based on the plastic strain tensor, named equivalent plastic strain $\varepsilon_{Eq}$and better discussed ahead.

Then, the relationships discussed between stresses and strains are:

| | |
|---|---|
| $\tilde{\sigma}$ , Stress ←→ $\tilde{\varepsilon}$ , Plastic Strain | *CURRENT STRESS STATE* |
| $\tilde{X}$, Kinematic Hardening ←→ $\tilde{\varepsilon}$ , Back strain | *MOTION OF THE YIELD SURFACE* |
| $R$ , Isotropic Hardening ←→ $\varepsilon_{Eq}$, Equiv. pl. strain | *EXPANSION OF THE YIELD SURFACE* |

The kinematic and the isotropic hardening functions have the dimensions of a tensorial and scalar stress, respectilvely. While eq. (3) refers to a yield function with just constant yield stress, only valid for an ideal perfectly plastic material, the general form of a realistic yield function incorporating isotropic and kinematic hardneing is:

$$f(\tilde{\sigma}) = (\tilde{\sigma} - X(\tilde{\varepsilon}))_{Eq} - \sigma_{y0} - R\left(\varepsilon_{Eq}\right) = 0 \qquad (4)$$

where the operator "equivalence", capable of transforming a tensor into a scalar according to a certain mathematical rule, is applied to the difference between the stress tensor and the kinematic hardening tensor At the momento no specific rue is considered for defining the equivalence operator.

The meaning of eq. (4) is that plastic strains generate permanent modifications of the yield surface through the two hardening functions; the isotropic hardening consists in the identical increase of the yield stress along whatever geometrical direction of the elementary material cube (e.g. principal directions), while the kinematic hardening consists in changes where the yield stress increases along certain directions and decreases along others.

Summarising, the current stress state can only be either placed inside the space delimited by the current yield surface ($f(\tilde{\sigma}) < 0$, elastic loading/unloading) or onto the inner side of such surface ($f(\tilde{\sigma}) = 0$, plastic loading); the yield surface can expand and translate in the stress space for preserving such condition. Then the inequality $f(\tilde{\sigma}) \leq 0$ always applies, with $f(\tilde{\sigma})$ evolving as a function of the plastic strain, according to the hardening functions.

After the evolutions of the yield surface is modeled, the incremental relationship between plastic strains and stresses can also be discussed. This in cremental relationship is called "**Flow Rule**" or "**Normality Rule**" and appears as follows:

$$d\tilde{\varepsilon} = \frac{\partial g(\tilde{\sigma},\tilde{X},R)}{\partial \tilde{\sigma}} d\lambda \qquad (5)$$

Where $g(\tilde{\sigma},\tilde{X},R)$ is a general plastic potential, e.g. a general scalar function depending on the stress tensor and on the hardening functions, while $\lambda$ is a kind of scale factor named "plasticity multiplier".
By referring to the principal reference system, the tensorial notation can be simplified component by component:

$$d\varepsilon_i = \frac{\partial g(\tilde{\sigma},\tilde{X},R)}{\partial \sigma_i} d\lambda \qquad (6)$$

Without going into detailed mathematics and complex demonstrations, we know that for usual metals plasticity the role of the plastic potential is played by the hardening function $f(\tilde{\sigma},\tilde{X},R)$ and the plasticity multiplier is the equivalent plastic strain $\varepsilon_{Eq}$, which has the dimension of a scalar strain and is the dual of the equivalent stress with through the plastic work function.
Then $\varepsilon_{Eq}$ depends on the whole definition of $\sigma_{Eq}$ and will be discussed ahead.
This kind of plasticity, where the yield function is used as plastic potential, is called "Associate Plasticity".
The flow rule for the associate plasticity is then:

$$d\tilde{\varepsilon} = \frac{\partial f(\tilde{\sigma},\tilde{X},R)}{\partial \tilde{\sigma}} \cdot d\varepsilon_{Eq} \qquad (7)$$

or, in single-components form,

$$d\varepsilon_i = \frac{\partial f(\tilde{\sigma},\tilde{X},R)}{\partial \sigma_i} d\varepsilon_{Eq} \qquad (8)$$

The normlaity rule, expressed in the principal reference system, states that the increment of plastic strain generated by a certain increment of stress is a vector perpendicular to the updated yield surface, at the surface point corresponding to the end of the stress increment. The modulus of the plastic strain incrementi s represented by the increment of the plastic multiplier. In other words, the three derivatives of the yield function deliver the direction of the plastic strain increment (versor with unit modulus) and $d\varepsilon_{Eq}$ delivers the modulus of such increment.
This mechanism is visualized in Figure 2-2, as the strain increment is normal to the yield surface at the point where the stress increment sets the current stress state (blue yield surface), while the orientation of the stress increment not related to any yield surface normal, before or after the stress increment.

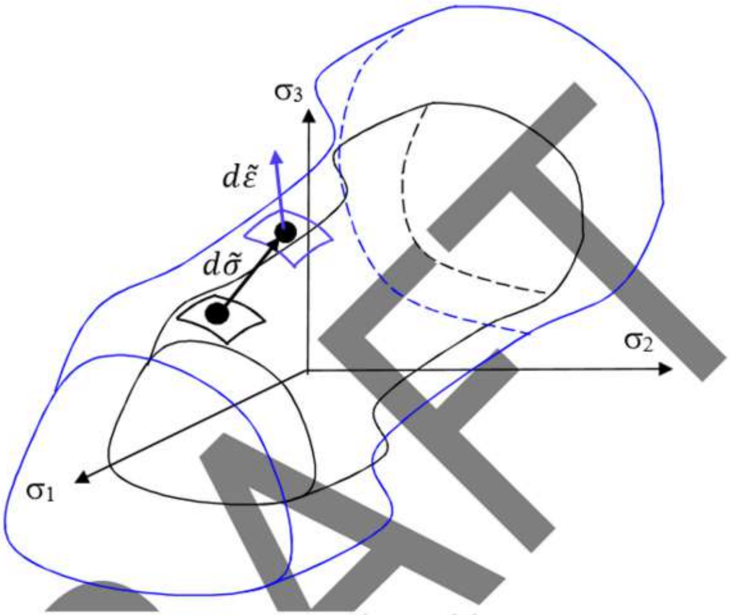

*Figure 2-2: Increments of stress and plastic strain*

Finally, the **Consistency Condition** must be imposed, expressing the condition that the yield surface only changes due to the increasing plastic strain, while it is independent of stress and hardening changes:

It is obvious that changes of the applied stress causing plastic strains also in turn affect the hardening functions and the yield surface, but if the stress change occurs without any plastic strain (e.g. elastic unloading or stress state moving onto the current yield surface), then no hardening change occurs and the yield surface itself is not going to be affected. This concept is implemented in eq. (9) below.

$$df = \frac{\partial f(\tilde{\sigma},\tilde{X},R)}{\partial \tilde{\sigma}} d\tilde{\sigma} + \frac{\partial f(\tilde{\sigma},\tilde{X},R)}{\partial \tilde{X}} d\tilde{X} + \frac{\partial f(\tilde{\sigma},\tilde{X},R)}{\partial R} dR = 0 \tag{9}$$

Given that the hardening functions depend on the plastic strain, the respective increments can be expressed according to the chain rule and the consistency condition is transformed as below:

$$df = \frac{\partial f(\tilde{\sigma},\tilde{X},R)}{\partial \tilde{\sigma}} d\tilde{\sigma} + \frac{\partial f(\tilde{\sigma},\tilde{X},R)}{\partial \tilde{X}} \cdot \frac{\partial \tilde{X}}{\partial \tilde{\varepsilon}} \cdot d\tilde{\varepsilon} + \frac{\partial f(\tilde{\sigma},\tilde{X},R)}{\partial R} \cdot \frac{\partial R}{\partial \varepsilon_{Eq}} \cdot d\varepsilon_{Eq} = \frac{\partial f(\tilde{\sigma},\tilde{X},R)}{\partial \tilde{\sigma}} d\tilde{\sigma} + \frac{\partial f(\tilde{\sigma},\tilde{X},R)}{\partial \tilde{\varepsilon}} \cdot d\tilde{\varepsilon} + \frac{\partial f(\tilde{\sigma},\tilde{X},R)}{\partial \varepsilon_{Eq}} \cdot d\varepsilon_{Eq} = 0 \tag{10}$$

Then, the stress increment can be obtained as a function of the strain increment and the material yield function:

$$d\tilde{\sigma} = -\frac{\frac{\partial f(\tilde{\sigma},\tilde{X},R)}{\partial \tilde{\varepsilon}} \cdot d\tilde{\varepsilon} + \frac{\partial f(\tilde{\sigma},\tilde{X},R)}{\partial \varepsilon_{Eq}} \cdot d\varepsilon_{Eq}}{\frac{\partial f(\tilde{\sigma},\tilde{X},R)}{\partial \tilde{\sigma}}} \tag{11}$$

The elastoplastic material may react to the appied stresses with an additive combination of plastic and elastic strains; given that the **Hooke elasticity law** applies to the elastic strains alone and recalling eq.(1), the following relationship applies:

$$d\tilde{\sigma} = [C] \cdot d\tilde{\varepsilon}^{EL} = [C] \cdot (d\tilde{\varepsilon}^{TOT} - d\tilde{\varepsilon}) \tag{12}$$

Where $C$ is the elasticity tensor of the material, based on Young modulus and the Poisson coefficient. If in the Hooke law (12) we substitute thestress increment from the Consistency condition (11) and the plastic strain increment from the Normality rule (7) we get:

$$-\frac{\frac{\partial f(\tilde{\sigma},\tilde{X},R)}{\partial \tilde{\varepsilon}} \cdot d\tilde{\varepsilon} + \frac{\partial f(\tilde{\sigma},\tilde{X},R)}{\partial \varepsilon_{Eq}} \cdot d\varepsilon_{Eq}}{\frac{\partial f(\tilde{\sigma},\tilde{X},R)}{\partial \tilde{\sigma}}} = C \cdot (d\tilde{\varepsilon}^{TOT} - \frac{\partial f(\tilde{\sigma},\tilde{X},R)}{\partial \tilde{\sigma}} d\varepsilon_{Eq}) \tag{13}$$

Which allows to derive the plastic multiplier $d\varepsilon_{Eq}$:

$$d\varepsilon_{Eq} = \frac{\frac{\partial f(\tilde{\sigma},\tilde{X},R)}{\partial \tilde{\sigma}} \cdot C \cdot d\tilde{\varepsilon}^{TOT} + \frac{\partial f(\tilde{\sigma},\tilde{X},R)}{\partial \tilde{\varepsilon}} \cdot d\tilde{\varepsilon}}{\frac{\partial f(\tilde{\sigma},\tilde{X},R)}{\partial \tilde{\sigma}} \cdot C \cdot \frac{\partial f(\tilde{\sigma},\tilde{X},R)}{\partial \tilde{\sigma}} - \frac{\partial f(\tilde{\sigma},\tilde{X},R)}{\partial \varepsilon_{Eq}}} \tag{14}$$

Where the term $\frac{\partial \tilde{X}}{\partial \tilde{\varepsilon}}$ within $\frac{\partial f(\tilde{\sigma},\tilde{X},R)}{\partial \tilde{\varepsilon}} = \frac{\partial f(\tilde{\sigma},\tilde{X},R)}{\partial \tilde{X}} \cdot \frac{\partial \tilde{X}}{\partial \tilde{\varepsilon}}$ expresses the function of Kinematic Hardening and the term $\frac{\partial R}{\partial \varepsilon_{Eq}}$ within $\frac{\partial f(\tilde{\sigma},\tilde{X},R)}{\partial \varepsilon_{Eq}} = \frac{\partial f(\tilde{\sigma},\tilde{X},R)}{\partial R} \cdot \frac{\partial R}{\partial \varepsilon_{Eq}}$ expresses the function of Isotropic Hardening. These two hardening functions represent the "ID card" of a material from the viewpoint of its plastic behavior, as the elasticity modulus and the Poisson coefficient are the ID card for the elastic properties.

If the plastic multiplier from eq. (14), also called "Equivalent Plastic Strain", is substituted within the Normality rule and the resulting expression is inserted within the Hooke law, then the incremental stress-strain relationship typically expressing the elastoplastic behavior is finally obtained:

$$d\tilde{\sigma} = [C] \cdot (d\tilde{\varepsilon}^{TOT} - \frac{\partial f(\tilde{\sigma},\tilde{X},R)}{\partial\tilde{\sigma}} \cdot \frac{\frac{\partial f(\tilde{\sigma},\tilde{X},R)}{\partial\tilde{\sigma}} \cdot C \cdot d\tilde{\varepsilon}^{TOT} + \frac{\partial f(\tilde{\sigma},\tilde{X},R)}{\partial\tilde{X}} \cdot \frac{\partial\widetilde{X(\tilde{\varepsilon})}}{\partial\tilde{\varepsilon}} \cdot d\tilde{\varepsilon}}{\frac{\partial f(\tilde{\sigma},\tilde{X},R)}{\partial\tilde{\sigma}} \cdot C \cdot \frac{\partial f(\tilde{\sigma},\tilde{X},R)}{\partial\tilde{\sigma}} - \frac{\partial f(\tilde{\sigma},\tilde{X},R)}{\partial R} \cdot \frac{\partial R(\varepsilon_{Eq})}{\partial\varepsilon_{Eq}}} \tag{15}$$

which, in case of vanishing Kinematic hardening, becomes the well known form

$$d\tilde{\sigma} = \left[ C \cdot - \frac{C \cdot \frac{\partial f(\tilde{\sigma},R)}{\partial\tilde{\sigma}} \cdot C \cdot \frac{\partial f(\tilde{\sigma},R)}{\partial\tilde{\sigma}}}{\frac{\partial f(\tilde{\sigma},R)}{\partial\tilde{\sigma}} \cdot C \cdot \frac{\partial f(\tilde{\sigma},R)}{\partial\tilde{\sigma}} - \frac{\partial f(\tilde{\sigma},\tilde{X},R)}{\partial R} \cdot \frac{\partial R(\varepsilon_{Eq})}{\partial\varepsilon_{Eq}}} \right] \cdot d\tilde{\varepsilon}^{TOT} = \left[C_{ep}\right] \cdot d\tilde{\varepsilon}^{TOT} \tag{16}$$

The elastoplastic constitutive law takes the incremental form where $\left[C_{ep}\right]$ is the material matrix which defines the nonlinear material properties all over the plastic straining histories of the given material. The elastoplastic stress-strain law can only be integrated by numerical methods (e.g. finite elements), except for few very simple special cases where the relationship can be simply integrated in closed form. It is worth noting that, frequently, structural metals are capable of undergoing large strains before failure, with consequent large displacements: this introduces geometrical nonlinearities in addition to the material nonlinearities originated by the elastoplasticity and already discussed above.
For better understanding the concept of geometrical nonlinearity, a simple example can be made: let suppose that the cantilever beam below, made of a perfectly elastic material, is loaded so that its tip is subjected to a "small" displacement (e.g. 1/100th of the beam lenght).

*ELASTIC LINEAR BEHAVIOUR:*

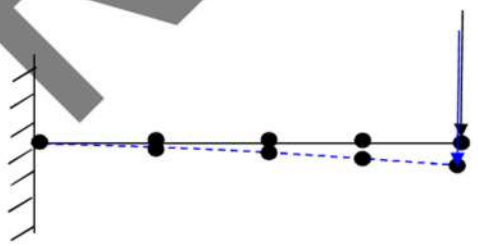

*Figure 2-3: small deflections in a cantilever beam*

Given that the deformed shape is very close to the undeformed one, the stiffness matrix is "almost" (in an engineering sense) the same of the undeformed beam.

$$\{u\} = [K]^{-1} \cdot \{F\} \tag{17}$$

With $u$ vector of nodal displacements (unknown), $K$ stiffness matrix (depending on material, shape and constraints of the beam) and $F$ vector of known generalized nodal loads.

After eq. (13) is solved the structure displacements are found by common matrix method (e.g. the method discussed in the course of *Costruzione di Macchine II*), the elastic strains and stresses can be retrieved.

$$\{\varepsilon\}=[B]\cdot\{u\}$$

(18)

With $B$ matrix dependent on the structure geometry (again, refer to the matrix method from *Costruzione di Macchine II*).

Finally the stresses are derived:

$$\{\sigma\}=[C]\cdot\{\varepsilon\} \qquad (19)$$

Where $C$ is the elasticity matrix of the material and eq.(19) states the generalized Hooke law.

*ELASTIC RESPONSE WITH GEOMETRICAL NONLINEARITIES:*

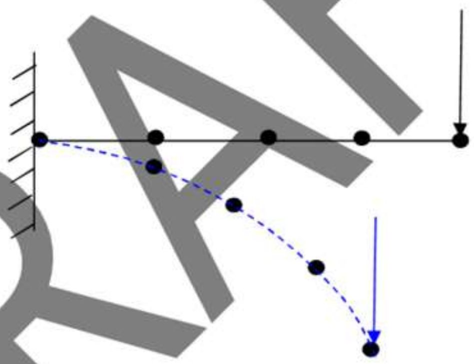

*Figure 2-4: Large displacements in a cantilever beam*

If the displacements are "large" (e.g. beyond 1/10 of the beam length), then the geometry of the deformed body differs too much from that of the initially undeformed body (e.g. the applied force becomes closer to the constraint as the beam deflects).

In such cases the stiffness matrix of the final deformed body cannot be assumed to be concident to that of the undeformed body, and the overall large deformation must be splitted in many steps o rncrements, each consisting of a smal deformation set, at the end of which a new stiffness matrix must be calculated. If the increments are sufficiently small, then the linearity assump\tion within each step is acceptable from an engineering viewopint (small approximations are allowed) and eqs. (17)-(19) are applied for each increment, using the tiffness matrix $[K_i]$ according to the deformed structure from the previous step. The elasticity matrix $[C]$ remains identical all over the analysis provided that the yield stress is not reached. Depending on the accuracy required an iterative procedure can be also implemented for further improving the approximation by deriving the stiffness matrix referred to the deformed shape at the end of the current step instead of that of the previous one.

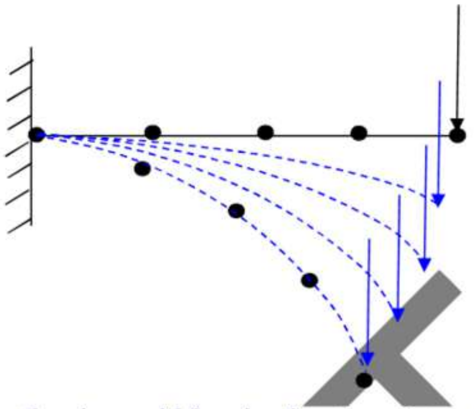

*Figure 2-5: Large displacements in a cantilever beam and deformed configurations at intermediate steps of a nonlinear analysis*

*ELASTOPLASTIC RESPONSE: MATERIAL NONLINEARITY + GEOMETRICAL NONLINEARITY*
- EXPLICIT INTEGRATION

Some materials exhibit nonlinear material response, (e.g. rubbers, …. ), where the parameters of the matrix are not constant $\tilde{\sigma} = [C_{nl}(\varepsilon)] \cdot \tilde{\varepsilon}$.

No real changes of solution strategy are necessary in this case and the same approach of the previous case can be used.

*ELASTOPLASTIC RESPONSE: MATERIAL NONLINEARITY + GEOMETRICAL NONLINEARITY*
- IMPLICIT INTEGRATION

Elastoplasticity usually is accompanied by large displacements so both causes of nonlinearity are coupled together.

At each analysis step the material matrix to be calculated $\left[C_{ep}\right]$ is not known a priori because, according to the highly nonlinear eq. (16), it depends on the material state at the end of the current increment (e.g. plastic loading, elastic unloading etc. etc.) . So also the matrices $[K]$ and $[B]$ will depend on the unknown state of the material at the end of the increment: such kind of problem requires the so-called Implicit Integration.

Iterative procedures are the used according to the follow scheme: for each load increment "$i$", an initial tentative prediction is made about the overall stiffness matrix at the end of the current increment based on that of the previous finished one; then, the tentative incremental displacements, strains and stresses (elastic predictor) are calculated with the usual criteria (eqs. 17-19 based on iteration zero $\left[{C_{ep-0}}^{i}\right]$ );

the stress increments are then used for calculating the current stress-point in the stress space while the strain increments are used for calculating the updated yield surface according to the hardening function of the material, better discussed ahead: if the stress points lies over the updated yield surface (within an admissible tolerance error) then the increment is complete and the next is initiated, otherwise a further iteration is made for the same increment by adjusting the stress increments (e.g. radial return), leading to a new estimate of $\left[\boldsymbol{C}_{ep-1}{}^{i}\right]$, a new set of strains and a new yield surface and a new check whether the stress state lies on the yield surface: such iterative adjustments are repeated until the check is satisfied and the increment is completed. Then a new incremental set of displacements and forces is applied and the iteration cycle starts again, until the last increment is made. If the convergence chek is not satisfied after a certain number of iterations the incremental loading step is reduced until a certain limit. If convergence is not obtained the analysis is stopped also without completing the application of the planned load and integration parameters must be refined for allowing finer increments an more iterations. A possible flow chart for the implicit integration algorythm is the followin one:

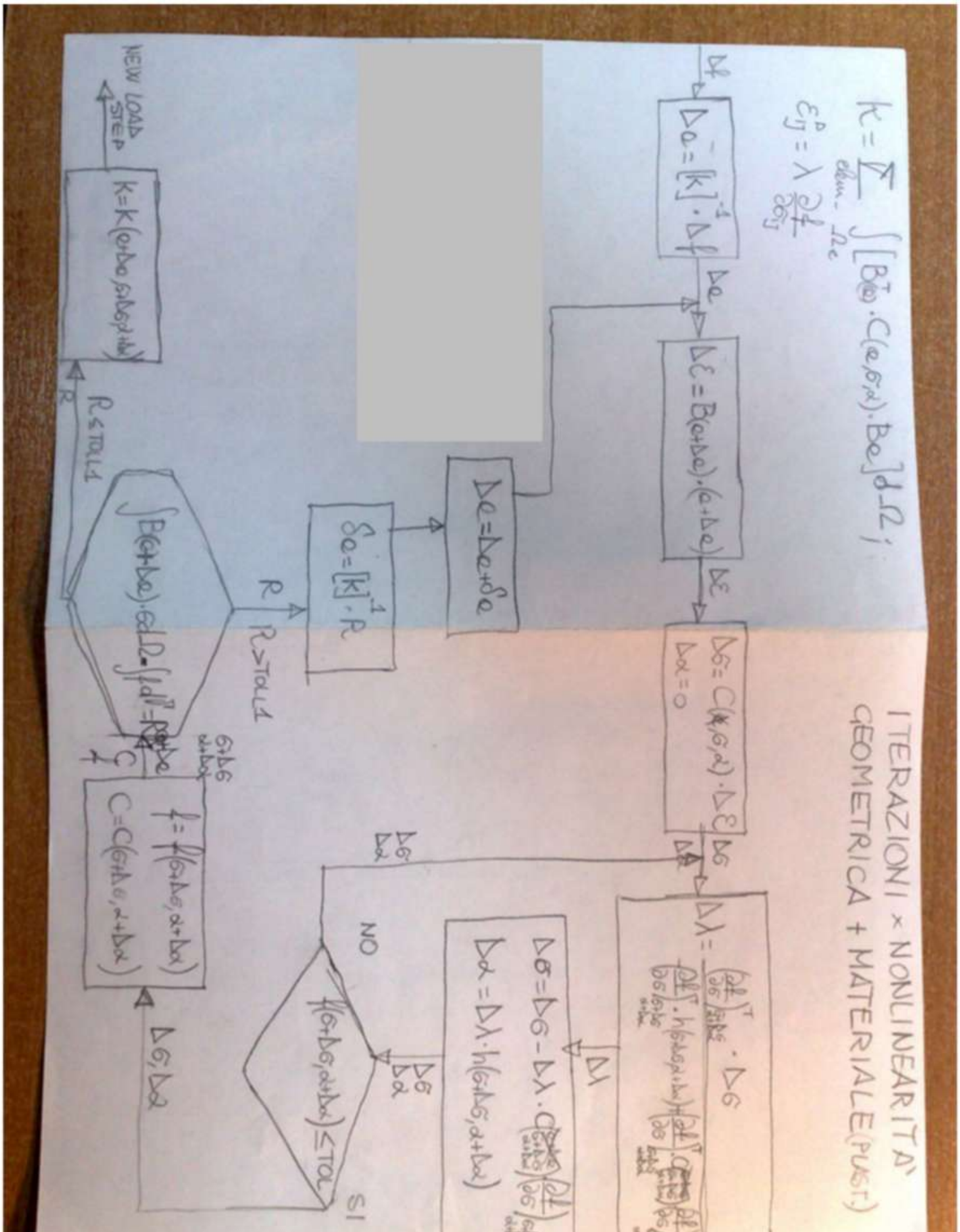

*Figure 2-6: Iterazioni FEM nonlineare implicito*

## 2.2 VON MISES YIELD FUNCTION

A "yelding function" describes a yield surface in the principal stresses space, which separates the elastic stress states from the elastoplastic ones.

For isotropic materials the yield occurrence depends on the value of the principal stresses but is independent of their sequence, e.g. all permutations of the same triplet of principal stresses is equivalent from the viewpoint of the yield.

In other words, the yield is independent of the reference system where the stress tensori s expressed, so the yield only depends on the three stress invariants.

The invariant of the stress tensor (I1, I2 ed I3) and of the stress deviatoric tensor ($J_1$, $J_2$ e $J_3$) are respectively expressed as follows:

$$\begin{aligned}
&I_1 = \sigma_1 + \sigma_2 + \sigma_3 \\
&J_1 = s_1 + s_2 + s_3 = 0 \\
&I_2 = (\sigma_1\sigma_2 + \sigma_1\sigma_3 + \sigma_2\sigma_3) \\
&J_2 = (s_1 s_2 + s_1 s_3 + s_2 s_3) = \sqrt{\frac{1}{6}\left[(\sigma_1-\sigma_2)^2 + (\sigma_1-\sigma_3)^2 + (\sigma_3-\sigma_2)^2\right]} \\
&I_3 = \sigma_1 \cdot \sigma_2 \cdot \sigma_3 \\
&J_3 = s_1 \cdot s_2 \cdot s_3
\end{aligned} \tag{1}$$

The point representing a general stress state can be identified by its cartesian coordinates $\sigma_1$, $\sigma_2$ e $\sigma_3$, (principal stresses) or by three cylindrical coordinates (Haigh-Westergaard coordinates) referred to the trisector of the positive octant (versor $\{1,1,1\}$) in the stress space as in :

$$\xi = \frac{I_1}{\sqrt{3}}; \quad \rho = \sqrt{2J_2}; \quad \theta = \frac{1}{3} Arcos\left(\frac{27}{2} \cdot \frac{J_3}{{\sigma_{Eq}}^3}\right) \tag{2}$$

Where $\xi$ is the axial coordinate along the above trisector, $\rho$ is the radial one and $\theta$ is the angular anomaly also called Lode Angle.

Due to the isotropy, the value of the Lode angle is insensitive to the permutations of the three principal stresses and spans between -30 and 30 degs.

For most metals, the hydrostatic stress (and the first stress invariant) is known to not affect the yield, then $\xi$ cannot affect the yield function and, in other words, the yield surface in the space of principal stresses $\{\sigma_1, \sigma_2, \sigma_3\}$, is a prism with a constant cross section along the stress space trisector axis.

Therefore the stress deviator, intrinsically devoid of any hydrostatic component, is sufficient to decsribe the elastoplastic response.

Furthermore, the above considerations imply that the intersection of the yield surface with the deviatoric plane $\sigma_1+\sigma_2+\sigma_3=0$, is representative of the entire yield surface.

The most known yield surface suitable for ductile materials is the von Mises crteria; according to this criteria, only the second deviatoric invariant and the corresponding radial coordinate $\rho$ affect the yield, which instead is insensitive to the Lode angle $\theta$ and to the third deviatoric invariant. Then, the cross section of the yield surface is circular and the overall surface is schematically drawn in Figure below.

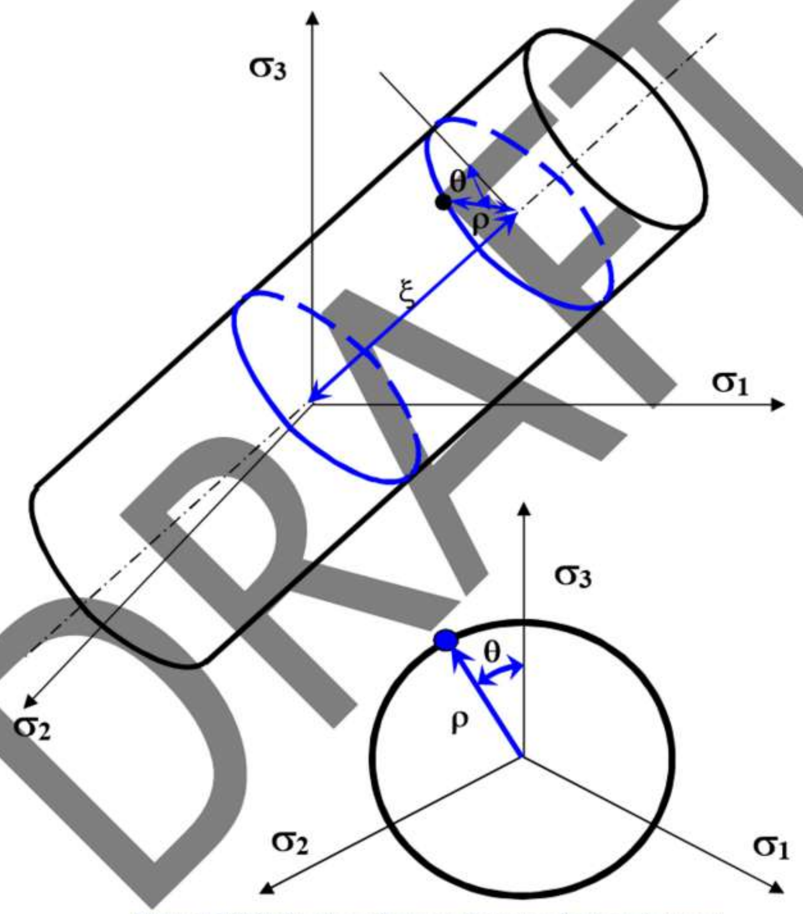

*Figure 2-7 Cylindrical coordinates in the space of principal stresses*

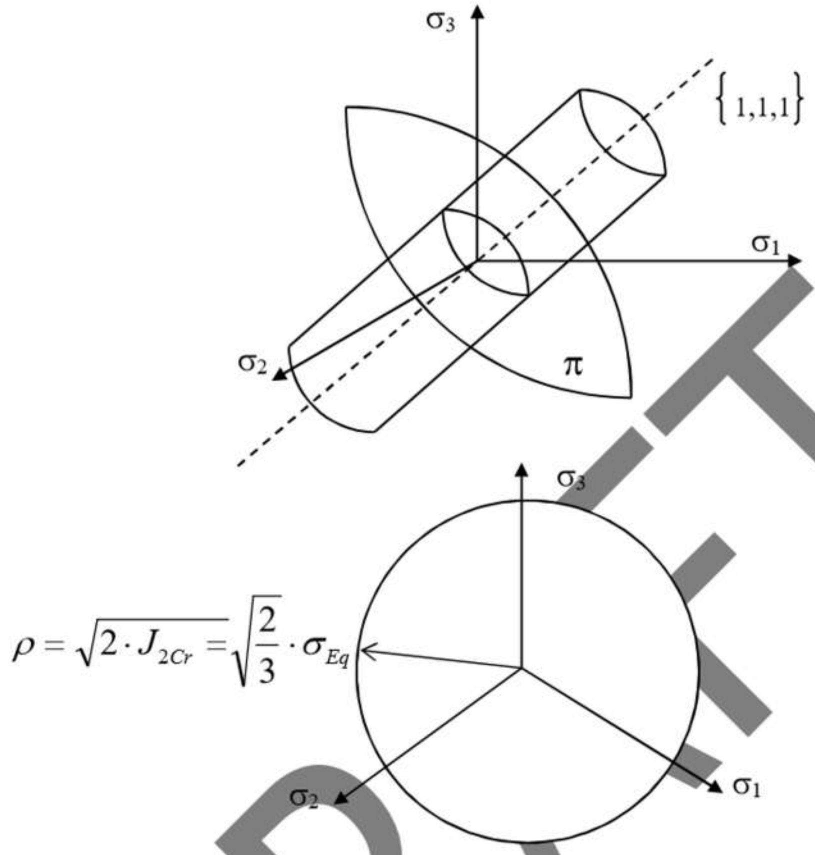

*Figure 2-8: von Mises hardening surface*

Given the cylindrical symmetry of the Mises yield surface, a common representation is that on the plane parallel to the cyilinder corss section (and perpendicular to the trisector axis) and passing through the origin, such plane being called Π and being identified by the equations $\xi = \frac{I_1}{\sqrt{3}} = 0$ or $\sigma_1+\sigma_2+\sigma_3=0$. According to the Von Mises criteria, the yield and the plastic flow take place as $J_2$ takes a critical value $J_{2CR}$, independendly of J3 and the Lode angle: then the cross section of the von Mises criteria is circular. The yield occurs when the point representing the current stress state lies onto the cylindrical yield surface with axis {1,1,1} and radius $\rho_{CR} = \sqrt{2J_{2Cr}}$.

The inner points to the yield surface, with $\rho < \rho_{CR}$ and $J_2 < J_{2CR}$, correspond to elastic stress states. The yield under uniaxial stress state occurs as the only applied stress equals theyield stress and the principal stresses are then $(\sigma_{yiel}, 0, 0)$; then the general combination of $(\sigma_1, \sigma_2, \sigma_3)$ for a triaxial stress state at the yield limit can be identified by imposing that their $J_2$ invariants have the same value:

$$J_2(\sigma_{yiel},0,0)=\sqrt{\frac{1}{6}\left[(\sigma_{yiel})^2+(\sigma_{yiel})^2\right]}=\sqrt{\frac{1}{3}}\sigma_{yiel}=J_2(\sigma_1,\sigma_2,\sigma_3)=\sqrt{\frac{1}{6}\left[(\sigma_1-\sigma_2)^2+(\sigma_2-\sigma_3)^2+(\sigma_1-\sigma_3)^2\right]} \tag{3}$$

This delivers the equivalent von Mises which is scalar value obtained from all principal stresses which can be directly compared to the yield stress for checking whether or not the stress state is elastic or plastic.

$$\sigma_{Eq}=\sqrt{\frac{1}{2}\left[(\sigma_1-\sigma_2)^2+(\sigma_2-\sigma_3)^2+(\sigma_1-\sigma_3)^2\right]}=\sigma_{yiel} \tag{4}$$

The envelope of all points ($\sigma_1$, $\sigma_2$, $\sigma_3$) of the stress space satisfying the above equation is the cylindrical Mises yield surface discussed before.

The yield function based on the Mises equivalent stress is

$$f(\boldsymbol{\sigma})=\sigma_{eq}-\sigma_{Yiel}=\frac{1}{2}\left[(\sigma_1-\sigma_2)^2+(\sigma_2-\sigma_3)^2+(\sigma_1-\sigma_3)^2\right]-\sigma_{Yiel}=0 \tag{5}$$

The following examples of application of the Mises formula help in visualizing the shape of the Mises surface itself.

Stress state A: $\sigma_A=\{100,0,0\}\Rightarrow$

$\Rightarrow \sigma_{eq\_A}=100;$

Stress state B: $\sigma_B=\sigma_A+\sigma_{HYDR}(50)=\{100,0,0\}+\{50,50,50\}=\{150,50,50\}\Rightarrow$

$\Rightarrow \sigma_{eq\_B}=\sqrt{\frac{1}{2}\left[100^2+100^2+0^2\right]}=100;$

Stress state C: $\sigma_C=\sigma_A+\sigma_{DEV}=\{100,0,0\}+\{-100,100,0\}=\{0,100,0\}\Rightarrow$

$\Rightarrow \sigma_{EQ\_C}=100;$

These three stress states can be represented by the following points in the stress space:

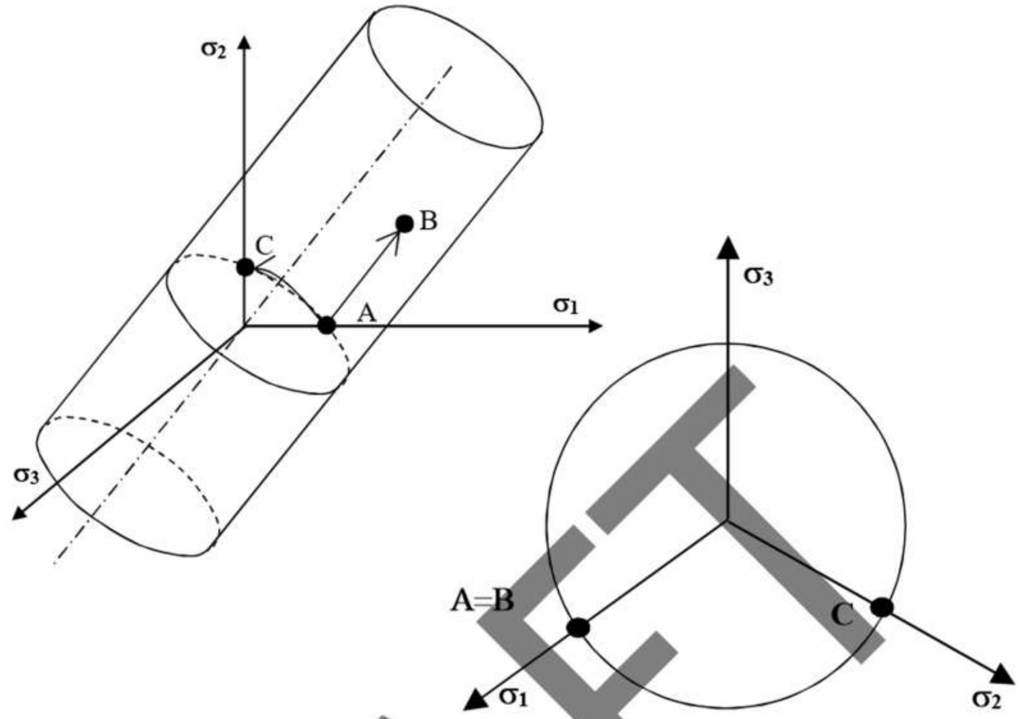

*Figure 2-9: invariancy of Mises yield crfiteria from Lade angle and ressure*

Points A and B only differ for a triaxial stress state then are aligned along the same generatrix, while point C lies on the same deviatoric plane of point A, identified by the equation $\xi = 100/\sqrt{3}$ (corresponding to a hydrostatic stress of 100/3=33.3).

The equal values of $\sigma_{Eq}$ for stress states A and B demonstrates that the hydrostatic stress has noeffect on the yield and that the Mises cross section is constant

The equal values of $\sigma_{Eq}$ for stress states A and C demonstrates that the Muses yield surface has a circular cross section, independent of the lode angle.

Special stress states are those calle "biaxial" or "plane", where one of the principal stress states is zero: if we assume $\sigma_3$=0 the possible combinations of $\sigma_1$, $\sigma_1$ determining the yield condition correspond to the intersection of the Mises cylinder with the plane $\sigma_3$=0 as in figure below:

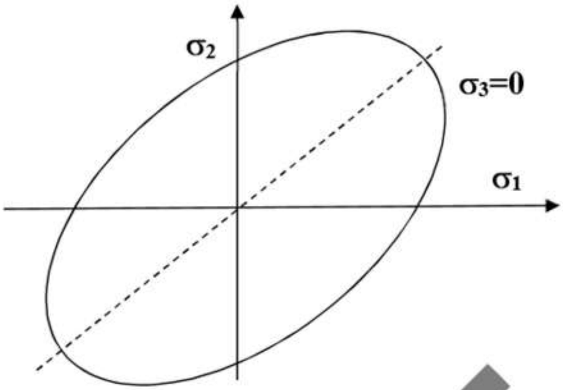

*Figure 2-10: intersection of Mises yield surface wth plane$\sigma 3=0$.*

## 2.3 HARDENING MODELS AND PRINCIPLES OF EXPERIMENTAL ASSESSMENT

Equation (5) deos not allow to properly describe the yield function of real elastoplastic materials, because the first yield stress $\sigma_{Yiel}$ is a material constant and this means that the yield surface represented in eq. (5) is unchangable. This is equivalent to suppose that after the applied stress reaches the first yield, the plastic strains flow without the need of any further increase of the yield stress, which is typical of the ideally-plastic materials like chewingum, clay, toothpaste and and play-doh for children. Real structural materials instead, like ductile metals, exhibit a very different "steady" stress-strain response where stress increments are always necessary for generating further plastic strains, as in the qualitative picture below:

FIGURA CON 2 CURVE PLASTICHE: UNA IDEALE COSTANTE + UNA REALE CRESCENTE

Recalling that the stress-point $\{\sigma_1,\sigma_2,\sigma_3\}$ during plastic straining must always lie onto the surface, the above stress increase required for plastic straining means that the yield surface itself must exhibit size-shape changes evolving with plastic straining, for ensuring the above contact between stress state and yield surface.

For visualizing the process of elastoplastic loading for a general material point within a loaded body, the evolving Mises surface together with the trajectory of the current stress-state point $\{\sigma_1,\sigma_2,\sigma_3\}$ can be seen from the upper plane-view or in the intersection/projection with the $\Pi$ plane:

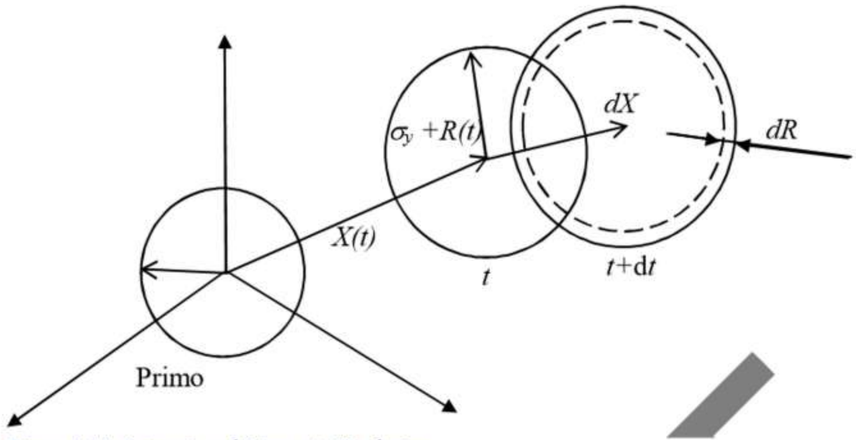

*Figure 2-11: Isotropic and Kinematic Hardening*

The starting unloaded state {0,0,0} corresponds to the origin, then an initially elastic loading may occur along any general combination of principal stresses (any trajectory on the Π plane), until the point $\{\sigma_1,\sigma_2,\sigma_3\}$ reaches the boundary of the initial yield surface eg. the material reaches its first yield: so far, no permanent plastic deformation has yet occurred.

*PLASTIC LOADING:*

If a further stress increase takes place attempting to move the point $\{\sigma_1,\sigma_2,\sigma_3\}$ outside the yield surface, then the yield surface undergoes a combination of motions (vector displacement **X** in the principal stress space) and enlargements (scalar radius increase $R$ ), so that at the end of that increment the new stress state is still adhering to the current updated yield surface.

During this infinitesimal (incremental) transformation the material is hardened (meaning that the yield surface is changed and the current yield stress is increased from its initial value $\sigma_{\text{Yiel}}$ ), while plastic strain increments occurred (meaning that the material point subjected to the told stress-strain history is permamently deformed).

*ELASTIC UNLOADING:*

If instead the stress increment starting at the border of the yield surface is aimed at going back inside the surface, then the yield surface does not undergo any change, the material does not harden and only elastic strains occur, with no plastic straining.

The modifications of the yield surface are promoted by the plastic straining or, more properly, by the energy associated at the local scale to the plastic work or the distortional work.

The two possible types of transformations of the yield surface are called Isotropic hardening, scalar, (size change in the form of radius increase), and Kinematic hardening, tensorial, (motion within the stress space).

Each material exhibits a different combination of the two types of hardening, and for the same material, each hardening term is function of the strain, the strain rate and the temperature.

In the simplified case that quastistatic tests at room temperature occur, each hardening term only depends on the current strain, meaning that the same given stress increment can be associated to different incremental plastic strains. In other words, the hardening depend on the entire loading (straining) history from the beginning of the plastic flow (first time the initial yield stress has been reached) until the current stress state.

This important property of the stress - plastic strain relationship is called "history-dependence" or also "path-dependence" and will be bettwer stressed out ahed by way of practical examples.

It is worth noting that the constancy of the cross section of the yield surface implies that stress increments parallel to the trisector axis do not generate any plastic straining nor any hardening / yield surface update.

If the realistic yield surface is modelled within the yield function together with its possible hardening transofrmations, then eq. (5) changes in eq.(6)

$$f(\boldsymbol{\sigma}, R, \mathbf{X}) = (\boldsymbol{\sigma} - \mathbf{X})_{eq} - R - \sigma_Y \tag{6}$$

In eq. (6) the von Mises equivalence operator is applied to the difference between the current stress tensor and the kinematic stress tensor, also colled "backstress" tensor.

The two hardening functions constitute the "identity card" of the material from the viewpoint of its plasticity response, similarly to how the Young modulus and the Poisson coefficient play the same role for the elasticity response: e.g. the difference between steel and aluminium in terms of elastic behavior is quantified by different values of $E$ and $\nu$ while their difference in terms of elastipalstic response is represented by different $X$ ed $R$.

The remarkable difference is that $E$ and $\nu$ are material constants while $X$ ed $R$ are material functions, not so easy to be measured-identified as the elastic ones are.

Also, both the hardening functions are related to the plastic strains but their real variables are not directly the components of the plastic strain tensor, while they just are derived from such components.

The Kinematic hardening depends on the "backstrain" $\alpha$, which is usually taken to be coincident to the entire plastic strain tensor $\tilde{\alpha} = \tilde{\varepsilon}$ so that $\tilde{X} = \tilde{X}(\tilde{\varepsilon})$, instead the Isotropic hardneing, $R(\varepsilon_{Eq})$, depends on the so-called "equivalent plastic strain" defined below:

$$d\varepsilon_{Eq} = \sqrt{\frac{2}{9}[(d\varepsilon_1 - d\varepsilon_2)^2 + (d\varepsilon_1 - d\varepsilon_3)^2 + (d\varepsilon_3 - d\varepsilon_2)^2]} \tag{7}$$

It is defined so that $\sigma_{\mathrm{Eq}}$ integrated all over $\varepsilon_{\mathrm{Eq}}$ delivers the same amount of distortional work of the integration of the entire stress-plastic strain tensors all over the same straining history.

Another common expression of (7) is based on the fact that plastic strains always deliver shape changes at local scale but leave unaltered the volume: this means that $\varepsilon_1 + \varepsilon_2 + \varepsilon_3 = 0$ and such condition inserted into eq. (7) delivers the so-called "deviatoric" expression of the equivalent plastic strain, fully equivalent to the previous:

$$d\varepsilon_{Eq} = \sqrt{\frac{2}{3}\left[d\varepsilon_1{}^2 + d\varepsilon_2{}^2 + d\varepsilon_3{}^2\right]} \tag{8}$$

The associative rule connecting the hardening functionals and their dual strain-related function through the yield function are similar to that relating the plastic strain to the tress:

$$\begin{aligned} d\varepsilon_{ij} &= \frac{\delta f}{\partial \sigma_{ij}} d\varepsilon_{Eq} \\ d\varepsilon_{Eq} &= -\frac{\partial f}{\partial R} d\varepsilon_{Eq} \\ d\varepsilon_{ij} &= -\frac{\delta f}{\delta X_{ij}} d\varepsilon_{Eq} \end{aligned} \quad \text{corresponding to} \quad \begin{aligned} \frac{\delta f}{\partial \sigma_{ij}} &= -\frac{\delta f}{\delta X_{ij}} \\ -\frac{\partial f}{\partial R} &= 1 \end{aligned} \tag{9}$$

Given the form of the yield function in eq. (6) , the increment of plastic strain is:

$$\begin{aligned} d\varepsilon_i &= \frac{\partial f}{\partial \sigma_i} d\varepsilon_{Eq} = \frac{\partial\left(3/2\left[\left(\sigma_i - X_i\right)'^2 + \left(\sigma_j - X_j\right)'^2 \left(\sigma_k - X_k\right)'^2\right]\right)^{1/2}}{\partial \sigma_i} d\varepsilon_{Eq} = \\ &= \frac{1}{2}\cdot\left(\ \right)^{-1/2}\cdot 2\cdot\frac{3}{2}\cdot\left(\sigma_i - X_i\right) d\varepsilon_{Eq}{}' = \frac{3}{2}\cdot\frac{\left(\sigma_i - X_i\right)'}{\left(\sigma_{ij} - X_{ij}\right)_{eq}} d\varepsilon_{Eq} \end{aligned} \tag{10}$$

Where the hardening functions *R* and *X*, respectively scalar and tensorial stresses, respectively depend on $\varepsilon_{Eq}$ and $\varepsilon_{ij}$, respectively scalar and tensor as well.

In general, the material characterization from the elastoplastic viewpoint consists of determining the hardening function of that given material, other than the first-yield stress wchich is the threshold between the elastic and elastoplastic responses.

Given that the yield function is $f = (\boldsymbol{\sigma} - \mathbf{X})_{eq} - R - \sigma_Y = 0$ , for determining the combination of both hardenings functions it is sufficient to measure the evolution of the equivalent stress and the equivalent plastic strain during monotonic loading tests where $\{\sigma_1, \sigma_2, \sigma_3\}$, $\sigma_{Eq}$, $\{\varepsilon_1, \varepsilon_2, \varepsilon_3\}$ and $\varepsilon_{Eq}$ progressively increase up to failure.

The smartest option for accomplishing the above task is that of loading “special” prismatic components, with simple uniform cross section, by “special” loads capable of generating a uniaxial stress state $\{\sigma_1, 0, 0\}$: such components are the smooth specimens (either with round or rectangular cross section) and the special loading mode is the simple tensile or compressive force, gradually increasing from zero until specimen failure.

The tensile test of round-section specimens is the ideal option, but also compressive tests on short cylinders and tensile tests on flat specimens with rectaingular cross section, eventually very thin if obtained from sheet metal, are common practice in material mechanics.

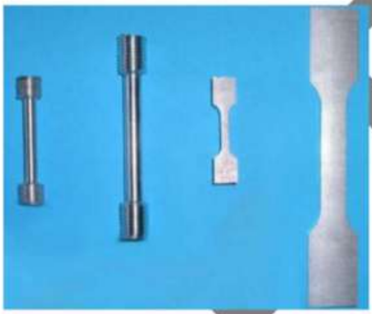

*Figure 2-12: Smooth Tensile specimen shapes (https://it.m.wikipedia.org/wiki/File:Tensile_specimen-round_and_flat.jpg)*

In general, the truss-like bodies are only subjected to an uniaxial stress state $\{\sigma_1, 0, 0\}$, uniform all oever the volume, with $\sigma_1$=load/area progressively increasing together with the load imposed by the testing machine: given the stress uniaxiality, the Mises formuyla yields $\sigma_{Eq} = \sigma_1$=Load/Area.

Also, the volume conservation of plastic strains $\varepsilon_1 + \varepsilon_2 + \varepsilon_3 = 0$ together with the geometrical / loading symmetry yields that the principal plastic strain components are in the form $(\varepsilon_1, -\varepsilon_1/2, -\varepsilon_1/2)$, so that the equivaent plastic strain becomes $\varepsilon_{Eq} = \varepsilon_1$ : then, by just measuring the axial stress and the axial strain at different instants during a tensile experiment, we get the equivalent stress-strain relationship.

If the material at hand has not any Kinematic hardening ( $X = 0$ ) and only exhibits isotropic hardening, then aseries of alternately tensile/compressive test would deliver the following picture 6:

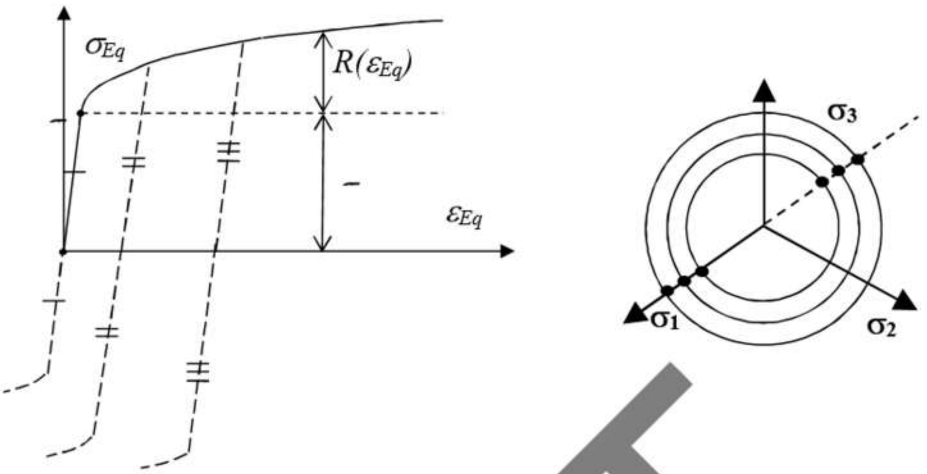

*Figure 2-13: Loading/unloading at dfferent test stages: Isotropic hardening curve and yield surfaces*

Given the symmetry of the isotropic hardening, each hardening level delivers the same yield stress in tension and compression. In this case, the functionof Isotropic hardening can be easily obtained as follows from a single monotonic test up to failure:

$$R(\varepsilon_{Eq}) = \sigma_{eq}(\varepsilon_{Eq}) - \sigma_Y = \sigma_1(\varepsilon_1) - \sigma_Y$$

Here the midpoint of each elastic segment remains over the horizontal axis while the amplitude of the elastic segment increases as the isotropic hardening occurs.

Although the hardening is correctly identified by the function *R* alone, in common practice the complete set of $\sigma_Y + R = \sigma_{Eq}$ is considered as the Isotropic hardneing curve, shortly named as the "material elastoplastic curve" or the "flow curve".

If instead the isotropic hardneing is negligible *R=0* and only yhe kinematic hardening occurs, then the loading/unloading of the material delivers the following curves in figure 7:

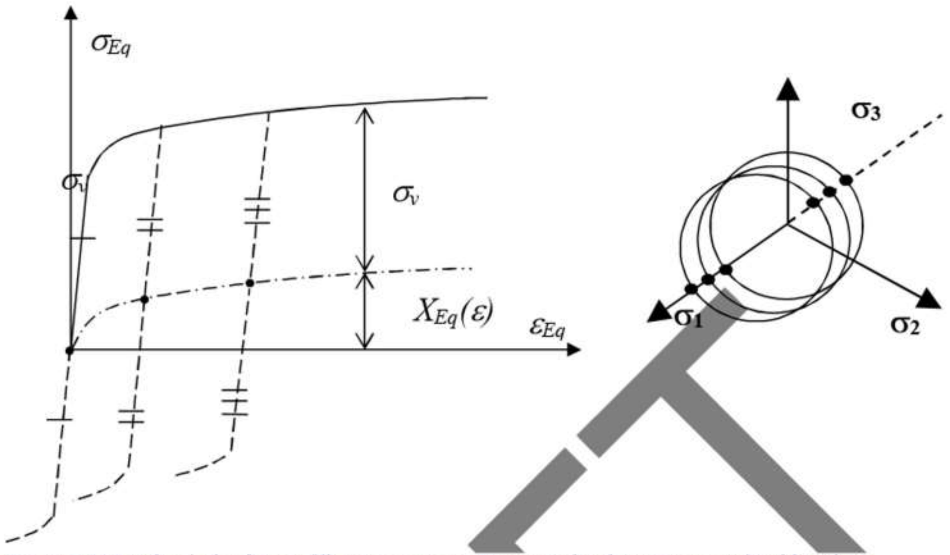

*Figure 2-14 Loading/unloading at dfferent test stages: Kinematic hardening curve and yield surfaces*

Here the midpoint of each elastic segment moves vertically as the isotropic hardening occurs, instead the amplitude of the elastic segment remains constant.

In this case, the kinematic hardneing function is identified by the average value of each loading/unloading yield stresses.

For each loading/unloading cycle a point of the kinematic hardening curve is obtained.

Finally, when the material exhibits both Isotropic and Kinematic hardening, successive loading/unloading cycles would deliver elastic segments with both increasing length and increasing average value.

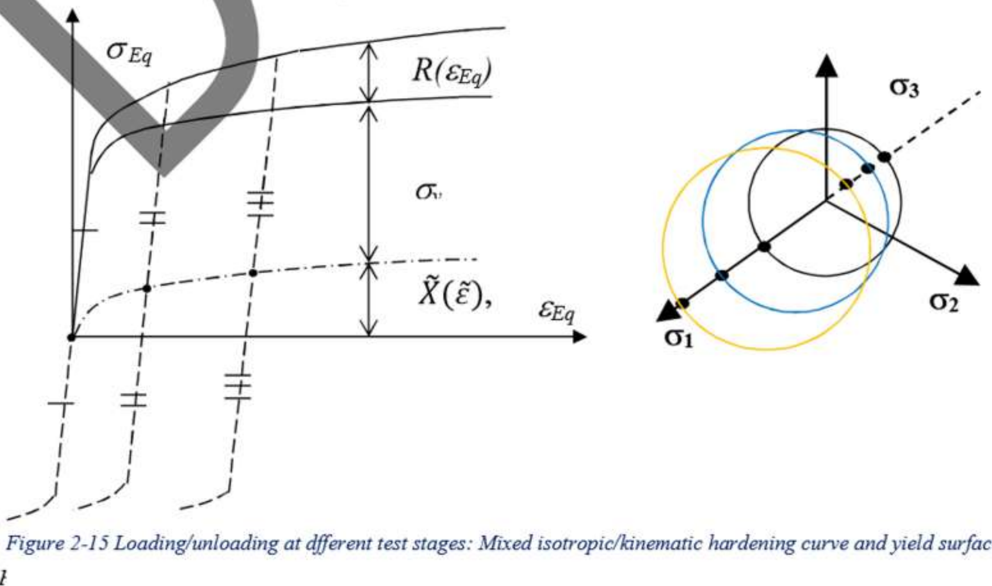

*Figure 2-15 Loading/unloading at dfferent test stages: Mixed isotropic/kinematic hardening curve and yield surfaces*

In this case, the increasing amplitude of elsatic cycles delivers the isotropic hardening $R$ and the incresaing height of the midopint of each elastic segment delivers the kinematic hardening $\tilde{X}$. Each elastic tension/compression cycle delievers a value of the scalar function $R(\varepsilon_{Eq})$ and a value of the tensorial function $\tilde{X}(\tilde{\varepsilon})$, .

Experiments always deliver discrete values of the hardening functions coupled to the corresponding relevant variables; then, arbitrary selection of the preferred kind of best-fit function can be made for approximating the experimental data.

While no special functions are commonly preferred in the literature for approximating $\tilde{X}(\tilde{\varepsilon})$, various known functions are available for approximating $R(\varepsilon_{Eq})$ :

Hollomon Law (Power Law):
$$\sigma_{Eq} = K \cdot {\varepsilon_{Eq}}^{N} \tag{10}$$

Ludwig Law:
$$\sigma_{Eq} = \sigma_0 + K \cdot {\varepsilon_{Eq}}^{N} \tag{11}$$

It is important to understand that eqs. above are just mathematical approximations which usually are found to nicely approximate the usual experimental data, while they not include any physics principle nor are derived from any exact formula. For the experimental results of some materials, none of the above formula works fine and a “simple” n-th order polynomial works better than them.

## 2.4 IRREVERSIBILITY & PATH-DEPENDENCE OF PLASTIC STRAINING

The incremental relationship between stress tensor and plastic strain tensor represents a dissipative (non-conservative) model and, then, the current strain state does NOT depend on the current stress state while it depends on the entire stress history ranging from the beginning of the plastic straining until the current state.

The following example can be of help in better experiencing this aspect.

**EXAMPLE:**

Let’s consider a rectangular sheet metal on the plane (x,y), thin enough that the two only non-zero principal stresses lie in the sheet plane and the third principal stress, normal to the plane, is zero because of the small thickness. Let's say that the material has a first-yield stress $\sigma_Y = 65\ MPa$, no kinematic hardneing and isotropic hardening according to the Ludwik law with the following parameters:

$$\sigma_{Eq} = 65 + 200 \cdot {\varepsilon_{Eq}}^{0.3} \tag{12}$$

This metal sheet must undergo two different stresses, each to be gradually applied from zero up to 120 MPa along the X direction and from zero up to 150 along the Y direction.

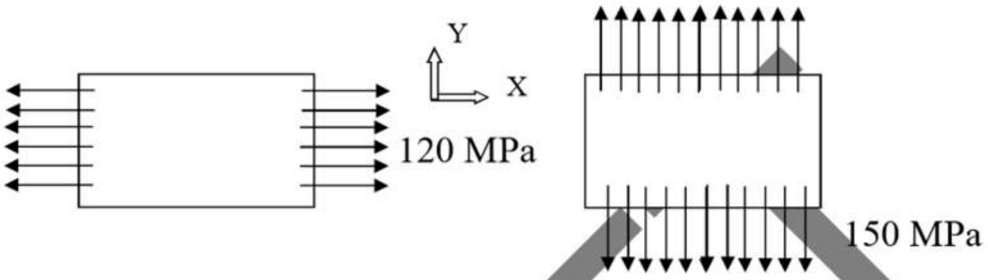

Figure 2-16 Sheet metal subjected to membrane normal loads in two directions

Two possible sequences are possible:

- case 1), the load along X followed by that along Y (path O-A-C in Figure),
- case 2) the load along the Y direction followed by that along X (path O-B-C in figure).

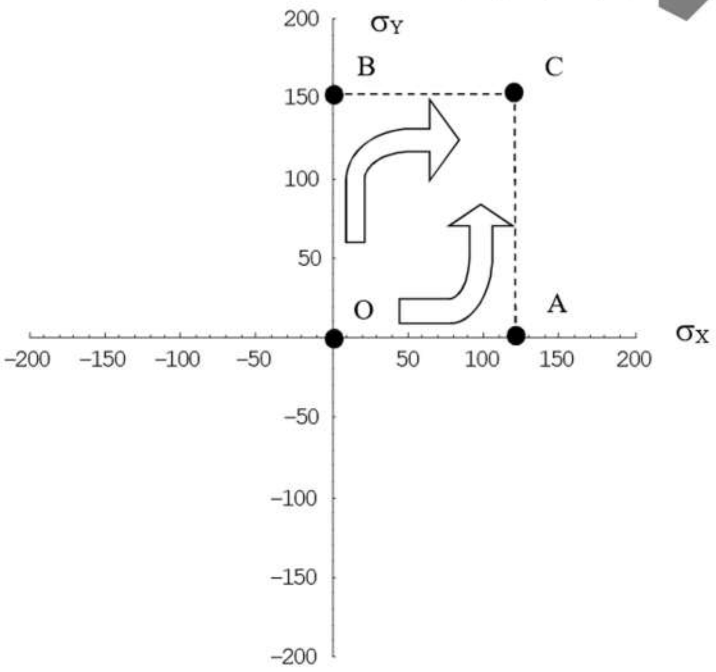

Figure 2-17 Two different possible stress paths from state O to state C

In both cases the final stress state is $\tilde{\sigma} = \{150{,}150{,}0)\}$ but the respective final strain states will be remarkably different to each other.

For simplifying the example all stress-strain increments will be treated as if they were infinitesimal also if they are not, assumed that as an acceptable approximation.

1) PATH O-A-C:

SEGMENT O-A

$\sigma_x$ initially increases within the elastic range and the point representing the stress state, $\tilde{\sigma} = \{\sigma_x, 0{,}0\}$ moves along the X axis until it crosses the border of the first-yield surface at 65 MPa.

Then $\sigma_x$ further increases and plastic strains develop, until point A in the stress space and 120 MPa are reached. After the path O-A is completed the flow stress is euqal to:

$$\sigma_{EqO-A} = \sqrt{\frac{1}{2} \cdot \left((120)^2 + (120)^2\right)} = 120\,MPa \tag{13}$$

Then, the stress increment from $\{65{,}0{,}0\}$ to $\{120{,}0{,}0\}$ generates plastic strains which, in the current approximate approach, are treated as if they were infinitesimal also if they are not.

Then, according to the material hardening function of eq. 12, the total equivalent plastic strain after O-A is

$$\varepsilon_{EqO-A} = \left(\frac{120-65}{200}\right)^{(1/0.3)} = 0.0135 \tag{14}$$

The stress surface is updated as in Figure below (red = initialy yield, red = current yield after O-A) and the path is elastic until first yield at 65 MPa (dashed line), elastoplastic in the successive part from 65 to 120 MPa (solid line arrow).

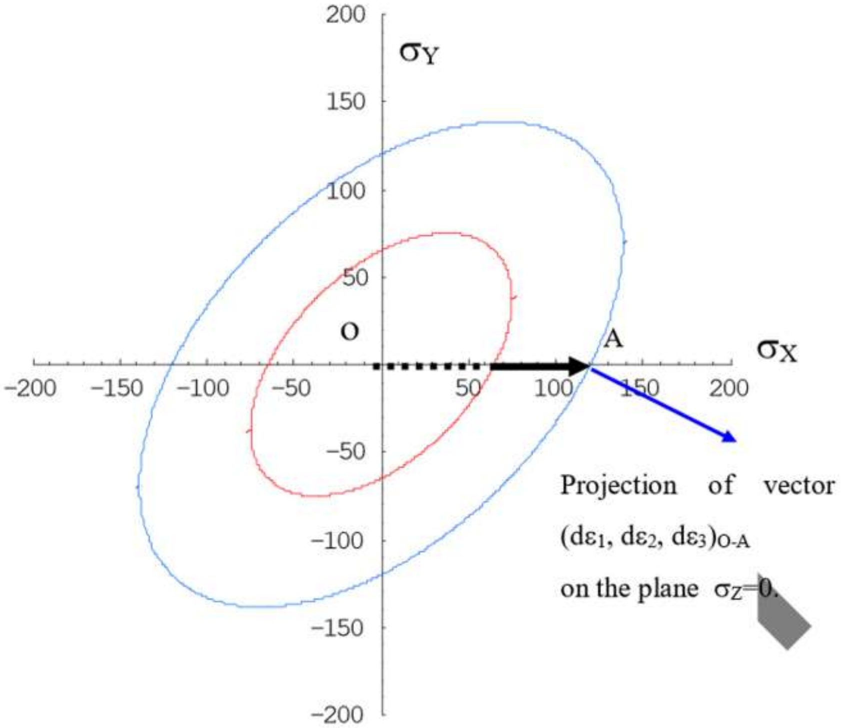

Projection of vector $(d\varepsilon_1, d\varepsilon_2, d\varepsilon_3)_{O\text{-}A}$ on the plane $\sigma_Z=0$.

*Figure 2-18 Yield surface after stress path O-A*

The plastic strain vector will then be normal to the current yield surface at point A; the ellipses and the blue arrow in Figure are respectively the intersection of the yield surfaces with the plane of equation $\sigma_Z=0$, and the projection of the plastic strain vector $(\varepsilon_1, \varepsilon_2, \varepsilon_3)$ on the same plane.

The semiaxes of the ellipses are inclied at 45 degrees, the normal to the ellipse at point A is inclined at 30 degrees with respect to the x axis (versor in the XY plane is $\left\{1, -\frac{1}{2}, 0\right\}$ ) and the normal to the overall cylindrical surface at point A has versor $\left\{1, -\frac{1}{2}, -\frac{1}{2}\right\}$. Then the normality rule stating that the strain incrementi is normal to the yield surface implies that:

$$\rightarrow \left(d\varepsilon_X, d\varepsilon_Y, d\varepsilon_Z\right) = \left(d\varepsilon_X, -\frac{d\varepsilon_X}{2}, -\frac{d\varepsilon_X}{2}\right) \qquad (15)$$

Which is the typical plastic strain state occurring in case of uniaxial stress.

The definition (8) of the Equivalent plastic strain delivers in this case:

$$\left|d\tilde{\varepsilon}\right| \cdot \sqrt{\frac{2}{3}} = d\varepsilon_{Eq} \Rightarrow \sqrt{d\varepsilon_X^{\ 2} + \frac{d\varepsilon_X^{\ 2}}{4} + \frac{d\varepsilon_X^{\ 2}}{4}} \cdot \sqrt{\frac{2}{3}} = d\varepsilon_{Eq} \Rightarrow$$
$$\Rightarrow d\varepsilon_X = d\varepsilon_{Eq} = 0.0135 \tag{16}$$

The plastic strain increment of the transformation O-A is applied to the unstrained material, then the total strain at the state A is coincident with the incremental strain O-A. Recalling eq. (15) gives:

$$\{\varepsilon_x, \varepsilon_y, \varepsilon_z\} = \{0,0,0\} + \{d\varepsilon_{x_{O-A}}, d\varepsilon_{y_{O-A}}, d\varepsilon_{z_{O-A}}\} = \{0.0135, -0.00675, -0.00675\} \tag{17}$$

and

$$\varepsilon_{Eq\ O-A} = d\varepsilon_{Eq\ O-A} = 0.0135$$

SEGMENT A-C

Now the normal stress σy = 150 MPa is progressively applied over the sheet metal while the load along the X axis is maintained, so performing the transformation A-C in the following Figure;

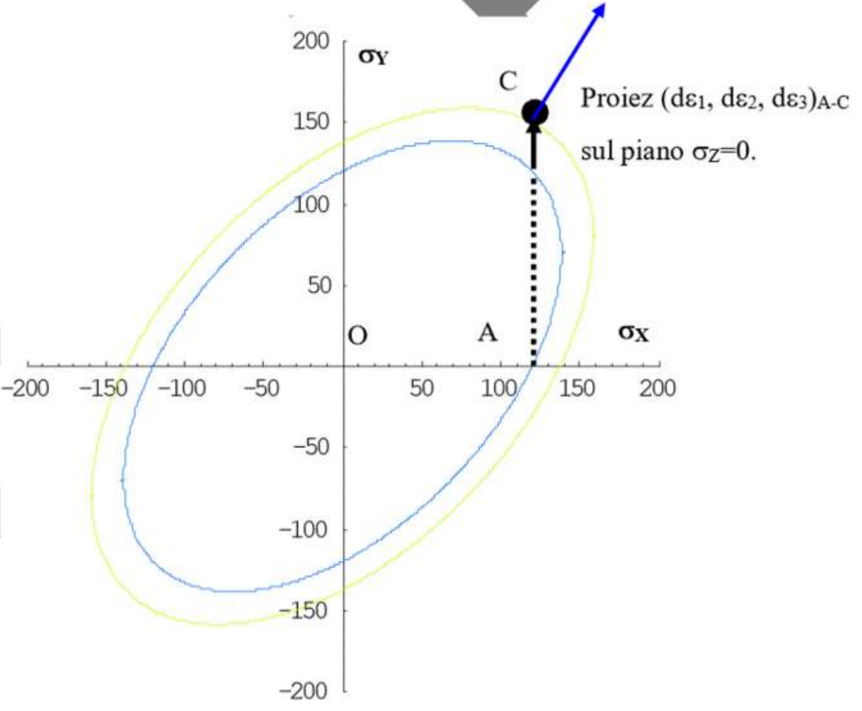

*Figure 2-19 Yield surface after stress path O-A-C*

The final value of the equivalent stress after the path O-A-C becomes :

$$\sigma_{EqO-A-C} = \sqrt{\frac{1}{2} \cdot \left((120-150)^2 + (120)^2 + (150)^2\right)} \approx 137.5 MPa \tag{18}$$

While σy is progressively applied, σEq initially decreases from its value of 120 MPa at the state A, while the yield surface remains unchanged together with the current yield stress of 120 MPa. Therefore the initial part of the transformation A-C is an "elastic unloading", represented by the dashed portion of the segment A-C.

At midpoint of the dashed portion of A-C the stress □Eq starts increasing again and, as σy becomes 120 MPa, the σEq has restored the value of 120 MPa. From now on, further increase of σy generates plastic strain increments, increases the yield stress and expands the yield surface until the final state C. The increase of yield stress up to 137.5 MPa implies the following equivalent plastic strain as the state C is reached:

$$\varepsilon_{EqO-A-C} = \left(\frac{137.5-65}{200}\right)^{(1/0.3)} = 0.034 \tag{19}$$

and the following increment of equivalent plastic strain in the transformation A-C:

$$d\varepsilon_{Eq\ A-C} = 0.034 - 0.0135 = 0.0205 \tag{20}$$

The modulus of the incremental plastic strain vector of the transformation A-C can be related to the increment of equivalent plastic strain in the same transformation :

$$\left|d\tilde{\varepsilon}_{A\text{-}C}\right| = \sqrt{3/2}\cdot d\varepsilon_{Eq-A-C} = \sqrt{3/2}\cdot(0.034-0.0135) = 0.0251 \tag{21}$$

The versor of the incremental platic strain can be found as the normal to the yield surface at point C; this would require the calculation of partial derivatives of the yield surface at the current point, which are conceptually very simple but would be not immediate by pen and paper; then are not carried out here.

The blue vector in Figure 2-19 Yield surface after stress path O-A-C represents the projection of the total incremental strain vector on the plane $\varepsilon_3=0.$, then the only considerations based on Figure 2-19 are that $d\varepsilon_{A-C_x}$ and $d\varepsilon_{A-C_y}$ are both positive while $d\varepsilon_{A-C_z}$ enters the plane of the drawing and is negative. The volume conservation at local scale implies that the sum of three principal plastic strains vanishes, then $\left|d\varepsilon_{A-C_z}\right| = d\varepsilon_{A-C_x} + d\varepsilon_{A-C_y}$.

Assumed that the versor of $d\bar{\bar{\varepsilon}}_{A-C}$ is found, the knowledge of its modulus allows to easily determine each of its components $\left\{d\varepsilon_{A-C_x}, d\varepsilon_{A-C_y}, d\varepsilon_{A-C_z}\right\}$.

The total plastic strain after the stress path O-A-C is the vectorial sum of $\bar{\bar{\varepsilon}}_{O-A-C} = d\bar{\bar{\varepsilon}}_{O-A} + d\bar{\bar{\varepsilon}}_{A-C}$

$$\left\{0.0135 + d\varepsilon_{A-C_x}, -0.00675 + \mathrm{d}\varepsilon_{A-C_y}, -0.00675 + d\varepsilon_{A-C_z}\right\}. \tag{22}$$

## 2) PATH O-B-C:

### SEGMENT O-B

The progressive application of $\sigma_Y$ = 150 MPa to the unloaded sheet delivers plastic strains as the stress sxceeds 65 MPa, according to the following formulae:

$$\begin{aligned} \sigma_{EqO-B} &= \sqrt{\frac{1}{2}\cdot\left((150)^2+(150)^2\right)} = 150\,MPa \\ \varepsilon_{EqO-B} &= \left(\frac{150-65}{200}\right)^{(1/0.3)} = 0.058 \end{aligned} \qquad (23)$$

The new current yield stress is obviously become 150 MPa and the yield surface is modified as in Figure 2-20

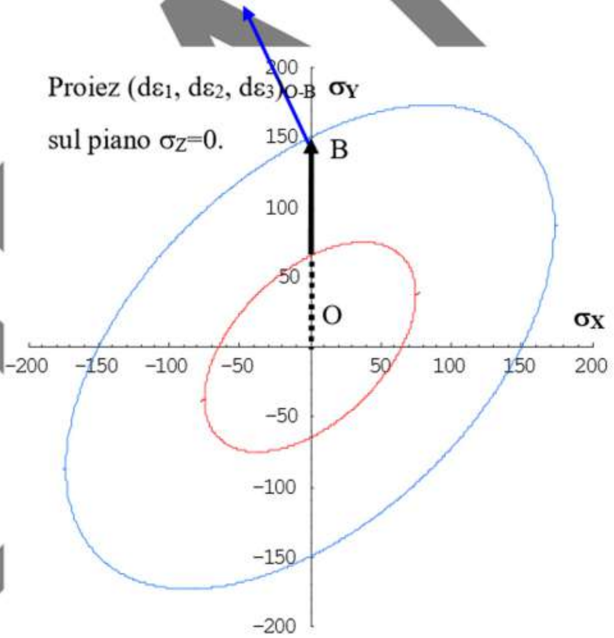

*Figure 2-20 Yield surface after stress apth O-B*

The incremental plastic strain vector is parallel to the normal to the yield surface at point (0,150,0), so its components are proportional to the direction (1, -1/2, -1/2); The modulus of the incremental plastic strain vector depends on the increment of equivalen t plastic strain according to the known formula below:

$$\left|d\tilde{\varepsilon}\right|_{O-B} = \sqrt{\frac{3}{2}}\, d\varepsilon_{Eq_{A-C}} = 0.071 \tag{24}$$

The normal to the yield surface at point B is proportional to the vector (1, -1/2, -1/2) and, recalling eq. (24), the plastc strain increment generated in the path O-B is a vector like

$$d\tilde{\varepsilon}_{O-B} = \left(-\frac{d\varepsilon_{Eq-O-B}}{2}, d\varepsilon_{Eq-O-B}, -\frac{d\varepsilon_{Eq-O-B}}{2}\right) = (-0.029,\ 0.058,\ -0.029) \tag{25}$$

SEGMENT B-C

As the stress σx = 120 MPa is progressively applied (transformation B-C) the equivalent stress decreases until reaching the value of eq. (26) as the state B is reached:

$$\sigma_{EqO-B-C} = \sqrt{\frac{1}{2}\cdot\left((120-150)^2 + (120)^2 + (150)^2\right)} \approx 137.5MPa \tag{26}$$

Obviously the yield stress cannot decrease so that the segment B-C corresponds to a fully elastic unloading represented by the dashed line in Figure 2-21 and the yield surface remains unaffected by the transformation B-C.

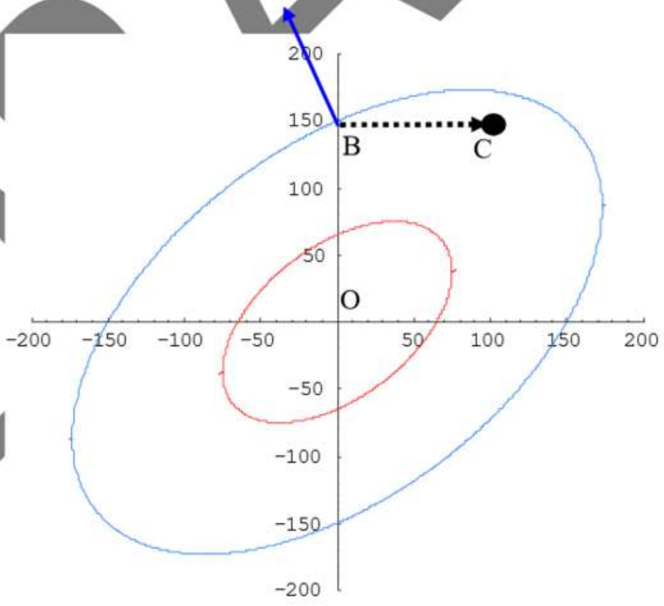

Figure 2-21 Yield sruface after stress path O-A-C

Then, the only plastic strain of the path O-B-C is generated during O-B:

$$d\tilde{\varepsilon}_{O-B} = (-0.029,\ 0.058,\ -0.029) \tag{27}$$

and also the yield stress at the end of the stress path O-B-C remains 150 MPa as it was after O-B.

The nit is clear that the stress paths O-A-C and O-B-C deliver different plasticity histories depite the final stress state is the same.

| | Path O-A-C | Path O-B-C |
|---|---|---|
| Yield stress | 137.5 MPa | 150 MPa |
| Equivalent plastic strain | 0.034 | 0.058 |
| Plastic strain along x | $0.0135 + d\varepsilon_{A-C_x}$<br>$(0.0135 < \varepsilon_{x_{O-A-C}} < 0.034)$ | -0.029 |
| Plastic strain along y | $-0.00675 + d\varepsilon_{A-C_y}$<br>$(-0.00675 < \varepsilon_{y_{O-A-C}} < 0.02725)$ | 0.058 |
| Plastic strain along z | $-0.00675 + d\varepsilon_{A-C_z}$<br>$(-0.00675 < \varepsilon_{z_{O-A-C}} < 0.02725)$ | -0.029 |

So also the shapes of two identical square sheet metals with edge length = 1, at the end of the two stress paths would be rather different:

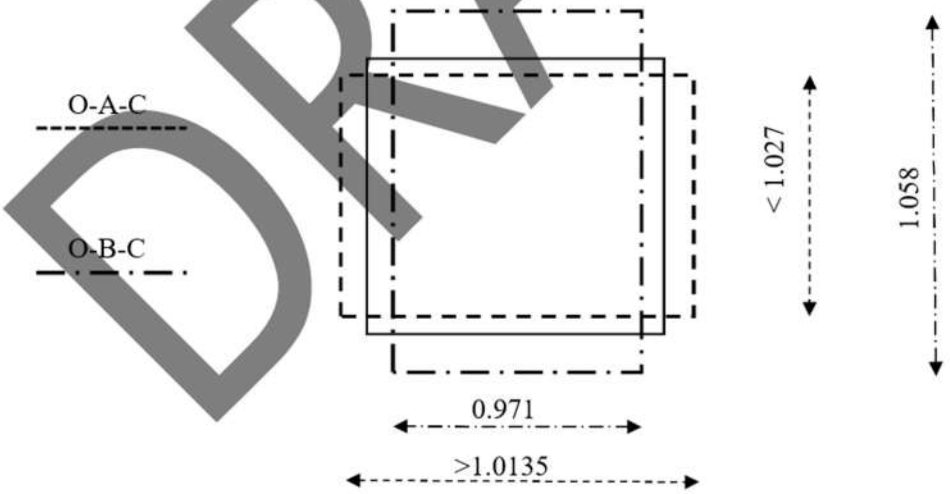

Above is demonstrated that reaching the same general stress state from two different paths in the stress space can deliver different deformation hitories and leaves the material in different plasticity conditions; this can also be visualized as trajectories on the plane $\sigma_{Eq} - \varepsilon_{Eq}$:

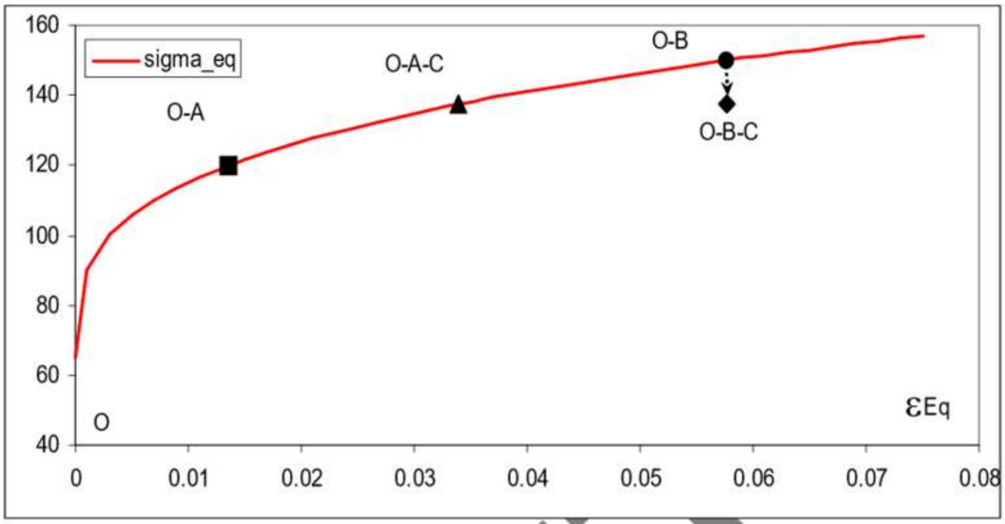

*Figure 2-22 Stress paths represented along the hardening curve (Isotropic) of the material*

The path O-A-C consists of a monotonic plastic loading until state C leading to a final state $\sigma_{Eq} = \sigma_{Yield} = 137.5\ MPa$ and $\varepsilon_{Eq} = 0.034$.

Instead the path O-B-C delivers plastic loading until state B with $\sigma_{Eq} = \sigma_{Yield} = 150\ MPa$ and $\varepsilon_{Eq} = 0.058$, then an elastic unloading occurs so that the current $\sigma_{Eq} = 150\ MPa$, but the plastic variables are not affected by elastic unloading so remain unaltered to the values achieved at the state B : $\sigma_{Yield} = 150\ MPa$ and $\varepsilon_{Eq} = 0.058$.

# 3 STRESS-STRAIN CHARACTERIZATION (STATIC)

## 3.1 PRELIMINARY CONSIDERATIONS

**Why to characterize structural metals and design structures in the plastic range**

The elastoplastic characterization is crucial for the mechanical design of structures and components aimed at high-tech applications, requiring the most advanced design techniques.

Typical structural applications heavily involving advanced techniques of mechanical design are those where the structures are required to perform both under "normal" operating conditions within the elastic range and under "special" load conditions within the effective failure and/or permanent plastic deformations limits appropriately identified.

An example very close to everyday life is that of automotive monocoques and substructures: they are required to remain elastic under the normal operating loads from from tire-terrain interaction, but are also required to perform adequately in case of crash and impact, by asdsorbing plenty of impact energy through extensive plastic deformation always preserving the safety of driver and passengers, meaning that no failure and specially limited deformations must occur.

Similar examples are possible in all fields of structural design like airspace vehicles (normal flight loads and accidental loads from emergency landings, envelope limits or engine failure), building engineering (normal static loads and special earthquake loads), nuclear and generally industrial plants (standard pressures and maximum rate overpressures in emergency conditions), etc.

As will be extensively discussed in the next chapters, also the failure condition of real structural materials is completely different from the basic assumption of a "failure stress", constant for each material, wich in the past was assumed as the only and general material failure limit.

Still today the so-called "failure stress" is listed in many official documents as a material propery, but its real meaning cannot be interpreted anymore as a general limit as it was typically done in the past.

In principle, for the same given set of standard and limit loads a structure might be overdimnsioned in an attempt to increase its safety, but the material research and modern design techniques clarified that various phenomena occur in a deformation/damaging structural process, so that an oversized structure may fail much sooner than a lighter well-designed one.

The ideal mantra for a perfect mechanical design is to manage the material response well enough to design a structure using the minimum amount of material and making it reach its very limit condition at the same time all over the structure, as the loads reach their emergency values.

The achievement of such targets also means at the same time weight, cost and environmental pollution decrease together with performance, durability and safety increase.

**Specimens shape for stress uniaxiality and uniformity**

The elastoplastic characterization consists of determining how the yield surface evolves as the plastic strain increases.

According to the hypotheses discussed in the previous chapters, the simplified case of elastoplastic characterization regards the material response under monotonically increasing loads, so that the isotropic hardening alone can be considered and the kinematic hardening is neglected, whose determination would require reverse loading signs.

Determining the isotropic hardneing by experiments means determining how the equivalent stress $\sigma_{Eq}$ evolves as a function of the equivalent plastic strain $\varepsilon_{Eq}$, during the monotonic loading up to failure of an arbitrary component/structure/specimen/body made of the material at hand.

For an arbitrary shape of the tested body and an arbitrary choice of loads/constraints, $\sigma_{Eq}$ depends on all three principal stress components (see eq. 4 of chapter 2.2) and, for each instant of a test, such principal stresses can be variable from a material point to another within the volume of the same component/structure/specimen/body.

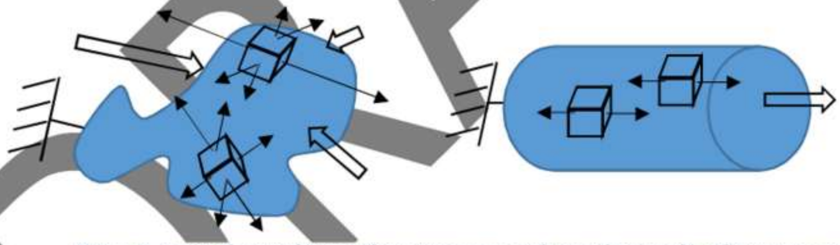

*Figure 3-1general triaxial/nonuniform stress state and special uniaxial/uniform stress state*

Then, for simplifying the calculation of $\sigma_{Eq}$ at each instant of the test, special combinations of component shape and applied loads/contraints should be adopted: the most convenient known choice is a simple prismatic specimen subjected to pure traction, so that, in principle, at each instant of a test the two following conditions apply:

- only the axial stress is present at each material point so that $\sigma_{Eq} = \sigma_Z$ (uniaxiality of the stress state)
- At each given instant of a test, $\sigma_Z$ and $\sigma_{Eq}$ have the same current value at whatever material point within the specimen (uniformity of the stress distributions), so that $\sigma_Z = F/A$ where $F$ is the current load and $A$ the current cross section.

The ideal tensile specimen is then a prism with constant cross section either circular (cylinder) or rectangular (parallelepiped) but, for holding the specimen into testing machines and for applying the tensile load, the so-called shoulders are usually provided as fillets connecting the constant cross section prism to larger cross sections at both ends, with either threaded connections or flat surfaces suitable for respectively screwing or clamping the specimens in the testing machine:

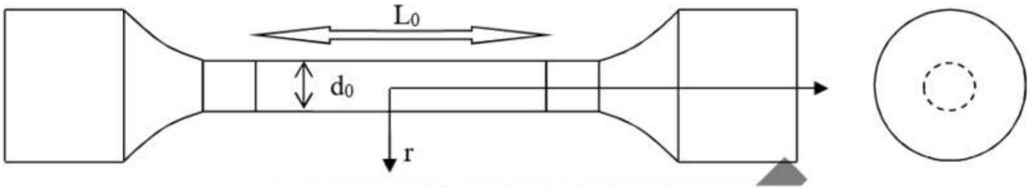

*Figure 3-2 Typical shape of a cylindrical tensile specimen*

The central part of the cylindrical zone is called gauge length of the specimen, it is long $L_0$ and is slightly shorter thant the overall cylindrical lenght. $d_0$ is the initial specimen diameter.

If the material to be characterized cames in the form of sheet metal or thin metal plate, then cylindrical specimens cannot be manufactured and flat specimens must be machined according to Figure 3-3:

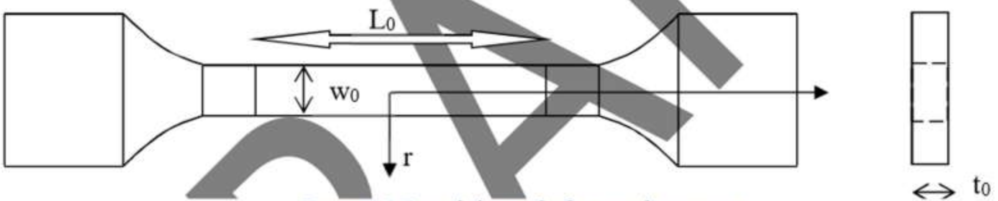

*Figure 3-3 Typical shape of a flat stensile specimen*

where the gage lenght is again $L_0$ but the rectangular cross section is wide $w_0$ and thick $t_0$.

It will be shown later that flat specimens generate a lot more dofficulties than round specimens in the material characterization at high plastic strains; then the machining of round specimens is highly recommended despite it can be slightly more time-consuming, also in case of not-too-thin plates (e.g. plate thickness exceeding 5 mm allows to machine round specimens by way of a reasonably accurate cnc equipment).

In the next sections the discussion will alwyas refer to round specimens, unless explicit reference is be made to flat specimens.

## 3.2 FIRST APPROXIMATION, ENGINEERING STRESS-STRAIN CURVE

The Engineering stress-strain curve is based on the three following assumprtions:

- The displacements and strains are small enough that the current deformed configuration of the specimen can be approximated to the original undeformed one;
- The stress state is uniform wherever whitin the gage length of the specimen;
- The stress state is unixial wherever whithin the gage length of the specimen;

Thanks to the stress uniaxiality $\sigma_{Eq} = \sigma_Z$, thanks to the stress uniformity$\sigma_Z = \frac{F}{A}$ and thanks to the small strain hypothesis $A \approx A_0$, with the last two terms being respectively the current cross section and the initial undeformed cross section. Therefore, the equivalent stress is

$$\sigma_{Eq} = \sigma_Z = \frac{F}{A_0} = \frac{F}{\frac{\pi}{4} \cdot {d_0}^2}\ , named\ \sigma_{Eng} \qquad (3\text{-}1)$$

As seen in eq. (16) of chapter 2.4, in case of uniaxial stress along $z$ the vector of principal plastic strains is of the type $\left\{-\frac{\varepsilon_z}{2}, -\frac{\varepsilon_z}{2}, \varepsilon_z\right\}$, therefore $\varepsilon_{Eq} = \varepsilon_z$; furthermore, the small deformation hypothesis implies that the first derivative of the axial displacement is accurate enough for expressing the strain:

$$\varepsilon_z \approx \frac{\partial w}{\partial z} = \frac{L - L_0}{L_0} \qquad (3\text{-}2)$$

Then, finally, the equivalent plastic strain can be expressed as:

$$\varepsilon_{Eq} = \varepsilon_z = \frac{L - L_0}{L_0}, named\ \varepsilon_{Eng}; \qquad (3\text{-}3)$$

The qualitative shape of an engineering flow curve is reported in Figure 3-4 and includes the known initial elastic segment ending at the yield stress $\sigma_y$, the curved segment from the first yield up to the maximum engineering stress also called Ultimate stress $\sigma_u$ and the final decreasing curved segment beginning at the ultimate stress and ending with the specimen fracture at the failure stress $\sigma_f$.

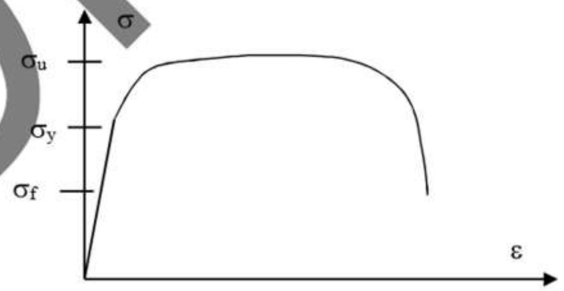

*Figure 3-4 Qualitative shape of an Engineering stress-strain curve*

The accuracy of the engineering curve is very low already at very low plastic strains (within 5%), because the first hypothesis which quits being validi s that of small displacements and infinitesimal strains.

**Second approximation, True stress-True strain curve**

As the hypothesis of small displacements – infinitesimal strains quites being accurate, the current geometrical configuration of the specimen cannot be approximated with the initial-undeformed configuration therefore two consequences occur on both the stress and the strain:

The stress cannot be based anymore on the current resisting cross section, because now $A \neq A_0$, then

$$\sigma_{Eq} = \sigma_Z = \frac{F}{A} = \frac{F}{\frac{\pi}{4} \cdot d^2},\ named\ \sigma_{True} \qquad (3\text{-}4)$$

As far as the stresses and strains are uniform within the specimen, the volume conservation from plastic strains can be applied to the entire constant-section volume of the specimen, then:

$$A_0 \cdot L_0 = A \cdot L \ \rightarrow\ A = A_0 \cdot \frac{L_0}{L} \qquad (3\text{-}5)$$

And substituting ( *3-5* ) in ( *3-4* ) delivers:

$$\sigma_{Eq} = \sigma_Z = \frac{F}{A} = \frac{F}{A_0} \cdot \frac{L}{L_0} = \frac{F}{A_0} \cdot \frac{L_0 + \Delta L}{L_0} = \sigma_{Eng} \cdot (1 + \varepsilon_{Eng}), \text{named } \sigma_{True-L} \qquad (3\text{-}6)$$

The difference between $\sigma_{True-L}$ and $\sigma_{True}$ is that the former is based on specimen length measurements, the latter is based on specimen diameter measurements.

They are nicely identical to each other as far as stresses and strains are uniform within the specimen but, as already mentioned, at necking onset they start to gradually diverge to each other until failure.

Also the axial strain cannot be expressed anymore by the first derivative of the axial displacement, because now $\varepsilon_z \neq \frac{\partial w}{\partial z}$, and a cumulative-incremental formulation must be used for reasonably calculating the total current strain, where the current finite elongation is broken in many small increments of elongation and the deformed configuration of the previous increment is taken as the undeformed configuration of the present increment:

$$\varepsilon_{Eq} = \varepsilon_z = \frac{L_1 - L_0}{L_0} + \frac{L_2 - L_1}{L_1} + \cdots + \frac{L_{i+1} - L_i}{L_i} + \cdots \ldots + \frac{L - L_{n-1}}{L_{n-1}} \qquad (3\text{-}7)$$

In infinitesimal form becomes:

$$\varepsilon_{Eq} = \varepsilon_z = \int_{L_0}^{L} \frac{\partial w}{\partial z} dL = \int_{L_0}^{L} \frac{dL}{L} = Ln\left(\frac{L}{L_0}\right) = Ln(1 + \varepsilon_{Eng}), named\ \varepsilon_{True-L} \qquad (3\text{-}8)$$

The stress-strain curve obtained by formulae ( *3-6* ) and ( *3-8* ) is called “elongation-based true curve” and its qualitative shape is reported in Figure 3-5 together with the engineering curve.

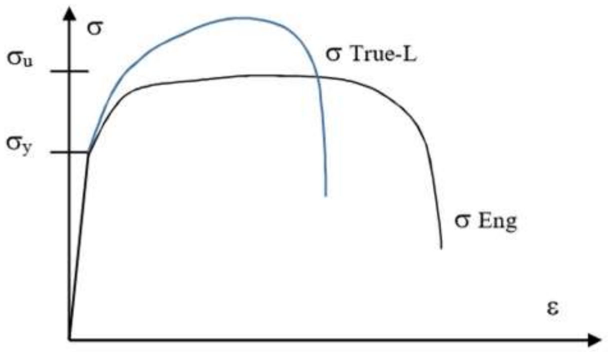

*Figure 3-5 Qualitative shape of Engineering and Elongation-based true cruves*

The elongation-based true curve has greater stresses and smaller strains than the engineering curve, resulting in a slightly shorter and steeper curve than the engineering one. It is fully accurate and representative of the real material response until a special condition occurs, called "necking", which is recognized as the phenomena changing the initially straigh profiles of smooth specimens into pronounced hourglass-shaped profiles.

The necking occurs when, due to microscopical imperfections in the shape or in the material, both stress and strain start concentrating around a single cross section of the gage length which progressively shrinks, while the remaining part of the specimen are not deformed/stressed anymore:

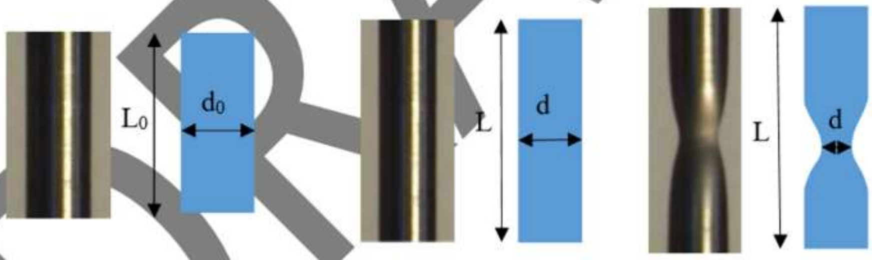

*Figure 3-6 Specimen shape (gage lenght): undeformed, pre-necking, post-necking*

The necking onset corresponds to the maximum of the tensile load during a test, as after such event the load progressivly decreases as the neck sections becomes progressively thinner and thinner, until failure which clearly occurs on the neck section.

Under such circumstances the stress-strain distributions are not uniform anymore and eqs ( *3-4* ) and ( *3-8* ) ( *3-5* ) quit to be valid, so that also the respective elongation-based true stress of eq. ( *3-6* ) and true strain of eq. ( *3-8* ) quit to deliver realistic results.

Then, after necking onset, the material of the neck section is deformed many times more than the material of all other cross sections of a specimen, also according to Figure 3-6 and Figure 3-7: this is why the neck section becomes the only meaningful location where the material can be characterized.

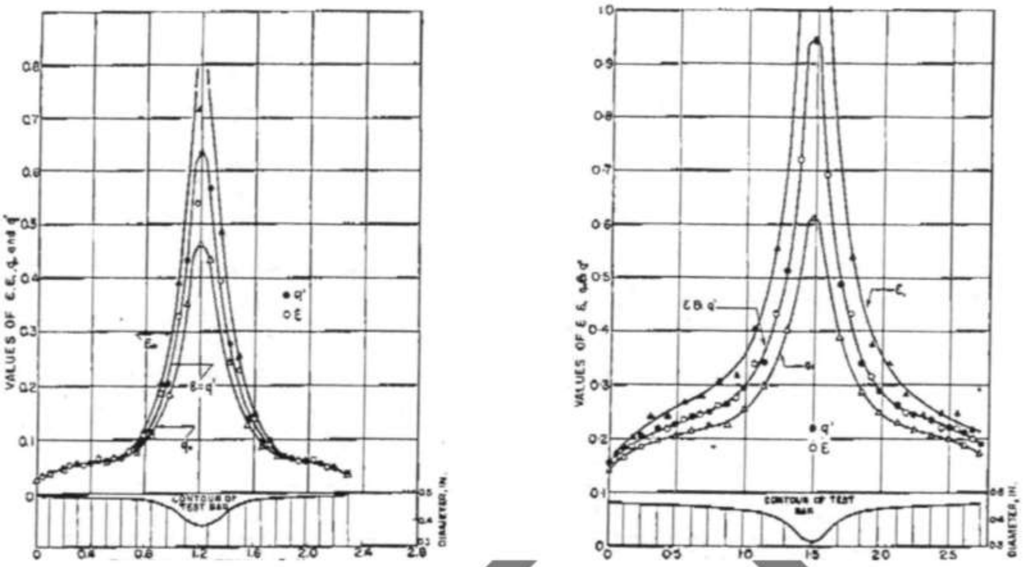

*Figure 3-7 Typical distributions of axial plastic along the axis of necked specimens CITE CREDITS MC …….*

Now eq. ( *3-9* ) based on the diameter *d* must be mandatorily adopted for the true stress, because the elongation-based expression does not capture anymore the minimum area at the neck section nor the corresponding neck-averaged axial stress represented by the ratio load/resisting area.

Also, during the post-necking phase, $\sigma_{Eq}$ progressively differs from $\sigma_{True}$ because the stress uniaxiality does not apply anymore, and the stresses distributions progressively become more and more nonuniform so that $\sigma_{True}$ merely becomes the neck-averages axial stress differing from local values of $\sigma_Z$ and $\sigma_{Eq}$, as will be better discussed in the next sections.

Then for this second-approximation material curve, eq. ( *3-4* ) is used also after necking onset but it is recognized to juset deliver an approximate estimate of $\sigma_{Eq}$:

$$\sigma_{Eq} \approx \sigma_Z \approx \frac{F}{A} = \frac{F}{\frac{\pi}{4}\cdot d^2},\ named\ \sigma_{True} \qquad (3\text{-}9)$$

Instead for the true strain a different consideration must be done, because the volume conservation leading to eqs. ( *3-7* ) and ( *3-8* ) cannot be applied anymore to the overall specimen volume: referring to Figure 3-6, the current *L* and *d* deliver the same original volume as *L₀* and *d₀* only until necking onset; after the necking initiates, the volume of the entire specimen clearly remains constant, but is not related anymore to the current values of *L* and *d* .

Then, after necking onset the volume conservation must be imposed to an ideal slice of material centered around the neck section, thin enough that its shape remains nearly cylindrical also during the necking evolution; its initial undeformed gage length is $dL_0$ instead of $L_0$ and its current deformed length is d$L$ instead of $L$ , as depicted in Figure 3-8 :

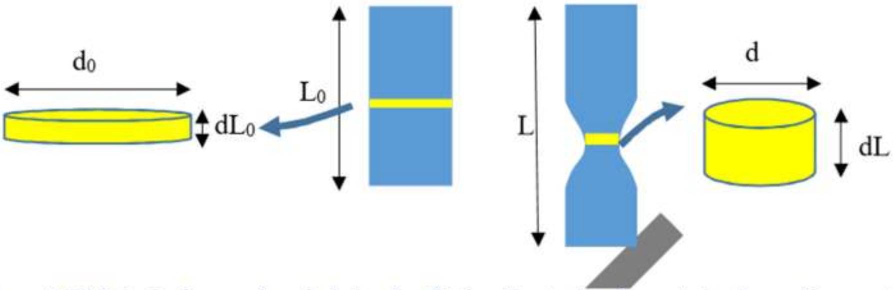

*Figure 3-8 Infinitesimal voume for calculating the effective, diamter-based true strain after necking onset*

Eq. ( *3-8* ) applied to such infinitesimal slice of specimen together with the related volume conservation deliver:

$$\varepsilon_{Eq} = \varepsilon_z = Ln\left(\frac{dL}{dL_0}\right) = Ln\left(\frac{A_0}{A}\right) = 2 \cdot Ln\left(\frac{d_0}{d}\right), \text{ named } \varepsilon_{True} \qquad (3\text{-}10)$$

Then, if diameter measurements can be taken during a tensile test, expressions ( *3-9* ) and ( *3-10* ) deliver the best possible estimate of the "effective", diameter-based true curve up to failure. If instead only elongation measurements are available, then eqs. ( *3-6* ) and ( *3-8* ) deliver the much less accurate "elongation-based" true curve.

Both elongation-based and section-based true curves are fully exact until necking onset and just experimental measurements approximations can spoil their accuracy during such stage;

After necking onset, the elongation-based true cruve quickly becomes useless as both stress and strain are unrealistic; instead the diameter-based true curve maintains a very good accuracy in the strain (which remains accurately representative of the necking-averaged equivalent strain) and just exhibits a moderately increasing error in the stress ($\sigma_{True}$ at failure is up to 20% higher than $\sigma_{Eq}$ for highly ductile metals).

In this document we will refer to the most accurate diameter-based true curve as simply the true curve; frequently in the literature the section-based true cruve is not even considered and therefore the concept of true curve refers to the poorly accurate elongation-based one.

The elongation-based and the diameter-based true curves are qualitatively reported in Figure 3-9 together with the engineering curve. Also the slope curve of the true curve is reported for the reason better detailed below.

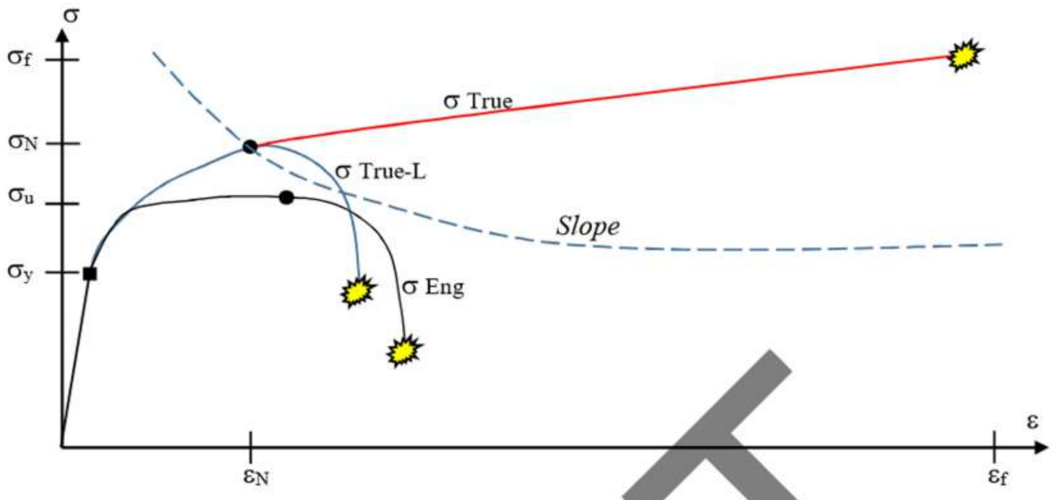

*Figure 3-9 Qualitative shape of the effective true cruve compared to the lengh-based stress-strain curves*

Given that the necking onset corresponds to the tensile instability and the maximum load, it can be identified also on the effective true curve by a simple mathematical condition;

$$\max load \rightarrow \frac{\partial F}{\partial \varepsilon_{True}} = 0; \rightarrow \frac{\partial(\sigma_{True} \cdot A)}{\partial \varepsilon_{True}} = \frac{\partial(\sigma_{True})}{\partial \varepsilon_{True}} \cdot A + \sigma_{True} \frac{\partial(\mathrm{A})}{\partial \varepsilon_{True}} = 0 \qquad (3\text{-}11)$$

But by definition

$$\varepsilon_{True} = Ln\left(\frac{A_0}{A}\right) \rightarrow A = A_0 \cdot e^{-\varepsilon_{True}} \rightarrow \frac{\partial(\mathrm{A})}{\partial \varepsilon_{True}} = A_0 \cdot e^{-\varepsilon_{True}} = -A \qquad (3\text{-}12)$$

Putting ( *3-12* ) in ( *3-11* ) delivers the condition for identifying the strain $\varepsilon_N$ at necking onset, based on the function expressing/approximating the true curve:

$$\frac{\partial(\sigma_{True})}{\partial \varepsilon_{True}} \cdot A - \sigma_{True} \cdot A = 0 \rightarrow \left.\frac{\partial(\sigma_{True})}{\partial \varepsilon_{True}}\right|_{\varepsilon_N} = \sigma_{True}|_{\varepsilon_N} \qquad (3\text{-}13)$$

Equation ( *3-13* ) shows that the necking onset occurs at the deformation $\varepsilon_N$ where the slope of the true curve equals the current value of the true stress, which is perfectly equivalent to say that the load reaches its maximum. Then the necking strain is the value of the abscissa in Figure 3-9 where the true curve is intercepted by its own slope curve.

Sometimes in experiments, the load is nearly constant for quite a long time and only small oscillations due to inertia and/or electronic noise from load cells affect the load reading: in such cases the identification of the necking onset from the load peak can deliver some inaccuracies, therefore the condition of eq ( *3-13* ) can be used for double-checking the value of necking strain from maximum load, reducing the risk of the above errors.

The effective true curve, based on diameter measurements, perfectly captures the evolving strain which concentrates at the neck section and the monotonically increasing local true stress, therefore it is rather accurate up to failure; on the contrary, the length-based true curve cannot account for a cross section shrinking much more than pthers in the specimen, then rapidly loses its accuracy after the necking onset and erroneously delivers an apparent material softening which, instead, only reflects the geometrical instability of the specimen due to the necking.

As a result, the effective (diameter-based) true stress and true strain at failure can be many times greater (2 to 20) than their length-based counterparts, while the effective true stresses at failure can be "just" 2-5 times greater than their elongation-based counterparts.

If the specimens exhibit a rectangular cross section, the optical measurement of the neck diameter cannot deliver the cross section; also two geometrical measurements, width *w* and thickness *t* of the section, do not deliver as well the area of the cross section after necking onset because such cross section becomes more and more distorted acording to Figure 3-10, so that the simple product of *t* by *w* is not adequate:

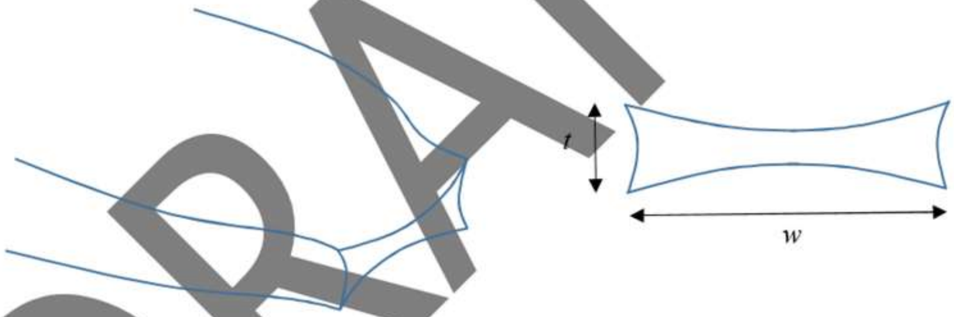

*Figure 3-10 Schematic shape of necked flat specimen*

This is the main experimental problem arising from the use of specimens flat specimens: no "simple" way exists for determining the current cross section after necking onset and, then, only the nominal elongation-based true curve can be easily determined by experiments.

When the specimen is very thin ($w_0/t_0 > 10$), the stress state is almost biaxial (the principal stress parallel to the thickness is nearly zero always and wherever) and two "in-plane" measurements or the use of DIC technique delivers reasonable accuracy, but for not-very-thin flat specimens, the problem of an experimental material curve extended up to failure is not solved today.

Usually iterative procedure based on finite elements (f.e.) are adopted, so that the material curve is changed until the load-elongation curves from f.e. closely copy those from experiments up to failure, but this procedure is not reliable as infinite material curves slightly differing in the last phases preceding failure can deliver the same f.e. results in terms of load-elongation.

A new procedure named *MVB* has been recently proposed in " *Mirone, Verleysen, Barbagallo - Tensile testing of metals: Relationship between macroscopic engineering data and hardening variables at the semi-local scale - International Journal of Mechanical Sciences 150 (2019) 154–167* " for converting the experimental enginnering curve into an estimate of the affective true curve, but it is not yet diffused in the current practice.

However also the application of the *MVB* procedure requires some efforts for being applied, therefore the stress-strain characterization via round specimens is always much more straightforward than that via flat specimens.

Unfortunately, another approximation also affects the true cruve, because the necking onset, together with quitting the stress uniformity, also quits the stress uniaxiality and triggers an increasing and increasing stress triaxiality. In fact also the radial and hoop stresses, which are null before necking, start to develop and increase after necking onset, togegher with the already-existing axial stress.

This is the reason why one more, third-approximation curve must be discussed for getting a really reliable and accurate material curve.

**Third approximation, necking-corrected equivalent stress-strain curve**

The necking affects whatever tensile test, as the buckling affects whatever compressive test.

Although being referred to different phases of the material response (the former is a typical elastoplastic phenomena, the latter occurs in the elastic range), both are geometrical instiabilities triggered by a combination of material properties and specimen structural response.

Fragile materials may break before the necking occurs but ductile structural metals typically undergo such instability, regardless of the smooth / notched shape of the tensile specimen:

*Figure 3-11 Necked specimens with and ithout notches: initial and necked shapes*

The strain at which necking initiates is a typical material constant, although high temperatures and/or high strain rates can remarkably change the whole material curve and anticipate / delay the necking onset according to eq. ( *3-13* ). Therefore, unless explicitly mentioned, we will refer to tests and material curves at room temperature and at static strain rates.

Realistic values of $\varepsilon_N$ and $\varepsilon_f$ for structural metals respectively vary in the range (0.03; 0.45) while the respecitve failure strains vary within (0.3; 1.45):

Indicative true strains at necking onset and at failure for different metals:

| | | |
|---|---|---|
| - Mild steel Fe-370 | 0.03 | 1.2 |
| - Titanium alloy TiAl4V6: | 0.07 | 0.3 |
| - Cold-worked Copper 99.9…%: | 0.05 | 1.3 |
| - Annealed Copper 99.9…%: | 0.15 | 1.5 |
| - Aluminium alloy 2020 – 6065 | 0.15 | 0.35 |
| - Medium grade steel C40 | 0.25 | 0.9 |
| - Stainless steel AISI304 | 0.4 | 1.4 |

The above data fully clarifies that the postnecking phase frequently affects the greater part of the elastoplastic life of structural metals, therefore the assessment of how the necking perturbates the stresses and strains in a tensile specimen is crucial for the material stress-strain characterization.

The discussion about the effective (diameter-based or section-based) True curve made in the previous section already clarified that, after necking onset, the neck becomes the only cross section where stresses and strains are to be calculated.

However in defining the true cruve we implicitly assumed that only a uniform axial stress was acting over the neck section, so that eq.(34) was used for estimating the equivalent stress.

Instead the real aspect of stress distributions before and after necking onset is depicted in Figure 3-12:

- first of all, the stress nonunifomity along the specimen axis (from a cross section to anoter) also applies within the neck section (from a radius value to another), thus the axial stress is not uniform and eq.(34) just delivers the section-averaged value of the current $\sigma_Z$ distribution along the radius.
- Secondly, also the radial and hoop stresses $\sigma_r$ and $\sigma_\vartheta$, not existing in a smooth specimen before necking, start to develop and increase as the necking proceeds. At the neck center $r = 0$, both $\sigma_r$ and $\sigma_\vartheta$ are identical to each other due to the cylindrical simmetry. At the outer radius, $r = d/2$, $\sigma_r$ vanishes because of the free surface equilibrium with no external pressure applied, while $\sigma_\vartheta$ usually assumes slightly negative (compressive) values.

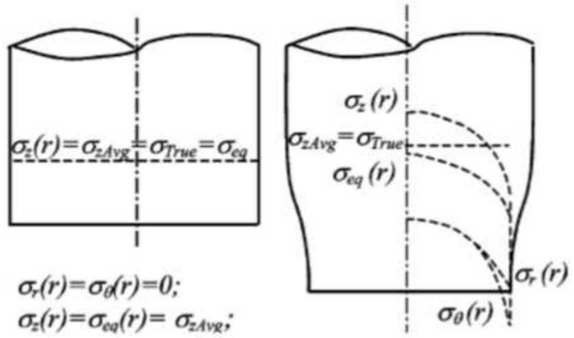

*Figure 3-12 Stress-Strain distributions before and after necking of a smooth tensile specimen*

Then, in principle, the complete set of three stress distributions $\sigma_Z(r)$, $\sigma_r(r)$ and $\sigma_\vartheta(r)$ should be calculated for successively deriving $\sigma_{Eq}(r)$ according to the von Mises formula. A similar procedure should be carried out for the principal plastic strains, so that the values of $\sigma_{Eq}(r)$ and $\varepsilon_{Eq}(r)$ are extracted at the neck center, where both them are maximum, delivering a point of the material curve of coordinates $(\varepsilon_{Eq}, \sigma_{Eq})$, corresponding to the given instant of the test. Repeating such procedure for an adequate number of instants during a tensile test delivers enough points to approximate the whole material curve and the function $\sigma_{Eq}(\varepsilon_{Eq})$ can be finally estracted by simple bestfitting techniques.

Independently of how the stress distributions are eventually calculated (which will be discussed ahead), the outcome of such axysimmetric stress state at the neck center affects the material curve by delivering values of $\sigma_{Eq}$ progressively decreasing with respect to $\sigma_{True}$ , according to Figure 3-13.

*G. Mirone / International Journal of Solids and Structures 41 (2004) 3545–3564*

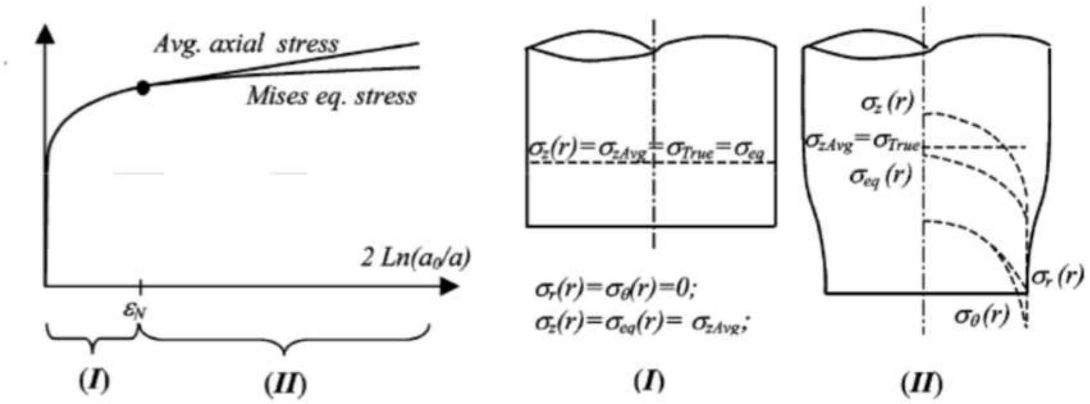

*Figure 3-13 Bifurcation between true cruve and flow curve after necking onset*

Before necking onset, phase I), the stress state is really uniform and uniaxial wherever in the specimen so that the two true stresses perfectly coincide with the equivalent stress.

After necking onset, phase II), the nominal length-based $\sigma_{True-L}$quickly falls (see Figure 3-9) and is completely unrealistic, the effective section-based $\sigma_{True}$ monotonically increases with a much more realistic trend and the real $\sigma_{Eq}$, also called flow stress if caming from a tensile test, progressively bifurcates below the true curve.

This bifurcation occurs because into $\sigma_{True}$ are incorporated increasing and increasing magnitudes of the hydrostatic stress as the necking proceeds: before necking is

$$\sigma_{Eq} = \sigma_{Eq} \text{ and } \sigma_H = \frac{\sigma_Z}{3} = \frac{\sigma_{Eq}}{3} \tag{3-14}$$

instead after necking is

$$\sigma_{Eq} = \sqrt{\frac{1}{2}[(\sigma_Z - \sigma_r)^2 + (\sigma_r - \sigma_\vartheta)^2 + (\sigma_Z - \sigma_\vartheta)^2]} \text{ and } \sigma_H = \frac{\sigma_Z+\sigma_r+\sigma_\vartheta}{3} \gg \frac{\sigma_{Eq}}{3} \tag{3-15}$$

It is known that the hydrostatic stress does not contributes to $\sigma_{Eq}$ (see Figure 2-9) but equally contributes to each single principal stress including $\sigma_Z$, its neck-averaged value $\sigma_{True}$ and its resultant load which is the current tensile force of a test; therefore the difference between $\sigma_{True}$ and $\sigma_{Eq}$ just expresses such hydrostatic stress.

A very useful parameter for expressing the amount of triaxiality related to the current flow stress is the so-caled Triaxiality Ratio or Triaxiality Factor:

$$T.F. = \frac{\sigma_H}{\sigma_{eq}} \tag{3-16}$$

Typically the $TF$ is equal to 1/3 for uniaxial stress states $\{\sigma_1, 0, 0\}$ and 0 for generalizad plane strain states $\{\sigma_1, \sigma_2, \sigma_3\}$ with $\sigma_2 + \sigma_3 = -\sigma_1$, including the special case of pure shear $\{\sigma_1, 0, -\sigma_1\}$.

The problem of determining the exact stress distributions over the neck section of a smotth specimen is not solved so far, although some approximate solutions are available. Three of them are introduced below and better detailed in the next sub-sections.

- The most famous by far is that due to P.W. Bridgman (1954), requiring considerable efforts in processing experimental data and returning an approximation within 15%;
- The most used in the literature is the "reverse engineering" method based on iterative trial-and-error inverse procedures: a tentative material curve, just accurate until necking onset, is introducend into a f.e. simulation of the smooth test and is changed iteratively in the postnecking segment until the load-elongation curve predicted by f.e. equals that from experiments. This method is moderately time-consuming and suffers of non-unique solutions

at very late strains before failure (e.g. different material curves can deliver the same load-elongation curve matching experiments).

- The most accurate and less time-consuming procedure due to Mirone (2004) is based on the observation that the necking-induced perturbation of stresses and strains is material-independent, similarly to what happens to the deformed shape of columns subjected to buckling: the onset of buckling depends on the material (through the elasticity modulus) but the deformed shape is similar-homotetic-identical independently of the material, only depending on the comparability of columns geometry and boundary conditions. The MLR method just consists of a unique corrective function suitable for all metals, capable of transforming the effective area-based true curve into the equivalent stress-strain curve only depending on the necking strain of the given material.

Whatever method is adopted for estimating $\sigma_{Eq}$, its curve always bifurcates from the true curve at necking onset and continues staying below $\sigma_{True}$ so that, at failure, $\sigma_{Eq}$ can be up to 25% lower than $\sigma_{True}$ in case of long postnecking phase. The longer is the postnecking phase of a material, the greater is their difference at failure, so that for materials exhibiting shorter strain ranges between necking and failure, smaller differences are expected between $\sigma_{Eq}$ and $\sigma_{True}$.

The qualitative evolution of all the stress-strain curves discussed so far is reported in Figure 3-14

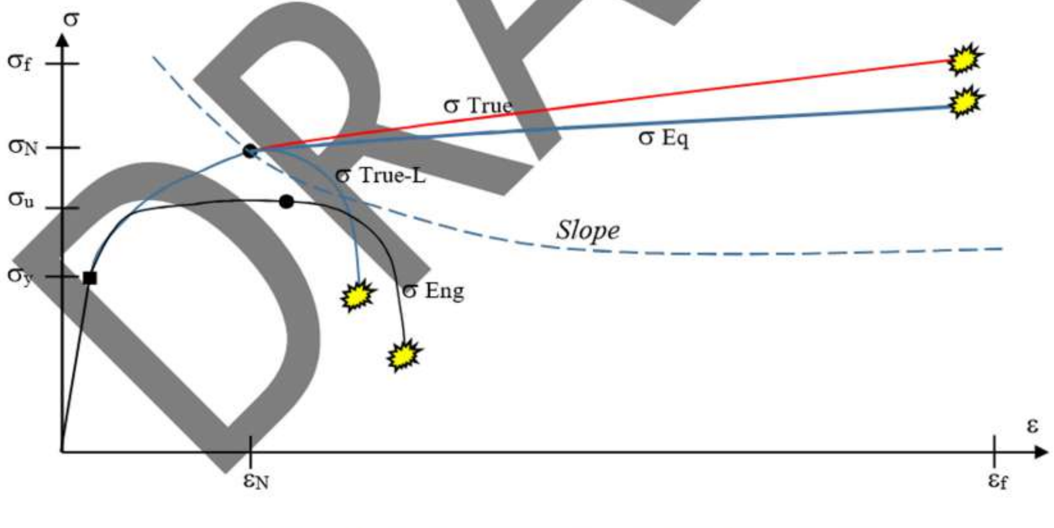

*Figure 3-14 Stress-strain curve according to all possible approximationss*

*BRIDGMAN METHOD*

It is based on the main approximation that plastic strains $\varepsilon_Z, \varepsilon_r, \varepsilon_\vartheta$ are uniform over the neck section (strain nonuniformity only applies along the specimen axis).

This implieas that also $\varepsilon_{Eq}$ and, in turn, $\sigma_{Eq}$ are uniform over the neck section, although the principal stresses $\sigma_Z, \sigma_r, \sigma_\vartheta$ are not uniform.

Without detailing the demonstration which is not of interest here, the results of the Bridgman method are that all plastic strains are perfectly determined by the true strain:

$$\varepsilon_Z = 2 \cdot Ln\left(\frac{d_0}{d}\right); \quad \varepsilon_r = \varepsilon_\vartheta = -\frac{\varepsilon_Z}{2} = -Ln\left(\frac{d_0}{d}\right); \quad \varepsilon_{Eq} = \varepsilon_Z = 2 \cdot Ln\left(\frac{d_0}{d}\right) \tag{3-17}$$

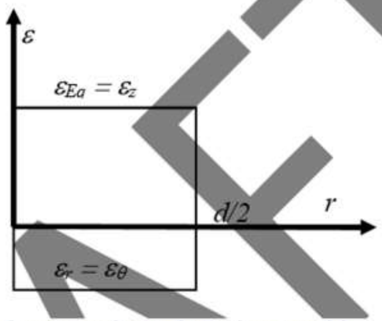

*Figure 3-15 Strain distribution acording to the Bridgman model*

While the stresses are approximated by the following expressions:

$$\begin{gathered}
\sigma_{Eq} = \frac{\sigma_{True}}{\left(1+4\frac{R}{d}\right)\cdot Ln\left[1+\frac{d}{4R}\right]} \\
\sigma_r(r) = \sigma_\vartheta(r) = \sigma_{Hyd}(r) = \sigma_{Eq} \cdot Ln\left[1 + \frac{d^2-4r^2}{4Rd}\right] \\
\sigma_Z(r) = \sigma_{Eq} + \sigma_{Hyd}(r) = \sigma_{Eq} \cdot \left(1 + Ln\left[1 + \frac{d^2-4r^2}{4Rd}\right]\right)
\end{gathered} \tag{3-18}$$

Where $R$ is the curvature radius of the necking profile at each instant of the test

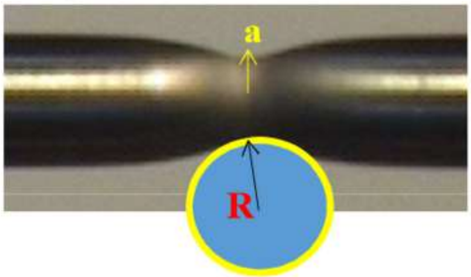

*Figure 3-16 Curvature radius of the necking profile*

The resulting stress distributions are qualitatively depicted in Figure 3-17.

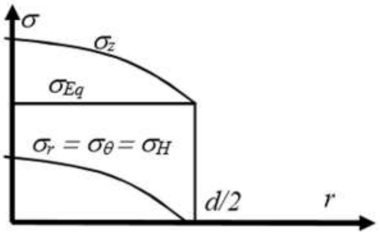

*Figure 3-17 Stress distributions along the neck radius accordin to the Bridgman model*

The term $1/\left\{\left(1+4\frac{R}{d}\right)\cdot Ln\left[1+\frac{d}{4R}\right]\right\}$, converting $\sigma_{True}$ into an estimate of $\sigma_{Eq}$ as visible in the first line of eq. ( *3-18* ), is the necking correction factor proposed by Bridgman.

*INVERSE METHOD*

The first tentative curve is an extension of the length-based true curve until necking onset, prolonged with arbitrary curved segments beyond necking onset up to the failure strain.

A f.e. simulation of the tensile test of smooth specimens is ran with the 1st material curve and the resulting load-elongation curve is compared to the experimental one: the comparison is accurate until necking but will underestimate-overestimate after necking onset. Depending on such comparison the postnecking curve is increased-decreased leading to the 2nd material curve and a new f.e. simulation is run, a new comparison is made of numerical/experimental load-elongation curves, a new material curve is guess, and so on, until the discrepancy of load-elongation curves from f.e. and from experiments will be lower than the desired tolerance.

Unfortunately, at high necking strains the very final part of a material curve will affect very small volumes of material as visible in Figure 3-18, so that its effect will be almost undetectable on the overall load-elongation curve from f.e.

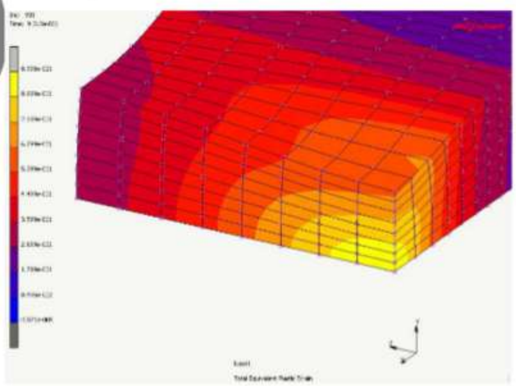

*Figure 3-18 Equivalent plastic strain distribution over a necked flat specimen*

This means that infinite curves bifurcating at the final stages of test will deliver the same load-elongation curve therefore the inverse method cannot deliver a really unique solution, although such non-unicity problem only affects the very final stages of a test.

*MLR METHOD*

This method, firstly proposed in *G. Mirone, A new model for the elastoplastic characterization and the stress-strain determination on the necking section of a tensile specimen - Int. J of Solids and Structures (2004), 41 (13) 3545-3564*, was based on the observation that the ratio of $\sigma_{Eq}$ averaged on the current neck section and divided by the true stress, $\sigma_{EqAvg}/\sigma_{True}$ , evolved according to an almost material-independent trend, provided that the post-necking strain, $\varepsilon_{True} - \varepsilon_N$, was assumed as the variable governing such trend.

This was observed by f.e. analyses of tensile tests of many different materials including different mild and high strenght steels, aluminium alloys, copper alloys.

Then the above ratio was approximated by a simple bestfit function as shown in Figure 3-18 and used for successfully correcting, after necking onset, the experimental true curves of many different materials studied since 2004.

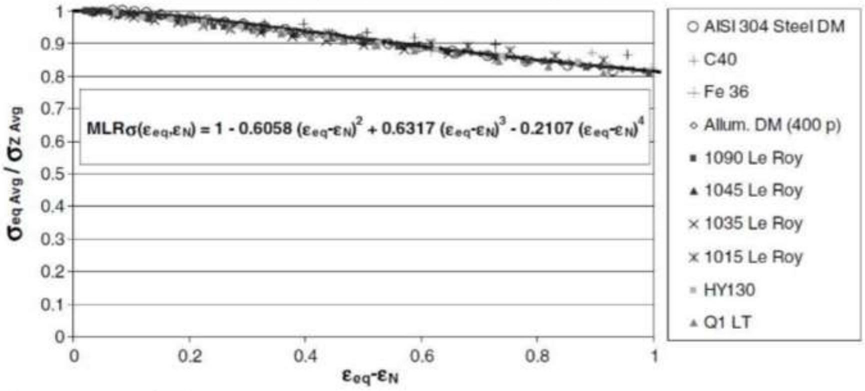

*Figure 3-19 MLR necking corrective function*

The principal stress functions were also derived in the original paper together with the MLR correction factor, but such further outcome is just secondary with respect to the main result consisting of the way for simply and accurately transforming the experimental true curve into a reliable estimate of the equivlant stress-strain curve.

## 3.3 TYPICAL FORMULAE FOR APPROXIMATING MATERIAL CURVES

The procedures discussed in the previous section allow to estimate a finite number of couples of values $(\varepsilon_{Eq}, \sigma_{Eq})$ from each tensile test, which can represent a set of discrete points in a stress-strain diagram. For using such set of data in a convenient way it is common practice to find mathematical functions approximating such data according to least square methods or even according to simple "eye-based" accuracy evaluations.

Therefore the mathematical form of the function selected for approximating such data is not-at-all related to the physics of plasticity or to the material response.

Nevertheless, some formulae are very known in the literature and are very frequently adopted, maybe also when their adoption is not suitable for the data at hand; in fact sometimes the mathematical function selected can prevent the accurate reproduction of data (e.g. a single quadratic function or n-th power function cannot accurately reproduce an experimental stress-strain behavior which is curved in a certain strain range and linear in another).

The simpler equation used for approximating stress-strain material curves is that by **Hollomon**:

$$\sigma_{Eq} = K \cdot {\varepsilon_{Eq}}^{n} \qquad (3\text{-}19)$$

With $K$ and $n$ material constants to be calibrated for identifying the material curve. A special feature of the Hollomon formula is that $n$, also called "hardening exponent", is coincident to the necking strain $\varepsilon_N$: in fact if eq. ( *3-19* ) is derived for finding the strain value where the condition $\partial\sigma_{Eq} / \partial\varepsilon_{Eq} = \sigma_{Eq}$ is satisfied, yields:

$$\partial\sigma_{Eq} / \partial\varepsilon_{Eq} = n \cdot K \cdot {\varepsilon_{Eq}}^{n-1} = K \cdot {\varepsilon_{Eq}}^{n} \rightarrow n = \varepsilon_{Eq} = \varepsilon_N \qquad (3\text{-}20)$$

The Hollomon equation copies quite well the experimental points over the pre-necking part of the Mises stress-strain curve, where it is conicindet to the true curve, of late-necking materials (e.g. $\varepsilon_N > 0.1$). After necking onset the true curves are quite often very close to being linear (see the MVB method in Mirone et al. 2019) and the Mises curves are governed by the MLR correction applied to such linear trends: therefore a single Hollomon power law is not very suitable for such postnecking range and, sometimes, two or more Hollomon laws with different parameters are used together, referred to different strain ranges.

Another issue of the Hollomon curve is that it predicts zero Mises strain at zero plastic strain, meaning zero yield stress: this is why the Hollomon curve can be adopted only after plastic strains is higher than a few perecnts, e.g. 0.02 to 0.05.

Therefore, when materials exhibit early necking ($\varepsilon_N < 0.1$) the Hollomon law is nearly completely unsuitable for describing the material curve.

Another very common equation for material curves is that by **Ludwik**, taking the following form:

$$\sigma_{Eq} = A + B \cdot \varepsilon_{Eq}{}^{n} \tag{3-21}$$

where $A$ is the yield stress, $B$ and $n$ describe the plastic curve. The hardening exponent $n$ h ere is not equal to the necking strain, as it was for the Hollomon curve. Th good point of this law uis that it correctly describes the non-zero yield stress at zero plastic strain.

Also different formulae are available in the literature for approximating material curves, like the **Voce** law, the **Swift** law and mix ed **many others**, which are not considered here.

However it is essential to bear in mind that all possible mathematical functions are just to be selected depending on their ability to nicely approximate the sperimental points, as they are not connected in any way to whatever physical consideration.

Therefore, despite it may be more time-consuming, frequently the best choice is that of breaking the experimental data in two or three strain ranges (e.g. early plasticity range for $0 < \varepsilon_{Eq} < 0.1$, pre-necking range for $0.1 < \varepsilon_{Eq} < \varepsilon_N$ and post-necking range for $\varepsilon_N < \varepsilon_{Eq} < \varepsilon_{fail}$) and adopting **simple polynomial best-fit** functions in each range, taking care to ensure continuity at the boundaries between two neighbouring strain ranges.

FIGURA CON ESEMPIO DATI EXP APPROSSIMATI CON Hollomon, Ludwik, polinomiale

# 4 INTRODUCTION TO DUCTILE DAMAGE – MECHANISMS AND MODELS

## 4.1 QUALITATIVE MECHANISMS OF DUCTILE FAILRUE

Materials failure does never occurs at the same time within an entire component or structure; instead it is a progressive phenomenon roughly evolving according to the following phases:

- Fracture initiation, usually occurs at a critical/weakest material point, sometimes in more critical points at the same time. It is a discrete event and has a null time duration:

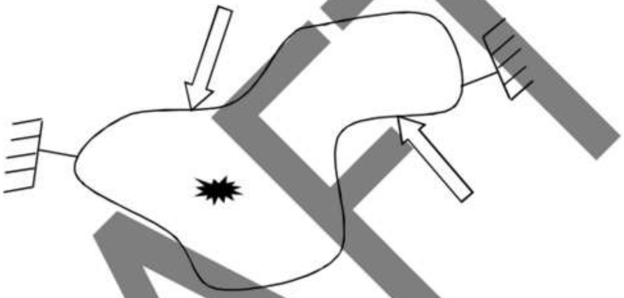

*Figure 4-1 Schematic of failure initiation at a single material point*

- Fracture propagation = fracture of material points close to the fracture initiation point: the envelope of failed material points is the fracture surface. It is a continuous process and, although can be very quick depending on the load, in principle it can be always stopped before complete propagation ad structure breaking; in this case the structure is partially damaged but macroscopically still intera, If the damage involves only internal points within the structure, it may seem apparently undamaged:

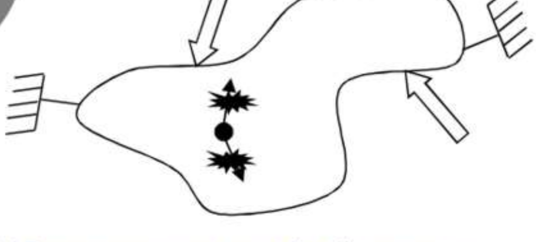

*Figure 4-2 Fracture propagation starting from the initiation site*

- Complete fracture = macroscopic breaking and separation of the structure/component in two or more fragments. It is a discrete event corresponding to the completion of the propagation phase :

*Figure 4-3 Fracture propagation until macroscopic component failure*

For ductile metals, fracture initiation at the local scale never occurs at fixed values of stress or strain for the given material: depending on the component shape, on the load type and the imposed constraint, failure may initiate at very different values of stress and strain for the same material, as qualitatively depicted in Figure 4-4;

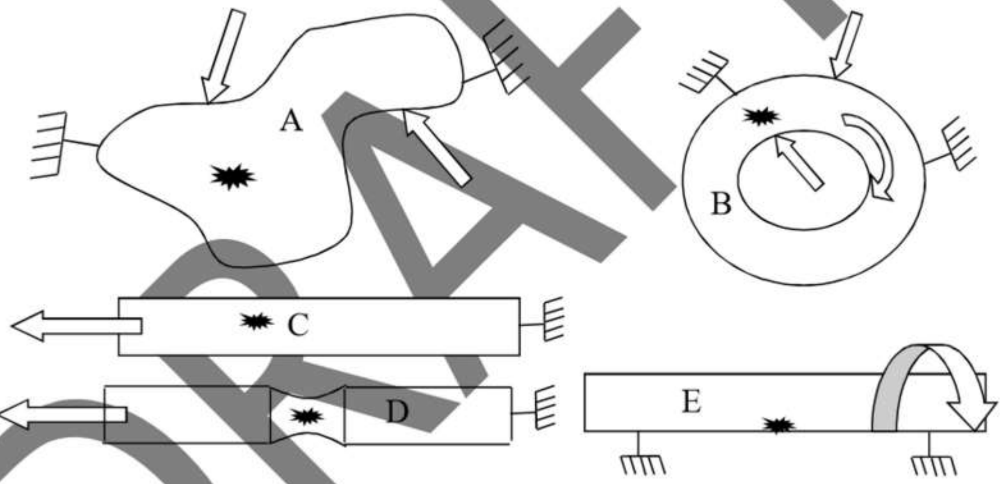

$$\tilde{\sigma}_A \neq \tilde{\sigma}_B \neq \tilde{\sigma}_C \neq \tilde{\sigma}_D \neq \tilde{\sigma}_E$$

$$\tilde{\varepsilon}_A \neq \tilde{\varepsilon}_B \neq \tilde{\varepsilon}_C \neq \tilde{\varepsilon}_D \neq \tilde{\varepsilon}_E$$

$$\sigma_{Eq\,A} \neq \sigma_{Eq\,B} \neq \sigma_{Eq\,C} \neq \sigma_{Eq\,D} \neq \sigma_{Eq\,E}$$

$$\varepsilon_{Eq\,A} \neq \varepsilon_{Eq\,B} \neq \varepsilon_{Eq\,C} \neq \varepsilon_{Eq\,D} \neq \varepsilon_{Eq\,E}$$

*Figure 4-4 Different failure modes under different loading-deformation modes*

According to the "classic" approach to failure, the local break of a given material initiates when $\sigma_{Eq}$ reaches a critical value, the so-called "failure stress" $\sigma_f$, independently of how the principal stresses are combined together (independently of the stress state) for delivering that value of $\sigma_{Eq}$: therefore the stress and strain tensors can be different from a stress state to another but the limit value of the equivalent stress at failure is fixed and common to whatever stress state as in eq. ( *4-1* ).

$$\sigma_{Eq} = \sigma_f \tag{4-1}$$

The bad news is that the "classical" approach is completely unreliable when moderate or large plastic strains are involved before failure: in such cases complex phenomenon occur going under the name of "Ductile Damage". Many different approaches are available in the scientific literature for mathematically describing the Ductile damage: none of them is still completely exact while all of them contribute to overall knowledge of the subject and allow more or less accurate predictions of failure initiation.

Independently of the many damage models available, the practical outcome from experiments referring to Figure 4-4 is that different stress states histories (different combinations of principal stresses during the load history) deliver different values of $\sigma_f$ and $\varepsilon_f$ for the same given material, according to eq. ( *4-2* ):

$$\begin{gathered} \sigma_{Eq_A} \neq \sigma_{Eq_B} \neq \sigma_{Eq_C} \neq \sigma_{Eq_D} \neq \sigma_{Eq_E} \\ \varepsilon_{Eq_A} \neq \varepsilon_{Eq_B} \neq \varepsilon_{Eq_C} \neq \varepsilon_{Eq_D} \neq \varepsilon_{Eq_E} \end{gathered} \tag{4-2}$$

In other words the classical reassuring concept that every material has its own *Failure Stress*, triggering failure initiation under whatever stress-strain history, is just a "legend" and cannot be adopted anymore for the advanced design of mechanical structures !!!

Therefore, also a single failure strain is of no use for predicting failure or for designing a structure with assigned failure limits, because neither the *Failure strain* at failure is a material constant !!!!

The above concept of different failure limits for different stress-strain histories on the same material is perfectly compatible with the concept that whatever stress-strain history is associated to the same hardening curve (also said "material constitutive curve").

In fact, assumed quasistatic straining at room temperature, whatever stress-strain history of a material complies with the same static Mises curve of that material: only the failure points move back and forth along such curve, depending on how the principal stresses are combined to each other for delivering each value of $\sigma_{Eq}$, according to Figure 4-5:

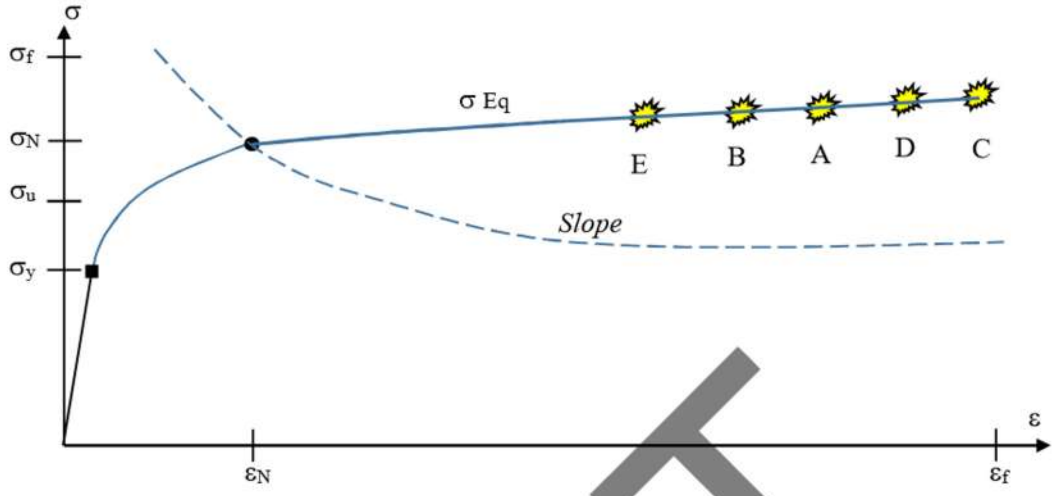

*Figure 4-5: Different failure points x different stress states along the same material curve*

The double infinity of different combinations of principal stresses delivering a given value of $\sigma_{Eq}$ (which expresses the second stress invariant), can be identified by the values of the first and the third-deviatoric stress invariants.

The two most used variables expressing the stress states based on the ratio of such stress invariants to the second one are the stress triaxiality *TF* (ratio of $\sigma_H/\sigma_{Eq}$, see eq. ( *3-16* )), and a normalized version of the Lode Angle already defined in chapter 2:

$$X = Cos(3 \cdot \theta) = \left(\frac{27}{2} \cdot \frac{J_3}{{\sigma_{Eq}}^3}\right) \qquad (4\text{-}3)$$

We could say that the two stress-state parameters respectively express the ratio of axial and angular coordinate of the Haigh-Westergaard cylindrical coordinates to the radial coordinate.

Other expressions similar to eq. ( *4-1* ) are available in the literature for expressing the Lode parameter (e.g. based on the Sine function or normalized over diffferent intervals), but their overall physical meaning remains unchanged as they always relate the angular coordinate to the radial one.

A single stress state can be then identified by three parameters, e.g. the principal stresses, the stress invariants or, still better, by the triplet $\sigma_{Eq}$, $TF$ and $X$.

The stress triaxiality $TF$ virtually extends in the range (- $\infty, \infty$), the Lode parameter $X$ lies within [-1, 1]. Typical values of the stress-state parameters for reference loading modes are reported in table below and plotted in Figure 4-6:

| | Principal stresses | TF | X |
|---|---|---|---|
| Uniaxial tension<br>(tension of smooth specimen) | $(\sigma_1, 0{,}0)$ | 1/3 | 1 |
| Torsion<br>(thin pipe or outer surface of solid cylinder in torsion ) | $(\sigma_1, 0, -\sigma_1)$ | 0 | 0 |
| Axisymmetric<br>(axis of round notched tensile spcimen) | $(\sigma_1, \sigma_2, \sigma_2)$ | (- ∞, ∞) | 1 |
| Generalized plane strain | $(\sigma_1, \sigma_2, -\sigma_1 - \sigma_2)$ | (- ∞, ∞) | 0 |
| Generalized Plane stress (S-shaped curve relating TF to X) | $(\sigma_1, \sigma_2, 0, )$ | $[-\sqrt{3}/_2, \sqrt{3}/_2]$ | [- 1, 1] |
| Equibiaxial tensile plane stress = special case of plane strain | $(\sigma_1, \sigma_1, 0, )$ | 2/3 | 0 |
| Equibiaxial compressive plane stress = special case of plane strain | $(0, \sigma_3, \sigma_3, )$ | -2/3 | 0 |

*Table 4-1: values of TF nd X for special stress states*

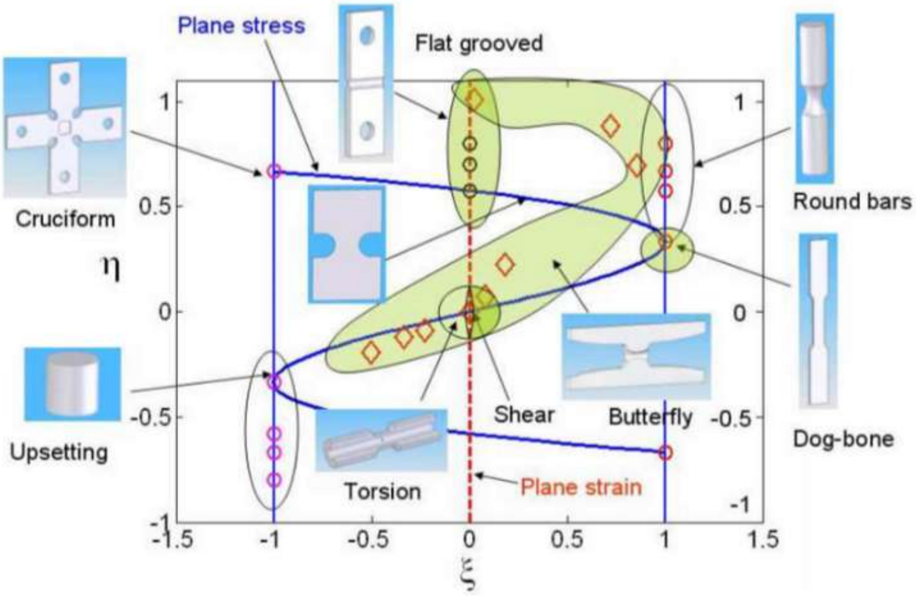

*Figure 4-6 Special Stress States in the plane TF - vs- f(X), see https://www.researchgate.net/figure/Stress-states-in-the-space-of-the-newly-defined-stress-triaxiality-h-H-and-the-Lode_fig7_302473743 , Namsu Park . If X is used instead of Lp the plot is roughly mirrored around the vertical axis (AGGIUNGI GRAFICO FATTO IN CASA CON X !!!)*

The “million dollars” question to which the damage mechanics still attempts to answer is: how can we design a structure (shape, size and constraints) capable of withstanding a certain set of loads, without relying on any critical value of the equivalent stress or equivalent plastic strain?
In other words, how can we predict whether our structure will start failing at its weakest material point when the stress-strain will be those of failure points E, B, A, D or C in Figure 4-5 ??? Failure initiation at point E will mean that the overall load carrying and deformation capabilities of the given structure are much lower than those of another structure (different shape, constraints, size etc.), made of the same material, whose weakest point starts failing at point C of the same material curve.
The search of the answer to the above question promoted the development of the Fracture Mechanics (about 1920) and of the Damage Mechanics (about 1970), two areas of modern Material Science of crucial importance in most fields of structural design such as aerospace, nuclear, automotive, naval, defence, forming-forging technology, special applications of building engineering, etc. etc.

The ductile damage is a phenomenon which progressively evolves at the microscopic local scale (single material points) and is usually modeled at a so-called mesoscale, intermediate between the micro-scale of single material points and the macro-scale of the structural component. The size of representative volume elements identifying such mesoscale, RVE, might be roughly within 0.1 mm$^3$ for metals, 1 cm$^3$ for fine-grained concrete and 10 cm$^3$ for thick-grained concrete.
The adoption of the RVE allows to discretize the volume of a structure and to assign the material properties homogeneized /averaged on the entire RVE to its center point.
At the initial stages of damage evolution the RVEs stress-strain response is just barely affected, at intermediate stages its load carrying capacity is progressively decreased until, at final stages, such load carrying capacity vanishes and the RVE representing the given material point within the specimen/component/structure is failed and can be “turned off”.
So far the macroscopic response of the structure (e.g. the overall load in a tensile specimen) is still nearly unaffected by damage and failure. Only after many material points close to each other have failed, the macroscopic damage shows up (a crack, a cluster of microvoids or a shear band) and further propagates until the complete failure of the specimen/component/structure.

Depending on the stress states (the different combinations of evolving principal stresses delivering the same evolving $\sigma_{Eq}$), two main types of damage evolution and failure modes exist: the triaxiality-dominated damage exhibiting a mechanism of microvoids nucleation, growth and coalescence, while shear-dominated damage showing slip failure surfaces according to preferential crystallographic planes and eventually instability along shear bands in dynamics.

Void nucleation originates where imperfections and inclusions are present: in fact despite structural metals at the macroscopic scale usually appear as nicely homogeneous, at the local scale they are non-homogenous and can be represented as a surrounding ductile metal matrix containing isolated dispersed stone-shaped harder inclusions (e.g. carbides, …. ) or internal bubbles and microvoids due to the metallurgical process.

If the mesoscale approach is adopted, the choice of RVE of the appropriate size allow to consider the metal as an homogenous medium whose local properties also reflect the discontinuities at the very microscale. Then the material properties averaged over RVE containing inclusions are suitable for expressing: a) the initial undamaged state where full adherence and continuity exists between matrix and inclusion , b) the intermediate state where the continuity is missing and the load carrying capacity of the RVE is deteriorating and c) the final stages where coalescing voids are leading to the failure of the RVE and total loss of its load carrying capacity.,

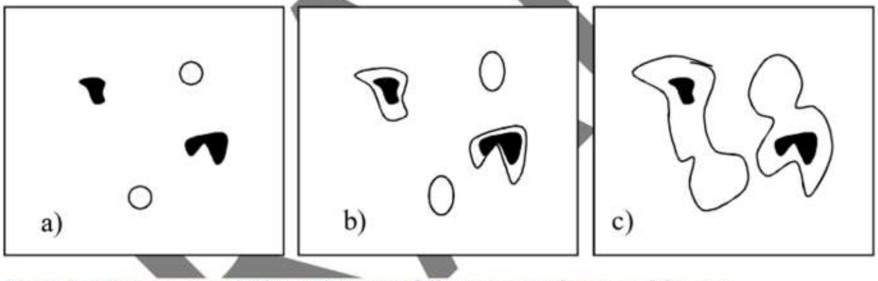

*Figure 4-7 Representative VOlume Element at different stages of strain and damage*

Together with the voids originating from detaching inclusions under applied load, also pre-existing voids may exist within the virgin undeformed metal, due to foundry processes, uncomplete gas evaquation etc.

A physically-based parameter adopted for quantifying the damage is the void volume fraction (e.g. Gurson-based models), another is the equivalent voided resisting cross section (Lemaitre-based models), however frequently also other non-physically-related conventional variables are successfully adopted in the literature.

The shear-dominated failure exhibit less “suggestive” mechanisms as “simpler” separation of the material along special slipping planes occurs, with just recognizable features from the metallographic viewpoint such as smooth, velvet-like fracture surfaces instead of rougher and more glass-like fracture surfaces in case of micrvoids-promoted high triaxiality failure.

Given such qualitative preliminary considerations, the "big problem" of materials damage is that local failure does not initiates just when the equivalent stress reaches a critical vaue typically called "material strength" or "failure stress"; Instead it initiates as infinite possible different values of the flow stress are reached for the same material, depending on how the two stress-state parameters $TF$ and $X$ evolved during each arbitrary deformation history.

We can say that the value of $\sigma_{Eq}$ alone cannot trigger local failure, as the same material point can fail at infinite different values of $\sigma_{Eq}$ depending on how evolved both $TF$ and $X$ all over the loading history. For a given ductile metal at failure, $\sigma_{Eq}$ from smooth tensile specimens (failing at neck center where $TF>1/3,\ X=1$ ) is greater than that from notched tensile specimens (can fail wherever on the minimum section with $TF>>1/3,\ X<=1$), while that from a tubular torsion specimen (fails on the surface with $TF\approx 0,\ X=0$) can be either greater or lower depending on how the failure of that material is sensitive to the Lode angle.

Furthermore, for ductile metals it is much more appropriate to identify each failure conditions by the equivalent plastic strain instead of the equivalent stress. This is mainly because hardening curves usually exhibit a low-slope, saturating attitude as qualiteatively depicted in Figure 4-5, which makes more resolute and accurate the identification of a curve point indicating failure by its horizontal coordinate (the equivalent plastic strain) than it is by its vertical coordinate (the flow stress).

Then, to characterize the damage response of a ductile material means to derive the relationship between all possible arbitrary evolutions of $TF, X$ and the corresponding values of $\varepsilon_{Eq}$ at local failure accodring;

Many material models from the literature are able to reproduce the failure from experiments related to a more or less wide range of $TF, X$ histories with reasonable accuracy, but the ability to exactly predict failure under whatever possible evolution of $TF$ and $X$ histories for a given material is one of the largest challenges still open for material scientists.

## 4.2 MICROVOIDS AND STRESS TRIAXIALITY : MC CLINTOCK AND RICE-TRACEY MODELS

Two of the most known earlier models relating $\varepsilon_{Eq}$, $TF$ and the growth of microvoids are due to McClintock (1968) and to Rice-Tracey (1969).

Mc-Clintock assumed that the material was organized in regular arrays of rectangular cells each including a single ellipsoidal void, according to Figure 4-8.

The growth of voids along their major semiaxis was related to the stresses along the same direction $\sigma_a$ and the transverse direction $\sigma_b$ so that, when the major semiaxis elongated enough to become euqal to the entire cell length, $a = l$, failure occurred. Assuming an Hollomon-like material curve, eq. ( 4-4 ) shows the strain at failure corresponding to the above limit situation.

$$\varepsilon_f = \frac{(1-n)\cdot Ln\left({}^{l_0}\!/_{b_0}\right)}{sinh\left[0.5\cdot\sqrt{3}\cdot(1-n)\cdot\left(\frac{\sigma_{a+\sigma_b}}{\sigma_{Eq}}\right)\right]+\frac{3}{4}\cdot\left(\frac{\sigma_{a+\sigma_b}}{\sigma_{Eq}}\right)} \qquad (4\text{-}4)$$

Where $n$ is the Hollomon hardening exponent and $\frac{\sigma_{a+\sigma_b}}{\sigma_{Eq}}$ is a close approximation of the triaxiality factor $TF$. This is the first case of a model capturing a partial relationship between the failure strain and the stress triaxiality.

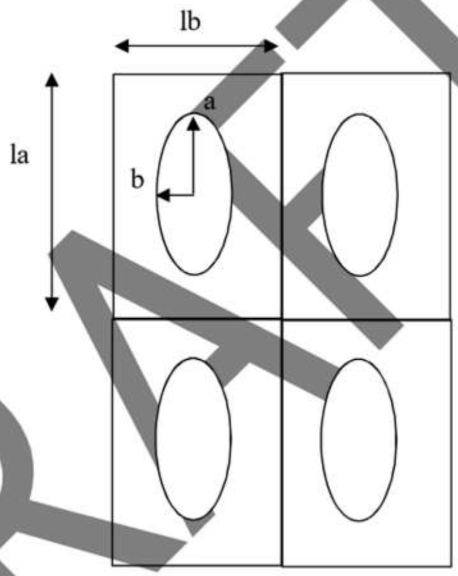

Figure 4-8 McClintock's array of voided cells

The model by Rice and Tracey assumed an arbitrarily large spherical cell containing a spherical void of radius $R_0$, according to Figure 4-9

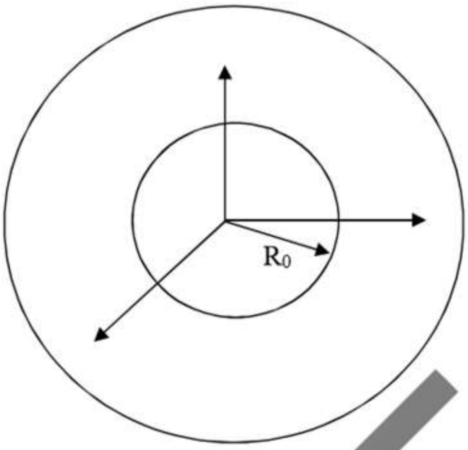

Figure 4-9 Undeformed Rice-Tracey unit cell containing a spherical void

They assumed that the presence of the void was perturbating the remote fields of radial displacement, stress and strain according to different arbitrary functions decaying with the distance from the void center, as in Figure 4-10

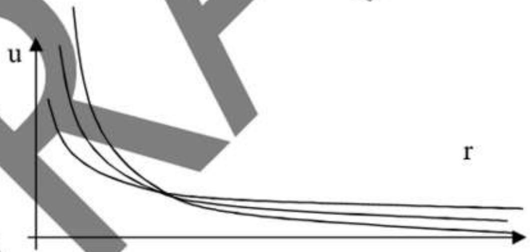

Figure 4-10 Arbotrarily perturbed displacement functions

They imposed the Rayleigh-Ritz minimization of a potential $Q$ based on the plastic work corresponding to the difference between remote stresses (nominal, "undisturbed" by the void) and local stresses (effective, affected by the void):

$$Q = \int_0^{\varepsilon_f} \left(\sigma_{Eq-Rem} - \sigma_{Eq-Loc}\right) \cdot d\,\varepsilon_{Eq} \tag{4-5}$$

Obtaining the growth speed of the spherical void along the three principal directions:

$$\dot{R}_k = \left[c \cdot \dot{\varepsilon}_{K-Rem} + D \cdot \dot{\varepsilon}_{Eq-Rem}\right] \cdot R_0 \tag{4-6}$$

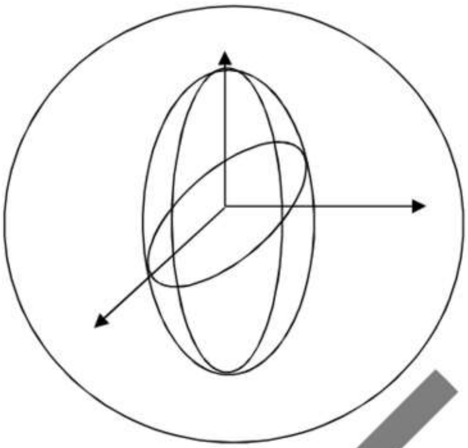

*Figure 4-11 Rice-Tracey unit cell and defomed spherical void becoming ellipsoidal*

with $c$ and $D$ material constants governing the microvoid evolution: $c$ expresses the change of void shape at constant volume because the principal plastic strains $\dot{\varepsilon}_{1-Rem} + \dot{\varepsilon}_{2-Rem} + \dot{\varepsilon}_{3-Rem} = 0$ and so do the corresponding "deviatoric" contribution to radius increments $c \cdot (\dot{\varepsilon}_{1-Rem} + \dot{\varepsilon}_{2-Rem} + \dot{\varepsilon}_{3-Rem})$, while the constant $D$ expresses the change of volume at constant shape because the "hydrostatic" or "dilatational" contribution of the radius increments, $D \cdot \dot{\varepsilon}_{Eq}$ , is equally applied along all three principal directions.

The $c$ coefficient was obtained to assume the following values:

$$C = 2 \quad \text{( HARDENING e/o HIGH TRIAX)}$$
$$C = \frac{2}{3} \text{( NO HARDENING e/o LOW TRIAX )} \qquad (4\text{-}7)$$

Mainly depending on the hardening, with a poor dependency on the stress triaxiality; instead $D$ was found to take the following form:

$$D = \frac{3\sigma^{\infty}}{4\sigma^{\infty}{}_{eq}} \quad \text{( HARDENING )}$$

$$D = 0.558\sinh\left(\frac{\sigma^{\infty}}{2\tau_y}\right) + 0.008\nu\cosh\left(\frac{\sigma^{\infty}}{2\tau_y}\right) \approx \qquad (4\text{-}8)$$

$$\approx (0.279 + 0.004\nu)Exp\left(\frac{3\sigma^{\infty}}{2\sigma_y}\right) \quad \text{( NO HARDENING )}$$

With a pronounced dependency on $\sigma_H/\sigma_{Eq}$, expressing the triaxiality factor, independently of the low/high hardening attitude of the material.
According to many experimental observations the dilatational term prevails on the deviatoric term in affecting the local strain field and generating the damage.

Whiel these models are not frequently used today in their original form for modeling the ductile damage, their great merit was that of demonstrating how and why the hydrostatic stress, completely ininfluent for the plastic stress-strain response of a material (the Mises stress is unaffected by $\sigma_H$), become essential in determining the damage evolution and, in turn, the failure of that material.

## 4.3 PRACTICAL OUTCOMES AND EXPERIMENTAL EVIDENCES OF THE RELATIONSHIP BETWEEN HYDROSTATIC STRESS AND DUCTILE DAMAGE

The early studies on ductile damage demonstrated that the same metal obeyes to the same Mises stress-strain material curve but can fail at different points along such material curve, as close to the curve origin (early failure) as larger are the triexiality values experienced by the material.
The best way for getting an immediate confirmation of such phenomenon is to test tensile specimens with and without notches. In fact the presence of a notch generates radial and hoop stresses $\sigma_r$ and $\sigma_\vartheta$ which, in turn, mean generating $\sigma_H$ and $TF$ in excess with respect to those of the smooth specimen.
The typical notched specimen is defined by its maximum diameter $D$, minimum diameter $d$ and notch profile radius $R$, according to Figure 4-12.

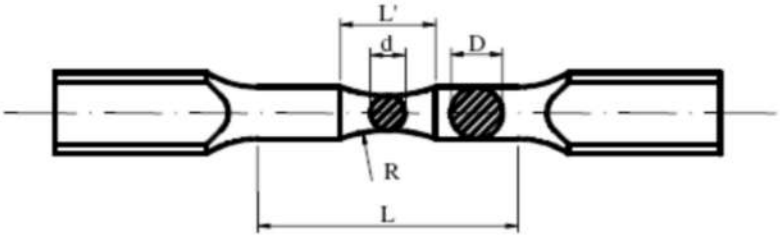

*Figure 4-12 Notched specimen shape*

The sharper is the notch (large values of $D/d$ and small values of $R$), the higher are the distributions of $\sigma_r$ and $\sigma_\vartheta$ over the minimum cross section of notched specimens for each given current load. A notch acts similarly to the necking, but its effect also exists at elastic and early plastic stages, long before the necking is actually initiated. When also the necking takes place on notched specimens the two effects act together with the imaginable outcome: magnified increase of stress triaxiality, accelerated damage growth and failure anticipation.

For showing such outcome, the true crues from various experiments performed in the past at the University of Catania are reported in Figure 4-13 and Figure 4-14, together with the respective Mises curves.

All tested specimens are machined with $D = 9mm$, $d = 6mm$ and $L = 55\ mm$, while the notch profile radius $R$ varies depending on the desired sharpness of the notch and is identified by the name *Rxx* of each notched specimen.

The discrete marks in the aforementioned plots represent the experimental true stress-true strain data points; in these figures the continous curves are obtained from finite elements simulations but similar curves might also express the bestfit functions of experimental data.

The dashed curves represent the $\sigma_{Eq}$-vs- $\varepsilon_{Eq}$ material curves: until necking onset they are perfectly overlapped to the true curves of smooth specimens, after necking onset the former curves bifurcate and run below the latter ones.

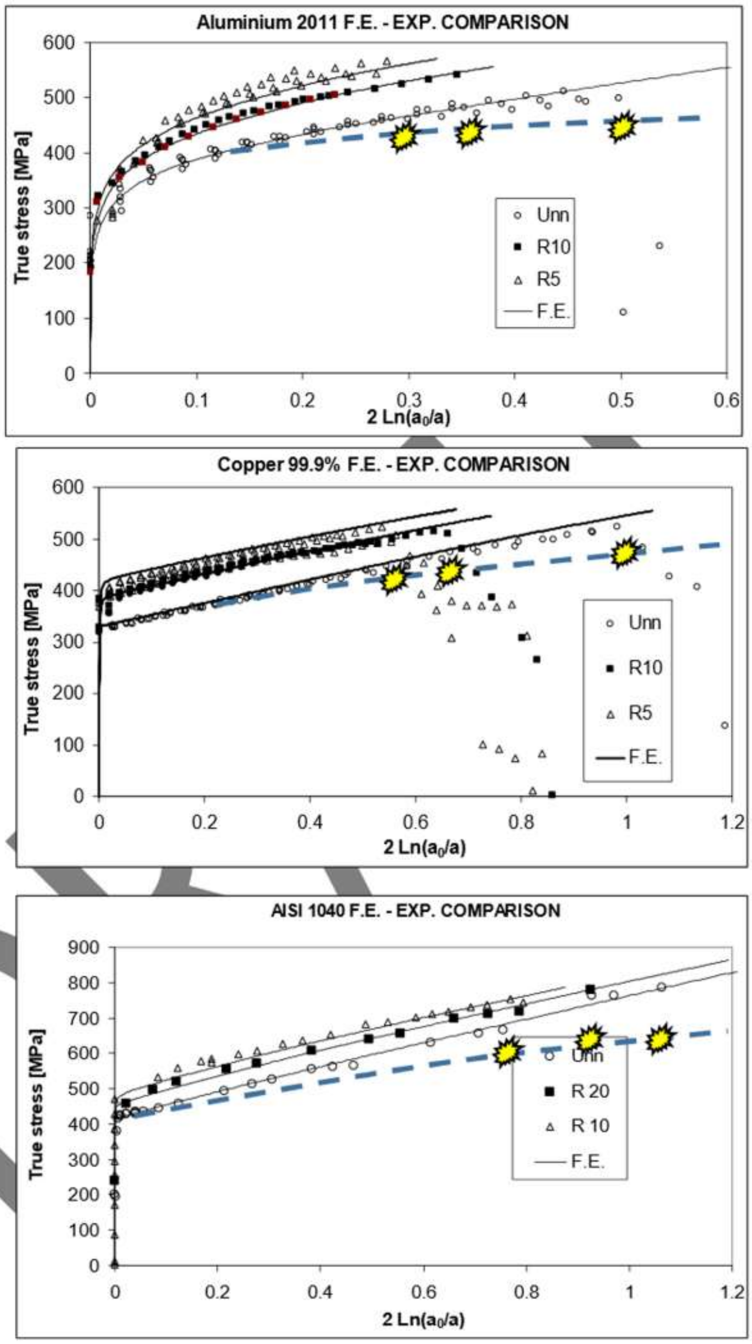

*Figure 4-13 Stress-strain cruves of smooth and notched tensile specimens of Al Alloy, Mild steel and cold-worked pure Copper*

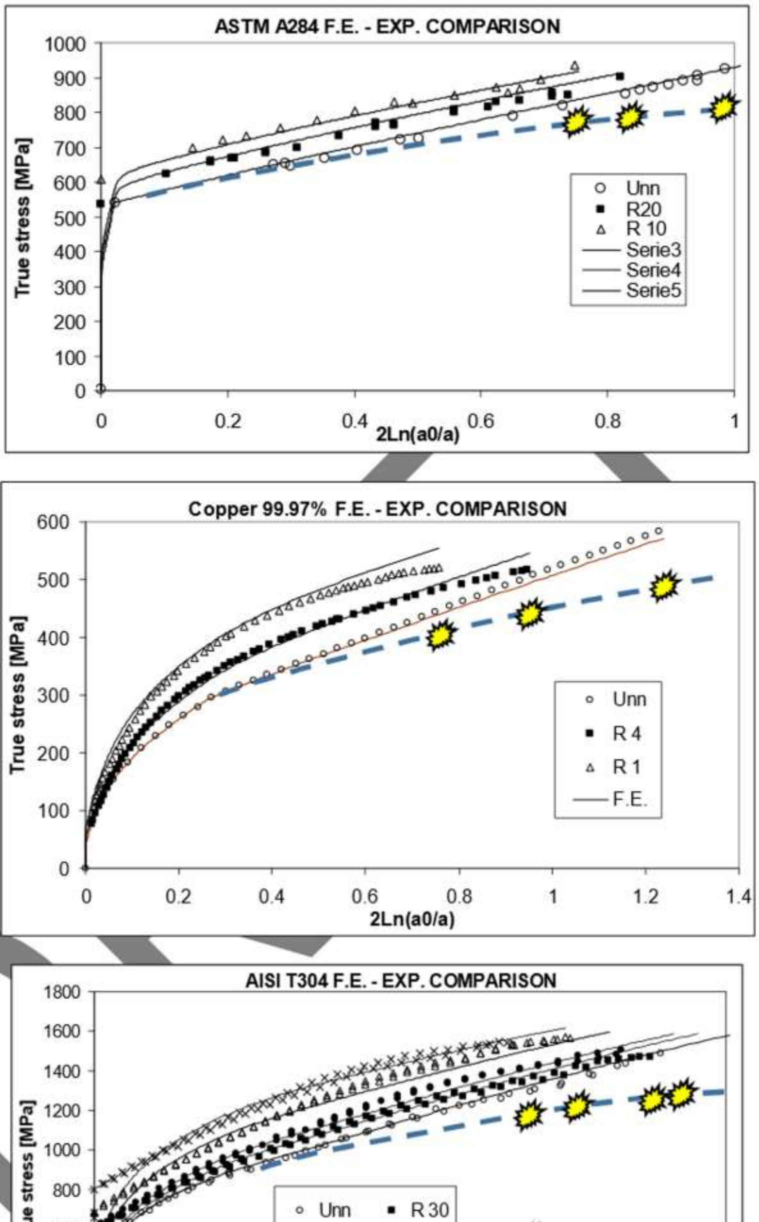

*Figure 4-14 Stress-strain cruves of smooth and notched tensile specimens of Annealed Copper, Fe370 and Stainless AISI304 steel*

As clearly visible in all figures, the sharper is the notch of a specimen the higher is its true curve.

This is because sharper notches induce greater amounts of $\sigma_H$ for each given $\sigma_{Eq}$ or, in other words, greater amount of stress triaxiality $TF$. Larger $\sigma_H$ also increase the axial stress $\sigma_Z$ together with the corresponding values of the current tensile force and the current $\sigma_{True}$.

Qualitative plots of $\varepsilon_{Eq}$ and $TF$ along the noralized radial abscissa of the neck section are reported in Figure 4-15 for smooth and notched specimens.

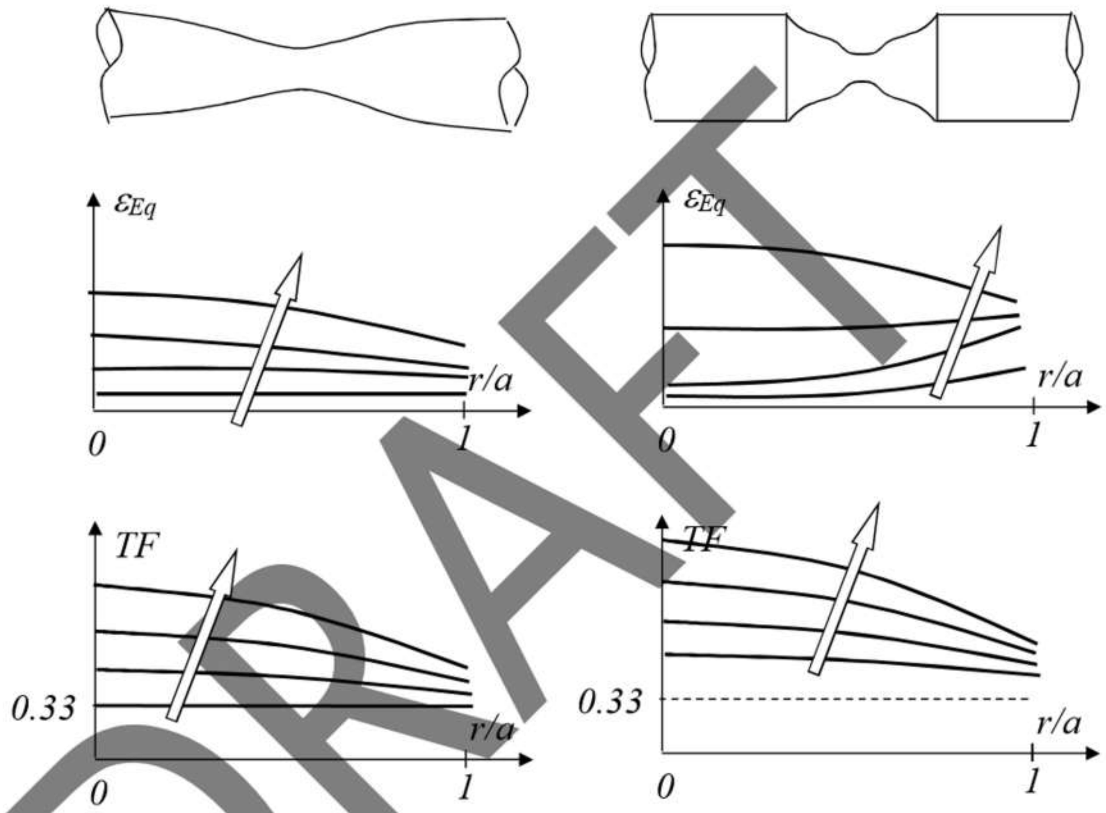

Figure 4-15Qualitative rRadial distribuition of $\varepsilon_{Eq}$ and $TF$ along the normalized neck radius r/a at different test stages

The same sharper notches so greatly affecting the true cruves do not affect the whole material curve, while only moving back and forth the failure points along such latter curve. Greater $TF$ generally means faster damage growth and lower failure strain, as if ductile materials tend to become fragile at higher stress triaxialities.

It is worth recalling that, for smooth and notched cylindrical tensile specimens, the nonuniformity of $\varepsilon_{Eq}$ along the radial abscissa is low enough that the strain can be assumed uniform and then $\varepsilon_{Eq} \approx \varepsilon_{True}$.

The stress triaxiality of smooth specimens remains equal to 1/3 until necking onset, then it grows until failure. For notched specimens similar trend occur with $TF > 1/3$ but constant until necking onset, then again increasing until failure.

The histories of $TF$ at the neck center during different experiments on smooth and notched specimens performed at UniCT are reported in the figures below.

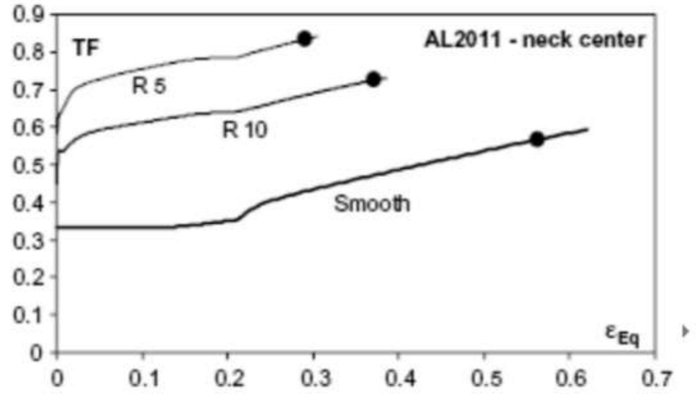

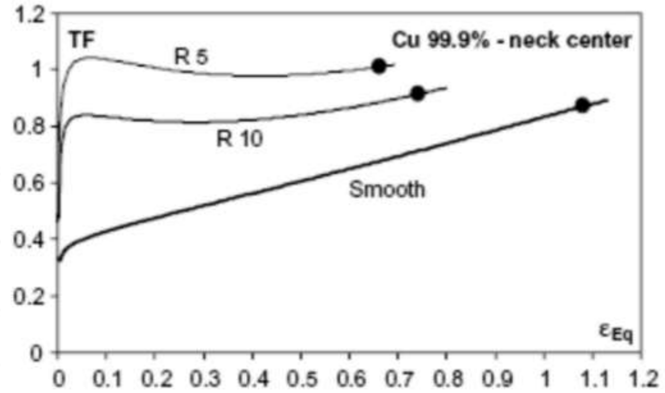

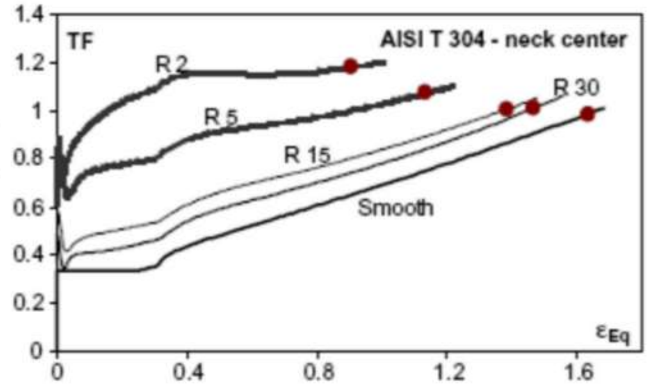

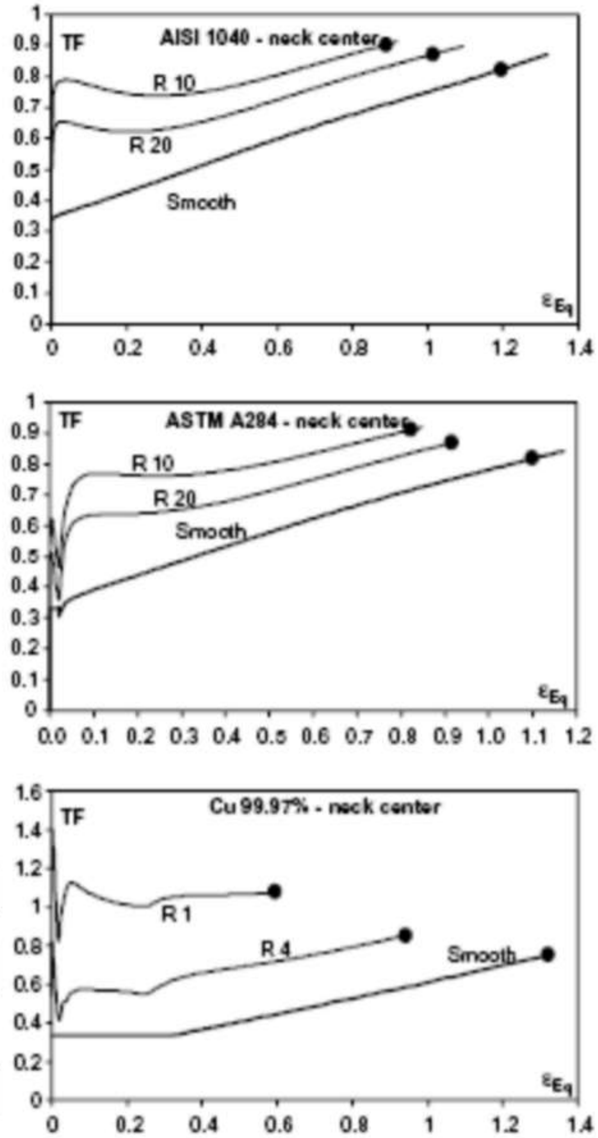

Figure 4-16 Triaxiality histories from different tensile tests . Mirone (2007)

Metals like the AL2011, AISI304 and CU99.97% (annealed) exhibit moderately late necking therefore the $TF$ of smooth specimens remains equal to 0.33 at initial stages of tests (e.g. respectively until strains of 0.2, 0.35 and 0.38).

Instead the 99.9% Copper (cold-worked), the AISI1040 and the ASTM A284 steels exhibit early necking and the $TF$ already starts increasing at the beginning of the tests.

Summarizing, the initial damage models by Mc-Clintok and by Rice-Tracey demonstrated that:

1) The same material can fail at different local values of $\varepsilon_{Eq} = \varepsilon_f$ (and $\sigma_{Eq} = \sigma_f$)

2) The parameter mainly affecting local failure initiation is the $TF$ : the greater it is, the faster grows the damage and the more anticipated is failure (the smaller is the failure strain $\varepsilon_f$).

In 1976 Mackenzie, Hancock and Brown shown the results of their extensive research with different smooth and notched steel specimens highlighting that, depending on the notch severity, the failure strain can decrease, as visible in Figure 4-17, from more than 0.7 of the notched specimen to less than 0.2 of the sharpest notch.

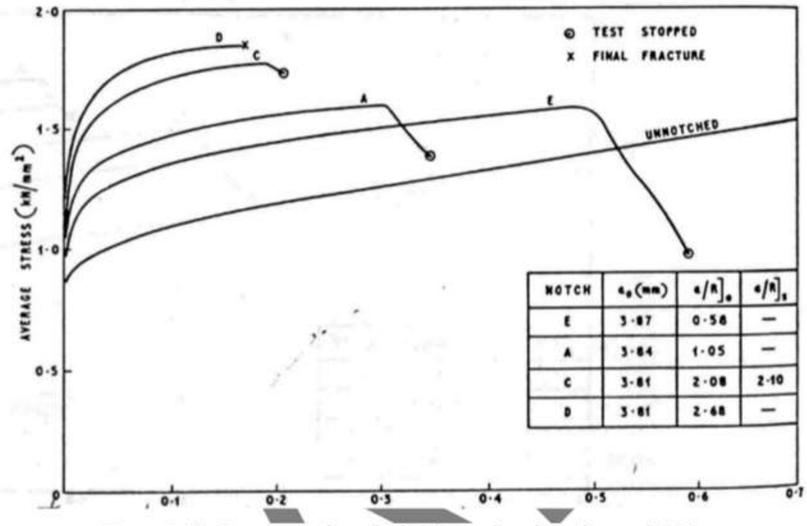

| NOTCH | $a_0$ (mm) | $a/R]_0$ | $a/R]_s$ |
|---|---|---|---|
| E | 3·87 | 0·58 | — |
| A | 3·84 | 1·05 | — |
| C | 3·81 | 2·08 | 2·10 |
| D | 3·81 | 2·68 | — |

Figure 4-17: Experimental results by Hancock and Mackenzie (1976)

In some of such curves is also visible a decreasing branch of the true cruves: such descending segments describe the fracture evolution which usually originates at the neck center and propagates all over the cross section.

In fact, as far as the cross section is "healthy" and not affected by macroscopic inner/outer cracks, the true stress always increases: when failure initiates at neck center a hole or a crack starts developing without being visible from outside, so the effective cross section decreases together with the resisting force, although the effective load/area ratio continues to increase. The apparent cross section detectable from outside is greater than the effective one while the measured load is the effective one, so the apparent load/area ratio starts to decrease.

Whenever a cross section-based true curve starts decreasing without temperature or other softening effects, an inner fracture is propagating inside the cross section: in such cases the beginning of fracture must be taken as the material limit, at the peak of the true curve with the corresponding failure strain.

The relationship between failure strains and stress triaxiality is reported in Figure 4-18 from the paper by Hanckck and Mackenzie, each curve an orientation of the orthotropic steel they tested.

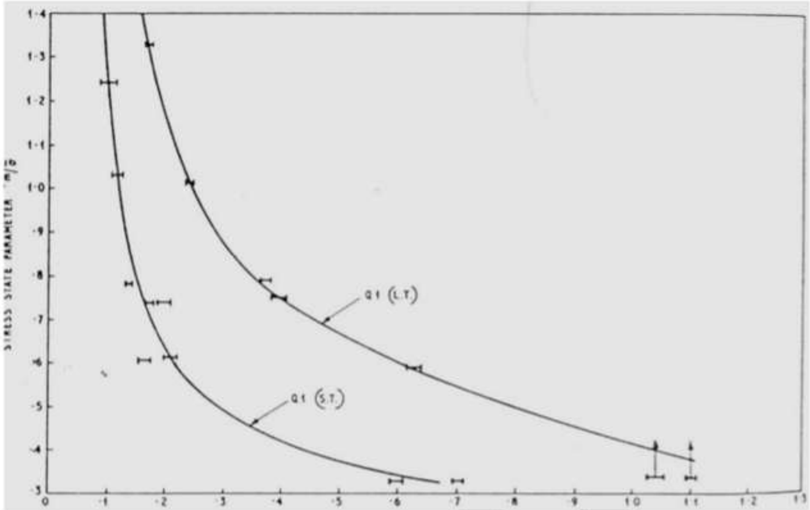

*Figure 4-18 Fracture strain vs. triaxiality values by Hancock and Mackenzie (1976)*

For describing the trend of $\varepsilon_f$ vs. $TF$ HAnckock and Mackenzie also proposed a relationship (HM model) based on the findings by Rice and Tracey:

$$\varepsilon_f = \varepsilon_{nucl} + \alpha \cdot Exp(-\frac{3}{2}TF) \qquad (4\text{-}9)$$

Where $\varepsilon_{nucl}$ and $\alpha$ are two material constants respectively expressing a nucleation strain where voids start being generated and a scale factor. According to this model large $TF$ clearly anticipate failure by decreasing the failure strain $\varepsilon_f$.

The outcome of the HM model calibrated for another material along short transverse and long transverse directions is compared to experiments in Figure 4-19.

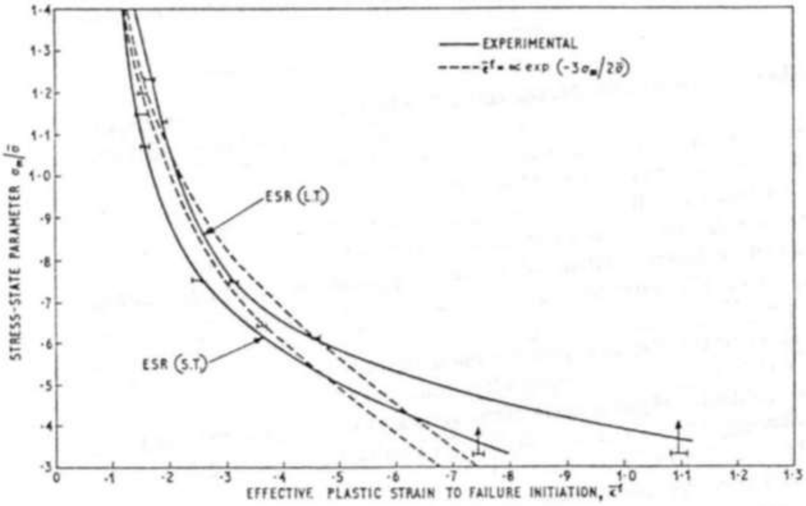

*Figure 4-19: Failure model by Hanckick and Mackenzie compared to experimental data*

As also the authors highlighted, a limit of such model was that the $TF$ was calculated at the beginning of each test and then assumed to be constant, while, instead, it is highly variable as the necking takes place as already pointed out before (see Figure 4-16). The consequences of assuming $TF = constant$ were that the model accuracy was either good at high triaxialities or at low triexialities, while not being able to accurately capture the failure strains at whatever $TF$.

Probably an integral-cumulative form of the HM model incorporating the variability of $TF$ might be much more versatile and suitable for better capturing failure at extreme triaxiality ranges.

Finally, some considerations about local quantities involved with failure.

The triaxiality factor TF in a cylindrical tensile specimen without any notch (smooth bar) is always maximum at the neck center, in fact failure often initiates at that material point.

Propagation of fracture to the entire cross section is quite fast but further strain occurs in the points surrounding the center area. So, when the specimen is completely broken in two halves, the fracture in the center area occured earlier than it does in the neighbours, and, in other words, fracture in center zone of the neck section is somehow more fragile than it is in the outer points of the neck section.

Then fracture surface of smooth bars has the typical "cup and cone" shape below:

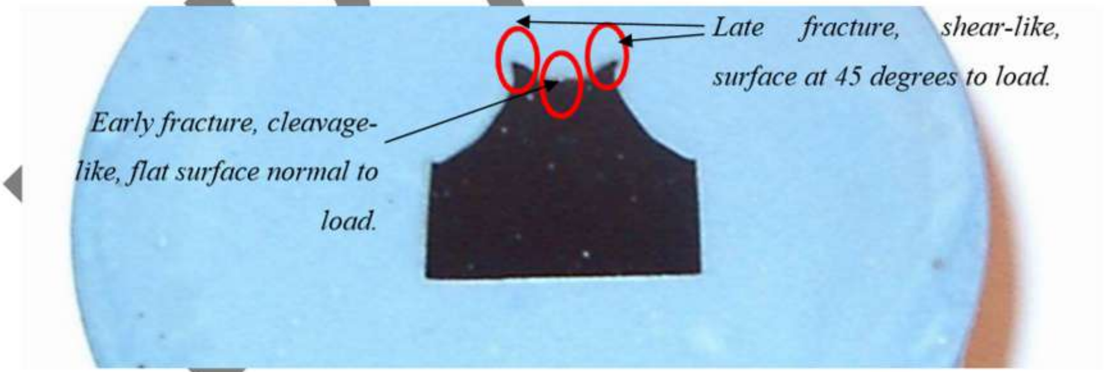

*Figure 4-20: typical cup-cone fracture of round tensile specimens - Mirone (2007)*

In Figure 4-20 is shown the half of a notched specimen exhibiting the cup-like surface, the other half obviously exhibits a cone-like fracture.

The initial flat fracture occurs at the equivalent strain $\varepsilon_f$; at such stage of the test the specimen still seems to be unbroken from outside, but it has a hole inside whose diameter corresponds to the flat fracture, therefore the effective resisting section is smaller than the apparent one.

Then fracutre propagates towards the outer surface of the specimen and further strains may occur in such zones.

In Figure 4-21 is also reported a couple of micrographs taken at the University of Catania from a smooth specimen of 99.9 Copper and from an R2-notched specimen of AISIT304 steel.

Large and more circular voids are always located close to the neck center (high triaxiality ensures that void volume increase is greater than the void shape variation), while, at outer radii of the neck section, no voids (notched bar fails too soon) or just smaller elongated voids (smooth bar fails late enough to nucleate and distort voids close to the outer surface) are present. This also is in agreement with the overall explanation provided by Rice and Tracey.

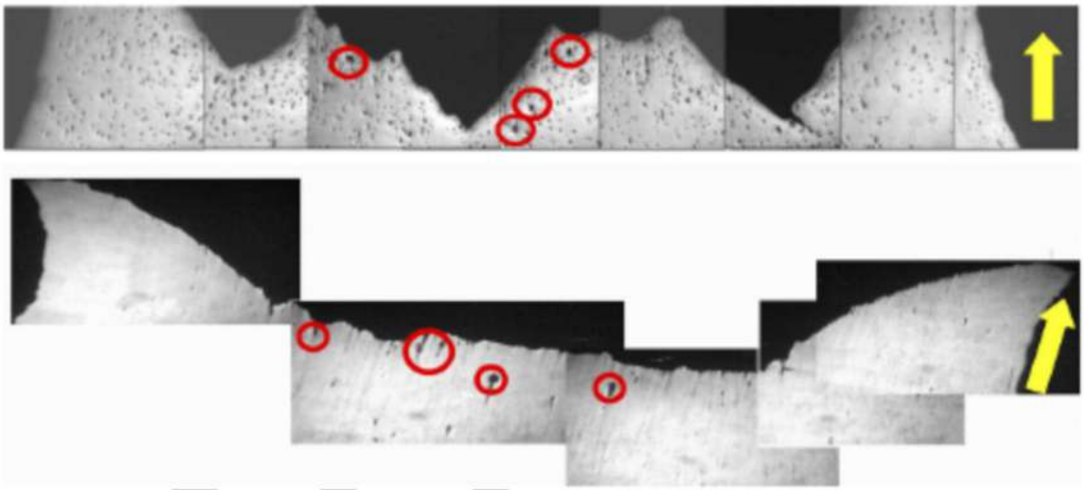

Figure 4-21 Micrographs of polished fractured specimens showing microvoids – Mirone (2007)

Beyond the introductory studies by Mc Clintock, Rice and Tracey, Hancock Mackenzie and Brown, two main approaches developed giving birth to the Damage Mechanics as an alternative to the Fracture mechanics; the latter was an already consolidated scientific segment of the material science in the seventies of 20th century, but it was not suitable for dealing with ductile structural metals.

The precursors of such two approachese to damage mechanics were Lemaitre-Cachanov (originating the Continuous Damage Mechanics) and Gurson-Tvergaard (originating the family of microvoids-based damage models).

After year 2000 a new family of damage models was introduced by the research group of prof. Wierzbicki at MIT, usually addressed as “Phenomenological Damage Models”.

## 4.4 CONTINUOUS DAMAGE MECHANICS (CDM) –INTRODUCTION AND LEMAITRE MODEL

In tutti i modelli derivati dalla trattazione di Lemaitre la variabile che quantifica il danneggiamento, pur essendo intimamente legata alla frazione di volume dei vuoti nel materiale non è definita esattamente come la porosità istantanea ma piuttosto come la frazione di superficie resistente elementare occupata da vuoti, quindi è legata alla intersezione (bidimensionale) che la sezione resistente ha con i vuoti tridimensionali all'interno del materiale, come indicato in Figura 4.1.1.

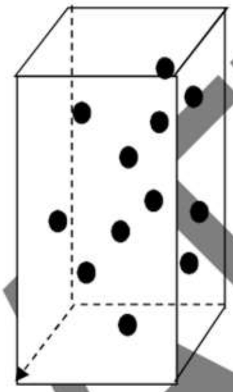

Definite come in figura le superfici attive e quelle "vuote", l'espressione analitica della variabile di danneggiamento D è:

$$D = \frac{S_D}{S} \qquad 4.1.1$$

Il valore che può assumere tale variabile ovviamente è compreso nell'intervallo (0,1), anche se i valori estremi, corrispondenti rispettivamente a materiale assolutamente compatto ed a materiale totalmente fratturato, non sono raggiungibili nella pratica considerato che, come accennato in precedenza, le condizioni di rottura si considerano raggiunte nell'istante in cui nel materiale ancora parzialmente integro e quindi caratterizzato da D<1, si innesca il processo incontrollabile e rapidissimo che comporta la caduta della tensione "true" sopportabile e la separazione fisica delle parti di materiale. Nel caso di comportamento isotropico del materiale anche in termini di evoluzione dei vuoti, il danno è quantificabile con lo scalare D ma, la stessa definizione è estensibile a variabili tensoriali quando le caratteristiche del materiale lo richiedano.

Da questa identificazione della variabile di danno segue che la tensione che sollecita i vari punti della sezione resistente elementare non è più pari a quella "macroscopica" *F/S* ma, in prima approssimazione, si può supporre che i vuoti interni costituiscano una riduzione di sezione non accompagnata dalle concentrazioni tensionali (FIGURA) caratteristiche di ogni discontinuità,

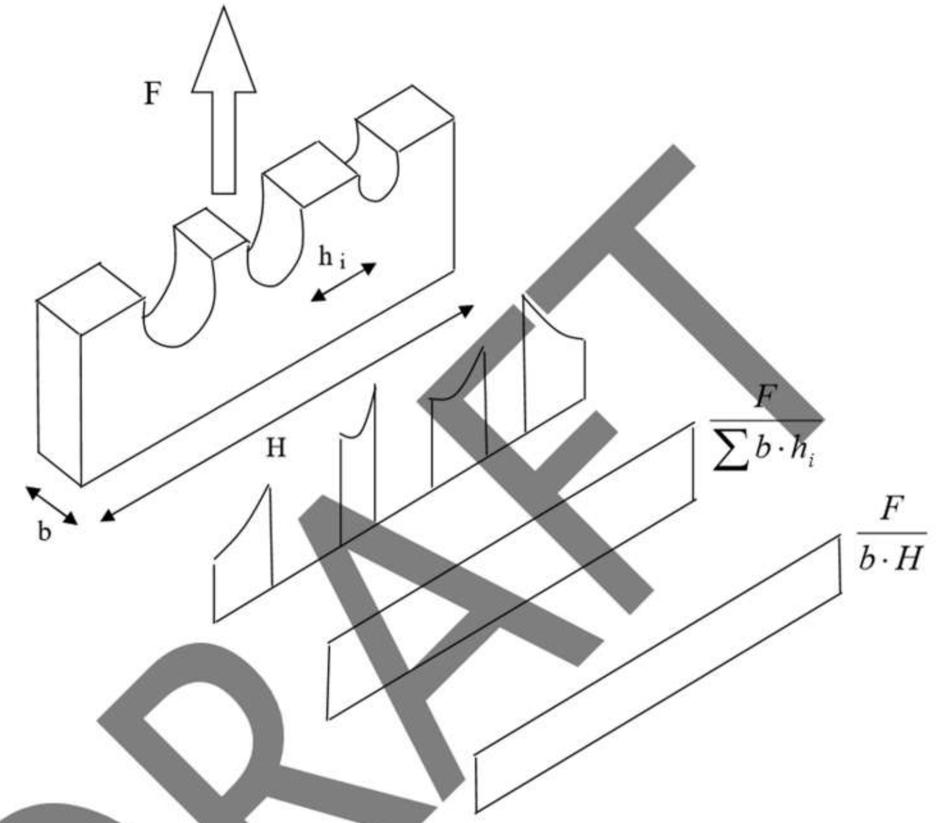

per cui la tensione effettiva diventa

$$\breve{\sigma} = \frac{F}{S - S_D} = \frac{F}{S\left(1 - \frac{S_D}{S}\right)} = \frac{F}{S(1-D)} = \frac{\sigma}{1-D} \qquad 4.1.2$$

Una utile conseguenza di come sono state definite queste variabili, è che da misurazioni del modulo elastico "apparente" in prove di trazione si può risalire al valore di danno secondo il criterio seguente:

$$\varepsilon^{el} = \frac{\breve{\sigma}}{E} = \frac{\sigma}{E(1-D)} = \frac{\sigma}{\breve{E}}$$

*quindi* 4.1.3

$$D = 1 - \frac{\breve{E}}{E}$$

Il modulo elastico soprasegnato è il modulo apparente nel senso che è quello misurato localmente in direzione *longitudinale* (*tramite strain gages* ) durante il generico ciclo di scarico del provino in avanzata fase plastica, per cui è indicativo di una rigidezza che corrisponde al materiale contenente una certa quantità di vuoti ovvero danneggiato, mentre $E$ è il modulo elastico del materiale vergine, in cui la porosità è solamente quella intrinseca del materiale.

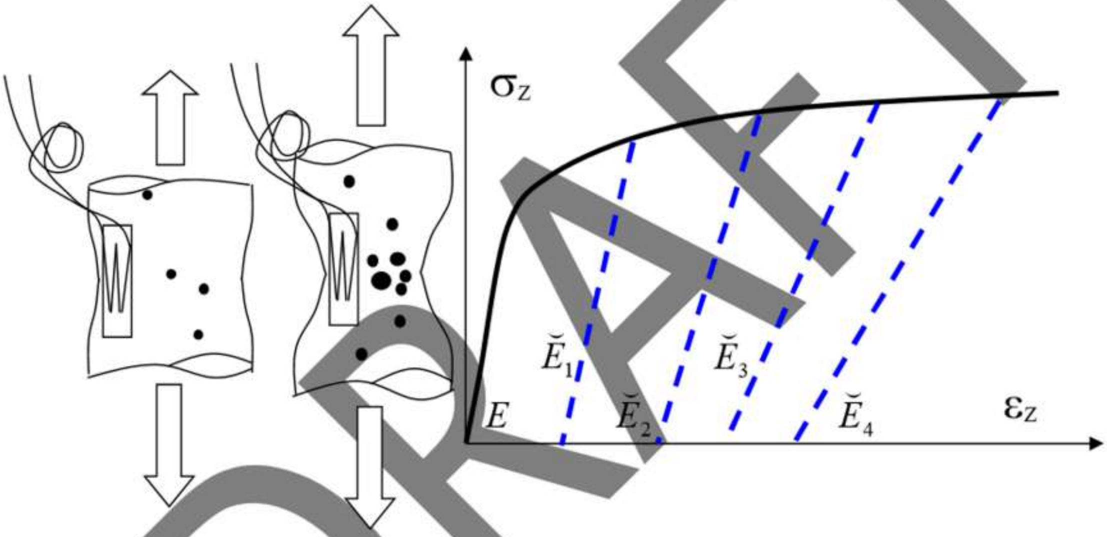

Ovviamente, la curva sperimentale ottenuta con gli estensimetri assomiglia alla curva true solo se l'estensimetro è applicato sulla sezione ristretta, e la coincidenza perfetta tra curva estensimetrica e curva true si avrebbe solamente per estensimetro di dimensioni infinitesime.

Inoltre un solo estensimetro non può seguire le deformazioni tipiche di materiali duttili (a qualche % perde efficacia e/o si scolla) quindi vengono incollati vari estensimetri in successione sulla stessa zone di provino.

La determinazione del legame che intercorre tra la variabile $D$ e le altre che caratterizzano il comportamento del materiale, passa attraverso la identificazione di un potenziale che, analogamente a quanto visto nei capitoli precedenti relativi al modello di comportamento elasto-plastico, metta in relazione tutte le variabili termodinamiche del fenomeno.

A questo proposito, per cominciare si riporta la distinzione fatta da Lemaitre tra variabili osservabili, variabili interne e variabili associate, secondo lo schema seguente:

| | | VARIABILI ASSOCIATE |
|---|---|---|
| Osservabili | Interne | |
| $\boldsymbol{\varepsilon}$ | | $\boldsymbol{\sigma}$ |
| T | | S |
| | $\boldsymbol{\varepsilon}^e$ | $\boldsymbol{\sigma}$ |
| | $\boldsymbol{\varepsilon}^p$ | $-\boldsymbol{\sigma}$ |
| | r | R |
| | $\mathbf{a}$ | $\mathbf{X}$ |
| | D | Y |

Le singole variabili, a parte quelle già definite come il tensore degli sforzi $\sigma$ o il danno $D$, sono:

- $\boldsymbol{\varepsilon}^e$ tensore di deformazione elastica, è la componente elastica del tensore di deformazione totale;
- $\boldsymbol{\varepsilon}^p$ tensore di deformazione plastica, componente plastica del tensore di deformazione totale;
- $\boldsymbol{\varepsilon}=\boldsymbol{\varepsilon}^e+\boldsymbol{\varepsilon}^p$ tensore di deformazione totale;
- r deformazione plastica cumulativa, scalare, ha le dimensioni di una deformazione (adimensionale) ed è la variabile che "pilota" l'evoluzione dell'hardening isotropico;
- **a** tensore di backstrain, è il tensore che rappresenta la deformazione che "pilota" l'evoluzione dell'hardening cinematico;
- R tensione di hardening isotropico, scalare, dimensionalmente è uno stress;
- **X** tensore di hardening cinematico, detto backstress, dimensioni di una tensione;
- Y densità di potenza di deformazione rilasciata, dimensionalmente è un lavoro, e corrisponde alla quanttà di energia liberata dal volume elementare a causa della perdita di rigidezza conseguente al crescere del danno.
- T temperatura del punto materiale;
- S entropia del punto materiale;

Il potenziale che, nell'ambito della "State Kinetic Coupling Theory", è utilizzato per ricavare il legame costitutivo elastoplastico di un materiale dotato di hardening isotropico e cinematico lineare, e soggetto a danneggiamento, ha la forma seguente:

$$F = \left(\breve{\boldsymbol{\sigma}}^{D} - \mathbf{X}\right)_{eq} - R - \sigma_y + F_D \qquad 4.1.4$$

Chiaramente la forma è la stessa del potenziale visto nel Cap. 2, a meno del fatto che adesso la variabile *D* influisce sulla tensione e che compare un nuovo termine $F_D$ che è responsabile della evoluzione del danneggiamento.

Considerato che una ipotesi preliminare sul termine $F_D$ è che in esso non compaiono esplicitamente i termini **σ**, **X** ed R, il legame di dualità tra variabili interne e variabili associate che resta determinato dal potenziale considerato è, per quanto riguarda le correlazioni tra deformazioni (plastica ed elastica), tensioni ed hardening, pressoché identico a quello già visto nel Cap. 2, solo che adesso è entrata in gioco la variabile *D* per cui:

$$d\varepsilon_{ij} = \frac{\partial F}{\partial \sigma_{ij}} d\varepsilon_{Eq}\left(1 - D\right) \qquad 4.1.5$$

Il moltiplicatore di plasticità λ resta sempre individuato dalla:

$$d\lambda = \frac{\left(C\dfrac{\partial f}{\partial \boldsymbol{\sigma}}\right)}{-\left(\dfrac{\partial f}{\partial \boldsymbol{\alpha}}\right) h(\boldsymbol{\alpha}, \boldsymbol{\sigma}) + \left(\dfrac{\partial f}{\partial \boldsymbol{\sigma}}\right) C \left(\dfrac{\partial g}{\partial \boldsymbol{\sigma}}\right)} d\boldsymbol{\varepsilon}$$

Con f funzione di snervamento ed F potenziale dissipativo che adesso contiene qualcos'altro (legato alla presenza del danno), oltre alla suddetta funzione.

Il potenziale FD deve poter esprimere la generica forma della legge di evoluzione del danno secondo una normality rule:

$$dD = \frac{\partial F_D}{\partial Y} \cdot d\lambda = \frac{\partial F_D}{\partial Y} \cdot d\varepsilon_{Eq} \cdot (1-D) \qquad 4.1.9$$

Dove la grandezza Y non ancora identificata dev'essere "duale" del danno nel senso dello stesso potenziale *Fd*.

The Lemaitre damage is related to something similar to the release of elastic strain energy (it's not a case if strain gage misurements can be used for measuring damage), then, a reasonable candidate for the function Y is expressed as follows:

$$Y = -\frac{1}{2} \cdot C_{ijkl} \cdot \varepsilon^e{}_{ij} \cdot \varepsilon^e{}_{kl} \qquad 4.1.6$$

Considerando che l'espressione dell'energia di deformazione elastica nel materiale danneggiato è:

$$\omega_e = \int \sigma_{ij} d\varepsilon^e{}_{ij} = \int C_{ijkl} \varepsilon^e{}_{kl} (1-D) d\varepsilon^e{}_{ij} = \frac{1}{2} C_{ijkl} \varepsilon^e{}_{kl} \varepsilon^e{}_{ij} (1-D) \qquad 4.1.7$$

diventa facile verificare che

$$Y = \frac{1}{2} \frac{\partial \omega_e}{\partial D}\bigg|_{\sigma = \cos t} \qquad 4.1.8$$

ovvero la variabile Y è proprio pari alla riduzione di energia elastica che si ha nel materiale quando questo subisce un incremento infinitesimo di danno mentre è sottoposto ad una tensione costante. SIMILAR TO THE G PARAMETER OF FRACTURE MECHANICS !!!!!

In pratica, per ricavare l'evoluzione del parametro di danno si è scelta una variabile duale che è funzione dell'energia di deformazione elastica perché l'effetto macroscopico del danno è, come visto, una riduzione del modulo di elasticità della sezione lorda e quindi proprio una perdita di energia di deformazione elastica.

Quindi, sulla base delle seguenti considerazioni pratiche Lemaitre ha costruito la prima forma di funzionale in grado di far scaturire la variabile danno.

- L'ammontare del danno è sempre correlato ad una forma di deformazione accumulata irreversibilmente, e di questo si tiene già conto con il termine $\varepsilon_{Eq}$ che compare nella 4.1.9.
- Quando la deformazione plastica equivalente inizia a crescere, è ragionevole pensare che la porosità del materiale ed il danno correlato non crescano sino al raggiungimento di una soglia

di deformazione $p_0$. Precedentemente a tale situazione, le irreversibilità legate alla deformazione plastica servono a far accumulare micro-stress o dislocazioni che successivamente genereranno microcricche. Questo aspetto può essere riprodotto inserendo in $F_D$ una funzione gradino o "Heavyside Function" del tipo $H|_{p_0}$.

- La velocità di crescita del danno è fortemente dipendente dal fattore di triassialità della sollecitazione agente, definito come il rapporto tra tensione idrostatica $\sigma_H$ e tensione equivalente $\sigma_{eq}$. Questa dipendenza è già presente nel termine Y, infatti scomponendo il generico tensore degli sforzi nelle sue componenti idrostatica $\sigma_H$ e deviatorica $\boldsymbol{\sigma}^d$ si ha:

$$\begin{aligned} Y &= \frac{1}{1-D}\int \sigma_{ij}\, d\varepsilon^{e}_{ij} = \frac{1}{1-D}\left[\int \boldsymbol{\sigma}^{d}_{ij}\cdot d\boldsymbol{\varepsilon}^{e\ d}_{ij} + \delta_{ij}\delta_{ij}\int \sigma_H \cdot d\varepsilon^{e}_{H}\right] = \\ &= \frac{1}{2(1-D)}\left[\frac{1+\nu}{E}\cdot\frac{\boldsymbol{\sigma}^{d}_{ij}\boldsymbol{\sigma}^{d}_{ij}}{1-D} + 3\cdot\frac{1-2\nu}{E}\cdot\frac{\sigma_H^{2}}{1-D}\right] = \\ &= \frac{\sigma_{eq}^{2}}{2E(1-D)^{2}}\left[\frac{2}{3}(1+\nu) + 3(1-2\nu)\left(\frac{\sigma_H}{\sigma_{eq}}\right)^{2}\right] = \frac{\sigma_{eq}^{2}}{2E(1-D)^{2}}R_\nu \end{aligned} \qquad 4.1.10$$

Il termine $R_\nu$ è detto funzione di triassialità dato che contiene al suo interno il fattore di triassialità TF ($\sigma_H/\sigma_{eq}$) definito precedentemente.

- Una relazione generica e qualitativa tra la velocità di danneggiamento e l'energia rilasciata è ottenibile considerando lineare il loro legame, per cui il potenziale sarà quadratico rispetto ad Y;

Tenendo conto di quanto esposto sopra il potenziale proposto da Lemaitre è:

$$F_D = \frac{Y^2}{2S(1-D)}\cdot H|_{\varepsilon_{Eq0}} \qquad 4.1.11$$

dove il termine al numeratore *2S* è scelto come costante di scala del materiale.

Pertanto, applicando la 4.1.9 alla 4.1.11 si ottiene la legge evolutiva del danno secondo Lemaitre, a partire dalla quale si sono sviluppate e continuano a nascere a tutt'oggi numerose varianti nelle quali si ritrovano piccoli o grandi "improvements" con i quali si tende a svincolare la trattazione dalle ipotesi semplificative che idealizzano il modello:

$$dD = \frac{\partial F_D}{\partial Y} \cdot d\varepsilon_{Eq} \cdot (1-D) = \frac{Y}{S} d\varepsilon_{Eq} \cdot H(\varepsilon_{Eq} - \varepsilon_{Eq\,0})$$

$$D(\varepsilon_{Eq}) = \int_0^{\varepsilon_{Eq}} \frac{Y}{S} d\varepsilon_{Eq} H\Big|_{\varepsilon_{Eq0}} = \int_0^{\varepsilon_{Eq}} \frac{\sigma_{eq}{}^2}{2ES(1-D)^2} R_v \cdot d\varepsilon_{Eq} \cdot H\Big|_{\varepsilon_{Eq0}} \qquad 4.1.12$$

Come <u>caso particolare</u>, se il materiale <u>è plastico ideale</u> oppure il danno comincia a crescere "tardi", quando l'hardening è piuttosto saturato ($\sigma_{eq}$ quasi indipendente da $\varepsilon_{eq}$) e se la sollecitazione rientra nella categoria del "<u>**proportional loading**</u>" (direzioni principali e quindi fattore di triassialità costanti), allora il danno risulta crescere linearmente con la deformazione plastica equivalente:

$$D(\varepsilon_{Eq}) = \frac{\sigma_{eq}{}^2}{2ES(1-D)^2} \int_0^{\varepsilon_{Eq}} d\varepsilon_{Eq} \cdot H\Big|_{\varepsilon_{Eq0}} = \frac{\widetilde{\sigma}_{eq}{}^2}{2ES} \cdot \left(\varepsilon_{Eq} - \varepsilon_{Eq\,0}\right)$$

I parametri che compaiono, S e □eq0, caratterizzano il materiale agli effetti del danneggiamento e sono da ricavare sperimentalmente, ad esempio, per quanto riguarda il termine S, tramite misurazioni del modulo di elasticità durante fasi di scarico all'interno di una prova di trazione.

Per quanto riguarda invece la <u>determinazione del valore **$\varepsilon_{eq0}$**</u>, deformazione di soglia a partrire dalla quale cui inizia a crescere il danno, come quasi tutte le grandezze relative alla crescita dei vuoti, anche questa secondo Lemaitre è variabile con la triassialità della sollecitazione. Pertanto, una volta determinato il valore $\varepsilon_{Uni\_0}$ relativo alla prova di trazione semplice sul materiale, per ricavare il valore $\varepsilon_{Tri\_0}$ corrispondente al generico carico triassiale occorre individuare analiticamente il fenomeno che comporta l'inizio della crescita di $D$.

In tal senso Lemaitre ipotizza che l'avvio del danneggiamento è legato al raggiungimento di un valore dell'energia di deformazione plastica immagazzinata irreversibilmente dal materiale (pari a quella complessivamente introdotta con la deformazione plastica meno la parte che viene dissipata in calore) che è caratteristico del materiale ovvero indipendente dalla triassialità.

$$\omega_{th} = \int_0^{\varepsilon_{ij}} \sigma_{ij} d\varepsilon_{ij} - \int_0^{\varepsilon_{Eq}} \sigma_y d\varepsilon_{Eq} = \int_0^{\varepsilon_{Eq}} \left(\sigma_{eq} - \sigma_y\right) d\varepsilon_{Eq}$$

In alcuni casi, lo yield stress su scala locale è approssimabile con il limite di fatica.

Se il materiale è plastico ideale ($\sigma_{eq}$ costante) sollecitato in campo rispettivamente monoassiale e pluriassiale, nell'ipotesi che lo stress di soglia monoassiale sia l'ultimate strength, la 4.14 all'istante in cui si raggiunge la deformazione di soglia sarà:

$$\omega_{th} = \left(\sigma_{u\_1} - \sigma_f\right)\varepsilon_{Th\_Uni} = \left(\sigma_u - \sigma_f\right)\varepsilon_{Th\_Tri}$$

La costanza del valore di soglia di tale energia permette, misuratone sperimentalmente il valore per il caso monodimensionale, di ottenere la deformazione di innesco del danno per qualsiasi altro valore di triassialità imponendo che l'energia plastica non dissipata in calore abbia un unico valore comune.

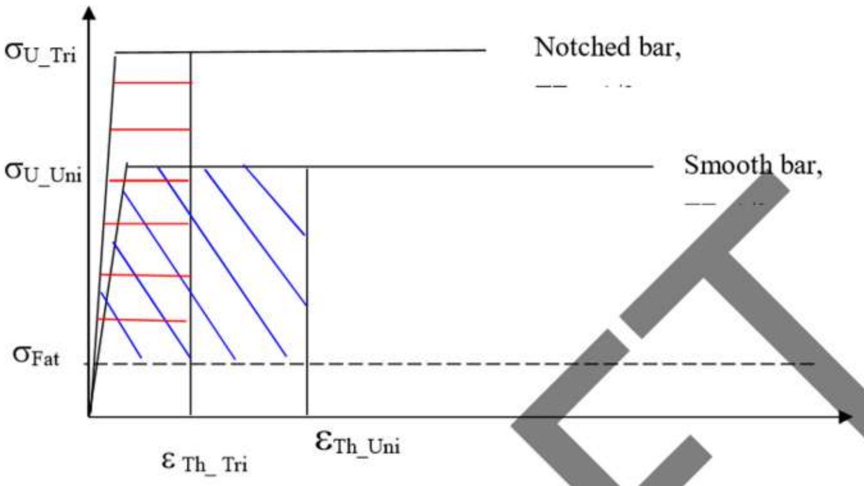

In caso di hardening non nullo non si fa più ricorso all'ultimate load ma si ricava ancora il threshold strain solo x il caso uniassiale, derivando gli altri con la costanza delle aree sottese dalla curva true:

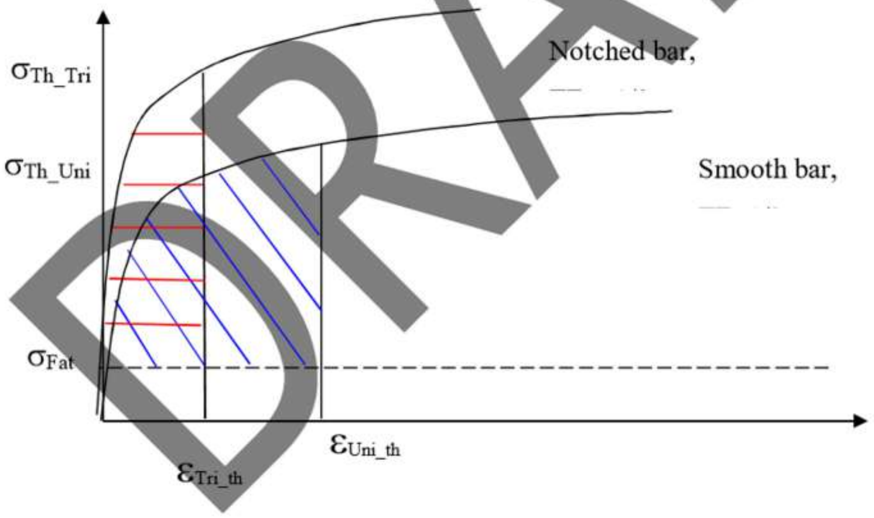

A questo punto, se la rottura della cella elementare di materiale avvenisse solo quando la superficie elementare è totalmente separata e D=1, allora il modello di danno così com'è basterebbe a prevedere la rottura ed a progettare di conseguenza

Invece la rottura su scala microscopica avviene quando il danno raggiunge un valore critico *Dcr<1*, che pertanto và ricavato per un dato materiale ed, eventualmente, anche per le diverse condizioni di rottura dello stesso materiale.

Secondo Lemaitre la rottura è determinato dal raggiungimento di un plafond nel rilascio di energia elastica, che è caratteristico del materiale. Secondo questa interpretazione, l'energia necessaria a formare o ad aumentare le superfici libere dei vuoti è esattamente quella fornita dalla perdita di rigidezza, ovvero l'energia elastica diventa un serbatoio di energia che viene quindi trasformata ad opera del fenomeno di danneggiamento. Non appena l'energia liberata dalla riduzione di rigidezza è cresciuta a tal punto da non poter essere tutta trasformata in nuove superfici di microvuoti o di decoesione delle impurità dalla matrice, il surplus di tale energia innesca l'instabilità che porta alla frattura della cella elementare. Nel modello di Lemaitre, l'andamento della densità energetica $Y$ al variare della deformazione plastica, tende a stabilizzarsi in prossimità della rottura sul valore caratteristico di cui sopra, indipendentemente dalla storia di carico del materiale. Analiticamente, la relazione ricavabile dalla ipotesi fatta è:

$$\int_0^{D_c} Y dD = \int_0^{D_c} \frac{{\sigma_{eq}}^2}{2E(1-D)^2} R_v dD = const. \qquad 4.1.15$$

Dopo aver determinato sperimentalmente un valore critico del danno, per esempio quello $D_{1c}$ relativo al caso monoassiale, la 4.1.15 permette di ottenere il valore del danno critico per qualunque altro andamento della triassialità del carico applicato: infatti uguagliando l'integrale precedente calcolato nel caso monoassiale a quello del caso multiassiale generico, si ricava la relazione che intercorre tra $D1c$ ed il generico $Dc$ al variare del parametro $R_v$ ovvero della triassialità.

Nel caso particolare di proportional loading uniassiale (trazione semplice con $R_v=1$) si ha:

$$\int_0^{D_{1c}} Y dD = \frac{\tilde{\sigma}^2{}_{eq\_u\_Uni}}{2E} D_{c\_Uni} \qquad 4.1.16$$

Per lo stesso materiale plastico ideale ma sottoposto adesso ad una generica triassialità costante (quindi sempre proprotional loading anche se non uniassiale):

$$\int_0^{D_c} Y dD = \frac{\tilde{\sigma}^2{}_{eq\_u\_Tri}}{2E} R_v D_{c\_Tri} \qquad 4.1.17$$

Uguagliando il valore ottenuto nel caso uniassiale ed in quello generico si ottiene:

$$D_{c\_Tri} = D_{c\_Uni} \cdot \frac{\sigma^2{}_{s\_u\_Uni}}{R_v \sigma^2{}_{s\_u\_Tri}}$$

4.1.18

Dove le tensioni equivalenti $\tilde{\sigma}^2_{eq\_u1}$ e $\tilde{\sigma}^2_{eq\_u}$ si riferiscono al valore che la curva costitutiva (unica per il dato materiale) assume a rottura del nelle due condizioni a differente triassialità:

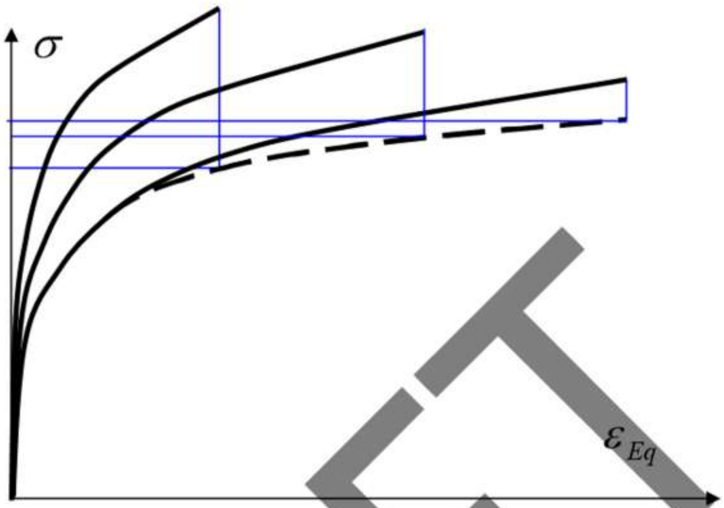

In questo caso, l'andamento del danno critico al variare della triassialità e dell'hardening (quest'ultimo influisce sulla differenza tra le tensioni), è il seguente:

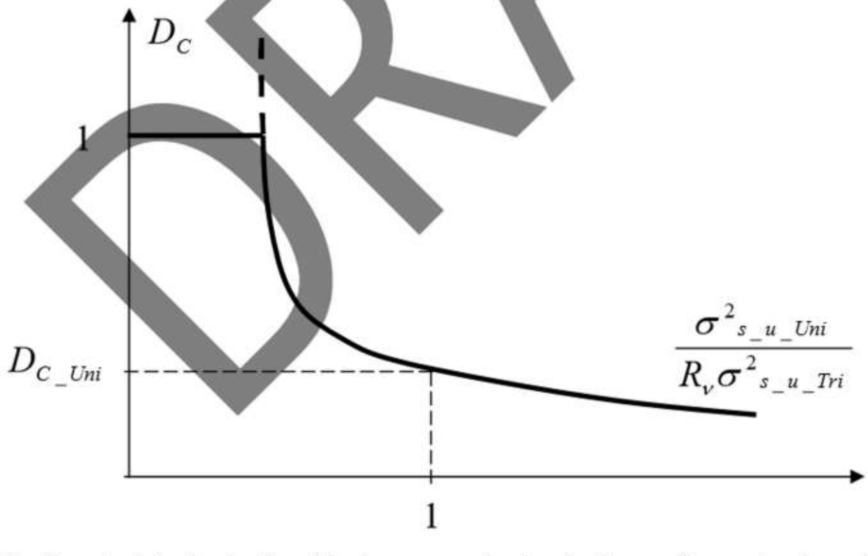

Se il materiale è plastico ideale ovvero ha hardening nullo, restando nella ipotesi di proportional loading si ha che la tensione equivalente a rottura ha un unico valore per qualunque triassialità, quindi :

$$D_c = \frac{D_{1c}}{R_\nu}$$

E la relazione diventa un ramo d'iperbole.

Noti sperimentalmente deformazione di soglia, deformazione critica e danno critico in caso monoassiale, $\varepsilon_{Th\_1}, \varepsilon_{Cr\_1,} D_{C\_1}$, se il materiale è plastico ideale allora il modello di danno di Lemaitre può essere espresso direttamente sotto forma di Criterio di Rottura per tutte le storie deformative a triassialità costante (proportional loading), ovvero legge che esprime direttamente la deformazione di Rottura locale al variare delle grandezze da cui essa dipende (strain plastico e triassialità):
L'espressione grezza della legge di danno in caso monoassiale e triassiale generico è:

$$D_{Uni}\left(\varepsilon_{Eq}\right) = \frac{{\sigma_{S\_Uni}}^2}{2ES} \cdot \left(\varepsilon_{Eq} - \varepsilon_{Th\_Uni}\right)$$

$$D\left(\varepsilon_{Eq}\right) = \frac{{\sigma_S}^2}{2ES} \cdot R_\upsilon \cdot \left(\varepsilon_{Eq} - \varepsilon_{Th}\right)$$

Esprimendo il valore a rottura della funzione di danno si ha:

$$D_{C\_Uni} = D_{Uni}\left(\varepsilon_{C\_Uni}\right) = \frac{{\sigma_{S\_Uni}}^2}{2ES} \cdot \left(\varepsilon_{C\_Uni} - \varepsilon_{Th\_Uni}\right) \Rightarrow \frac{{\sigma_{S\_Uni}}^2}{2ES} = \frac{D_{C\_Uni}}{\left(\varepsilon_{C\_Uni} - \varepsilon_{Th\_Uni}\right)}$$

$$D_C = D(\varepsilon_C) = \frac{{\sigma_S}^2}{2ES} \cdot R_\upsilon \cdot (\varepsilon_C - \varepsilon_{Th}) \qquad \Rightarrow \frac{{\sigma_S}^2}{2ES} = \frac{D_C}{R_\upsilon \cdot (\varepsilon_C - \varepsilon_{Th})}$$

Quindi sostituendo si ha la legge di danno "raffinata" per il caso particolare in esame (materiale perfettamente plastico e TF costante):

$$D_{Uni}\left(\varepsilon_{Eq}\right) = D_{C\_Uni} \cdot \frac{\left(\varepsilon_{Eq} - \varepsilon_{Th\_Uni}\right)}{\left(\varepsilon_{C\_1} - \varepsilon_{Th\_1}\right)}$$

$$D\left(\varepsilon_{Eq}\right) = D_C \cdot R_\upsilon \cdot \frac{\left(\varepsilon_{Eq} - \varepsilon_{Th}\right)}{\left(\varepsilon_C - \varepsilon_{Th}\right)}$$

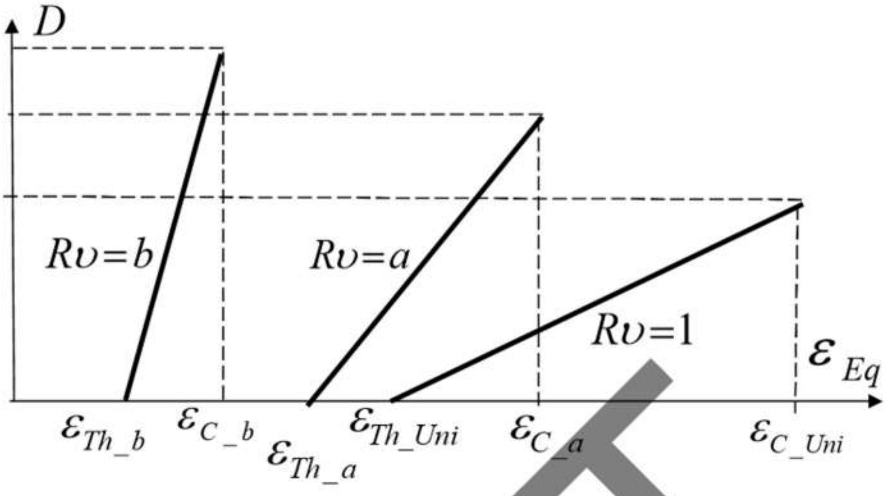

Se $D_C = D_{C\_Uni} = 1$ allora le deformazione a rottura soddisfa la seguente relazione:

$$\frac{\left(\varepsilon_C - \varepsilon_{Th}\right)}{\left(\varepsilon_{C\_Uni} - \varepsilon_{Th\_Uni}\right)} = \frac{1}{R_\upsilon}$$ e descrive i seguenti andamenti al variare di ν:

:

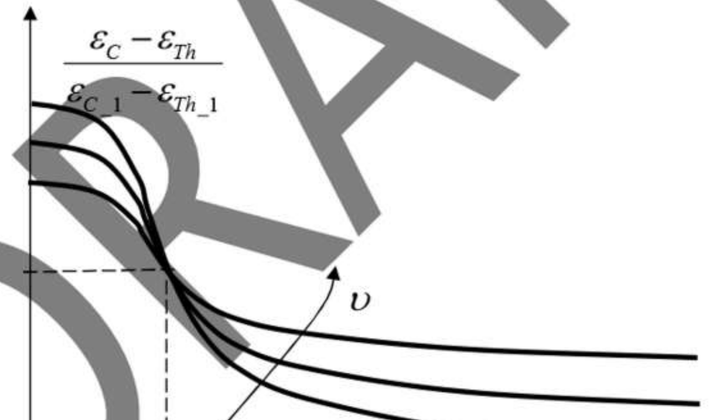

Si noti come le curve soprastanti assomigliano qualitativamente a quelle proposte in precedenza da Rice e Tracey ovvero da Hanckock e Mackenzie.

Se mai fosse stato necessario, ecco una ulteriore evidenza del fatto che elevate triassialità limitano la vita del materiale abbassandone la percentuale di vuoti compatibile con la capacità di sopportare carichi.\

## 4.5 OTHER CDM MODELS

A partire dalla data di creazione dei primi modelli di evoluzione del danno ad opera di Lemaitre, nella prima metà degli anni 80, se ne sono succeduti numerosi altri da parte di autori inquadrabili nella stessa scuola di pensiero, ognuno dei quali ha proposto variazioni alla forma di quella parte del potenziale dissipativo da cui deriva l'andamento della funzione *D*, ed al criterio di variazione del danno critico a causa delle diverse triassialità possibili.

Di seguito vengono discussi quattro tra i vari modelli che costituiscono lo sviluppo della trattazione di Lemaitre, e precisamente, in ordine cronologico, quelli dovuti agli autori W. H. Tai & B. X. Yang del 1986, W.T. Jun del 1992, S. Chandrakanth & P. Pandey del 1995, ed N. Bonora del 1997. Si premette che in tutti i modelli descritti di seguito vengono date per scontate le premesse che portano alla definizione del legame espresso dalla 4.1.9 in cui vengono associate le variabili di danno e di densità di energia elastica rilasciata, tramite il potenziale $F_D$.

**Modello di Bonora**

Il più recente dei modelli riportati risale al 1997 ed è dovuto ad un ricercatore Italiano, N. Bonora. Il potenziale dissipativo funzione del danno è:

$$F_D^{IV} = \frac{Y^2}{2ES^{IV}(1-D)} \frac{(D_c - D)^{\frac{\alpha-1}{\alpha}}}{\varepsilon_{Eq}^{2N+1}} \qquad 4.2.22$$

Il significato dei simboli è quello già descritto precedentemente ma, ovviamente, il fatto che le costanti *S* ed $\alpha$ vengano differenziati da un modello all'altro tramite apici serve a sottolineare che sono costanti che hanno espressioni analitiche e significati fisici diversi in ognuna delle teorie esposte. Applicando la normality rule tra funzione di danno e densità energetica $Y$, e successivamente sostituendo a tale fattore la sua espressione in termini di tensione equivalente, modulo elastico e danno *D,* si ottiene:

$$dD = \frac{\sigma_{eq}^2}{2ES^{IV}(1-D)^2} R_\nu \frac{(D_c - D)^{\frac{\alpha-1}{\alpha}}}{\varepsilon_{Eq}^{2N+1}} d\varepsilon_{Eq} \qquad 4.2.23$$

Se la curva costitutiva è di tipo esponenziale $\sigma_{Eq} = K \cdot \varepsilon_{Eq}^N$, nella 4.2.23, si ottiene:

$$dD = \frac{K^2}{2ES^{IV}} R_\nu \frac{(D_c - D)^{\frac{\alpha-1}{\alpha}}}{\varepsilon_{Eq}} d\varepsilon_{Eq} \qquad 4.2.24$$

Nel solito caso ideale in cui la prova di trazione su un provino liscio consenta di mantenere uniassialità perfetta ovvero il fattore di triassialità TF costante e pari ad 1/3 ($R_v$=1), la determinazione della costante di scala del modello si ottiene integrando la 4.2.24 tra l'innesco del danno e la rottura:

$$\int_{D_=}^{D_{C\_Uni}} \left(D_{c\_Uni} - D\right)^{-\frac{\alpha-1}{\alpha}} dD = \int_{\varepsilon_{Th}}^{\varepsilon_{C\_Uni}} \frac{K^2}{2ES^{IV}} R_\upsilon \frac{1}{\varepsilon_{Eq}} d\varepsilon_{Eq}$$

$$\frac{K^2}{2ES^{IV}} = \frac{\left(D_{c\_Uni} - D_0\right)^{\frac{1}{\alpha}}}{\alpha \cdot Ln \dfrac{\varepsilon_{C\_Uni}}{\varepsilon_{Th}}} \qquad 4.2.25$$

in cui compare la deformazione di innesco del danno senza pedice perché, secondo Bonora, tale deformazione è una costante del materiale e non dipende dallo stato di sollecitazione.

Sostituendo questa espressione nella precedente si ottiene la legge di evoluzione del danno nel caso di materiale con curva costitutiva esponenziale e carico a triassialità generica:

$$\int_{D_0}^{D_C} \left(D_c - D\right)^{-\frac{\alpha}{\alpha-1}} dD = \frac{\left(D_{c\_Uni} - D_0\right)^{\frac{1}{\alpha}}}{\alpha \cdot Ln(\dfrac{\varepsilon_{c\_Uni}}{\varepsilon_{Th}})} \cdot \int_{\varepsilon_{Th}}^{\varepsilon_C} \frac{R_\nu}{\varepsilon_{Eq}} \cdot d\varepsilon_{Eq} \qquad 4.2.26$$

Integrando questa espressione tra inizio danneggiamento e rottura, una volta per carico uniassiale puro e l'altra per carico triassiale costante generico, si ottiene che:

$$\frac{1}{\alpha}\left(D_c - D_0\right)^{\frac{1}{\alpha}} = \frac{\left(D_c - D_0\right)^{\frac{1}{\alpha}}}{\alpha \cdot Ln \dfrac{\varepsilon_{C\_Uni}}{\varepsilon_{Th}}} Ln\left(\varepsilon_{C\_Uni} - \varepsilon_{Th}\right) \quad \text{( IDENTITY)}$$

$$\left(D_c - D_0\right) = \frac{\left(D_c - D_0\right)^{\frac{1}{\alpha}}}{Ln \dfrac{\varepsilon_C}{\varepsilon_{Th}}} Ln\left(\varepsilon_C - \varepsilon_{Th}\right) R_\nu \qquad 4.2.27$$

e dividendo membro a membro le due espressioni precedenti resta definita una relazione che costituisce il criterio di rottura:

$$Ln\left(\frac{\varepsilon_C}{\varepsilon_{Th}}\right) = \frac{1}{R_\nu} Ln\left(\frac{\varepsilon_{C\_Uni}}{\varepsilon_{Th}}\right) \qquad 4.2.28$$

ovvero

$$\varepsilon_C = \varepsilon_{Th}\left(\frac{\varepsilon_{C\_Uni}}{\varepsilon_{Th}}\right)^{\frac{1}{R_v}} \qquad 4.2.29$$

I parametri del modello di Bonora da determinare sperimentalmente con delle prove di trazione sono, analogamente a quanto vale per gli atri modelli, la costante di scala S''', le deformazioni di innesco e fine del danneggiamento, e l'esponente α''' tramite misurazioni del valore di danno in punti interni al range di deformazioni suddetto e successivo best fitting.

All models derived from the Lemaitre idea have the main weakness: it is the way the model constants are derived. In fact, they assume that tension tests induce proportional loading so that, for example, Rv = 1 all over the strain history of a smooth tensile specimens. This is not true because necking greatly changes the traxiality and, if these changes are not included in the calculation of damage constants, large approximations are expected.

Di seguito si riportano i risultati sperimentali di prove di trazione a differenti triassialità effettuate in passato presso il DIIM (*La Rosa, G., Mirone, G., Risitano, A., 2001. Effect of stress triaxiality corrected plastic flow on ductile damage evolution in the framework of continuum damage mechanics. Eng. Fract. Mech. 68 (4), 417–434*), ed i relativi andamenti simulati di triaxialità, danno e deformazione di rottura.

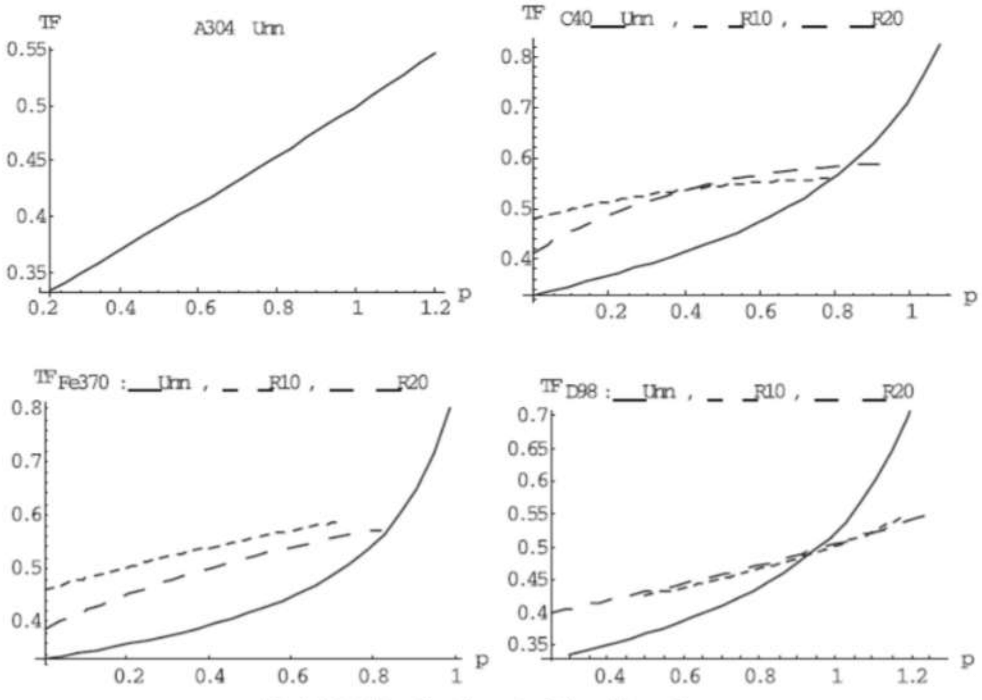

Fig. 7. Triaxiality ratio at the centre of the necking section.

*Figura....* Mirone La Rosa Risitano 2001

Si vede ad esempio che il TF, calcolato tramite misure sperimentali ottiche del raggio di curvatura del necking ed applicazione della formula di Bridgman, per provini lisci in C40 ed FE370, arriva quasi a triplicare il suo valore nominale di 0.33 prima di rompersi.

Il modello di Bonora è stato quindi applicato sia con l'ipotesi di TF costante pari a quello nominale, sia con una stima alla Bridgman della suaeffettiva variazione, ottenendo l'effetto seguente:

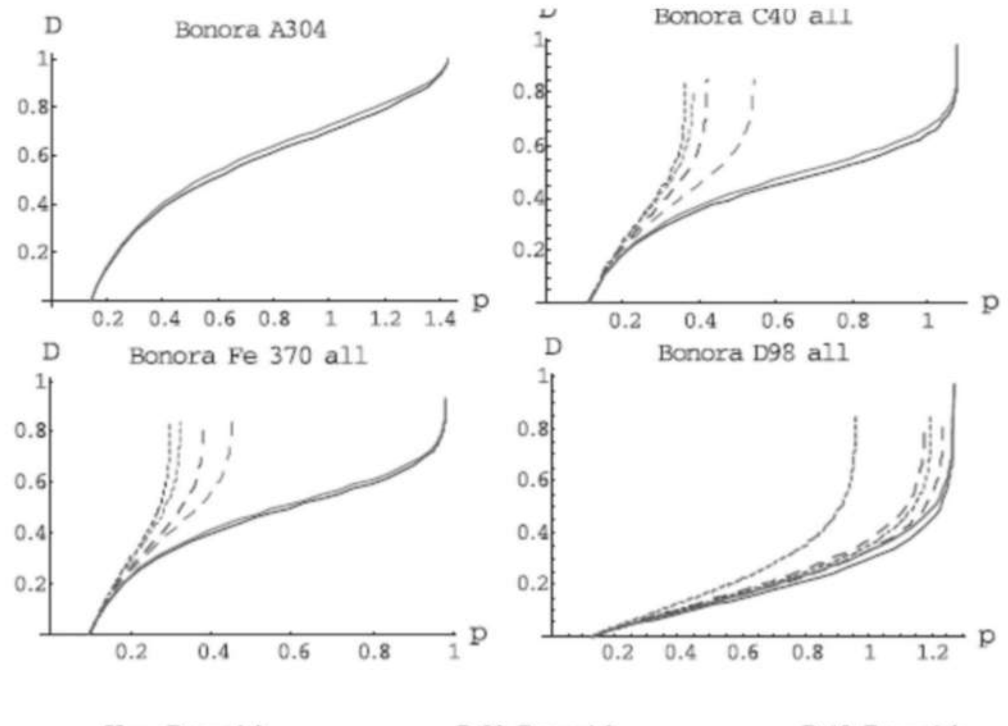

*Figura….* Mirone La Rosa Risitano 2001

in alcuni casi (acciaio D98 che è un AISI 304 inox), l'aumento di triassialità messo in conto con il necking, produce un rallentamento della crescita del danno e quindi un aumento della deformazione di rottura: questo è chiaramente impossibile ed evidenzia che i modelli derivati dalla formulazione di Lemaitre sembrano richiedere alcuni miglioramenti.

## 4.6 PHENOMENOLOGICAL MODELS –WIERZBICKI'S RESEARCH GROUP

The research group organized by Prof. Wierzbicki at the Crashworthiness Lab of the MIT, in the early 2000s, authored a rich series of papers proposing an approach to the damage model which, in the opinion of the writer, is still today the most sounding and accurate and is adopted as a reference in most advanced industrial applications such as automotive, aerospace, defence.

In *Y. Bao, T. Wierzbicki / On fracture locus in the equivalent strain and stress triaxiality space, International Journal of Mechanical Sciences 46 (2004) 81– 98*, the evolution of $TF$ was analysed for the first time taking into account its variability during a test, due to large strain and necking. Therefore they introduced the concept of averaged stress triaxiality at the critical material points within the specimen, the component or the structure:

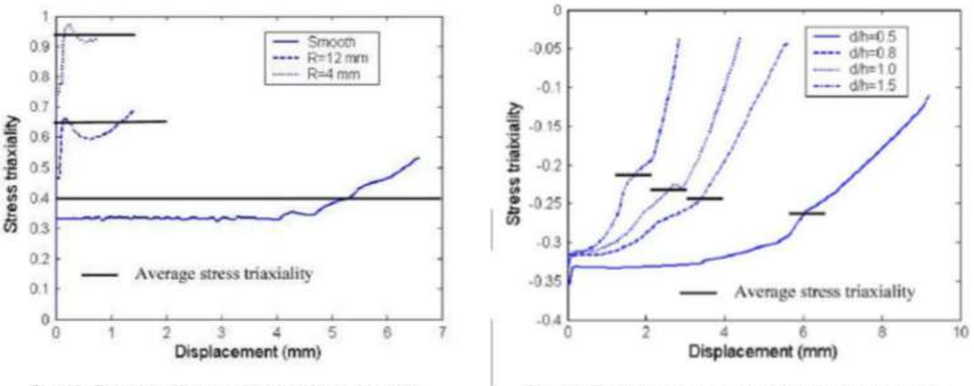

Fig. 19. Evolution of stress triaxiality for tensile tests.

Fig. 16. Evolution of stress triaxiality for upsetting tests.

*Figure 4-22 Variability of TF at critical material points during tests and average values – Bao and Wierzbicki (2004)*

In Figure 4-22 they shown such variability during different tests of a 2024-T351 Aluminium alloy subjected to various mixes of compression-shear-tension. The history-averaged stress triaxialities, $TF_{Avg}$, also compared to the varying $TF$ histories, are calculated as the average of functions $TF(\varepsilon_{Eq})$ according to eq. ( *4-10* ):

$$TF_{Avg} = \left(\frac{\sigma_H}{\bar{\sigma}}\right)_{av} = \frac{1}{\bar{\varepsilon}_f}\int_0^{\bar{\varepsilon}_f} \frac{\sigma_H}{\bar{\sigma}}\, d\bar{\varepsilon}, \quad = \frac{1}{\varepsilon_f}\cdot\int_0^{\varepsilon_f} TF\cdot d\varepsilon_{Eq} \qquad (4\text{-}10)$$

By simply plotting $TF_{Avg}$ vs. $\varepsilon_f$ from all the tests, they obtained the trend in Figure 4-23 expressing the possible envelope of a failure criteria:

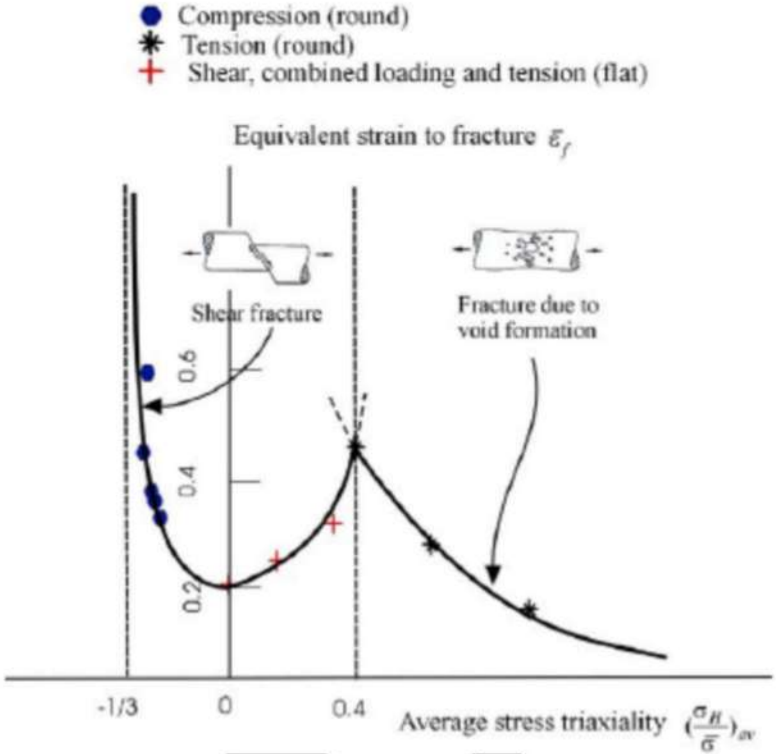

*Figure 4-23 Failure strain vs. TFAvg for a 2024-T351 Al. Alloy, according to Bao and Wierzbicki (2004)*

The overall trend was approximated by three different functions respectively applied to the range of mixed compression-shear ($TF_{Avg}$ between -1/3 and 0), the range of mixed tension-shear ($TF_{Avg}$ between 0 and 0.4) and the range of pure tension with different notches ($TF_{Avg}$ beyond 0.4).

$$\begin{aligned}
&\bar{\varepsilon}_f = 0.1225 * \left(\frac{\sigma_H}{\bar{\sigma}} + \frac{1}{3}\right)^{-0.46} \quad \text{for } \sigma_H/\bar{\sigma} = -1/3\text{–}0. \\
&\bar{\varepsilon}_f = 1.9 * \left(\frac{\sigma_H}{\bar{\sigma}}\right)^2 - 0.18 * \left(\frac{\sigma_H}{\bar{\sigma}}\right) + 0.21 \quad \text{for } \sigma_H/\bar{\sigma} = 0\text{–}0.4, \\
&\bar{\varepsilon}_f = 0.15\left(\frac{\sigma_H}{\bar{\sigma}}\right)^{-1} \quad \text{for } \sigma_H/\bar{\sigma} = 0.4\text{–}0.95.
\end{aligned} \tag{4-11}$$

For the first time, the tension of smooth specimen is not associated to the ideal uniaxial case and to a stress triaxiality of 0.33: the post-necking increase of $TF$ makes $TF_{Avg} = 0.4$, as visible from the abscissa marking the border between the $TF_{Avg}$ range of shear-tension tests and that of the pure tension tests.

The generalised form of the Bao-Wierzbicki damage model for a random material is:

$$\begin{aligned}
\varepsilon_f &= A_1 \cdot \left( TF_{AVG} + \frac{1}{3} \right)^{A_2} && \text{for} TF_{AVG} \in (-0.33,0) \\
\varepsilon_f &= B_0 + B_1 \cdot TF_{AVG} + B_2 \cdot TF_{AVG}{}^2 && \text{for} TF_{AVG} \in (0,0.4) \\
\varepsilon_f &= \frac{C}{TF_{AVG}} && \text{for} TF_{AVG} > 0.4
\end{aligned} \tag{4-12}$$

with $A$, $B_0$, $B_1$, $B_2$, $C$ material constants to be calibrated from experiments on the material at hand. Indeed, the use of the Bao-Wierzbicki material model in the present form is only possible in the ideal case of proportional loading where $TF$=constant all over a test and $TF_{Avg} = TF$ whose value can be simply obtained from the initial undeformed geometry of the specimen/component/structure.

In any real general case variable $TF$ histories occur, therefore the use of eqs. ( *4-12* ) is uncomfortable because, for calcuating $TF_{Avg}$, one should already know $\varepsilon_f$ which instead is the final unknown to be obtained from the model itself.

Starting from the above consideration a different form the the Bao-Wierzbicki model was proposed in Mirone (2007), where the last of eqs. ( *4-12* ), suitable for tension of axisymmetric specimens with whatever notch, was simply put in the form of an integral equation with the unknown being the upper integration limit.

$$\varepsilon_f = \frac{C}{TF_{AVG}} = \frac{C}{\dfrac{1}{\varepsilon_f} \cdot \displaystyle\int_0^{\varepsilon_f} TF d\,\varepsilon_{Eq}} \Rightarrow \int_0^{\varepsilon_f} TF d\,\varepsilon_{Eq} = C \tag{4-13}$$

Eq. ( *4-13* ) states that local failure occurs when the integral of $TF$ reaches a critical value $C$ which is a material constant.

During tensile tests of smooth / notched specimens the stress triaxiality always increases, starting from initial values which depends on the initial geometry (0.33 for smooth specimen, higher values for notched specimens).

Thus, the integral in ( *4-13* ) is a monotonically-increasing quantity, starting from zero at first yield, cumulating the combined effects of plastic strain and stress triaxiality and also expressing how close to failure a material point is, all over its strain range until complete failure. Therefore such integral has all the features of a damage function and is just renamed and intended as in eq. ( *4-14* ):

$$D\left(\varepsilon_{Eq}\right)=\int_{0}^{\varepsilon_{Eq}} TF d\,\varepsilon_{Eq}$$
$$D\left(\varepsilon_{f}\right)=\int_{0}^{\varepsilon_{f}} TF d\,\varepsilon_{Eq}=C=Dcr \qquad (4\text{-}14)$$

In other words, the integral of $TF$ expresses the current damage value and failure locally occurs when the damage function reaches its critical value, now called $D_{Cr}$.

In principle the B-W damage model for tensile tests can be calibrated with a single test (it has a single material constant), e.g. the smooth specimen, for finding the value of $D_{Cr}$ for that material, and then the model can be used for predicting failure of whatever notched specimen in tension made of that material.

Clearly, the B-W model cannot be used for failure predictions by simple pen-and-paper calculations: instead finite elements (f.e.) simulations of the specimen/component/structure must be ran with the approrpiate material curve and the damage integral function of eq. ( *4-14* ) must be calculated at each element / node of the f.e. model. When at a certain node the function will reach its critical value, the element containing that node can be removed from the f.e. mesh and the macroscopica damage of the specimen/component/structure is initiated.

In principle the furthe propagation of the fracture might be simulated by extending the procedure to the other nodes/elements of the structure, but in practice the failure propagation is always very strongly affected by the mesh size of the f.e. model and no generally valid propagations can be obtained.

This is why the ductile damage models are fully appropriate for accurately predicting failure initiation but are less suitable for correctly predicting fracture propagation.

Other damage models published since 2005 shown that also the Lode parameter $X$ of eq. ( *4-3* ) directly affects the damage evolution and ductile failure.

In in *T. Wierzbicki_, Y. Bao, Y. Lee, Y. Bai, Calibration and evaluation of seven fracture models, International Journal of Mechanical Sciences 47 (2005) 719–743*), , and in *L Xue and T. Wierzbicki, Ductile fracture characterization of aluminum alloy 2024-t351 using damage plasticity theory, International Journal of Applied Mechanics, Vol. 1, No. 2 (2007) 267*–304, the averaged deviatoric parameter $X_{Avg}$ is presented as a parameter moving up and down the curves $\varepsilon_f\left(TF_{Avg}\right)$, according to the qualitative picture of Figure 4-24. Clearly, if $\varepsilon_f$ is plotted against both variables $X_{Avg}$ and $TF_{Avg}$ a 3D surface is obtained as in Figure 4-25, where the former parameter is called η and the latter ζ .

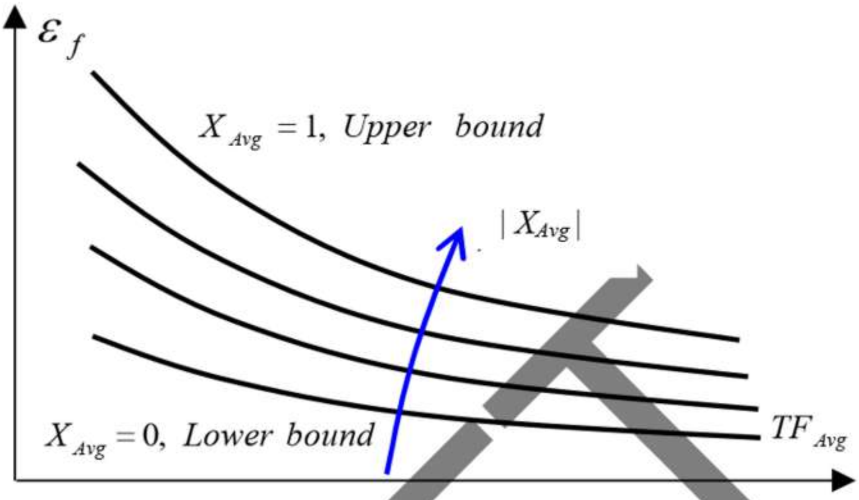

*Figure 4-24 Qualitative effect of Lode parameter and stress triaxiality on failure strain*

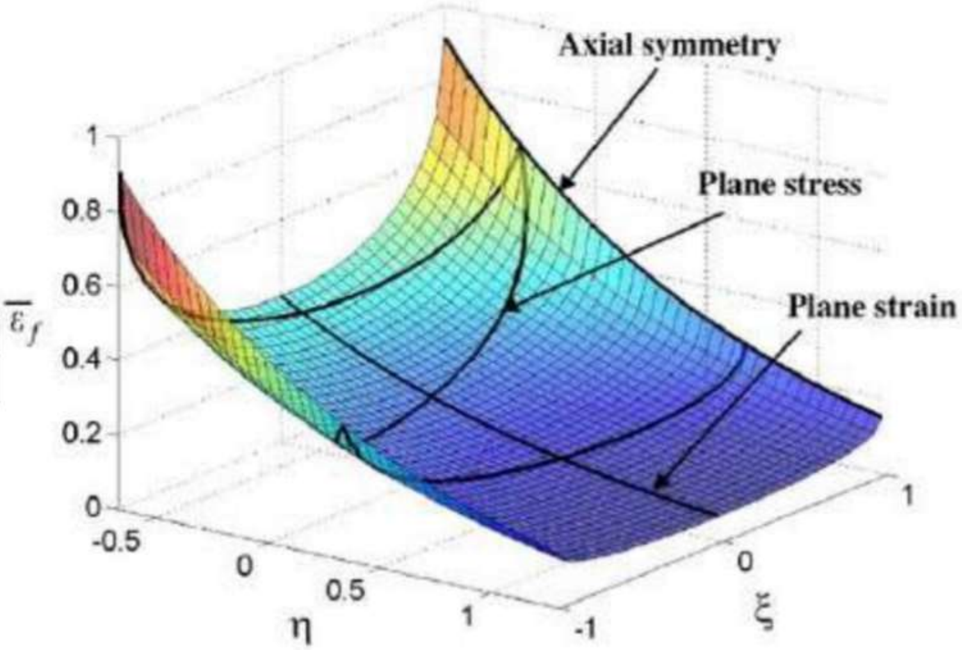

*Figure 4-25 X-W failure surface of an high stresngth steel - Xue and Wierzbicki (2009)*

The B-W model of Figure 4-23 is coincident to the X-W model of Figure 4-25 only for $X_{Avg}$ =1 and $TF_{Avg} > 0.4$, referred to axisymmetric tension specimens with and without notch. Instead at lower triaxialities the B-W model reported results from torsion, shear and compression tests where $X_{Avg}$ differed from 1.

Referring to the approach of Figure 4-25, the W-et-Al. And the X-W model expresses the upper bound curve ($X_{Avg}$ =1, Axisymmetric stress states) and the lower bound curve ($X_{Avg}$ =0, Plane Strain stress states) as in eq. ( *4-15* )

$$\begin{aligned} \varepsilon_f^{Axi} &= C_1 \cdot Exp\left(C_2 \cdot TF_{Avg}\right) \ \text{ for } X_{Avg} = 1 \\ \varepsilon_f^{PS} &= C_3 \cdot Exp\left(C_4 \cdot TF_{Avg}\right) \ \text{ for } X_{Avg} = 0 \end{aligned} \tag{4-15}$$

$C_1$ and $C_3$ are positive scale factors while $C_2$ and $C_4$ are negative exponents to express the decreasing dependence of $\varepsilon_f$ on $TF_{Avg}$.

The set of 4 constants must be calibrated for each material, based on a set of experiments including at least 4 differenc combinations of $TF_{Avg}$ and $X_{Avg}$.

For describing the failure at intermediate values of $X_{Avg}$ between 0 and 1, the W-et-Al. model adopted the following expression of a fracture criteria:

$$\left[\left(\frac{\varepsilon_f^{Axi} - \varepsilon_f}{\varepsilon_f^{Axi} - \varepsilon_f^{PS}}\right)^{1/N} + X^{1/N}\right]_{TF_{Avg}=Costante} = 1 \tag{4-16}$$

where for the the term $N$ is the hardening exponent (or the strain at necking onset). In the X-W model the fracture criteria remains identical but $N$ i soane more caibration constant for the given material instead of being the necking strain.

Solving for $\varepsilon_f$ delivers:

$$\varepsilon_f = \varepsilon_f^{Axi} - \left(\varepsilon_f^{Axi} - \varepsilon_f^{PS}\right) \cdot \left(1 - X^{1/N}\right)^N \tag{4-17}$$

and substituting eq. ( *4-15* ) in ( *4-17* ) returns:

$$\varepsilon_f\left(TF_{Avg}, X_{Avg}\right) = C_1 \cdot e^{C_2 \cdot TF_{Avg}} - \left(C_1 \cdot e^{C_2 \cdot TF_{Avg}} - C_3 \cdot e^{C_4 \cdot TF_{Avg}}\right) \cdot \left(1 - X_{Avg}{}^{1/N}\right)^N \tag{4-18}$$

Eq. ( *4-18* ) plotted against $TF_{Avg}$ and $X_{Avg}$ delivers a surface like that of Figure 4-25, where different sets of calibrated material constants clearly deliver different surfaces.

As already discussed for the B-W model, a failure criteria including history-averaged variables like $TF_{Avg}$ and $X_{Avg}$ cannot deliver the failure strain without knowng the evolution of such history-averaged variables, so the damage functions must be calculated from the outcome of f.e. analyses and compared to their limiting values at each step of a load history.

The fully predictive capability of these models is only possible when the Lode parameter and the stress triaxiality are constant, so that their average values can be already known at the beginning of the test. In such case the combination of failure strains can be reported in the plot of Figure 4-26.

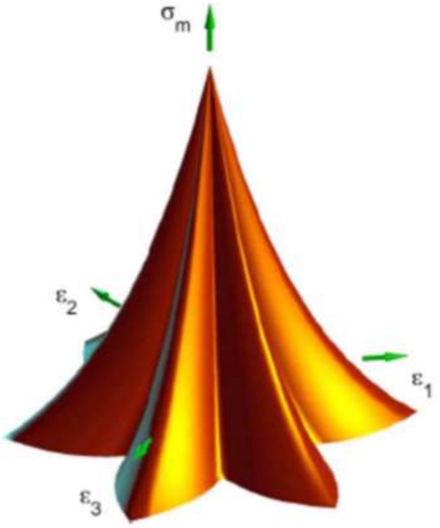

*Figure 4-26 Failure strains in case of proportional loading - Xue Wierzbicki (2007)*

## 4.7 PHENOMENOLOGICAL MODELS BY COPPOLA ET AL. AND BY MIRONE & CORALLO.

In *T. Coppola, L. Cortese, P. Folgarait, The effect of stress invariants on ductile fracture limit in steels, Engineering Fracture Mechanics 76 (2009) 1288–1302*, the upper and lower bound curves of eq. ( *4-15* ) are still valid but a different criteria is adopted for expressing the effect of intermediate values of $X_{Avg}$.

Coppola et al. considered that, for whatever given $TF_{Avg}$, the flow stresses at failure for $X_{Avg} = 0$ (generalized plane strain) and those for $X_{Avg} = 1$ (axisymmetric stress state) stay in the same ratio of the Mises stress to the Tresca stress:

$$\frac{\sigma_{Axi}}{\sigma_{PS}} = \sqrt{\frac{3}{2}} \qquad (4\text{-}19)$$

Coppola et al. also assumed that the flow curves evolve according to the Hollomon law $\sigma_{Eq} = k \cdot \varepsilon_{Eq}{}^{N}$, therefore eq. ( *4-19* ) can be put in terms of failure strains:

$$\frac{\varepsilon_f{}^{Axi}}{\varepsilon_f{}^{PS}} = \sqrt{\frac{3}{2}}^{1/N} \qquad (4\text{-}20)$$

which sets a relationship between upper and lower bound curves. This relationship is proposed for determining the upper bound cruve from experiments of pure torsion or tube flattening, where the variability of $TF_{Avg}$ and $X_{Avg}$ is less pronounced han it is in case of tensile specimens with and without notch. The mathematical form of the upper bound is stille as in eq. ( *4-15* ).

The dependence of $\varepsilon_f$ on $X_{Avg}$ proposed by Coppola et al. is expressed by eq. ( *4-21* ), with α, β and γ material constants to be calibrated from experiments at intermediate values of $X_{Avg}$.

$$g(X)=\frac{\alpha}{Cos\left(\beta\cdot\frac{\pi}{6}-\frac{1}{3}ArcCos\ (\gamma\cdot X)\right)} \qquad (4\text{-}21)$$

For a given set of material constants, g(X) is a reductive function which decreases the upper bound curve due to intermediate values of $X_{Avg}$ between -1 and 1; it obviously equals 1, leaving unaltered the upper bound, for $X_{Avg}=1$, according to equation ;

$$\varepsilon_f=\mathrm{C}_1\cdot Exp(-\mathrm{C}_2\cdot TF)\cdot[g(X)]^{1/N} \qquad (4\text{-}22)$$

When β = γ = 1, *g(X)* delivers the Tresca criterion, while the trends of the $g(X)$ function calibrated for two metals are reported in Figure 4-27. If only β = 1 then the dependence on the Lode parameter is independent of its sign and *g(X)* is symmetrical around the pure shear of $X=0$.

In case of proportional loading $X$ ad $TF$ are constant so eq. ( *4-22* ) can be used, in case of non-proportional loading either the average values might be used in eq. ( *4-22* ) or, according to Coppola et al., the integral form in eq. ( *4-23* ) might be adopted.

$$D=\int_0^{\varepsilon_f}\frac{Exp(\mathrm{C}_2\cdot TF)}{\mathrm{C}_1\cdot[g(X)]^{1/N}}\cdot d\varepsilon_{Eq} \qquad (4\text{-}23)$$

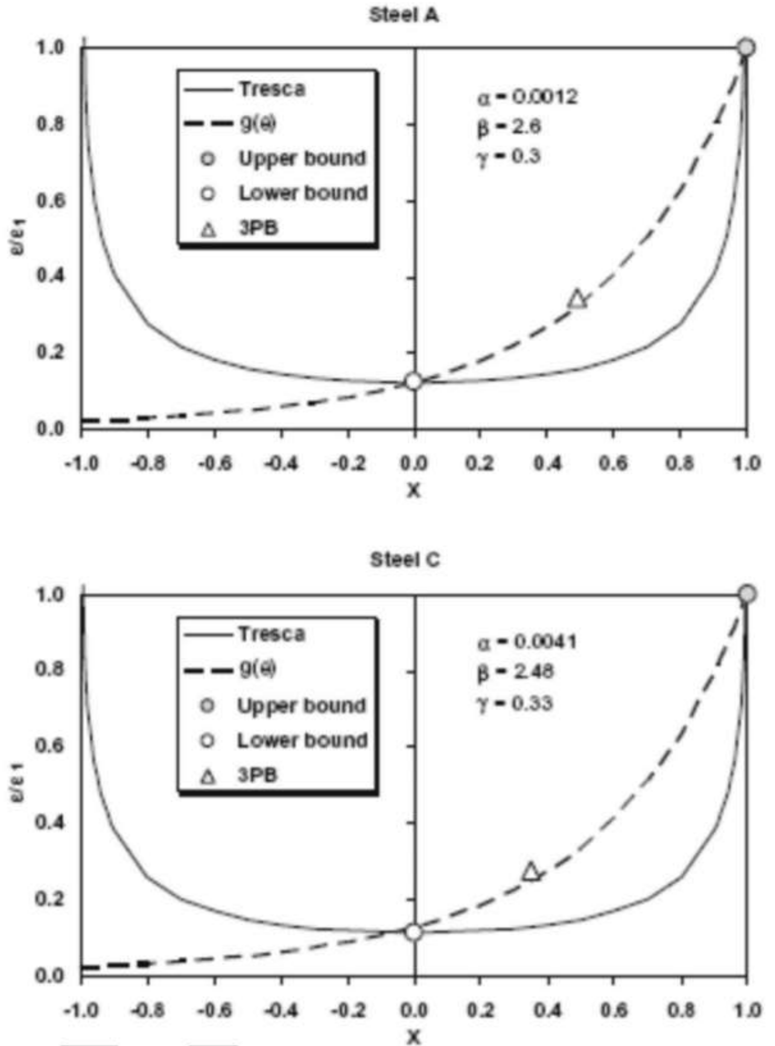

*Figure 4-27 Trends of the function g(X) calibrated for two steels, - Coppola et al. (2009)*

In *Mirone G. and Corallo D., Stress–strain and ductile fracture characterization of an X100 anisotropic steel: Experiments and modelling, Engineering Fracture Mechanics 102 (2013) 118–145*, another damage model is proposed, starting from the B-W model and adding a dependence on $X$. The critical damage $D_{Cr}$ of the Bao-Wierzbicki model still applies to the case $X = 1$ (upper bound for axisymmetric tension), and the effect of $X < 1$ is included in the formula ( *4-24* ).

$$D4(\varepsilon_{Eq}, TF, X) = \frac{\int_0^{\varepsilon_{Eq}} TF \cdot d\varepsilon_{Eq}}{C_0 + C_1 \cdot \left(1 - Cos\left(X \cdot \frac{\pi}{2}\right)\right)^{C_2}} \qquad (4\text{-}24)$$

Imposing that for $X = 1$ the B-W model must be obtained follows that $C_0 + C_1 = 1$ so that the independent maerial constants are two and the model can be rearranged in

$$D_4 = \frac{\int_0^{\varepsilon_f} TF \cdot d\varepsilon_{Eq}}{\mathrm{C}_0 + (1 - \mathrm{C}_0) \cdot \left[1 - \left(1 - Cos\left(X \cdot \frac{\pi}{2}\right)\right)^{C_2}\right]} \leq D_{Cr} \tag{4-25}$$

The material constant $C_0$ expresses the ratio of $\left(\int_0^{\varepsilon_f} TF \cdot d\varepsilon_{Eq}\right)/D_{Cr}$ for a general stress history with $X = 0$ while the material constant $C_2$ identifies the behavior at intermediate values of $X$.

If $D_{Cr}$ is only taken from pure tension and a single couple of $C_0$ and $C_2$ constants is considered, then the model $D_4$ is symmetric with respect to the sign of the Lode parameter. If Instead different trends are encountered in tension and compression, then the model can be repeated specularly based on $D_{Cr}^-$ from compressive tests and $C_0{}^-$ and $C_2{}^-$ from tests at negative $X$.

The generalized plane strain condition $X = 0$ sets a common boundary condition for both halves of the $D_4$ model so eq. ( *4-27* ) applies and relates to each other the material constants $C_0$ and $C_0{}^-$.

$$\frac{\int_0^{\varepsilon_f} TF \cdot d\varepsilon_{Eq}\Big|_{X>0}}{D_{Cr}} = C_0 = \frac{\int_0^{\varepsilon_f} TF \cdot d\varepsilon_{Eq}\Big|_{X>0}}{D_{Cr}{}^-} = C_0{}^- \tag{4-26}$$

The effect of the Lode parameter is collected in the function of eq. ( *4-27* ), plotted in Figure 4-28 for the positive range of $X$ alone.

$$D_4 = \frac{\int_0^{\varepsilon_f} TF \cdot d\varepsilon_{Eq}}{\mathrm{C}_0 + (1 - \mathrm{C}_0) \cdot \left[1 - \left(1 - Cos\left(X \cdot \frac{\pi}{2}\right)\right)^{C_2}\right]} \leq D_{Cr} \tag{4-27}$$

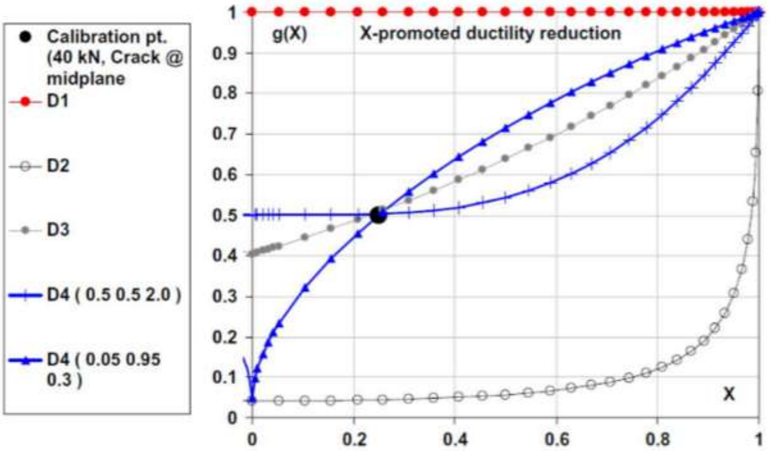

*Figure 4-28 Ductility reduction due to the Lode parameter in D4 damage model - Mirone and Corallo (2009)*

In case of non-proportional loading paths and variable $X$, different options might be adopted:

the simplest is that of changing $X$ with its current average value, another is that of changing $X$ with its cumulate, the third is that of integrating the whole expression ( *4-25* ) instead of integrating the numerator alone.

The adoption of $X_{Avg}$ has the side effect that its increase/decrease during a stress history leads to possible material "healing", which is not puhisically sounding at all.

The siple integral of $X$ would deliver the same effect for large $X$ values maintained over small failure strains or small $X$ values maintained up to large failure strains: $X \approx 1$ maintained until $\varepsilon_f = 0.1$ generates the same integral of $X \approx 0.1$ maintained over a larger strain range up to $\varepsilon_f = 1.0$. Maybe this feature is realistici and desirable maybe it is not, further experiments are necessary for ascertaining such possibility.

The third option, consisting of an overall integral with the stress triaxiality at the numerator of a fraction and the Lode parameter at its denominator, sets a coupling between the current values of $X$ and $TF$ which might complicate the model with no special reasons to expect in advance special improvements, which however might arrive unexpected.

This is why further work in such direction might lead to rather interesting results.

## 4.8 GENERAL CONSIDERATIONS FOR TRANSFORMING A DAMAGE MODEL IN A FAILURE CRITERIA

For all damage models including a dependence on $TF$ and $X$, the consideration about monotonically increasing cumulative expressions applies for taking into account the variability of such parameter during a stress-strain history.

The simplest and most general form of failure criteria is that of expressing the ratio of the current strain over the failure strain corresponding to the current values of the average/integrated $TF$ and $X$, according to eq. ( *4-28* ), to be implemented in f.e. codes and to be calculated at each step on each element/node/gauss point.

$$D = \frac{\varepsilon_{Eq}}{\varepsilon_f^{\,*}} = \frac{\varepsilon_{Eq}}{\varepsilon_f\left(\int_0^{\varepsilon_{Eq}} TF\,d\varepsilon_{Eq},\ \int_0^{\varepsilon_{Eq}} X\,d\varepsilon_{Eq}\right)} \le 1 \qquad (4\text{-}28)$$

It is important to underline that $\varepsilon_f$ in ( *4-28* ) is re-calculated at each step during a stress-strain history and changes together with the evolution of $TF$ and $X$ which can either increase or decrease; therefore

$\varepsilon_f$ before failure usually differs from the effective failure strain of that given stress history, and only at last step before failure $\varepsilon_f$ will really reflect the actual failure strain.

Instead in case of proportonal loading histories (e.g. where $TF$ and $X$ are constants), the value of $\varepsilon_f$ is known at the beginning of the loading history and reflects the real failure strain.

Assuming proportonal loading whenever $TF$ and $X$ are subjected to the usual spontanous variations due to the large straining can lead to considerable errors, as demonstrated in *G. Mirone, D. Corallo, A local viewpoint for evaluating the influence of stress triaxiality and Lode angle on ductile failure and hardening, International Journal of Plasticity 26 (2010) 348–371.*

In case of proportional loading the failure strain can be then represented as a function $\varepsilon_f(TF, X)$ which might also be determinied per discrete points, from experiments at different combinations of $TF$ and $X$, then bestfitted by whatever appropriate two-variables function.

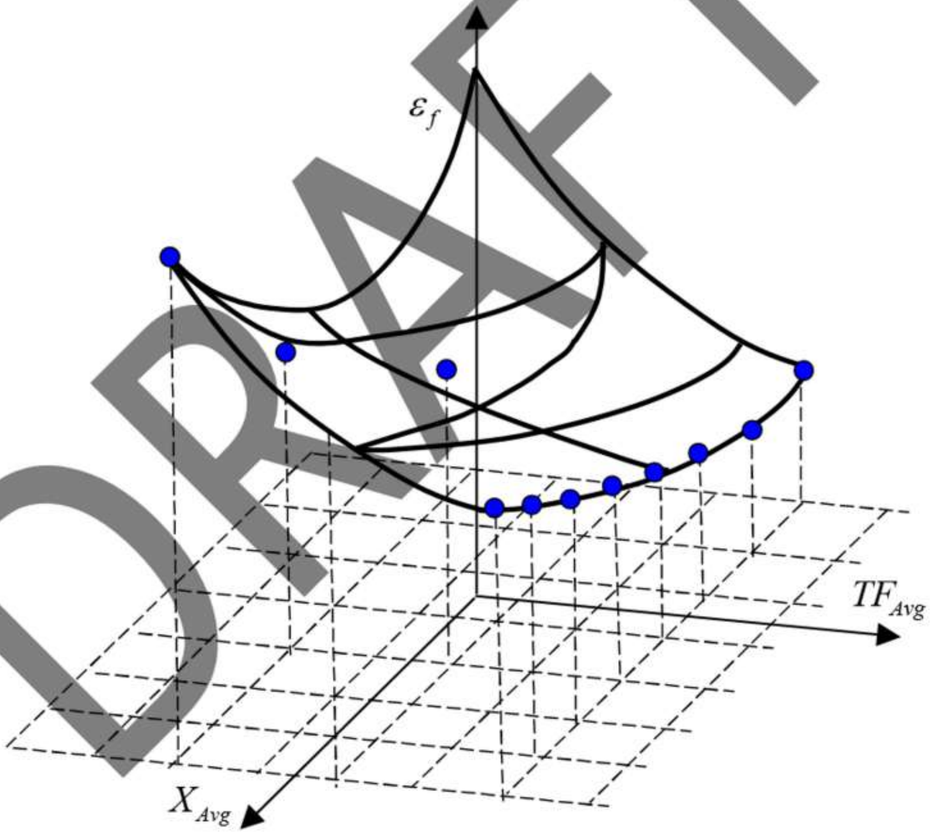

*Figure 4-29 General failure surface identifying $\varepsilon_f$ as a function of $TF, X$*

A grid of points in the plane $TF, X$ should be set for identifying the corresponding experiments, then the failure strains of those experiments might describe the sruface and can be approximated by bestfit techniques.

The combinations of $TF, X$ corresponding to the most typical tests are reported in Figure 4-30 according to Wierzbicki et al. (2009).

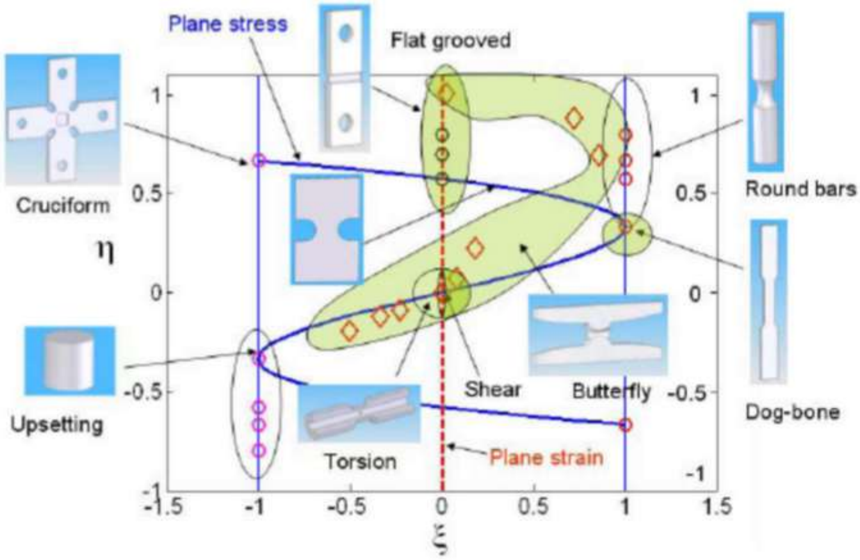

*Figure 4-30 Combinations of TF and X corresponding to the most typical tests and stress-strain histories – Wierzbicki et al. (2008)*

**POSSIBILI AGGIUNTE:**

1) **RAGIONAMENTO SU CRITICAL STRESS SURFACE**
2) **BIBLIOGRAFIA ARTICOLI**
1) **SINTESI ARTICOLI EFM 2007, IJP 2010-2013**
2) **EFFETTO LODE ANGLE SU YIELD SURFACE (BAI-WIERZ. , BIGONI)**
3) **ANISOTROPIA PLASTICA E CRITERIO DI HILL**
4) **METODO DOPPIA CAMERA X CURVA TRUE EXP. ANISOTROPA**

# 5 HIGH STRAIN RATE EFFECT AND DYNAMIC ELASTOPLASTICITY

## 5.1 APPLCATION AREAS AND INTRODUCTION TO THE DYNAMIC RESPONSE OF STRUCTURAL MATERIALS

Stuctural metals may exhibit remarkable differences in their elastoplastic response depending on the deformation speed also called strain rate. High strain rate loading occurs in many important structural applications such as vehicles impact and crash tests, debris impact and ballistic protection, metal forming/forging, etc.

*Anthony Taylor OWENS – Ph.D. thesis (2007)*

*https://pdfs.semanticscholar.org/f5e5/a63c0b3ff59e88abb1cd1b2548cc99110347.pdf*

The loading rate, commonly identified in terms of strain rate, can have a wide range of effects on critical material properties such as elastic modulus, yield stress, failure stress, and failure strain.
Gray [1] outlined several specific examples where materials are employed under high strain rate conditions. Automotive crashworthiness is one such example. Several areas of the vehicle are designed to function as energy absorbing mechanisms in the event of a crash, such that the decelerations seen by the driver are not so harsh that they cause severe bodily injury.

*Figure 5-1 Typical applications of dynamic elastoplasticity*

Even though the body is constrained by a harness, the head and neck of the driver is still susceptible to injury. In order to design structures that will absorb energy properly, the material behavior must be understood and characterized for conditions similar to the actual loading conditions.Another group of examples is in the aerospace industry. Often, spacecraft or other orbital bodies come into contact with foreign debris that may be traveling at high relative velocities. Also, jet engines, which have extremely high operating speeds, may ingest foreign objects, causing severe shock loads. Containment of debris in the event of catastrophic engine failure is another issue in jet engine design that involves highly transient loading. In some cases, fragments have pierced the engine casing and severely damaged hydraulic components that are vital for aircraft control.

Other examples include turbine blade design where cavitation is a concern, protective armor in defense applications, as well as ballistic devices where propellants and explosives interact with casings. There are many more real life applications where materials are deployed and expected to perform under high strain rate conditions.

## 5.2 INTRODUCTION TO HIHG STRAIN RATES EFFECTS: COUPLING TO THERMAL EFFECTS AND SIMPLE MATERIAL MODELS

Structural metals usually exhibit a remarkable sensitivity to the strain rate $\dot{\varepsilon}$; its main effect is to increase the flow stress at each strain and more generally to push upward the elastoplastic material curve at static rates.

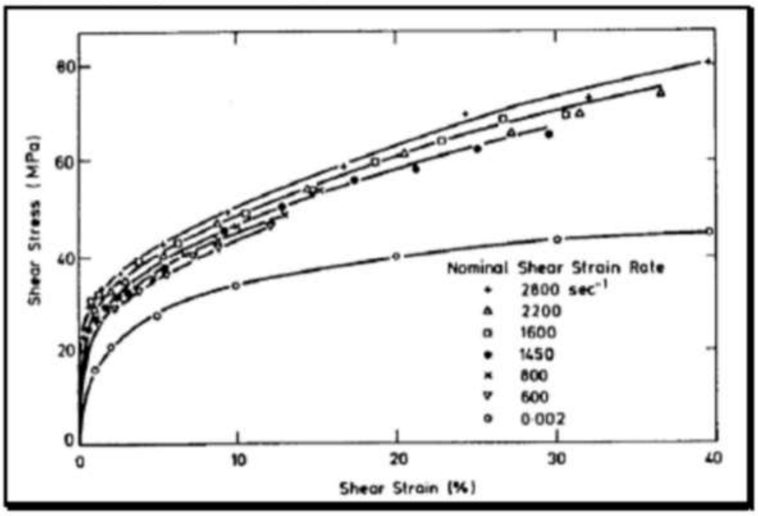

*Figure 5-2: Static and dynamic flow curves of a commercial aluminium alloy – A. Ruggiero, Ph.D. thesis, ().*

As an esample, in Figure 5-2 are reported different flow curves for an aluminium alloy at different strain rates, showing that the greater is $\dot{\varepsilon}$ the greater is the flow stress at given strain and the higher is the material curve with respect to the reference case at static strain rate.

Also the "length" of the flow curve (or the ductility e.g. the failure strain $\varepsilon_f$) can be affected by the strain rate; while the height of the curve always increases with $\dot{\varepsilon}$, the ductility can be either increased or reduced by $\dot{\varepsilon}$ depending on the material at hand.

Given that the strain rate effect usually consists of an increase of the material curve, in the next sections it is also called "dynamic amplification" of the flow stress.

The high strain rate loading is accompanied by temperature increase and possible thermal effects, as the the mechanical work generated by stress and plastic deformation is always converted into heat: if the strain rate is low then the "plastic heat" is dissipated in the environment and low or no temperature increase occurs in the component. If instead the deformation processi s fast, then the heat cannot be dissipated in the envoronment with sufficient speed and then the temperature of the deformed body increases.

The temperature increase is the fraction $\beta$ of the heat corresponding to the plastic work generated in the infinitesimal volume unit:

$$W = \beta \cdot \frac{1}{\varrho \cdot C_V} \cdot \int_0^{\varepsilon_f} \sigma_{Eq} \cdot d\varepsilon_{Eq} \qquad (5\text{-}1)$$

With $\varrho$ and $C_V$ respectively being the material density and the specific heat at constant volume. The fraction constant, called Taylor-Quinney coefficient, is $\beta \approx 0$ at low-static rates (roughly $\dot{\varepsilon} < 0.01$) and $\beta \approx 1$ at high rates (roughly $\dot{\varepsilon} > 1$).

Whatever it is the cause of the temperature increase (it can be either an external heating, an internal strain rate-promoted heating or a combination of them), the effect of temperature increase usually consists of a reduction of the flow stress at given strain and a lowering of the material curve with respect to the reference curve at room temperature (Troom). Figure 5-3 reports the flow curves for a stainless steel at different constant temperatures imposed via climatic chamber between Troom (35 C) and 300 C.

Given that the temperature usually makes lower the material curve and "softer" the material, its effect is called Thermal Softening.

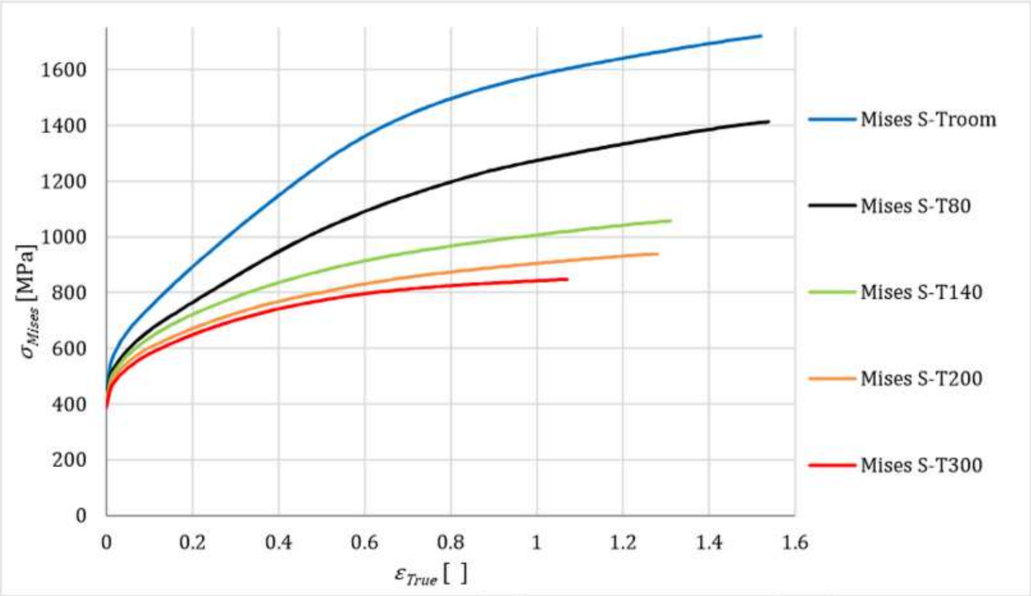

*Figure 5-3: Effect of thermal softening for the AISI 3044 stainless steel (Mirone et al. 2019)*

The material sensitivity to the temperature is also influenced by the crystallographic arrangement of the metals: body-centered cubic (BCC) metals like ferritic steels, tantalum, tungstenium, niobium etc., exhibit a remarkable sensitivity to both temeprature and strain rate while face-centered cubic metals (FCC) like Copper, Silver and Gold, are less sensitive to the temperature changes.

The sensitivity of Hexagonal close-packed (HCP) metals (beryllium, cadmium, magnesium, titanium, zinc) to the temperature is intermediate with respect to those of BCC and FCC metals.

Similar considerations might apply for the strain rate sensitivity, although each single material or alloy is a case on its own.

Below are introduced some of the most known material models describing how the high strain rate / temperature together affect the elastoplastic response of materials.

## JOHNSON-COOK MODEL

The most famous formulation, due to by Johnson and Cook in 1983, is implemented in most commercial FEM codes. It includes the strain-rate and temperature material sensitivities according to:

$$\sigma = \left(A + B \cdot \varepsilon_p^n\right) \cdot \left(1 + c \cdot \ln \dot{\varepsilon}^*\right) \cdot \left(1 - T^{*m}\right) \qquad (5\text{-}2)$$

It is worth noting that the first parenthesis expresses the reference material curve (at static rate and room temperature) according to the Ludwik formula, the second parenthesis expresses the dependence in the strain rate alone (material constant *c*), and the third parenthesis expresses the thermal softening alone (material constant *m*).

$\dot{\varepsilon}^*$ * and T* are defined with the relation:

$$\dot{\varepsilon}^* = \frac{\dot{\varepsilon}_p}{\dot{\varepsilon}_0} \text{ and } T^* = \frac{T - T_r}{T_m - T_r} \qquad (5\text{-}3)$$

where $\varepsilon_0$ is the reference strain-rate where no appreciabel strain rate effect exists for that material, and Tm and Tr are respectively the melting temperature and the reference (room) temperature.

The static material curve might also be expressed according to any other bestfitting formula, buti s the dynamic and thermal constributions (second and third parentheses of ( *5-2* ) is left unaltered, the resulting formulation remans of the Johnson-Cook type.

COWPER-SYMONDS MODEL

A simpler and older model of strain-rate sensitivity alone was proposed by Cowper and Symonds in 1957 according to the following equation:

$$\sigma_{yd} = \sigma_{ys} \cdot \left( 1 + \left( \frac{\dot{\varepsilon}_p}{D} \right)^{1/p} \right) \qquad (5\text{-}4)$$

where D and p are two model parameters, σys is the static flow stress and σyd is the dynamic flow stress affected by the strain-rate.

The static material curve might also be expressed according to the Ludwik law or to whatever any other formula leaving unaltered the Cowper-Symonds nature of the dynamic amplification law.

ZERILLI-ARMSTRONG MODEL

The model proposed by Zerilli and Armstrong in 1987, based on the theory of mechanical dislocations, assumes that the flow stress is the sum of an internal stress and a thermally-activated stress depending on the strain rate and the temperature.

The most general formulation of the Zerilli-Armstrong model is expressed as:

$$\sigma = c_0 + B_0 \cdot \exp\left(-\left(\beta_0 - \beta_1 \cdot \ln \dot{\varepsilon}_p\right) \cdot T\right) + K \cdot \varepsilon^n \qquad (5\text{-}5)$$

where c0, b0, β0, β1 and K are model parameters describing the dynamic amplification and the thermal softening features for the given material.

Again, $c_0 + K \cdot \varepsilon^n$ is the static flow curve approximated by a Ludwik functions, while the $B_0 \cdot Exp(\ldots.)$ term expresses the combined effect of strain rate (dynamic amplification) and temperature (thermal softening).

GENERAL COMMENTS ABOUT PLASTICITY MODELS WITH TEMP AND STRAIN RATE

In general, two philosophies exist for modeling the hardneing of materials with thermal softening and dynamic amplification: The multiplicative approach (like the J-C model) and the additive approach (like the Z-A model). The most general expressions for such two approaches are respectively reported below:

$$\sigma_{Eq}\left(\varepsilon_{Eq}, T, \dot{\varepsilon}_{Eq}\right) = \sigma_{St}\left(\varepsilon_{Eq}\right) \cdot S(T) \cdot R\left(\dot{\varepsilon}_{Eq}\right) \tag{5-6}$$

$$\sigma_{Eq}\left(\varepsilon_{Eq}, T, \dot{\varepsilon}_{Eq}\right) = \sigma_{St}\left(\varepsilon_{Eq}\right) + S(T) + R\left(\dot{\varepsilon}_{Eq}\right)$$

In eq. ( *5-5* ) the effects of $\varepsilon_{Eq}$, $T$ and $\dot{\varepsilon}_{Eq}$ are supposed to be "uncoupled" so that these three variables independently affect three separate functions.

According to a more general viewpoint, only the reference curve at $T \approx 25\ C$ and $\dot{\varepsilon}_{Eq} \approx 0\ s^{-1}$ remains dependent on the strain alone, while the thermal softening and the dynamic amplification depend on a mix of all vaiables according to the general form below:

$$\begin{aligned} \sigma_{Eq}\left(\varepsilon_{Eq}, T, \dot{\varepsilon}_{Eq}\right) &= \sigma_{St}\left(\varepsilon_{Eq}\right) \cdot S\left(T \varepsilon_{Eq}, T, \dot{\varepsilon}_{Eq}\right) \cdot R\left(\varepsilon_{Eq}, T, \dot{\varepsilon}_{Eq}\right) \\ \sigma_{Eq}\left(\varepsilon_{Eq}, T, \dot{\varepsilon}_{Eq}\right) &= \sigma_{St}\left(\varepsilon_{Eq}\right) + S\left(\varepsilon_{Eq}, T, \dot{\varepsilon}_{Eq}\right) + R\left(\varepsilon_{Eq}, T, \dot{\varepsilon}_{Eq}\right) \end{aligned} \tag{5-7}$$

The coupling of $\varepsilon_{Eq}$ and $T$ has been demonstrated by static tests at various temperatures and the coupling of $T$ with $\dot{\varepsilon}_{Eq}$ has been demonstrated by dynamic tests at different temperatures and different strain rates, in recent studies at the University of Catania.

However the hardening functions depending on $\varepsilon_{Eq}, T, \dot{\varepsilon}_{Eq}$ are still an open issue in the scientific community, as no certainty currently exist in this regard and different models are more or less appropriate for different materials.

## 5.3 METHODS FOR CHARACTERIZATION AT HIGH STRAIN RATES

The testing of materials at high strain rates is performed by different types of experimental equipment, according to the synthesis proposed by Ramesh :

- Quasistatic rates, ($0 – 10^{-2}$ s-1): Universal testing machines (usually electrically motor-driven), displacement-control tests at fixed elongation speeds.;
- Low Strain rates, ($10^{-2}$ – 1 s-1): macchine idrauliche di fatica, provini piccoli per limitare problemi di inerzia, accuratezza prove in controllo di spostamento a velocità traversa fissata (accuracy in displacement/velocity control lower than for motor-driven machines);

- Intermediate strain rates, (1 – $10^2$ s-1): Drop tests, specially designed hydraulic machines incorporating freeplay-and-impact devices or other architectrures for minimizing machine inertia effects;
- Impact and low-ballistic High strain rates, ($10^2$ – $10^4$ s-1): Hopkinson bar tests;
- Ballistic High strain rates ($10^4$ – $10^5$ s-1): Taylor tests;
- Very High strain rates, spallation and hypervelocity impacts ($10^5$ – $10^6$ s-1): Flyer plate impact tests;

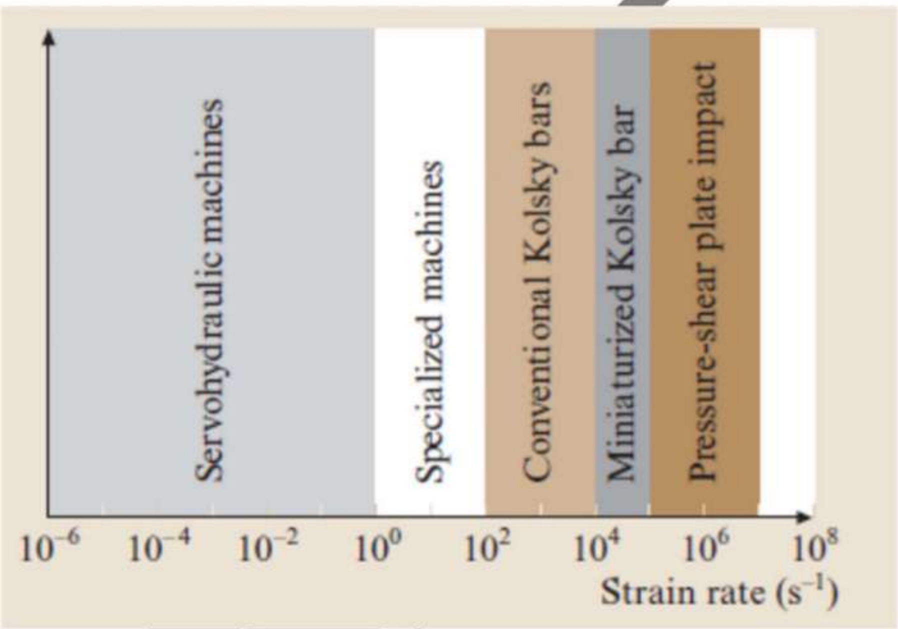

*Figure 5-4: Equipment families ofr synamic testing at different strain rates (Ramesh, 200?)*

The reasons why high strain rate tests cannot be made by standard testing machines (electrical or hydraulic), are mainly of two types:

- the mobile elements of heay machines (crossheads, clamps etc.) cannot reach the speeds required for generating the desired strain rates in the specimen;
- the frames stiffness of the testing machine is not infinite and inertial loads may induce substantial vibrations through the specimens affecting its equilibrium and the load cells readings.

The Labortoary equipment available at the University of Catania include motor-driven testing machines, hydraulic testin machines and an Hopkinson bar facility.

# 6 THE HOPKINSON BAR FOR HIGH STRAIN RATE TESTING

## 6.1 THE HOPKINSON BAR IN 500 WORDS

At strain rates beyond 10 s-1, inertial loads and stress wave transmission within the specimens become too relevant for being neglected; therefore the typical machines for static and fatigue testing are not suitable for dynamic testing.

In fact, two main issues affect the load measurements: the first is the vibration of the machine frame and fixtures, generating load oscillations which cannot be captured by conventional load cells based on resistive strain gauges; the second issue is the wave propagation within the specimen which causes different loads at specimen ends, generating specimen acceleration and load /stress gradients within the specimen.

Furthermore, the small size of dynamic specimens required for minimizing inertia issues, makes almost impossible to measure load and elongation over specimen with conventional in-situ means, although modern optical non-contac techniques allow for accurate strain measurements also with very small specimens.

These issues led to the invention of the Split Hopkinson Bar, where load and elongation of the specimen at nearly-constant strain rate can be inferred from strain measurements on much more suitable locations, e.g. the surface of long bars undergoing uniaxial stress states.

The apparatus consisted of two long bars (input and output bars respectively), connected to both ends of a specimen.

A strain wave, theoretically square, is generated along the input bar by either impacting its free end with a "striker" (usually a bar segment of same diameter and material of the input bar) or be pre-stressing a segment of the bar and suddenly releasing it..

FIGURA A PENNA SCHEMA SHPB con onde incidente-riflessa-trasmessa

The generated wave, called "incident wave", travels along the input bar toward its end where the specimen is connected. The incident wave will be then partially reflected into the input bar as a backward-traveling strain wave ("Reflected wave") and partially transmitted into the specimen. The wave entering the specimen will quickly travel to the other specimen end (the specimen is much shorter than the bars and than the input wave length), where the output bar is connected, so that part of it will be reflected back into the specimen and the other part will be further transmitted along the output bar, resulting in the so-called "Transmitted wave".

Now, according to procedures and relationships which will be discussed ahead in more detail, the measurement of the reflected strain wave and of the transmitted strain wave allows to derive the specimen elongation speed and the axial load of the specimen, respectively, which can be then further translated in engineering strain rate and stress.

Strain waves traveling in the bars are measured by strain gauges at given positions along the bars, so they are represented by strain-versus-time recordings at the proper time and space resolution (typically in the order of megasamples per seconds and a few millimiters as the size of strain gauges, respectively) Then, as engineering strain rate and engineering stress are obtained as functions of time, simple integration of the former also delivers the engineering strain.

Special requirements about the position of strain gauges along the bars derive from the opportunity of recording separately the incident wave and the reflected wave along the input bar preventing their superposition, but this will be better discussed ahead.

Also, according to different possible architectures of the Hopkinson bar, the incident wave can be compressive, tensile or torsional and can be generated by impact (in the first two cases alone) or by instant release of an elastic preload of a portion of the input bar (in all three cases).

The latter architecture is discussed in more detail ahead in this document.

## 6.2 AXIAL ELASTIC WAVES TRAVELING ALONG BARS

( https://www.physicsclassroom.com/ )

A mechanical wave is a disturbance that is created by a vibrating object and subsequently travels through a medium from one location to another, transporting energy as it moves. The mechanism by which a mechanical wave propagates itself through a medium involves particle interaction; one particle applies a push or pull on its adjacent neighbor, causing a displacement of that neighbor from the equilibrium or rest position. As a wave is observed traveling through a medium, a crest is seen moving along from particle to particle. This crest is followed by a trough that is in turn followed by the next crest. In fact, one would observe a distinct wave pattern (in the form of a sine wave) traveling through the medium. This sine wave pattern continues to move in uninterrupted fashion until it encounters another wave along the medium or until it encounters a boundary with another medium. This type of wave pattern that is seen traveling through a medium is sometimes referred to as a **travelling wave**.

Traveling waves are observed when a wave is not confined to a given space along the medium. The most commonly observed traveling wave is an ocean wave. If a wave is introduced into an elastic cord with its ends held 3 meters apart, it becomes confined in a small region. Such a wave has only 3 meters along which to travel. The wave will quickly reach the end of the cord, reflect and travel back in the opposite direction. Any reflected portion of the wave will then interfere with the portion of the wave incident towards the fixed end. This interference produces a new shape in the medium that seldom resembles the shape of a sine wave. Subsequently, a traveling wave (a repeating pattern that is observed to move through a medium in uninterrupted fashion) is not observed in the cord. Indeed there are traveling waves in the cord; it is just that they are not easily detectable because of their interference with each other. In such instances, rather than observing the pure shape of a sine wave pattern, a rather irregular and non-repeating pattern is produced in the cord that tends to change appearance over time. This irregular looking shape is the result of the interference of an incident sine wave pattern with a reflected sine wave pattern in a rather non-sequenced and untimely manner. Both the incident and reflected wave patterns continue their motion through the medium, meeting up with one another at different locations in different ways. For example, the middle of the cord might experience a crest meeting a *half crest*; then moments later, a crest meeting a *quarter trough*; then moments later, a *three-quarters crest* meeting a *one-fifth trough*, etc. This interference leads to a very irregular and non-repeating motion of the medium. The appearance of an actual wave pattern is difficult to detect amidst the irregular motions of the individual particles.

It is however possible to have a wave confined to a given space in a medium and still produce a regular wave pattern that is readily discernible amidst the motion of the medium. For instance, if an elastic rope is held end-to-end and vibrated at just the right frequency, a wave pattern would be produced that assumes the shape of a sine wave and is seen to change over time. The wave pattern is only produced when one end of the rope is vibrated at just the right frequency. When the proper frequency is used, the interference of the incident wave and the reflected wave occur in such a manner that there are specific points along the medium that appear to be standing still. Because the observed wave pattern is characterized by points that appear to be standing still, the pattern is often called a **standing wave pattern**. There are other points along the medium whose displacement changes over time, but in a regular manner. These points vibrate back and forth from a positive displacement to a negative displacement; the vibrations occur at regular time intervals such that the motion of the medium is regular and repeating. A pattern is readily observable.

The diagram at the right depicts a standing wave pattern in a medium. A snapshot of the medium over time is depicted using various colors. Note that point A on the medium moves from a maximum positive to a maximum negative displacement over time. The diagram only shows one-half cycle of the motion of the standing wave pattern. The motion would continue and persist, with point A returning to the same maximum positive displacement and then continuing its back-and-forth vibration between the up to the down position. Note that point B on the medium is a point that never moves. Point B is a point of no displacement. Such points are known as **nodes** and will be discussed in more detail later in this lesson. The standing wave pattern that is shown at the right is just one of many different patterns that could be produced within the rope.

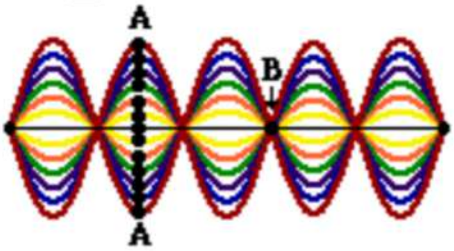

GENERAL CONCEPTS ON MECHANICAL WAVES PROPAGATING IN SOLIDS

Unixial waves (stress, strain, displacement) propagating along slender bodies (bars) can be expressed as functions of time and of position along the bar. The approximate hypothesis of unixiality ensures the everything is uniform all over the cross sections at each given instant.

A propagating wave can be represented at fixed time along a certain length of bar or at a fixed location of the bar during a certain time interval. The law connecting both represrntation states that the Wave length is equal to the propagation speed times the frequency: $\Lambda = C \times f$

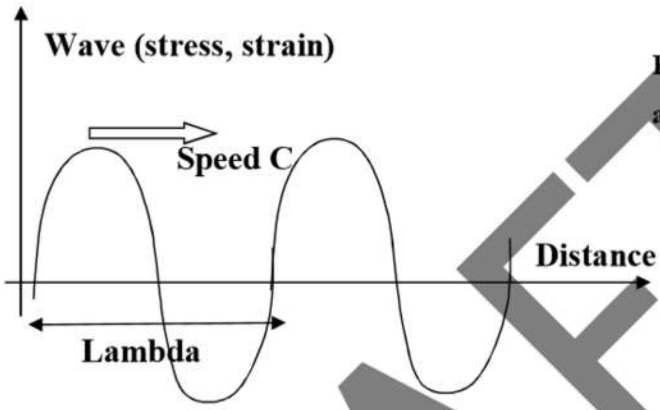

**Fotografia tratto di barra ad istante "t":**

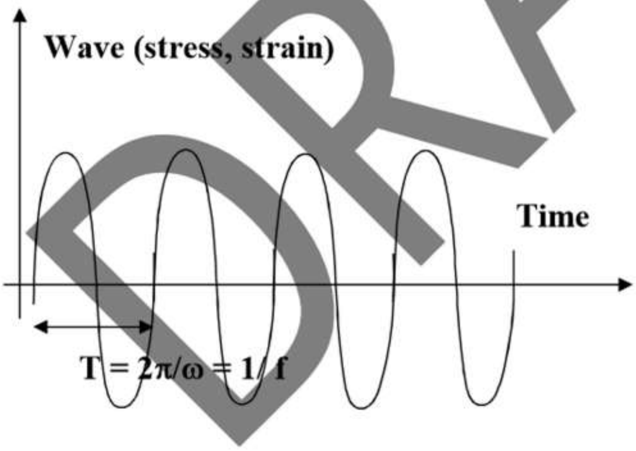

**Andamento al variare del tempo sulla sezione "x" della barra:**

Each general wave can be decomposed in the sum of sinusoids having frequency multiple of the base frequency 1/T; the Fourier series formula allows to calculate amplitude and phase shift of each sinoidal component at given frequency, also called harmonic component of the general wave. The zero-order harmonic is a constant expressing the average value of the wave.

In the special case which the general wave is already sinusoidal on its own, then the average value is null and thewave itself is coincident to the only harmonic component present in the series, so that the spectrum istogram of the wave (plot of the amplitude of the i-th harmonics vs. their frequency normalized to the base frequency) has a single bar.

:

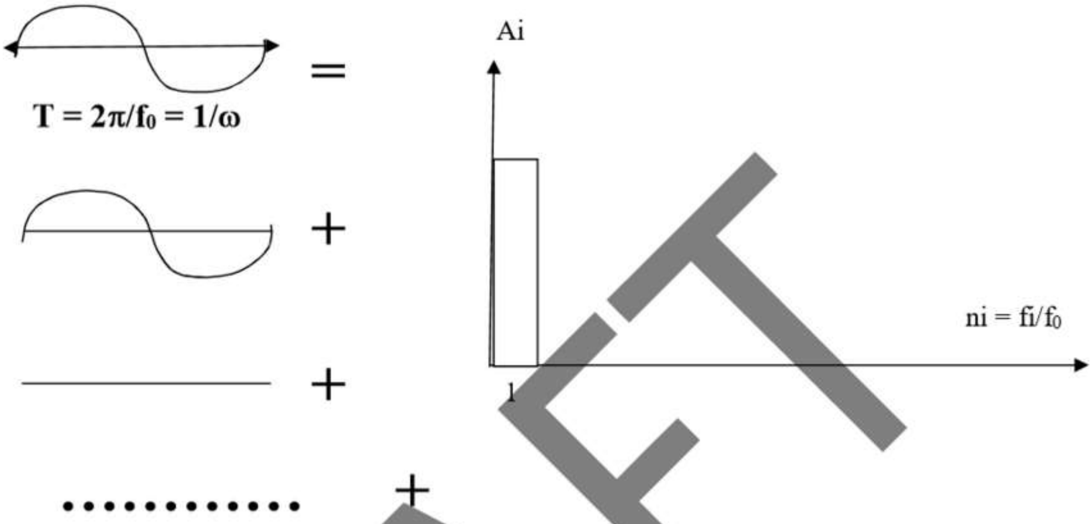

As the general wave is "really" general (e.g. triangular, trapzoidal, random-shaped etc.), a greater number of harmonics is present in the Fourier series approximating it and the spectrum istogram is flatter, made of more bars:

Usually the amplitude of the harmonics decreases with their frequency (higher-order harmonics have lower amplitudes than lower-order ones).

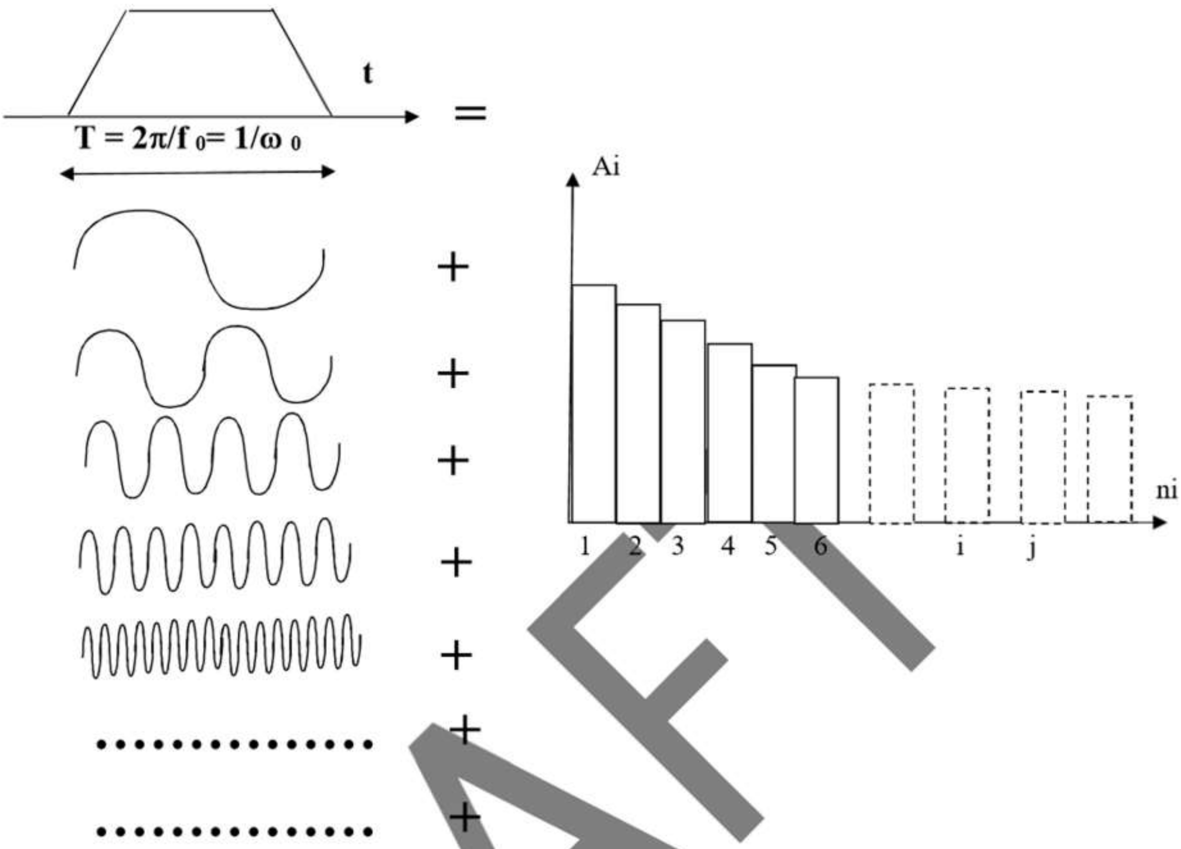

In principle, all elastic waves propagate in solids at the sound of speed $C_0 = \sqrt{\frac{E}{\rho}}$ .Instead their propagation speed slightly decreases as their frequency increases, according to Figure 6-1.

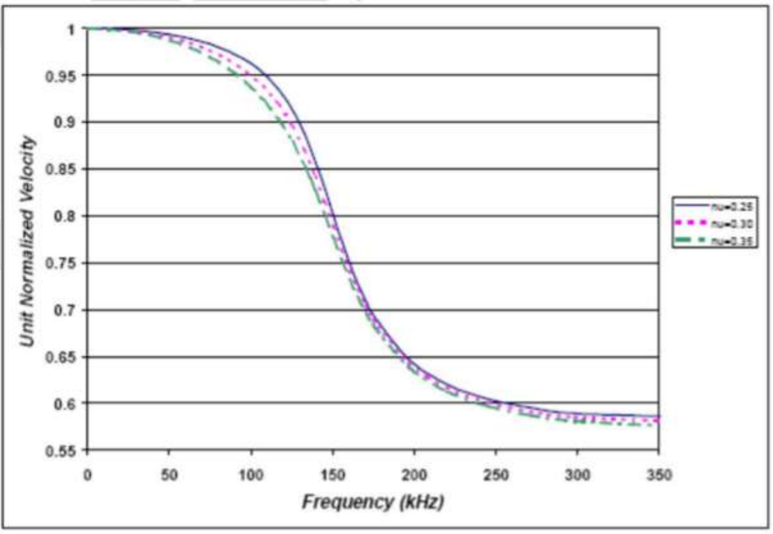

*Figure 6-1 Normalized propagation speed of elastic waves in solids vs. frequency*

Therefore lower-order harmonics run faster than higher-order ones and, after some time from their departure, the former waves covered more distance than latter.

This explains why an elastic wave tends to progressively change its shape as it is measured at different locations along the same bar: the difference of speed means that he phase shift of harmonics at various locations along the bar tends to differently increase with respect to its value at the initial location where the wave is generated.

From a practical viewpoint this means that, for example, a perfectly reactangular wave generated at a certain location of a bar slightly loses it sharp corners if it is recorded 3 meters far from the starting location and tends to become e quite rounded wave if it is recorded at further 10 meters ahead.

## WAVE PROPAGATION ALONG A BAR

Let's consider an elastic wave propagating along the elementary segment of a bar of constant cross section and homogeneous material:

The forces acting on both faces of the bar segment are :

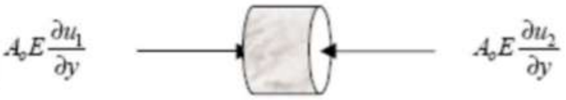

The above forces are equilibrated by the inertia force acting on the whole bar segment:

$$A_oE\frac{\partial u_1}{\partial y} - A_oE\frac{\partial u_2}{\partial y} = A_o dy\rho\frac{\partial^2 u_1}{\partial t^2} \tag{6-1}$$

(time variability of u much smaller than space variability, so du1/dy differs from du2/dy but du1/dt similar to du2/dt: this allows to take the acceleration of section 1 representative of the entire bar segment)

The propagation speed is approximately assumed to be equal to the sound speed in the medium:

$$C_o = \sqrt{\frac{E}{\rho}} \tag{6-2}$$

Deriving *E* and substituting in ( *6-1* ) the axial equilibrium of the bar segment becomes:

$$C_o^2\left[\frac{\partial u_1}{\partial y} - \frac{\partial u_2}{\partial y}\right] = \frac{\partial^2 u_1}{\partial t^2}dy \tag{6-3}$$

Given that the axial displacements function of the bar is contibuous, the displacements at the segment ends are related to each other:

$$u_2 = u_1 + \frac{\partial u_1}{\partial y} dy \qquad (6\text{-}4)$$

Deriving ( *6-4* ) implies:

$$\frac{\partial u_2}{\partial y} = \frac{\partial u_1}{\partial y} + \frac{\partial^2 u_1}{\partial y^2} dy \qquad (6\text{-}5)$$

and substituting in eq. ( *6-3* ) delivers:

$$\boxed{C_o^{\,2} \frac{\partial^2 u_1}{\partial y^2} = \frac{\partial^2 u_1}{\partial t^2}} \qquad (6\text{-}6)$$

Which is the equation describing the longitudinal wave propagating along the bar

Expressing the spatial derivative of displacement as the strain and the latter as a function of the stress, yields:

$$E \cdot \frac{\partial}{\partial y}\left(\frac{\partial u_1}{\partial y}\right) = E \cdot \frac{\partial}{\partial y}(\varepsilon_1) = \frac{\partial \sigma_1}{\partial y} \qquad (6\text{-}7)$$

and substituting ( *6-7* ) in ( *6-6* ) yields the most known form of the wave equation:

$$\boxed{\frac{\partial \sigma_1}{\partial y} = \rho \cdot \frac{\partial v_1}{\partial t}} \qquad (6\text{-}8)$$

The general solution of the differential wave equation is:

$$u = f(y-ct) + g(y+ct) = u_i + u_r \qquad (6\text{-}9)$$

where *f* is a forward-traveling wave ("incident") and *g* is a backward-traveling ("reflected") wave. The sign of both waves can be equal or opposite, depending on how the bar ends are constrained.

The elastic strain of the bar at a given section is the spatial derivative of both terms of the axial displacement or, in other words, is the sum of two strain componets also identified as incident and reflected:

$$\varepsilon_{input} = \frac{\partial u_{input}}{\partial y} = \frac{\partial u_{input}}{\partial (y-ct)} \cdot \frac{\partial (y-ct)}{\partial y} = f' + g' = \varepsilon_i + \varepsilon_r \qquad (6\text{-}10)$$

Instead the speed of the bar at a given section is the time derivative of both terms of the axial displacement, yielding:

$$v = \frac{\partial}{\partial t}(u) \;=\; \frac{\partial f}{\partial (y-ct)} \cdot \frac{\partial (y-ct)}{\partial t} + \frac{\partial g}{\partial (y+ct)} \cdot \frac{\partial (y+ct)}{\partial t} \;=\; c \cdot (-f' + g') = c \cdot (-\varepsilon_i + \varepsilon_r) \qquad (6\text{-}11)$$

## 6.3 MECHANICAL IMPEDANCE AND WAVES REFLECTION/TRANSMISSION AT INTERFACES

K. F. GRAFF. , WAVE MOTION IN ELASTIC SOLIDS, Docer Inc. New York.

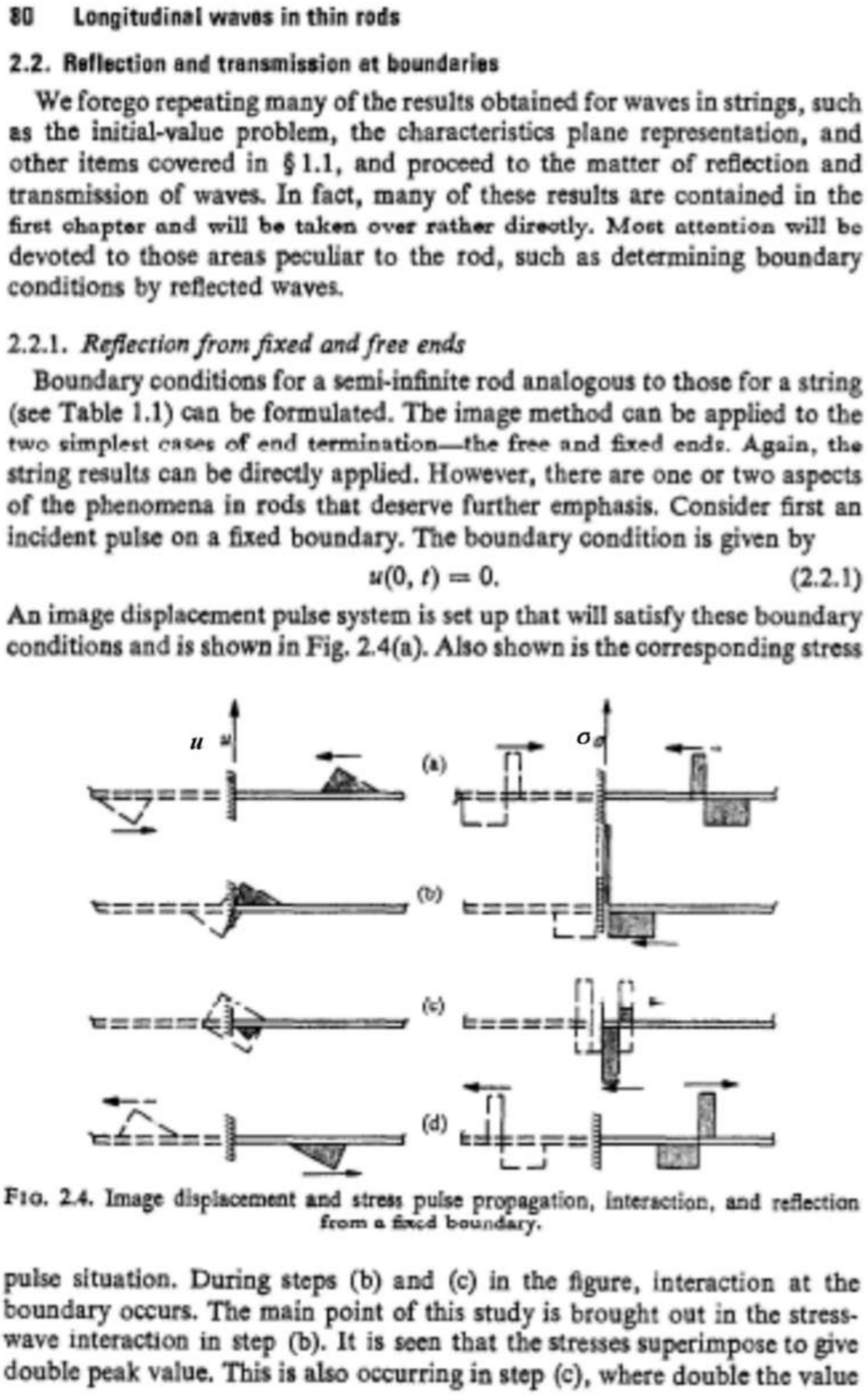

### 2.2. Reflection and transmission at boundaries

We forego repeating many of the results obtained for waves in strings, such as the initial-value problem, the characteristics plane representation, and other items covered in § 1.1, and proceed to the matter of reflection and transmission of waves. In fact, many of these results are contained in the first chapter and will be taken over rather directly. Most attention will be devoted to those areas peculiar to the rod, such as determining boundary conditions by reflected waves.

#### 2.2.1. *Reflection from fixed and free ends*

Boundary conditions for a semi-infinite rod analogous to those for a string (see Table 1.1) can be formulated. The image method can be applied to the two simplest cases of end termination—the free and fixed ends. Again, the string results can be directly applied. However, there are one or two aspects of the phenomena in rods that deserve further emphasis. Consider first an incident pulse on a fixed boundary. The boundary condition is given by

$$u(0, t) = 0. \qquad (2.2.1)$$

An image displacement pulse system is set up that will satisfy these boundary conditions and is shown in Fig. 2.4(a). Also shown is the corresponding stress

FIG. 2.4. Image displacement and stress pulse propagation, interaction, and reflection from a fixed boundary.

pulse situation. During steps (b) and (c) in the figure, interaction at the boundary occurs. The main point of this study is brought out in the stress-wave interaction in step (b). It is seen that the stresses superimpose to give double peak value. This is also occurring in step (c), where double the value of the compressive part is evident. This *stress multiplication* phenomenon is characteristic of the fixed boundary. Proceeding to part (d), after interaction has occurred, it is seen that the reflected stress pulse is identical to the incident pulse. Thus, compression has reflected as compression and tension as tension. This also is a characteristic of the fixed boundary.

Now consider a free-end boundary condition, as given by

$$\partial u(0, t)/\partial x = 0. \tag{2.2.2}$$

Again apply the image method to the reflection problem. The appropriate image system is shown in Fig. 2.5(a). As is evident in the interaction steps (b) and (c), there is a doubling effect, but the doubling is associated with the *displacement* at the end and not the stress. This latter is, of course, always zero. Continuing to step (d), it is seen that the reflected stress pulse is opposite to the incident pulse; thus compression has reflected as tension and vice versa. This *stress reversal* is a characteristic of the free end.

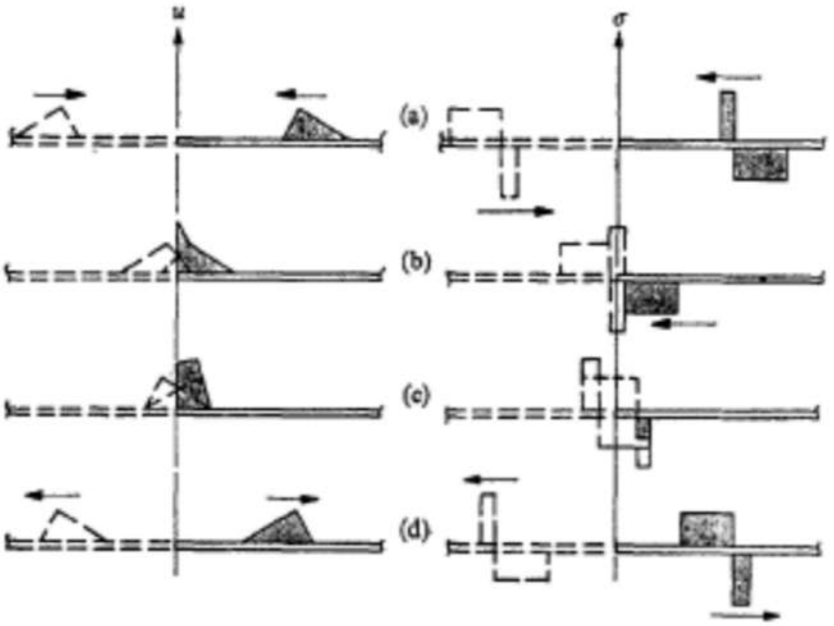

FIG. 2.5. Image displacement and stress pulse system for propagation, interaction, and reflection from a free end.

There are several practical implications of the stress-reversal phenomenon for a free end, all basically related to the fact that if the incident wave is compressive, it will reflect as a tension wave. For example, one of the earliest experimental techniques for determining pulse characteristics employed this phenomenon.† Briefly, the method involves attaching a small pellet or 'time

---

† Hopkinson, B. (1914). *Phil. Trans. R. Soc.* **A 213**, 437. This is mentioned in the *Introduction* (§ 1.3). See Kolsky [18, pp. 87–91] for a more detailed description of the method.

piece' to the end of a rod using a thin layer of grease. Such an interface is capable of transmitting compression but not tension. When a compressive wave reaches the end of the rod, it transmits across the interface and then reverses sign. At the moment the interface stress drops from compression to zero and attempts to pass into tension, the pellet flys off due to the trapped wave momentum in the pellet. From a knowledge of the pellet length and flyoff velocity, it is possible to deduce many of the pulse characteristics.

A second application of the phenomenon is the determination of the dynamic tensile strengths of brittle materials [1, 15]. When the reflected wave causes the tensile strength of material to be reached, fracture abruptly occurs and the end of the test rod flys off in the manner of the time piece. The stress reversal phenomenon is of great importance in ballistic impact situations. Stress waves propagating through thick slabs behave in the same manner as in the rod on encountering a free boundary. It is possible, under the stress reversal, for a 'spall' to be torn from the free surface and to fly off with high velocity again due to tensile failure of the material.

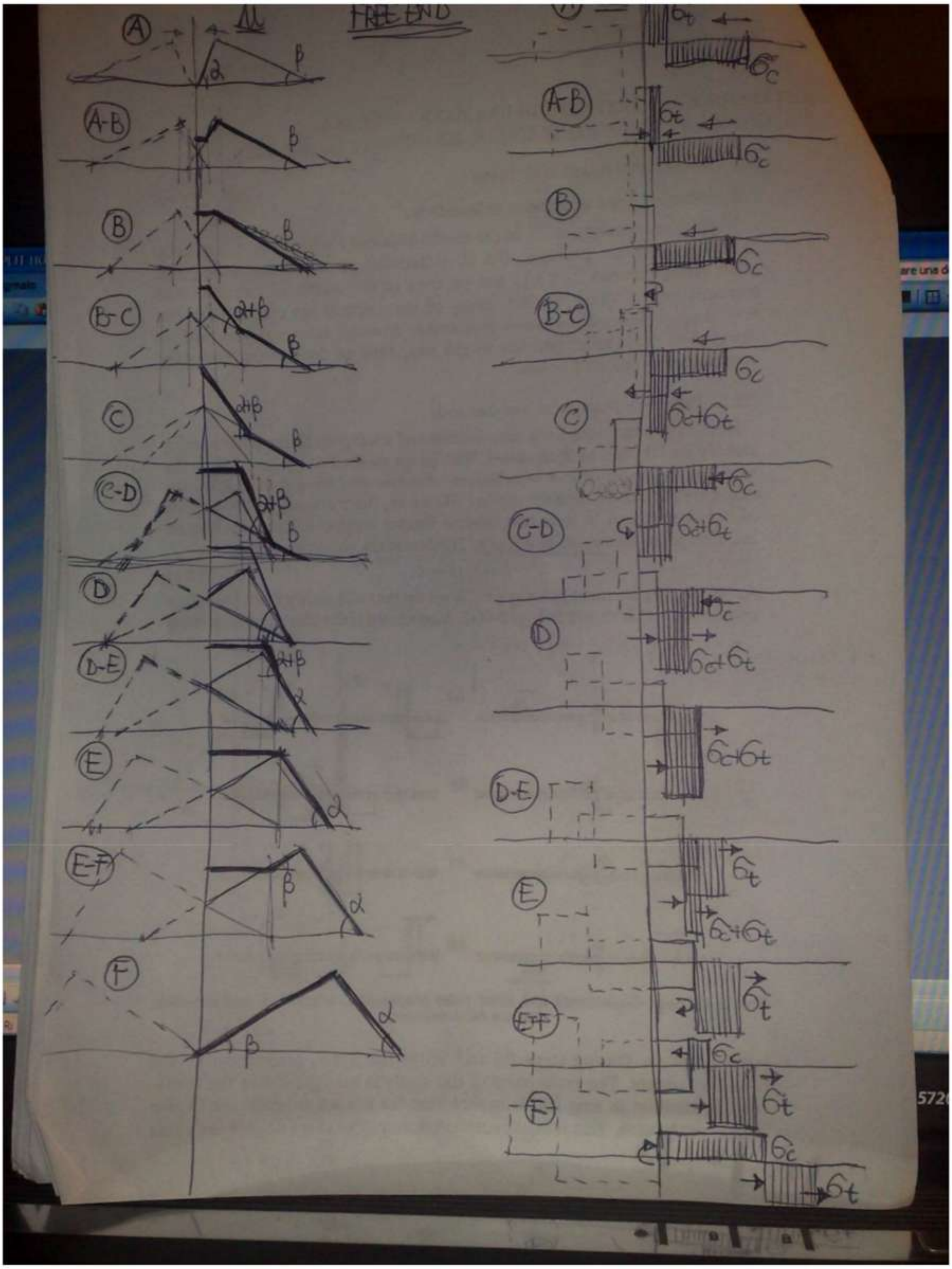
FREE END
A
A-B
B
B-C
C
C-D
D
D-E
E
E-F
F
α
β
α+β
σt
σc
σc+σt

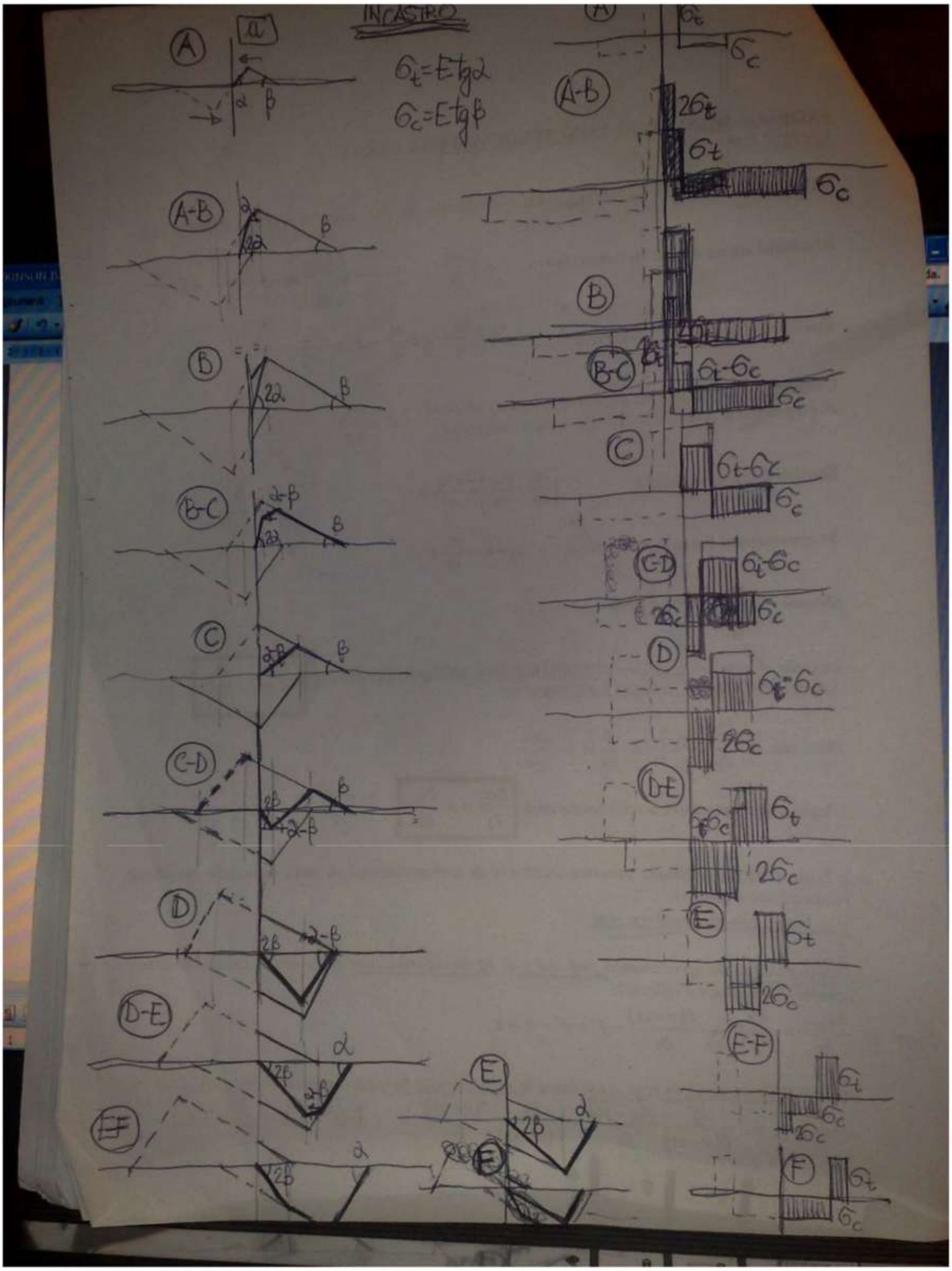
INCASTRO
a
$\sigma_t = E\,tg\alpha$
$\sigma_c = E\,tg\beta$
A
A-B
B
B-C
C
C-D
D
D-E
E
E-F
F
α
β
2α
α-β
2β
$\sigma_t$
$\sigma_c$
$2\sigma_t$
$\sigma_t - \sigma_c$
$2\sigma_c$

## SYINTHESIS OF WAVE REFLECTION MECHANISMS

Let's assume two bars in contact; an elastic wave is generated at the free end of the bar "A" and propagates toward the interface between the two bars. As the incident wave reaches the interface it is partially transmitted into a wave traveling along the bar B, partially reflected back as a retroceding wave into the bar B.

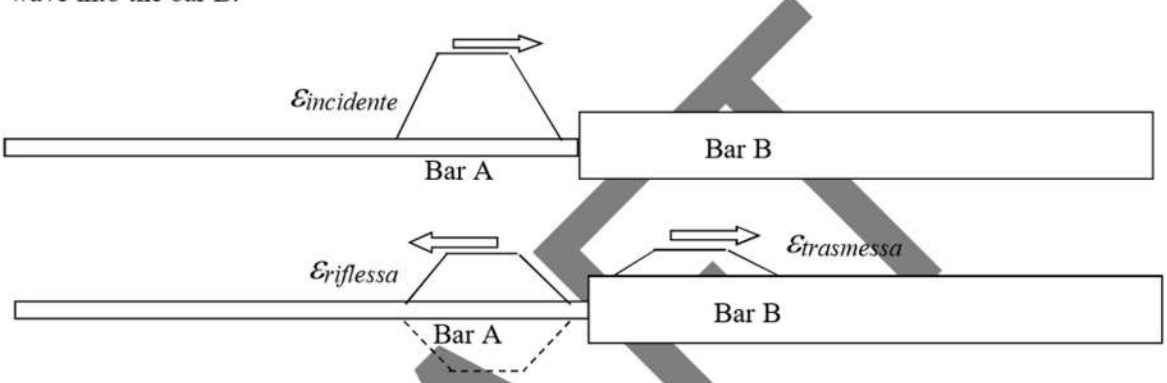

The sign of the reflected wave can be equal or opposite to that of the incident wave, depending on the relationship between inertia and stiffness features of the two bars. The transmitted wave has always the same sign of the incident one.

Also the amplitude of the transmitted/reflected waves depends on theinterplay of inertia and stiffness of the two bars; the parameter combining such features is called mechanical impedance and is defined as follows:

$$Z_i = S_i \cdot \sqrt{E_i/\varrho_i} \qquad (6\text{-}12)$$

The amplitudes of reflected / transmitted waves depends on the transmission/reflection coefficients:

$$\varepsilon_r = \alpha_r \cdot \varepsilon_i$$
$$\varepsilon_t = \alpha_t \cdot \varepsilon_i \qquad (6\text{-}13)$$

Where the coefficients are based on the bar impedances according to the following expressions:

$$\alpha_r = \frac{Z_B/Z_A - 1}{Z_B/Z_A + 1} \quad \alpha_t = 2 \cdot \frac{Z_B/Z_A \cdot S_A/S_B}{Z_B/Z_A + 1} \qquad (6\text{-}14)$$

If the bar B is much more rigid/heavy than the bar A then the reflected wave has the same sign of the incident wave and their amplitudes are close to each other, while the transmitted wave has a small amplitude ($\alpha_r \approx 1$ and $\alpha_t \approx 0$).

If instead the bar B is much lighter and softer than the bar A, then the incident wave is nearly integrally transmitted and the sign of the reflected wave is opposite of that of the incident wave ($\alpha_r \approx -1$ and $\alpha_t \approx 1$).

The limit conditions are the fixed-end constrained beam (bar B has infinite section, elastic modulus and density so that $Z_B \approx \infty$, $\alpha_r = 1$ and $\alpha_t = 0$) and the free-end beam (bar B has zero section, elastic modulus and density so that $Z_B \approx 0$, $\alpha_r = 1$ and $\alpha_t = 0$)

## 6.4 THEORY OF THE HOPKINSON BAR FOR THE MEASUREMENT OF STRESS, STRAIN, STRAIN RATE

ARCHITETTURE SISTEMI DI GENERAZIONE DELL' ONDA INCIDENTE

The split Hopkinson bar test is the most commonly used method for determining material properties at high rates of strain. Significant advancements implemented from the areas of testing techniques, numerical methods, and signal processing have improved the accuracy and repeatability of high strain rate testing. Constant strain rate tests can be performed at strain rates approaching $10^4$ $s^{-1}$ relatively easily.

In the split Hopkinson bar test, a short cylindrical specimen is sandwiched between two long elastic bars, as shown in figure 1.1. The bars are generally made of a high strength alloys with diameters in the range 10 – 50 mm and a length between 2 and 10 meters. *( M. A. KAISER, master thesis).*

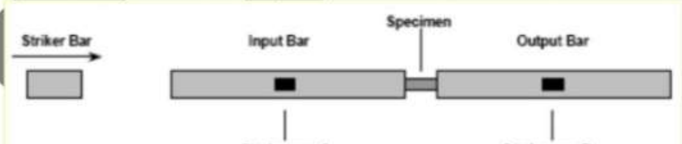

The incident wave can be generated either by launching a striker bar on the input bar as in the above scheme (striker-impact architecture), or by preloading a segment of the input bar and suddenly releasing the preload (direct tension architecture), as in the below scheme.

**AGGIUNGERE DISEGNO INPUT BAR SISTEMA DI BLOCCAGGIO (NOI, THRONDHEIM, ANCONA)**

In the first case the incident wave length is twice the length of the striker and its amplitude is proportional to the impact speed of the striker:

$$\lambda = 2 \cdot L_{Striker}$$
$$\varepsilon_i = \frac{\rho \cdot V_{Striker} \cdot c}{2 \cdot E_{bar}} \qquad (6\text{-}15)$$

Instead in the second case the wave length is twice the length of the preloaded semgent of the bar and its amplitude is half that of the preload before release.

$$\lambda = 2 \cdot L_{Preload}$$
$$\varepsilon_i = \frac{F_{Preload}}{2 \cdot E_{bar} \cdot S_{bar}} = \frac{\varepsilon_{Preload}}{2} \qquad (6\text{-}16)$$

The reasons why the incident wave has a length twice the control-length (of the striker or of the preloaded input bar segment) and an amplitude half the magnitude of the control-force (impact force or preload force), can be easily derived from the rules of elastic waves reflection-transmission at interfaces.

In principle the incident waves are perfectly rectangular (flat parallel impact of the striker or instantaneous release of the preload), in practice they are trapezoidal with more or less rounded vertices (uneven impact of the striker, finite time for completing the release of the preload).

The generated incident wave travels along the input bar until it reaches the interface with the specimen, then it is partially reflected back and partially transmitted to the specimen; the wave entering the specimen travels toward the other interface (between specimen and output bar) and then it further propagates along the output bar.

If the stress / strain waves traveling along the bars remain under their elastic limits, then the load and the elongation of the specimen can be calculated from the recorded strain histories of the bars.

Under certain deformation conditions, qualified later, only two important strain pulses need be identified. These are the reflected pulse and the pulse transmitted through the specimen.

The wave generated in both ways is not really rectangular because in the first case the impacting faces of striker and input bar are never completely planar nor perfectly parallel to each toher, in the second case the release of the preload is never perfectly instantanous but requires a certain (short) time for being completed.

**AGGIUNGERE DISEGNO DI ONDA TRAPEZIA EI VS. TIME CON INDICATO RISE TIME**

The incident waves generated in Hopkinson bars are then typically trapezoidal with the initial ramp requiring a time named "rise time". Typical rise times are in the range 1-10 microseconds for impact waves and 10-100 microseconds for preload-release waves.

## WAVES REFLECTION AT BARS-SPECIMEN INTERFACES AND DERIVATION OF THE ENGINEERING STRESS-STRAIN-STRAIN RATE OF THE SPECIMEN.

At the end of the input bar, the incident wave is partially reflected and partially transmitted into the specimen. The wave entering the specimen travels to the second interface (between specimen and output bar) where it is again partially transmitted along the output bar and partially reflected back into the specimen. The bakward wave in the specimen travels to the first interface (specimen-input bar) where is further splitted into a barckward wave into the input bar and a forward wave into the specimen. Given that the specimen lenght is much shorter than the bars lenght and than the incident wave length (it is a basic prerequisite for the Hopkinson bar), the traveling time into the specimen is very short: therefore many reflections occur at both ends of the specimen at very short time intervals and the first wave entering the specimen is somehow trapped into the specimen traveling back and forth between the two interfaces.

Furthermore the impedance of the specimen is small compared to the impedance of the bars, therefore at each reflection, the wave reflected into the specimen has the same sign of the pre-reflection one and their amplitudes are summed.

The two considerations above imply that a repeated step-like increase of the load occurs within the specimen, progressively stressing and straining the specimen up to failure.

For determining the load / elongation history of the specimen and, in turn, the engineering stress-strain curve of the material, the following considerations apply.

According to the general solution of the wave equation, the elastic wave on a certain section of the input bar while the specimen is subjected to load can be expressed by eq. 6-17.

$$u_{input} = f(y - c \cdot t) + g(y + c \cdot t) = u_r + u_r \qquad (6\text{-}17)$$

Where $f$ is the incident wave (forward-traveling) and $g$ is the relfected wave (backward-traveling).

An elastic wave can be expressed in terms of displacement, strain or stress: here the axial displacement $u$ is considered.

Given the usual impedances of bars and specimens of Hopkinson bar systems, the sign of the reflected wave $g$ is opposite to that of the incident wave $f$.

Instead the wave on a general section of the output bar only includes the transmitted wave (forward-traveling) because very often the specimen is broken much before the transmitted wave reflects at the free end of the output bar and travels back to the section where the wave is measured.

$$u_{output} = h(y - c \cdot t) = u_t \tag{6-18}$$

Where *f, g* and *h* are functions of *y*, axial coordinate along the bars, and of *t*, time. *c* is the nominal sound speed in the bars.

The time dependence of the functions describes the propagation speed and the direction of motion: when *c*t* is subtracted to the wave is forward-traveling, when *c*t* is summed the wave is backward-traveling.

Instead the dependency of wave functions on the bar abscissa *y* describes the shape of the function: if the waves were perfectly rectangular then the functions *f, g* and *h* were discrete step functions of *y*; in case of more realistic trapezoidal waves each function above begins with a linear segment extending over the spatial length corresponding to rise time (*c*t<sub>r</sub>*), then becomes constant. Real waves may have very have rounded corners and might also be described by various types of bestfit functions of *y*.

Differentiating the displacements with respect to the position *y,* the strains of the bars at the given cross section are obtained, useful for successively deriving the load on the specimen:

$$\begin{aligned} \frac{\partial u_{input}}{\partial y} &= \frac{\partial f}{\partial (y-ct)} \cdot \frac{\partial (y-ct)}{\partial y} + \frac{\partial g}{\partial (y+ct)} \cdot \frac{\partial (y+ct)}{\partial y} = f' + g' = \varepsilon_i + \varepsilon_r \\ \frac{\partial u_{output}}{\partial y} &= \frac{\partial h}{\partial (y-ct)} \cdot \frac{\partial (y-ct)}{\partial y} = h' = \varepsilon_t \end{aligned} \tag{6-19}$$

Instead differentiating with respect to the time are obtained the motion speeds of the same cross section, useful for successively deriving the elongation speed of the specimen:

$$\begin{aligned} \frac{\partial u_{input}}{\partial t} &= \frac{\partial f}{\partial (y-ct)} \cdot \frac{\partial (y-ct)}{\partial t} + \frac{\partial g}{\partial (y+ct)} \cdot \frac{\partial (y+ct)}{\partial t} = -c \cdot f' + c \cdot g' = c \cdot (-\varepsilon_i + \varepsilon_r) \\ \frac{\partial u_{output}}{\partial t} &= \frac{\partial h}{\partial (y-ct)} \cdot \frac{\partial (y-ct)}{\partial t} = h' = -c \cdot \varepsilon_t \end{aligned} \tag{6-20}$$

The strain at the bar ends can be converted in stress by the Hooke law and, then, in load by simple multiplication times the bar cross section $A_b$: Then the loads at the two specimen interfaces with bars can be calculated as follows:

$$\begin{aligned} F_{inp} &= E_b \cdot (\varepsilon_i + \varepsilon_r) \cdot A_b \\ F_{out} &= E_b \cdot (\varepsilon_t) \cdot A_b \end{aligned} \tag{6-21}$$

At initial stages of the specimen loading, the two above forces are not equal and opposite to each other because the specimen undergoes an accelerated motion and the net difference between the two interface forces provides the momentum for such acceleration. After a certain transitory the specimen equilibrium is acheved (velocity becomes constant the acceleration vanishes) so that the above forces compensate to each other.

The time necessary for achieving the equilibrium is called "ringing time" and usually equals 1-to-3 wave travels within the specimen.

Finally, the current load deforming the specimen is approximated as the average of the two above loads:

$$F_{Avg} = \frac{F_{inp} + F_{out}}{2} = \boxed{\frac{E_b \cdot A_b}{2} \cdot (\varepsilon_i + \varepsilon_r + \varepsilon_t)} \tag{6-22}$$

Under the hypotheses of validity of the engineering stress-strain curve, (small displacements/infinitesimal deformation and stress uniaxiality), he current average load divided by the specimen cross section $A_S$ delivers the current engineering stress:

$$\sigma_S = \frac{F_{Avg}}{A_S} = \frac{F_{inp} + F_{out}}{2 \cdot A_S} = \boxed{\frac{E_b \cdot A_b}{2 \cdot A_S} \cdot (\varepsilon_i + \varepsilon_r + \varepsilon_t)} \tag{6-23}$$

***(3-waves equation of stress)***

If the bars are equal to each other and the inertia of the specimen is approximately assumed to be negligible, the two forces at specimen ends are equal to each other and no initial transitory occurs before specimen equilibrium then:

$$F_{inp} = F_{out} \Rightarrow \varepsilon_i + \varepsilon_r = \varepsilon_t \tag{6-24}$$

Therefore the engineering stress becomes:

$$\boxed{\sigma_S = \frac{E_b \cdot A_b}{A_S} \cdot (\varepsilon_i + \varepsilon_r)} \tag{6-25}$$

***(2-waves equation of stress)***

or

$$\boxed{\sigma_S = \frac{E_b \cdot A_b}{A_S} \cdot \varepsilon_t} \tag{6-26}$$

***(1-wave equation of stress)***

In principle the three experssions are coincident to each other, but if the initial loading transitory causes substantial specimen disequilibrium during the ringing time, then the 2-waves and 1-wave equations may be affected by large approximations, while the 3-waves equation remains more accurate.

For deriving the strain rate on the specimen, the current speeds of the two bar ends can easily deliver the overall elongation speed of the specimen:

$$\dot{L} = v_{output-}v_{input} \tag{6-27}$$

Under the hypotheses of validity of the engineering stress-strain curves (small displacements/infinitesimal deformation and stress uniaxiality), the overall elongation speed of the specimen divided by the undeformed gage length, delivers the engineering strain rate:

$$\dot{\varepsilon}_S = \frac{v_{output} - v_{input}}{L_S} = \frac{1}{L_S} \cdot \left( \frac{\partial u_{input}}{\partial t} - \frac{\partial u_{output}}{\partial t} \right) = \frac{c}{L_S} \cdot (-\varepsilon_i + \varepsilon_r + \varepsilon_t) \qquad (6\text{-}28)$$

Assuming again indentical bars and negligible speciment inertia (instantaneous specimen equilibrium), then $\varepsilon_i + \varepsilon_r = \varepsilon_t$ and the final one-wave expression of the engineering strain rate becomes:

$$\boxed{\dot{\varepsilon}_S = \frac{2 \cdot c}{L_S} \cdot \varepsilon_r} \qquad (6\text{-}29)$$

***Engineering Strain Rate of the Specimen:***

The simple time integration of the engineering strain rate finally delivers the current engineering strain :

$$\boxed{\varepsilon_S = \frac{2 \cdot c}{L_S} \cdot \int_0^t \varepsilon_r \cdot dt_r} \qquad (6\text{-}30)$$

***Engineering Strain of the Specimen:***

It is worth noting that the elongation between bars is the "very-gross" specimen elongation, including the deformation contributions from specimen shoulders, fillets and any other part of the specimen exceeding the gage length, similar to the crosshead motion of static testing machines. This makes eq. ( *6-28* ) still less accurate than usual engineering strain measurements, typically based on clip-gage elongation measurements of the gage length alone instead of th than the entire gross specimen elongation.

In case of ductile metals the engineering approach and the elongation-based true approach derived from the engineering one, are too inaccurate and the "section-based" true aproach must be adopted for determining the stress-strain curve.

In these cases, the above concepts only remain valid for the determination of the current load by eq. ( *6-22* ), while optical methods are necessary for determining how the current specimen diameter evolves; then $\varepsilon_{True}$ and $\sigma_{True}$ are determined with the same procedures already duscussed for the static tests, while $\dot{\varepsilon}_{True}$ is finally obtained by simple time derivation.

## CONTROLLABLE PARAMETERS IN HOPKINSON BAR TESTING AND EFFECTS OF THE INCIDENT WAVE ON THE TEST CONDITIONS

Assuming ideal rectangular incident waves, the two controllable parameters of the Hopkinson bar test are the amplitude $\varepsilon_i$ and the wave length of the incident wave. In case of striker impact these parameters are respectively governed by the length of the impactor and by its speed according to eq. ( *6-15* ).

Instead in case of preload release (direct tension Hopkonson bars) the above parameters are governed by the preload magnitude and by the length of the input bar segment subjected to the preload, accordidng to eq. ( *6-16* ).

The magnitude of the incident wave sets the amount of energy entering the specimen per unit time and, then, the strain rate; instead the length of the incident wave sets the integrationlimit in eq. ( *6-30* ) and the upper strain at theend of the test. Obviously, given a certain wavelength sufficient for deforming the specimen up to failure, longer waves will not have any further effect and the part of incident wave exceeding the failure time will be totally reflected back into the input bar.

The same considerations apply for trapezoidal waves, according to Figure 6-2:

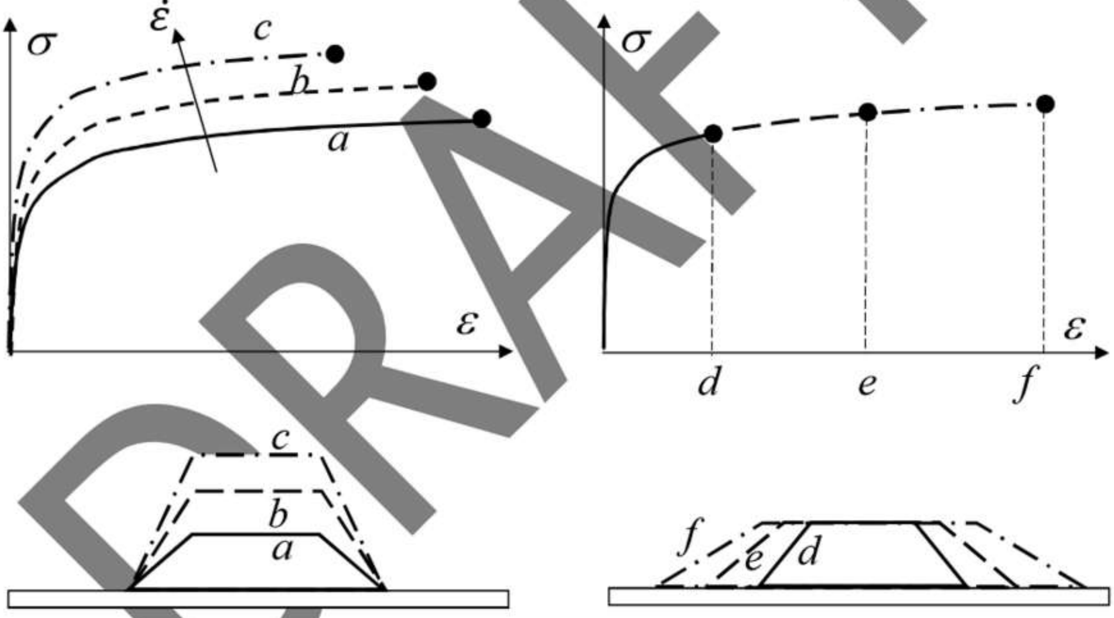

*Figure 6-2 Effect of the incident wave amplitude/wavelength on the specimen stress/strain/strain rate*

Clearly, when the amplitude of the incident wave is increased maintaining the same wavelength, the strain rate increase with the same integration time also accompanied by an increase of the final strain achieved: in other words, increasing the incident wave amplitude increases both the strain rate and the final strain achieved in the specimen.

Instead increasing the incident wave length only increases the final strain achieved in the specimen.

The effect of the rise time (initial ramp of the incident wave) is that of making the strain rate on the specmen to initially increase with an approximately linear ramp, untile the plateau is reached (constant strain rate phase of the test). The rise time roughly lies in the range 1 - 100 microseconds, which depending on the tested material and the specimen size correspond to a few percents of plastic strain (0.01 – 0.05).

In any case the elastic range of the specimen response is always included within the rise time, so the yield stress cannot reflect the dynamic amplification of the high strain rate value at the plateau.

The above considerations show that the Hopkinson bar test is a displacement-controlled test, as the controllable / prescribed law is that of elongation vs. time.

# 7 THE HOPKINSON BAR @ UNICT

## 7.1 OVERALL SIZE AND MAIN DIMENSIONS OF THE EQUIPMENT

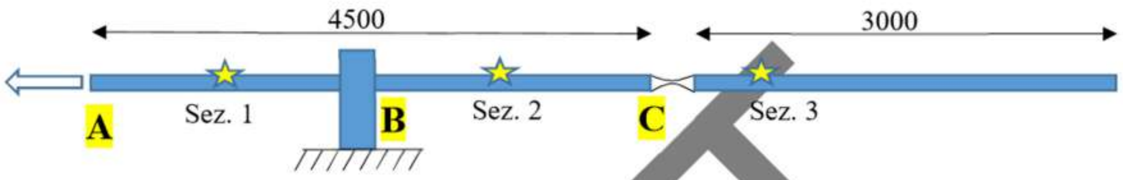

*Figure 7-1 Overall view of the Hopkinson bar equipment available at the Mechanics Laboratory of the University of Catania*

The split Hopkinson tensile bar (SHTB) available at the Iniversity of Catania is roughly 7.5 m long, 1 m wide and 1.3 m high. The current bars are made of Al7075 alloy with 16 mm diameter.

The input bar is 4.5 m long, it is simply supported with 7 low-friction teflon supports and is connected at section A with a 100 kN hydraulic jack, necessary for applying the tensile preload (see Figure 7-1and Figure 7-2),

At section B the input bar passes through a hole in a rigid wall fixed to the frame, so that a clamping device applied to such cross section of the input bar prevents it from passing through the hole in the wall and, then, allows to stretch the segment A-B of the input bar by simply pulling the jack (in the leftward direction according to the viewpoint of the pictures) and to generate the desired preload over the segment A-B. The clamping device applied onto the bar, as better discussed ahead, can be quickly released, so releasing the preload and transforming the static preload into the incident traveling.toward the specimen.

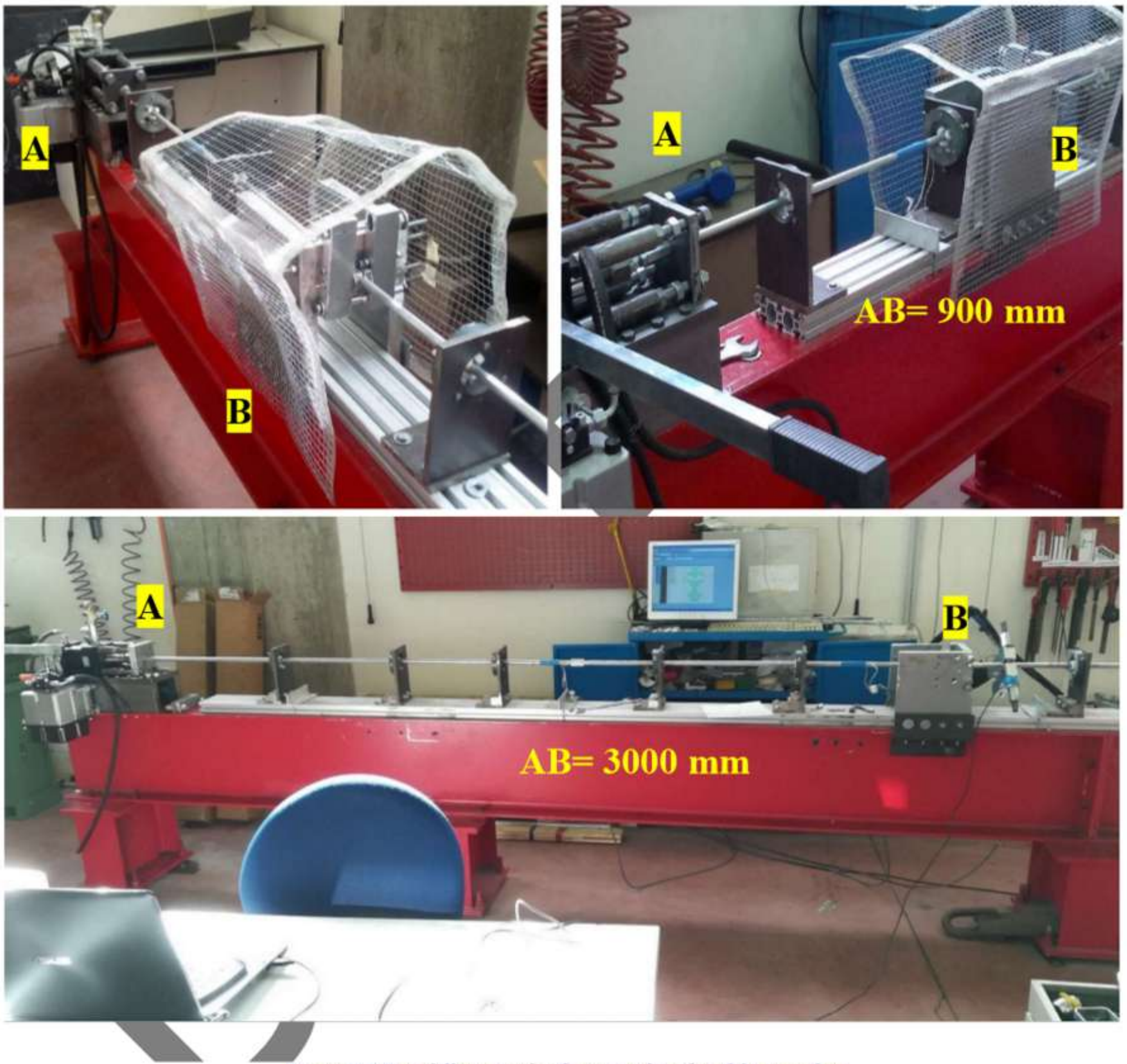

*Figure 7-2 Two different preload segment lengths of the input bar*

The current length of segment A-B is 3 metres buti t can be easily adjusted by simply moving the wall back and forth along the frame of the SHTB (the setup with A-B=900 mm is visible in Figure 7-2). At the endpoint C of the input bar an M8 threaded connection is machined for either connecting round specimens with the same threaded connection or an M8 threaded adapter for flat specimens (see ahead). The other end of the specimen is connected in the same way to the output bar, but in this case the M8 thread is left-handed for simplifying the specimen installation.

At the other end of the output bar a mass of roughly 300 grams is hanged with the scope of momentum trap, in order to prevent / reduce the broken specimen halves from being impacted to each other at the test end, which deforms/damages the broken specimen halves and spoils successive microscopical anaysis of fracture surfaces.

According to the classical theory of Hopkinson bar, given the overall length of 4500 mm of the input bar, the maximum lenght of the preloaded segment A-B was 1500 mm and the strain gauge for reading the incident and reflected wave was to be placed at a section "SG" far 3000 mm from A: in this way a 3000 mm and 600 microseconds incident wave was generated, and the position of the specimen at section SG was suitable for recording the incident and the reflected way clean and separate from each other, without any overlap. This would have enabled to determine $\dot{\varepsilon}_S$ and $\varepsilon_S$ bt equations ( *6-29* ) and ( *6-30* ).

Instead our technique for measuring $\dot{\varepsilon}_S$ and $\varepsilon_S$ is based on optical measurement from high speed camera acquisitions, which makes unnecessary the recording of a clean reflected wave $\varepsilon_r$ on the input bar and, then, enables to extend the preloaded segment A-B virtually up to the entire input bar. And longer prelod means longer incident waves and the possibility of estending the range of strain rates in the low-end of Hopkinson bar testing: experimens at $\dot{\varepsilon}_S \cong 300\ s^{-1}$ during up to 1200 microseconds have been successfully performed with rather long specimen (9 mm gage length plus 9 mm fillets and shoulders) made of very ductile metals, which according to the standards SHTB procedure would have required input bars twice times longer or more.

In other words, speed camera acquisitions and optical strain measurements allow to extend the lower threshold of possible strain rates of a given SHTB equipment at half the minimum values enabled by the standard strain measurement based on the reflected wave.

Also, the strain measurement by optical measurement is much more accurate than the reflected wave one, because the former can refer to the specimen diameter orto the proper specimen gage lentth, while the latter one can only refer to the total gross specimen length.

The upper strain rate achieved so far with the same specimens ( 9 mm gage length + 9 mm fillets and shoulders) is 3500 $s^{-1}$ with roughly 75 kN preload.

The current limit is the clamping system which can hold the input bar without slip only up to 75 kN preload. A larger/stronger clamping system enabling to get closer to the limit of the system (100 kN for the jack and the bars) should enalbe strian rates close to 5000 s-1.

## 7.2 SUSPENSION/ALIGNMENT DEVICES, PRELOAD AND CLAMPING

The supports of input and output bars are based on three 120 deg-angulated screws per each piece (see Figure 7-3), ending with a cylindrical teflon tablet (10 mm diameter 6 mm high).

The locknut system allows to register the position of the supported bar section

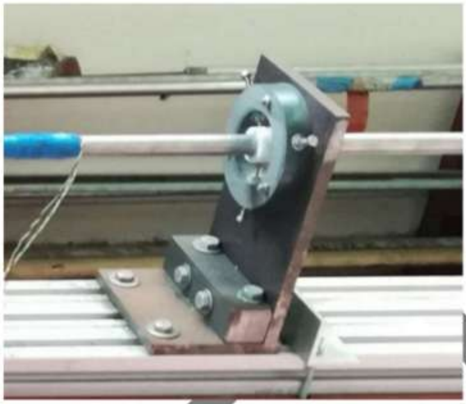

*Figure 7-3 bar support with registering screws and teflon tabletss*

The jack for applying the preload is rated to 100 kN and 50 mm stroke. As the section B of the input bar is locked against the wall by way of the clamping system and the preload is applied by pulling the section A with the jack, the latter section is locked to the ground too, by way of the column-and plate system in Figure 7-4. While the locking of section B is functional for preloading/releasing the input bar, the locking of section A is made for preserving the jack and its seals from the pressure bursts due to the successive wave reflections occurring there. A detail of the locking at section A is provided in Figure 7-4. This locking does not require any fast-release system as it is unlocked a

Fter each test and re-armed before starting the successive test.

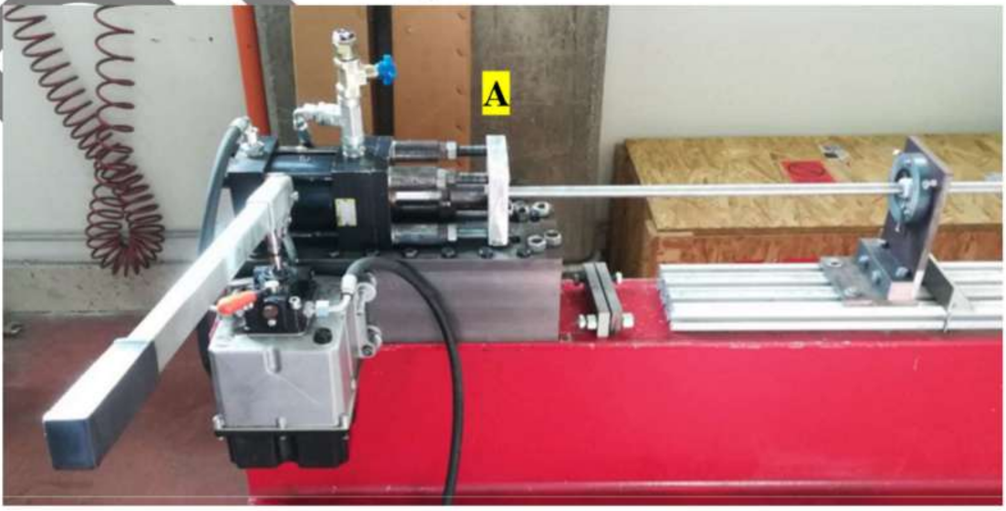

*Figure 7-4 Plate-and-columns locking of section A after preload.*

## 7.3 CLAMPING / FAST RELEASE SYSTEM, FRAGILE ELEMENT, SHAPE OF THE INCIDENT WAVE

The locking system of section B instead requires a fast release system for transforming the static preload into the incident wave. In the ideal case that the release duration is zero (instant release) a perfect rectangular step-like wave is generated; in real systems the release duration ranges from less than 10 to more than 100 microseconds and the corresponding incident waves are more or less trapezoid-shaped. The duration of the initial rampi s the rise time $t_r$.

The fast-release locking system is based on a couple of nutcracker-like clamps schematised in Figure 7-5 where the fulcrum is a fragile element in the lower side, generating the force $F_F$, the reaction is the contact force generated by the input bar when it is pushed radially by the clamps, $F_B$, the action is the actuation force generated by tightening the nuts of the M16 threaded bar, $F_A$.

The disassembled clamping system is also visible in Figure 7-6 where a washer-shaped load cell is installed for measuring the actuation force while the M16 bolts are tightened.

The input bar seats machined in each clamp are slightly threaded for increasing friction, delivering an overall friction coefficient around 0.6.

The distances $a$ and $b$ are aimed at ensuring a grip of the clamping sysyem suitable for locking the bar under a tensile force of 100 kN: considering that we want a friction force of 100 kN with a coefficient of 0.6, a normal contact force around $\frac{100\,kN}{2\cdot 0.6}$85 kN is necessary over each half side of the clamped bar surface; selecting a ratio $a/b \approx 3$ the equilibrium of each clamp implies that for locking the bar under 100 kN tensione the fragile element must undergo $F_F \approx 120\,kN$ without breaking and the actuation force must equal $F_A \approx 40\,kN$. The M16 threaded bar enables to get the latter actuation force by hand-tightening the bolts with a wrench where a tubular extension 400-500 mm long is installed.

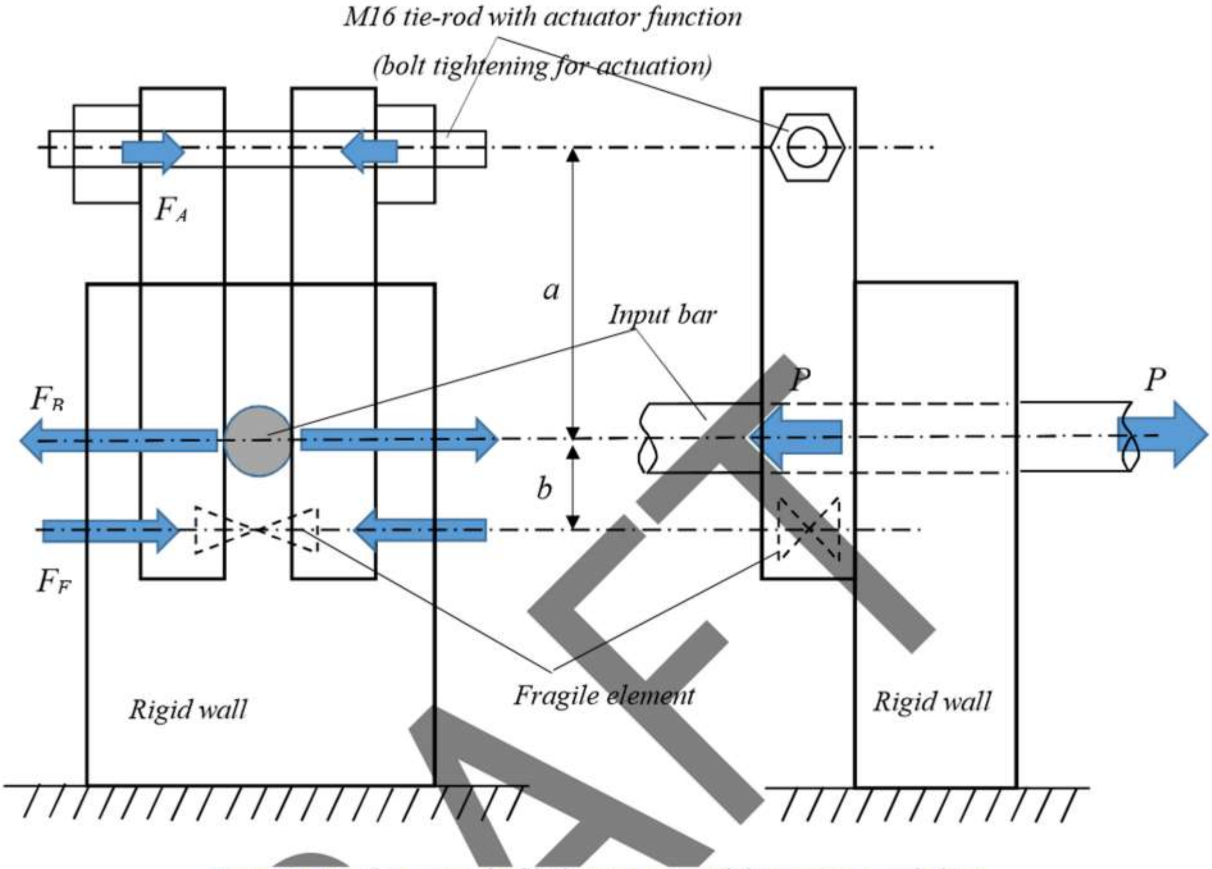

*Figure 7-5 Fast-release nutcracker-likeclamping system with forces acting on each clamp*

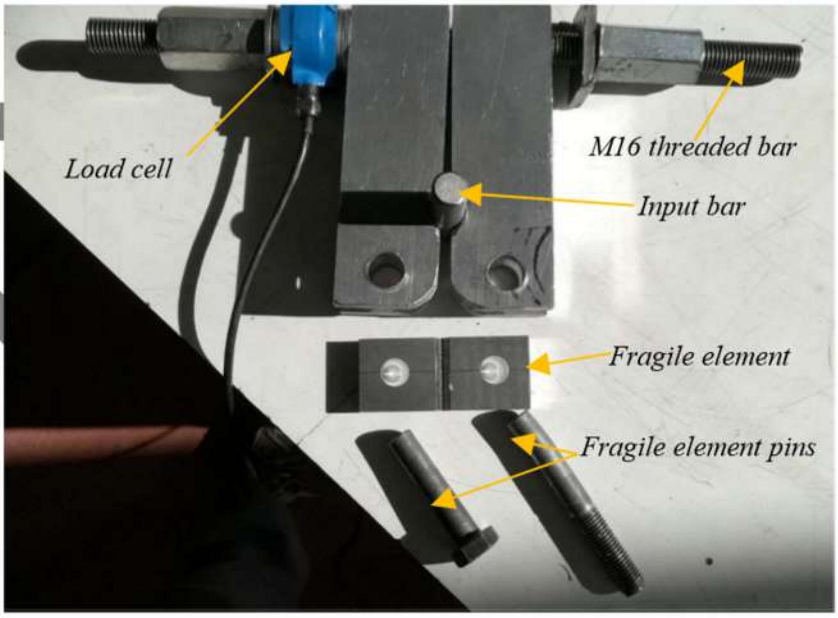

*Figure 7-6 Disassembled clamping system*

After the clamping force and the input bar preload force are respectively generated by tightening the M16 bolts and then by pulling the hydraulic jack, the endpoint A must be locked and the trigger-based recording system system armed: then the test is started by increasing the tightening force until the fragile element breaks and the preload is released.

In principle the necessary force for breaking the fragile element should be just slightly greater than that necessary for preventing the input bar from slipping through the clamps as the hydraulic jack applies the preload. Instead in the real case a certain margin is necessary between the two loads, so the rupture force of the fragile is at least 10% greater than that ensuring the non-slipping condition between input bar and clamps.

## 7.4 MAIN FEATURES OF STRAIN GAUGES BRIDGES AND DIGITISING/ACQUISITION SYSTEM

For acquiring the strain waves traveling along the bars, at least three couples of strain gauges are installed at opposite ends of diameter of three different cross sections of the bars;

1) the first couple of strain gauges (cross section #1) is installed at a cross section within the preloaded segment A-B of the input bar; it is necessary for controlling the static preload;
2) the second couple is applied on the input bar at a cross section #2 within the segment B-C (between the end section of the preloaded segment and the specimen attachment); given the availability of the speed camera at UniCT and the possibility of optical strain measurements, this couple of strain gauges is not used for the usual recording of the reflected wave but it only delivers the mix of incident + reflected waves useful for the three wave assessment of the specimen equilibrium at early stages of each test;
3) the third couple of strain gauges is applied to the output bar (cross section #3) beyond the specimen attachment, for measuring the transmitted wave;.

Two strain gauges are installed at opposite ends of an arbitrary diameter per each selected cross section because this setup allows to eliminate possible bending contributions affecting the recording of single strain gauge configurations.

.Given the average time duration of a SHTB test (within 1000 microseconds) and the need of acquiring an appropriate number of measurements at appropriate time intervals (around 100 measurements at 10 microseconds each), the 250 kHz badwidth and 1 Msample/second sample rate specifications of the acquisition and a/d conversion installed hardware are appropriate.

## 7.5 QUICK DESCRIPTION OF LABVIEW /DEWETRON CONTROL TOOLS

……………. IN PROGRESS : BASIC INFO X HANDLING THE SYSTEM ………

## 7.6 TESTING PROCEDURE : CLAMPING SETUP AND OPERATION

a) First step of testing procedure is to fully extend the jack (possibly retracted from previous tests) and to install the clamps, assembled but slack /not toghtened, over the bar section B just protruding out of the hole in the fixed wall (Figure 7-7).

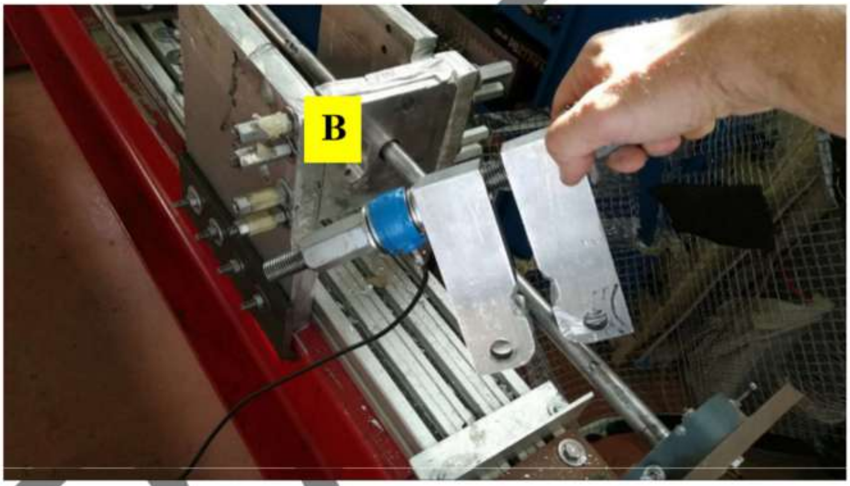

*Figure 7-7 Clamping system installation*

b) Then the a safety iron net is closed around the clamps for preventing the projection of fragments after the fragile ruptire and the clamps tightening can be started, as in Figure 7-8.
The tightening continues until the the reading of the button-shaped load cell informs that the threshold value of $F_A$ is reached, ensuring that no slippage occurs between the tightened clamps and the input subjected to the desired bar preload (the greater the desired preload the greater the necessary threshold tightening force).

*Figure 7-8 Clamping system tightened at end of test preparation: further tightening ruptires the fragile element and starts the test*

c) As the clamps are sufficiently tightened and section B is properly held, the input bar is gradually pulled at its section A by operating the hydraulic jack, until the strain gauge reading from section #1 informs that the desired bar preload is achieved.

d) Then the endpoint A is fixed to the ground (for reducing pressure overbursts on the jack), the triggers for strain gage acquisition are armed (either by decreasing signal at section #1 or by increasing signal at section #2) and the specimen is installed between the two bars;

e) Finally, the clamping system is further tightened until the fragile element breaks, releasing the preload and running the whole test. It is worth noting that also the fragile element must be designed for ensuring its failure at the desired load.

As the clamps break open and section B is set free, the preload of magnitude $P$ virtually becomes a couple of wave,s each of amplitude $P/2$ and wavelength AB, one (filled in yellow) traveling forward toward the specimen, the other (filled in green) traveling backward toward the section A, according to Figure 7-9:

*Figure 7-9 Static preload transformed in two traveling waves*

The green wave already starts at secion A, therefore as the clamps break it is just reflected by the fixed-end constraint of section A into a forward-traveling wave of the same sign (tension) which concatenates with the yellow wave.

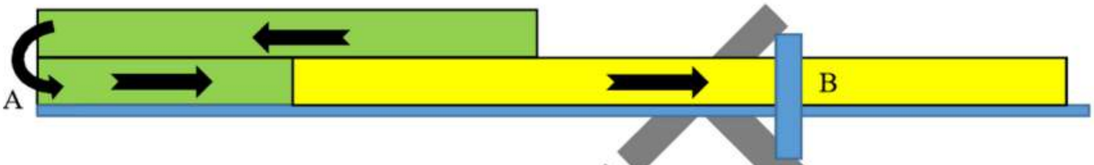

*Figure 7-10 traveling waves from preload*

In this way, according to the rules of uniaxial elastic waves propagation, the static preload $P$ over the segment AB of the input bar became a forward-traveling incident wave of load amplitude $P/2$ and wavelength 2AB, as already discussed in eq. ( *6-16* ).

## 7.7 OTHER EXISTING ARCHITECTURES OF HOPKINSON BAR SYSTEMS

*A.T. OWENS Master Thesis*

Another technique was developed by Nicholas [17] who used a threaded specimen placed in between the two bars (Fig. 1.9). A compression collar was placed around the specimen, and the threads were tightened until the collar was slightly preloaded. The wave was generated by a compressive impact and first passed through the collar as a compressive wave, leaving the specimen unloaded initially. At the end ofthe transmitter bar, the wave reflected as a tensile wave. The compression collar, being unable to resist the tensile wave, allowed the specimen to be loaded in tension.

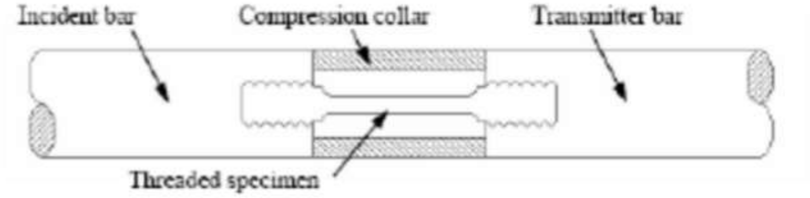

Another setup, used by Staab and Gilat [19], used a clamping mechanism to store energy in the incident bar. A clamp was placed on the bar at some distance from the end opposite the specimen. A static tensile load was applied to the end, and as the clamp was released, the tensile stress wave propagated towards the specimen. By using a fracture pin, the clamp could be released almost instantaneously. In the setups prior to this one, the length of time of the loading pulse was dependant on the length of the striker bar (Fig. 1.7). This setup had an added advantage that the length of the loading pulse is related to the length of the bar where the energy is initially stored. Thus, by placing the clamp farther away from the load application point, the time duration of the pulse could be varied. For the setup used by Staab and Gilat, loading pulses could be produced in excess of 500 microseconds. Previous setups had only produced loading pulses in the range of 100-200 microseconds.

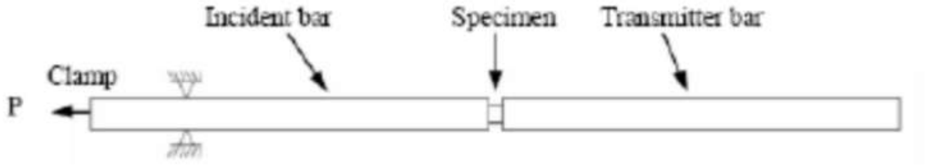

Researchers have also used hollow bullets to produce a tensile stress wave. Ogawa [20] used one such setup to study the impact-tension-compression behavior of pure irons. In these setups, the incident bar had some type of an anvil on the impacting end. A cylinder traveled along the incident bar and contacted the anvil as shown in the Fig. 1.12. The impact resulted in a tensile pressure pulse in the incident bar loading the specimen to failure.

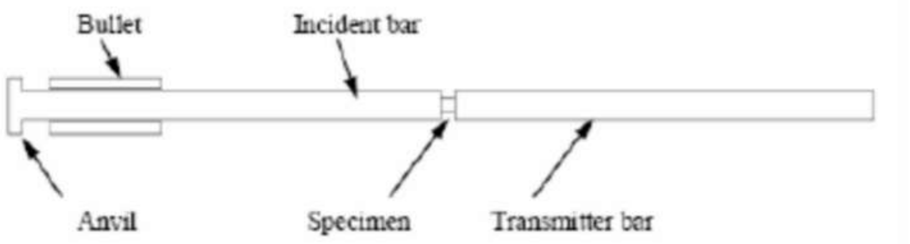

The previously mentioned setups are just some of the basic types of setups typically used in SHTB testing. Many variations of these configurations have been derived and used in the last few decades. The advent of high speed data acquisition techniques as well as the introduction of resistance strain gages, quartz and piezoelectric transducers, as well as other high frequency response measurement systems has opened up many doors for testing of dynamic stress-strain response.

INTERFACCIA BARRE-PROVINO

*A.T. OWENS*

PROVINI FLAT A SPESSORE VARIABILE::

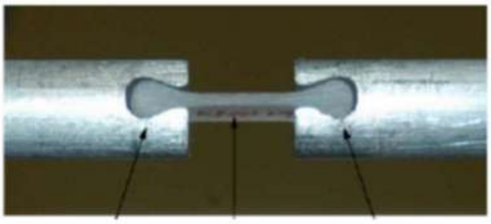

UNICT: PROVINI FLAT DA LAMIERA  Molto più  affidabile. Tutti con colla/resina, UniCT senza (grazie a camera rapida abbiamo elongaz. Provino e non interessano scostamenti da distanza estremi barre )….

UNICT: ATTACCHI FILETTATI  SU PROVINI CILINDRICI.

PROBLEMI SENSORISTICA

*A.T. OWENS*

DIMENSIONI STRAIN GAGE

Considering a harmonic wave that is the form of a cosine function, the peak value of the wave is located at the center, and the average can be found by integrating across the period.

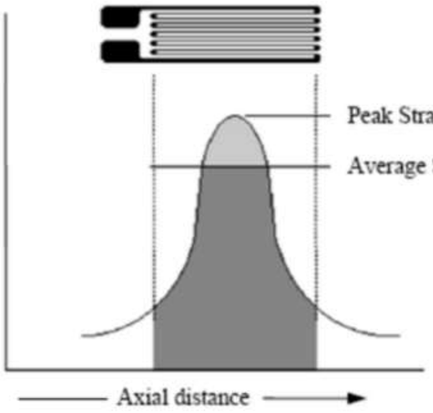

Figure 3.3: Peak vs. average strain (from *Vishay Measurements Group*)

Thus, for a cosine function with amplitude of unity, the measured strain will be,

$$\varepsilon_{MEASURED} = \frac{C_0}{L} \int_{-\frac{2C_0}{L}}^{\frac{2C_0}{L}} \cos(2\pi f t)\,dt \,.$$

where $L$ is the gage length, $f$ is the frequency, and $C_0$ is the wave speed. Figure 3.4 shows the frequency response for a number of different potential gage lengths available for this setup. It was determined that a gage length of 1.5 mm would be a suitable choice for this application.

# 8 APPENDIX - A: ANALYSIS OF EXPERIMENTAL DATA FOR FOR AREA-BASED TRUE CURVES (STATIC AND DYNAMIC TESTS)

## 8.1 OPTICAL DEFORMATION MEASUREMENTS FROM VIDEO ACQUISITIONS

The standard theory of Hopkinson bar prescribes that the strain on the specimen is obtained from the reflected wave $\varepsilon_r$ (see eqs. …….). But, as already duscyssed in previous sections, $\varepsilon_r$ just delivers the speed at which input and output bars separate to each other (e.g. the time derivative of the distance BC between specimen ends).

Apart from issues about overlapping disperion of incident and regflected waves, in case of tensile specimens the distance BC expressesthe gross specimen elongation also including contributions from shoulders, threaded or other kinds of specimen/bars connections and so on. Therefore the classical procedure for strain derivation from $\varepsilon_r$ is poorly accurate and and a more reliable procedure based on optical measurements is discussed here.

Apart from the derivation of single frames from either normal speed or high speed video acquisitions, the same procedure can be applied to static and dynamic tests with small differences only related to the way of synchronizing load readings with optical deformation readings.

The procedure discussed below is referred to round cross section specimen as the diameter measurement delivers the effective cross section necesary for calculating both true stresses and true strains, which cannot be directl derived from a single optical measurement of width in case of flat specimens. However recent findings (Mirone et al. 2018) show that conversion functions can be obtained for deriving the current cross setion from simple (optical) elongation measurements of properly selected gage lengths, also in case of flat specimens. As a further alernative, optical strain measurements and cross section derivation for flat specimens can also be based on the digital image correlation (DIC) technique, at least up to certain strain levels.

The following procedure describes how to extract pictures at proper time intervals from a video of the deforming specimen, and pasting / scaling them within a vectorial drawing software so that dimensions can be taken.

Provided that the video recordings are are made with adequate resolution (at least HD), that the framing encloses the deforming specimen in as larger frame portions as possible (e.g. the specimen length covers 80% of the picture or more) and that no optical distortion is ensured by camera/subject alignemnt and by focal length of camera lenses (90 mm or more), the accuracy of optical measurements is more than satisfactory (e.g. error within 1-2- %).

PROCEDURA STANDARD

1) Incollare su autocad tramite incolla speciale/bitmap indipendente dalla periferica la fotografia detta "immagine zero" del provino ripreso mentre si trova poggiato su un pannello verticale o "a tavolino" con accanto due righelli/parti di calibro/riferimenti di lunghezza nota, rispettivamente disposti paralellamente a larghezza ed altezza fotogramma. Al momento della foto i righelli devono stare sul piano medio dei provini cilindrici o sul piano superiore dei provini flat.

2) copiare una alla volta circa 30 immagini estratte Tramite Virtual Dub dal video della prova tramite CTRL+1, e incollarle su autocad tramite incolla speciale / bitmap indipendente dalla periferica

   Si parte dal frame precedente la rottura (ultimo fotogramma provino intero) e si va indietro fino al frame iniziale del filmato, chiamiamolo "frame 1". Vicino al momento della rottura i frames estratti saranno più ravvicinati (1 ogni 3 – 5 – 10), verso inizio prova più "Laschi" (1 ogni 50 – 100 – 500).

   Importante non cambiare lo zoom né salvare il file durante questa procedura, il che significa fare uno zoom abbastanza lontano tale che le immagini incollate si vedano piccole ma affiancandole in righe/colonne rientrano tutte nella schermata visibile. Lo zoom va settato con un paio di tentativi all'incollaggio della prima immagine, stimando la dimensione del riquadro disponibile in grado di contenere tutte le circa 30 immagini previste:

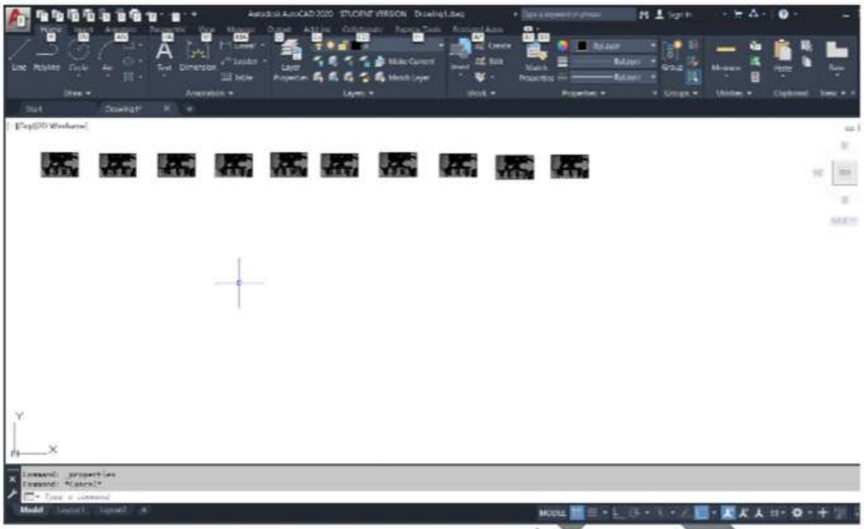

3) Fare in modo che tutte le 30 immagini del filmato siano scalate con la stessa scala, sia pure arbitraria (momentaneamente): per fare questo selezionarle tutte, cliccare il tasto destro / si apre un menù a tendina su cui cliccare "properties" che apre una finestra:

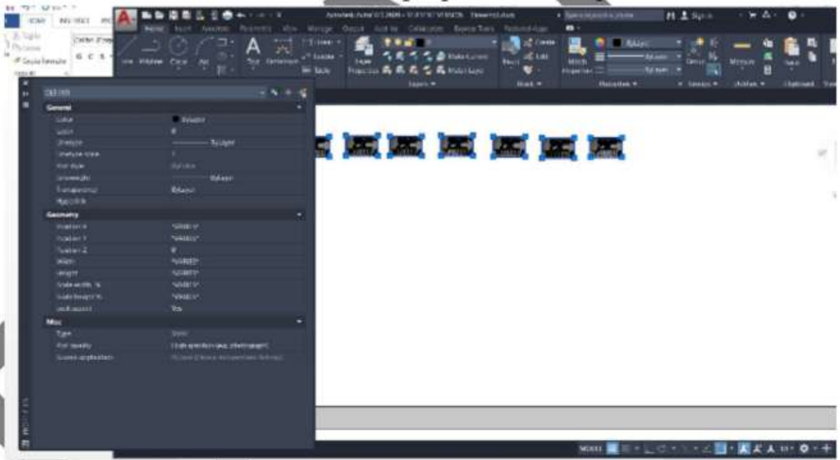

In questa finestra cliccare sul "yes" attivo di default accanto al "blocca proporzioni", cambiare in "no" x sbloccare proporzioni, quindi assegnare il fattore di scala 100 sia per la scala verticale sia per la scala orizzontale al posto del valore "VARIES" che normalmente si trova di default.

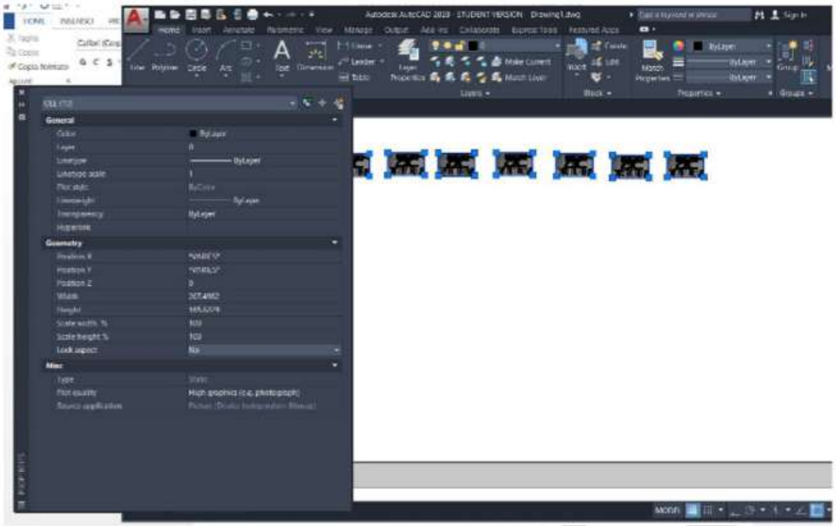

Adesso le immagini dovrebbero avere tutte le stesse dimensioni sia pure arbitrarie, verificare a campione che sia così x sicurezza.

4) Scalare l'immagine zero tramite:
   a) quotare il righello orizzontale e quello verticale su tratti + lunghi possibile;
   b) calcolare i due fattori di scala come rapporti tra le lunghezze reali dei due righelli (contare le tacche) / e le rispettive quote autocad;
   c) Analogamente a quanto già visto al punto 3, cliccare sull'immagine zero col tasto destro, si apre il menù a tendina su cui cliccare "properties" che apre la relativa finestra:

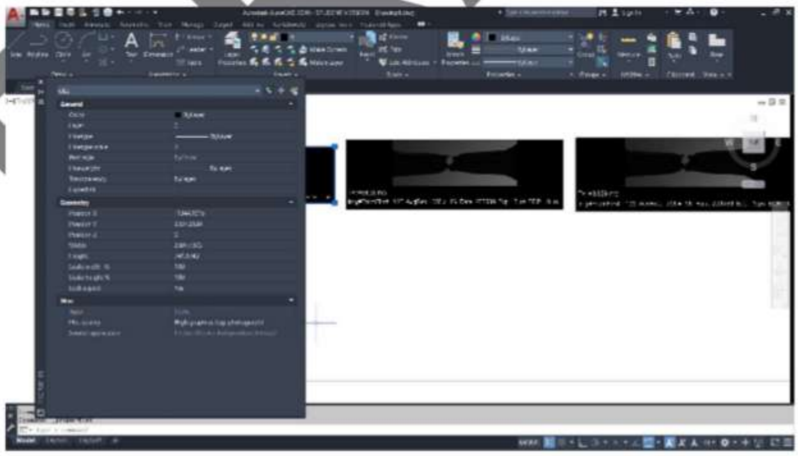

In questa finestra cliccare su "yes" attivo di default accanto al "blocca proporzioni", cambiare in "no" per sbloccare le proporzioni immagine, quindi assegnare i due fattori di scala orizzontale e verticale appena calcolati (normalmente sono diversi tra loro)i; attenzione al formato percentuale (per scalare del 15.7548% il valore da inserire è 115.7548).

Adesso le quote dei righelli dovrebbero essere esatte al centesimo, se non lo sono si ripete il punto 3 a partire dal calcolo delle due scale e le si riapplicano. Appena e quote dei due righelli risultano corrette l'immagine zero è "esatta" in entrambe le direzioni verticale/orizzontale, quindi può essere usata come riferimento per misurare otticamente tramite quotatura tutte le reali dimensioni di interesse del provino indeformato (diametri, lunghezze, gole intaglio, distanze spigoli, centri foro etc.etc.) che spesso con il calibro sono difficili da prendere (per es. intagli acuti o lunghezze prive di spigoli vivi netti) ovvero meno accurate di quelle ottiche.

5) Scalare tutte le immagini del filmato per adeguarle all'immagine zero esatta, tramite:
   a) Quotare due riferimenti sul provino del frame 1 del filmato, uno verticale ed uno orizzontale (per es. diametro max o diam. Min. provino x direzione orizzontale, lunghezza tratto cilindrico o distanza tra 2 vertici intaglio per direz. verticale, etc. etc.),
   b) Calcolare le due scale orizz. e vert. tra immagine 1 del filmato con il provino ancora indeformato ma in macchina di prova, ed immagine zero "esatta" nelle 2 direzioni ma provino poggiato "sul tavolino". Per esempio quota orizzontale da diametro max e quota verticale sulla lunghezza del tratto utile: sulla foto 0 in scala esatta il diametro sarà 3.2 mm e la lunghezza 9.1 mm; sull'immagine 1 del filmato, ancora in scala random dalla fine del passo 3), il diametro max risulta per es. 166,45 e la lunghezza 515.72..
   c) Selezionare TUTTE le IMMAGINI del FILMATO (ovviamente non l'immagine zero) e, tramite la solita sequenza tasto destro/proprietà/sblocca proporzioni applicare loro le due scale pari a 3.2/166.45 in orizzontale e 9.1/515.72 in verticale.

In teoria adesso anche le 30 immagini estratte dal filmato sono scalate in maniera "esatta" e permettono di effettuare le misure ottiche anche a provino deformato fino a rottura.

Verificare a campione che:

   d) i frames da filmato hanno tutti le stesse altezza/larghezza;
   e) le parti di provino o di altri oggetti inquadrati dalla camera che non hanno subito deformazioni (per es. zone afferraggi nei provini piatti, parti filettate nei cilindrici, altri riferimenti a parti di macchina o ad elementi sullo sfondo) devono avere le stesse identiche quote dall'immagine zero "a tavolino" fino all'immagine pre-rottura.

## VARIAZIONI RISPETTO ALLA PROCEDURA STANDARD:

Quando si testano provini flat, i righelli per l'immagine zero possono essere facilmente anche accostati ai provini già montati sulla macchina di prova ed allontanati poco dopo l'inizio del filmato (x es. nei 5 secondi di pausa tra inizio video e partenza macchina prova): in questi casi le immagini zero "a tavolino" sono ridondanti e si potrebbero omettere, considerando come immagine di riferimento per le misure esatte da righello il frame 1 del filmato che vede i righelli rpima di essere rimossi.

COMANDO COPIA-INCOLLA ALTERNATIVO:

Una procedura alternativa prevede di incollare le immagini quasi una sull'altra "a mazzetto" tramite il CTRL+V, sempre annotando i numeri di ogni immagine su un foglio a parte:

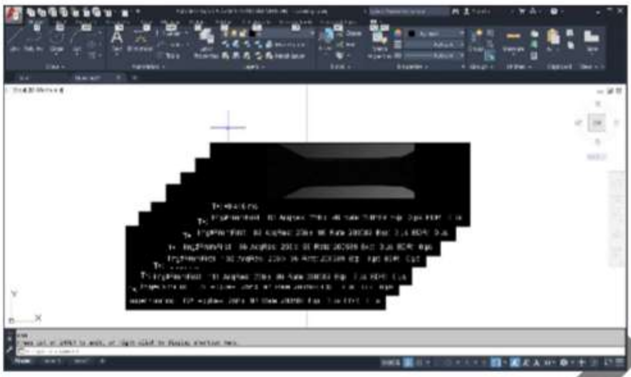

Al trentesimo frame incollato si verifica la dimensione comune delle foto come in 3) e si può poi zoomare come si vuole avanti e indietro per spostarle immagini una per una in modo che non siano più sovrapposte e possano essere quotare:

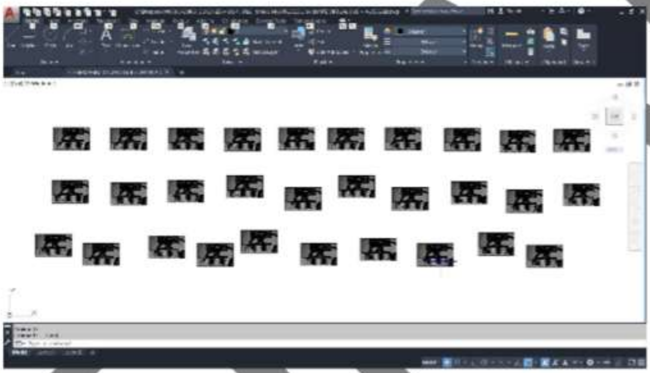

questa modalità fa risparmiare con un CTRL*V invece di tre click dell'incolla speciale/bitmap per ogni immagine e in qualche caso ha permesso di ottenere tutte le immagini uguali già a fine incollaggio facendo quindi risparmiare qualcuno dei 6 click di mouse del passo 3) (il controllo va sempre fatto, se poi si trovano le scale entrambe già pari a 100 si evita di sbloccarle e scrivere 100, 100); per contro però questa procedura alternativa richiede lo spostamento manuale delle 30 immagini.

Inoltre è stato verificato che in alcuni casi anche le immagini incollate in sovrapposizione con CTRL+V non hanno le stesse scale/dimensioni (probabilmente dipende da scheda video, versione autocad, sul pc, etc.) e bisogna quindi ugualmente eseguire il pareggiamento delle dimensioni tramite il passo 3) svolto per intero..

## 8.2 LOAD DERIVATION AND LOAD / DEFORMATION DATA SYNCHRONIZATION

In case of static tests, the load is simply recorded by the testing machine and stored in machine-files to be opened by spreadsheets (e.g. Excel).

Usually in such machine-files, after general information data like date, time, room temperature, test name etc., the first data column delivers the time values at the selected sample rate (e.g. time at 0.01 seconds intervals), then two more data columns report the current load (in kN or N) and the displacement of the machine head (in mm or m).

In case of Hopkinson bar tests, the load-vs-time readings are obtained from the transmitted wave of the output bar. In this case the transmitted wave is recorded together with the other waves traveling along the input bar, into a text file from the strain gauge acquisition system.

Then the time-vs-trasmitted wave amplitude has to be extracted from the overall acquisition file and the wave amplitude is multiplied by elasticity modulus and cross section diameter of the bar according to eq. ( *6-26* ). If the strain gauges placement along input and output bars ensure the possibility of separately reading the incident, reflected and transmitted waves, then the three-waves equation for the load in eq. ( *6-22* ) can be used.

In whatever of the two above ways, the load-vs-time data is obtained at the end of such procedure.

If the video acquisitions are synchronized by hardware with the testing machine or the SHTB acquisitions, then the time readings of the loads correspond to those of the camera frames.

If instead the testing machine/SHTB system are not synchronizaed to the video camera by any hardware triggering system, then a certain delay occurs between the two respective time readings and a post-processing synchronization has to be made by simply finding the value of such delay and by adding it to a reading or subtracting it to the other reading.

The physical phenomena suitable for such post-processing synchronization is the specimen ruputure, as it is usually detectable by visible fracture and/or separating specimen halves in the video recording, and by sudden load drop in the testing machine recording file.

Then the operating procedure is:

1) Identify the first video frame where the specimen is broken and its time (see figure …..)

ADD FIGURE OF UNBROKEN-BROKEN VIDOE FRAMES WITH TIME VALUES

2) Plot the load-vs-time curve from the testing machine and identify the FIRST INSTANTS time at which the load drops

ADD FIGURE OF LOAD-VS-TIME PLOT WITH HIGHLIGHTED FAILURE INSTANT

3) Calculate the delta-time to be added to the camera time (or the machine time) or to be subtracted to the machine time (to the camera time).

Once the optical measurements from the camera frames (elongations, shrinking diameters or any other distance betwee reference points on the specimen) are synchronized with the loads from the testing machine, whatever experimental load/displacement and stress-strain curve can be easily obtained.

## 8.3 CHRONIZATION

Here is described the procedure for joining data from load acquisitions and displacements/strains acquisitions in roder to derive the two main elements for each material characterization at given strain rate / temeprature condition: namely the flow curve $\sigma_{Eq}(\varepsilon_{Eq})$ and the strain rate history $\dot{\varepsilon}_{Eq}(\varepsilon_{Eq})$.

…………………. IN PROGRESS ………………..

## 8.4 EXAMPLES OF TESTING DATA

In figura sono riportate le letture sulle sezioni principali 2 e 3 rilevanti secondo la teoria standard della Hopkinson bar; (la sez. 1 serve teoricamente solo a misurare il precarico ed a triggerare l'acquisizione appena si rompe il fragile e viene rilasciata l'onda incidete; in realtà alcune info utili possono venire pure da tale sezione).

Le onde sono espresse in Newton sulle barre per immediatezza di interpretazione, ma per i calcoli classici della SHTB tali onde vanno espresse in termini di deformazione sulle barre per l'applicazione delle opportune formule viste in precedenza. Visto che sezione e materiale delle barre sono fissati, la conversione dall'una all'altra serie di grandezze è banale.

Con barre molto più lunghe dell'attuale e/o con precarichi molto più corti sulla stessa barra attuale, la sez. 1 avrebbe fornito le onde incidente e riflessa separate temporalmente l'una dall'altra. Visto che avere la riflessa "pulita" non ci serve perché lo strain lo misuriamo direttamente sul provino per via ottica, possiamo rinunciare alla riflessa per ottenere in cambio di poter allungare il precarico e l'onda incidente, il che significa maggiore durata della sollecitazione del provino e possibilità di rompere provini duttili anche a strain rates "bassi" rispetto allo standard delle SHTB, (anche 200 s-1)

A causa di quanto sopra, dopo i primi 550 microsecondi circa l'onda incidente letta sulla sez. 1 risulta sovrapposta alla riflessa che è già "di ritorno". Volendo estrapolare una stima della riflessa, si può comunque derivarla dalla incidente che rimane costante per circa 1200 microsecondi, meno la sovrapposizione di incidente-riflessa che è la registrazione globale della sez. 1 a partire dai 550 microsecondi.

## 8. REFERENCES

1) Lecture notes, G. Mirone, Università di Catania.
2) G. MIRONE , D. CORALLO, R. BARBAGALLO, Experimental issues in tensile Hopkinson bar testing and a model of dynamic hardening, International Journal of Impact Engineering, 103 (2017), 180–194.
3) G. MIRONE, D. CORALLO, R. BARBAGALLO, Interaction of strain rate and necking on the stress-strain response of uniaxial tension tests by Hopkinson bar, Procedia Structural Integrity, V. 2, (2016), 974–985.
4) MIRONE G., CORALLO D., Experimental issues and interpretation of the necking phenomena in the dynamic characterization via Hopkinson Bar, EPJ Web of Conferences 94, 01002 (2015).
5) MIRONE G., Development of a shape memory alloy – activated clamping device for split hopkinson tension bars, Exp. Techniques, 29-2 (2015), 3-15.
6) G. MIRONE, The Dynamic Effect Of Necking In Split Hopkinson Tensile Testing, Mechanics of Materials, 58 (2013) 84–96. (Q1)
7) Attività di ricerca in corso presso il DICAR e l'ex DII dell'Università di Catania: - Sviluppo di un sistema di rilascio rapido per SHTB, - Effetto del Necking in prove di trazione ad alti strain rates.
8) STRAIN RESPONSE OF PARTICULATE COMPOSITES UNDER HIGH RATES OF LOADING, Anthony Taylor Owens, A Thesis Submitted to the Graduate Faculty of Auburn University in Partial Fulfillment of the Requirements for the Degree of Master of Science Auburn, Alabama, August 4, 2007.

9) ADVANCEMENTS IN THE SPLIT HOPKINSON BAR TEST, by Michael Adam Kaiser, Thesis submitted to the Faculty of the Virginia Polytechnic Institute and State University in partial fulfillment of the requirements for the degree of Master of Science in Mechanical Engineering, Dr. Alfred Wicks, Chairman Leonard Wilson Dr. William Saunders May 1, 1998, Blacksburg, Virginia
10) AN OPTICAL METHOD OF STRAIN MEASUREMENT IN THE SPLIT HOPKINSON PRESSURE BAR Steven David Swantek Thesis submitted to the Faculty of the Virginia Polytechnic Institute and State University in partial fulfillment of the requirements for the degree of Master of Science in Mechanical Engineering
11) EXPERIMENTAL METHODS FOR MATERIAL CHARACTERIZATION AT HIGH STRAIN-RATE: ANALYTICAL AND NUMERICAL IMPROVEMENTS, Marco Peroni, ph. D. Thesis, april 2008, Politecnico di Torino.
12) WAVE MOTION IN ELASTIC SOLIDS, K. F.. Graff, Dover Inc., 1975, New York.
13) G.Mirone, P.Verleysen, R.Barbagallo, Tensile testing of metals: Relationship between macroscopic engineering data and hardening variables at the semi-local scale, International Journal of Mechanical Sciences, Volume 150, January 2019, Pages 154-167